

Local Heat Transfer and Stress Analysis of Direct Chill Casting Process

Dissertation

Zur Erlangung des akademischen Grades

Doktoringenieur

(Dr.-Ing.)

Vorgelegt von

M.Sc. Gaurav Abhay Kulkarni

Geb.am 05.10.1989

In Aurangabad, India

Genehmigt durch die

Der Fakultät für Verfahrens-und Systemtechnik
der Otto-von-Guericke-Universität Magdeburg

Gutachter:

Prof. Dr.-Ing. Eckehard Specht

Institut für Strömungstechnik und Thermodynamik, Universität Magdeburg

Jun.-Prof.Dr.-Ing. Daniel Juhre

Institut für Mechanik, Universität Magdeburg

Prof. Dr.-Ing. Udo Fritsching

Institut für Werkstofftechnik, Universität Bremen

Preface

This dissertation is submitted to Otto von Guericke University, Magdeburg for the degree of Doctor of Philosophy. The research described herein was conducted under the supervision of Prof. Ekehard Specht between October 2015 and November 2018. To the best of my knowledge, this work is original, except where suitable references are made to previous works. Neither this, nor any substantially similar dissertation has been submitted for any degree, diploma or qualification at any other university or institution.

Gaurav Abhay Kulkarni
Magdeburg, 12.11.2018

Acknowledgement

First and foremost I would like to extend my gratitude to my supervisor Prof. Dr.-Ing. E. Specht for providing me the opportunity to work with him and pursue a doctorate degree. His approach of simplifying complex problems has always been a source of motivation for me. He entrusted me with the freedom to pursue novel research methodologies and his guidance was vital for finishing this work. A special mention to Dr.-Ing. H. Böttcher and his colleagues from AMAG casting GmbH for many informative discussions. The exchange of knowledge was helpful for bridging fundamental research and industrial implementation.

I would like to thank Dr.-Ing. H. Woche and Dr.-Ing. A. K. Nallathambi for the frequent discussions and collaboration towards problem solving. They bestowed there immense research experience in the field of experimental and numerical analysis of casting processes upon me. Their doors were always open for me whenever I was in doubt. For helping to take my first steps with infrared thermography and quenching experiments, I would like to M.Sc. Y. Fang.

The research presented in this work was largely funded by DFG Graduate Research School GKMM - 1554, Micro-Macro-Interactions of Structured Media and Particle Systems. This multidisciplinary platform was very helpful in expanding my horizon beyond my research field. I thank the colleagues from GKMM for the numerous discussions, the scientific exchange and the cooperation over the project period. I would like to thank the secretaries Frau. M. Ruhbaum and Frau C. Hasemann for their continuous support with administrative work.

I thank my colleagues and friends of the Institute of Thermodynamics and Combustion as well as former scientists of the Institute of Thermodynamics and Combustion for their support. The exchanges and discussions of our scientific and certainly sometimes less scientific theses were very productive and gave me much joy. I thank my students for their project, bachelor or master theses for their dedication and commitment. I would also like to thank Prof. A. S. Dhoble and Prof. P. M. Padole from VNIT, Nagpur India for sparking my interest in the field of research and development at a young age. The mantras impart by them are a constant source of motivation for me.

I have an incredible family, their unconditional support has been paramount. I thank my parents Abhay and Madhuri Kulkarni, who are the reason for my existence and establishment. I would like to thank my brother and sister in law Aroha and Amruta for their continuous support. I especially thank my grandfather and my father and mother in law and other relatives who wish to see me holding doctorate title. The best gift I have received so far in my life is my wife Gauri and I am grateful for her exceptional love and immense support. Her efforts are incredible and I absolutely find no words to express my feelings towards her.

Abstract

Controlling the rate of cooling during the start-up phase of the Direct-Chill (DC) casting process is challenging and crucial as this region is highly prone to defect formation. During the DC casting process, primary cooling in the mold is followed by secondary cooling in which the partially solidified shell impinges with cooling water from an array of jets. The start-up phase of DC casting is the most critical phase because of its transient nature. This results in varying thermal boundary condition for the same set of parameters. The defect formation can be reduced by controlling the heat extraction in the secondary cooling zone. Hence, an accurate knowledge of boundary condition and the transient phenomenon occurring during the process is required for process optimization.

In order to analyze the boundary condition, the secondary cooling region is further divided in impingement zone and free falling zone on the basis of turbulence in the water stream. Experiments are conducted in laboratory replicate the DC casting process, to obtain the relations of various casting parameters on the boiling curve, in different zones. The thermal history data on the back side of the metal sheet is recorded with an infrared camera. This data is further analyzed in conjecture with 2D energy balance equation to obtain the temperature on the quenching side and hence the boiling curve.

The effect of various parameters like water quality and temperature, jet velocity and angle, metal thickness, casting speed, initial temperature and kind of metal are studied. It has been observed that the heat transfer in the impingement zone is less sensitive to changes in the quenching parameters, because of high turbulence in the water stream, whereas the free falling zone is sensitive to changes in parameters. During the experimental analysis, it has been found that if the temperature of the surface is high as it enters the free falling zone, water is ejected away from the surface. This phenomenon is dominant in the start-up phase, because of less diffusion of heat in the axial direction. Water ejection causes less and uneven cooling in the bottom region. So experimental analysis to quantify the effect of these parameters on water ejection is conducted. It has been noticed that water ejection is sensitive to various parameters. The boiling curves for impingement zone and free falling zone obtained from the experimental analysis for various parameters were incorporated in an FE model to predict the occurrence of ejection. These results were validated with experimental analysis to get a better physical understanding of ejection phenomenon.

In order to study the effect of various parameters on the DC casting process, the results from experimental analysis were used as boundary conditions in an in-house FE model, coupling the thermal, metallurgical and mechanical field. An isothermal staggered approach is followed to couple the thermal and mechanical fields along with temperature dependent material properties. The growing domain is simulated by adding new elements in the casting direction.

The thermal boundary conditions are validated with temperature measurements from industry. With the understanding of water ejection phenomenon, the temperature profiles from industrial measurements are matching well with the simulation results. The evolution of temperature and stresses in the start-up phase of the casting process are analyzed. The start-up phase is focussed to analyze the origin of the hot tear and other failures. In order to understand the influence of water ejection on the process, a hypothetical case with no water ejection is used to conduct comparative analysis. It has been observed that because of water ejection, compressive stress exists in the bottom region. This will give a chance for cracks if formed to heal. Without water ejection, the ingot undergoes high stresses at high temperature, increasing the susceptibility for failures.

The presented thermo-mechanical process model along with validated thermal boundary conditions. The effect of various casting parameters on the thermal boundary conditions is extensively studied with experimental analysis. This work, not only provides a deep understanding of heat transfer in the secondary cooling region, but also provides a qualitative understanding of the evolution of stresses in the DC casting process. This understanding is a powerful tool for improving the quality and optimization of the process in industry.

Keywords: Direct chill casting, Jet impingement quenching, Heat Transfer Analysis, Hot Tear, Boiling Curve , Wetting front.

Zusammenfassung

Die Steuerung der Abkühlungsgeschwindigkeit während der Startphase des Stranggießverfahrens (Direct Chill Casting) ist eine Herausforderung und entscheidend, da dieser Prozessabschnitt sehr anfällig für die Bildung von Defekten ist. Während des Stranggießverfahrens folgt der Primärkühlung in der Kokille die Sekundärkühlung, bei der die teilweise erstarrte Schale mit Kühlwasser aus einem Düsenfeld beaufschlagt wird. Die Anlaufphase des DC-Gießens ist aufgrund steigender Gießgeschwindigkeit die kritischste Phase. Dies führt zu veränderlichen thermischen Randbedingungen bei gleichzeitig hoher Kühlgeschwindigkeit. Die Fehlerbildung kann durch Steuerung des Wärmeentzugs in der sekundären Kühlzone reduziert werden. Daher ist eine genaue Kenntnis über die Randbedingungen und der während des Prozesses auftretenden Wärmeübergangsmechanismen für die Prozessoptimierung erforderlich. Um die Randbedingungen zu analysieren, wird der sekundäre Kühlbereich weiter unterteilt in Aufprallzone und Freifallzone. Diese Aufteilung wird auf Grundlage der Turbulenz im Wasserfilm definiert. Dazu werden Experimente im Labor durchgeführt, die das Stranggießverfahren nachstellen. Untersucht wird die Abhängigkeit zwischen verschiedenen Gießparametern und der Siedelinie, wobei in verschiedene Kühlzonen differenziert wird. Das thermische Verhalten während der Abkühlung des Metallblechs wird auf der Rückseite mittels Infrarotkamera aufgezeichnet. Diese Daten werden, in Verbindung mit einer zweidimensionalen Energiebilanzgleichung zur Beschreibung der Wärmeleitung in der Platte, analysiert, um die Temperatur auf der mit Wasser beaufschlagten Plattenseite und somit die Siedekurve zu erhalten. Die Auswirkungen verschiedener Parameter wie Wasserqualität, Wassertemperatur, Strahlgeschwindigkeit und Strahlwinkel, Plattendicke, Gießgeschwindigkeit, Anfangstemperatur und Art des Metalls wurden untersucht. Es wurde beobachtet, dass die Wärmeübertragung in der Aufprallzone aufgrund von starken Turbulenzen im Wasserstrom weniger empfindlich, während die Freifallzone empfindlich auf Änderungen der untersuchten Parameter reagiert. Während der experimentellen Analyse wurde beobachtet, dass Wasser von der Oberfläche weggeschleudert wird, wenn die Temperatur der Plattenoberfläche zu Beginn der Freifallzone hoch ist. Dieses Phänomen ist in der Startphase aufgrund von Wärmeleitung in axialer Richtung dominant und verursacht eine geringe und ungleichmäßige Kühlung stromabwärts. Daher wurde eine experimentelle Analyse durchgeführt, um den Effekt der genannten Parameter auf dieses Phänomen zu quantifizieren. Es wurde beobachtet, dass das Ejection-Phänomen empfindlich auf Parameteränderungen reagiert. Die Siedekurven für die Aufprallzone und die Freifallzone, die aus der experimentellen Analyse für verschiedene Parameter resultieren, wurden in ein FE-Modell aufgenommen, um das Auftreten des Ejection-Phänomens vorherzusagen. Diese Ergebnisse wurden mit experimentellen Analysen validiert, um ein besseres physikalisches Verständnis dieses Phänomens zu erhalten. Um die Auswirkung verschiedener Parameter auf das Stranggießverfahren zu untersuchen, wurden die Ergebnisse der experimentellen Analyse als Randbedingungen in einem hausinternen FE-Modell verwendet, wobei das thermische, metallurgische und mechanische Verhalten mittels einem isothermer

gestaffelter Ansatz gekoppelt wurde. Dabei wurde der anwachsende Strang simuliert, in dem neue Gitterelemente in Gießrichtung hinzugefügt werden. Die thermischen Randbedingungen wurden mit Temperaturmessungen aus industriellen Messungen validiert. Es wurde gezeigt, dass mit der Berücksichtigung des Ejection-Phänomens die Temperaturprofile von industriellen Messungen mit den Simulationsergebnissen gut übereinstimmen. Des Weiteren werden Temperaturfeld sowie resultierende Spannungen in der Startphase des Gießprozesses analysiert, um den Ursprung von Warmrissen zu analysieren. Es wurde beobachtet, dass durch das Ejection-Phänomen Druckspannungen stromabwärts auftreten, die Risse zurückbilden können. Tritt das Ejection-Phänomen nicht auf, wird der Strang hohen Spannungen bei hoher Temperatur ausgesetzt, was die Anfälligkeit für Ausfälle erhöht. Diese Arbeit präsentiert ein thermomechanisches Prozessmodell mit validierten thermischen Randbedingungen. Die Auswirkung verschiedener Gießparameter auf die thermischen Randbedingungen wird mit experimentellen Analysen intensiv untersucht. Diese Arbeit liefert nicht nur ein tiefes Verständnis zum Wärmetransport im sekundären Kühlbereich, sondern auch ein qualitatives Verständnis der Spannungsentwicklung während des Stranggießverfahrens. Dieses Verständnis ist ein leistungsfähiger Ansatz zur Verbesserung der Qualität und Optimierung des Prozesses in der Industrie.

Schlüsselwörter: Stranggießen, Düsenfelder, Abschrecken, Wärmetransportanalyse, Warmriss, Siedekurve, Benetzungsfront

Contents

| | |
|--|------------|
| Preface | iii |
| Acknowledgement | v |
| Abstract | vii |
| Zusammenfassung | ix |
| 1 Introduction | 1 |
| 1.1 Overview and Motivation | 1 |
| 1.2 Description of DC casting process for Aluminium Alloys | 2 |
| 1.3 Quality Issues in DC casting | 3 |
| 1.3.1 Hot Tearing | 3 |
| 1.3.2 Cold Cracking | 6 |
| 1.3.3 Ingot Distortion | 7 |
| 1.3.4 Macrosegregation | 7 |
| 1.3.5 Other Defects | 9 |
| 1.4 Purpose | 10 |
| 1.5 Overview | 11 |
| 2 Literature Review | 13 |
| 2.1 Secondary Cooling | 13 |
| 2.2 Boiling Water Heat Transfer | 14 |
| 2.3 Experimental Analysis | 16 |
| 2.4 Inverse code: Obtaining Boiling Curve | 17 |
| 2.5 Thermo-Mechanical Aspect of DC casting | 18 |

| | | |
|----------|---|-----------|
| 3 | Eulerian Steady State Solution of Boiling Curve for Impinging Water Jet on Moving and Stationary Hot Metal Plate | 21 |
| 3.1 | Introduction | 21 |
| 3.2 | Experimental Method | 21 |
| 3.2.1 | Setup | 21 |
| 3.2.2 | Experimental Sample | 22 |
| 3.2.3 | Experimental Results | 23 |
| 3.3 | Analysis Method | 23 |
| 3.3.1 | Advection | 24 |
| 3.3.2 | Eulerian Steady State | 25 |
| 3.4 | Heat flux as a function of position | 28 |
| 3.5 | Heat flux as a function of temperature | 30 |
| 3.6 | Results and discussion | 30 |
| 3.6.1 | Boiling Curve | 30 |
| 3.6.2 | Comparison with Inverse Model | 33 |
| 3.6.3 | Front Width | 34 |
| 4 | Heat Transfer Analysis of Moving Metal Sheet with an Array of Jets | 35 |
| 4.1 | Introduction | 35 |
| 4.1.1 | Mechanism of Heat Transfer | 35 |
| 4.2 | Results and Discussion | 37 |
| 4.2.1 | Influence of Water Quality | 39 |
| 4.2.2 | Temperature of Water | 41 |
| 4.2.3 | Jet Velocity | 43 |
| 4.2.4 | Jet Impingement Angle | 45 |
| 4.2.5 | Thickness of Metal Sheet | 46 |
| 4.2.6 | Casting Speed | 49 |
| 4.2.7 | Initial Temperature of Metal Sheet | 51 |
| 4.2.8 | Kinds of Metal | 52 |

| | | |
|--------------|--|---------------|
| 5 | Heat Transfer Analysis of Stationary Metal Sheet with an Array of Jets | 57 |
| 5.1 | Introduction | 57 |
| 5.1.1 | Mechanism of Heat Transfer | 58 |
| 5.2 | Results and Discussion | 60 |
| 5.2.1 | Influence of Water Quality | 62 |
| 5.2.2 | Temperature of Water | 63 |
| 5.2.3 | Jet Velocity | 66 |
| 5.2.4 | Jet Impingement Angle | 68 |
| 5.2.5 | Thickness of Metal Sheet | 70 |
| 5.2.6 | Initial Temperature of Metal Sheet | 72 |
| 5.2.7 | Kind of Metal | 74 |
| 6 | Water Ejection - Phenomenon and Physical Understanding | 77 |
| 6.1 | Introduction | 77 |
| 6.2 | Boiling Curve | 80 |
| 6.3 | Width of Impingement Zone | 82 |
| 6.4 | Mechanism of Heat Transfer | 83 |
| 6.5 | Simulation of Water Ejection | 84 |
| 6.6 | Results and Discussion | 85 |
| 6.6.1 | Temperature of Water | 86 |
| 6.6.2 | Thickness of Metal Sheet | 87 |
| 6.6.3 | Casting Speed | 87 |
| 6.6.4 | Jet Velocity | 88 |
| 6.6.5 | Jet Impingement Angle | 88 |
| 6.6.6 | Initial Temperature of Metal Sheet | 89 |
| 6.6.7 | Quality of Water | 89 |
| 6.7 | Critical Casting Speed | 90 |
| 7 | Implementing Laboratory Results to Industrial DC Casting Process Simulation | 93 |
| 7.1 | Extending Laboratory Results for DC Casting | 93 |
| 7.2 | Mathematical Modeling of DC Casting Process | 95 |
| 7.2.1 | Thermal Modeling | 95 |

| | | |
|----------|---|------------|
| 7.2.2 | Solidification Model | 96 |
| 7.2.3 | Mechanical Modeling | 98 |
| 7.3 | Thermal and Mechanical Boundary Condition | 101 |
| 7.4 | Casting Parameters | 102 |
| 7.4.1 | Material Properties | 102 |
| 7.4.2 | Casting Speed | 105 |
| 7.4.3 | Water Flow Rate | 106 |
| 7.5 | Analysing Experimental Results from DC Casting | 106 |
| 7.6 | Thermal Boundary Condition during Secondary Cooling | 109 |
| 7.6.1 | Boiling Curve | 110 |
| 7.7 | Simulation of DC Casting | 113 |
| 7.7.1 | Computational Domain | 113 |
| 7.8 | Results | 114 |
| 7.8.1 | Thermal Results | 114 |
| 7.8.2 | Mechanical Results | 119 |
| 7.9 | Critical Casting Speed | 127 |
| 7.10 | Formation of Meniscus | 128 |
| 8 | Conclusion | 131 |
| | Bibliography | 135 |
| I | Appendix | 141 |
| | List of Publications | 147 |
| | List of Thesis Supervised | 149 |
| | Curriculum Vitae | 151 |

1. Introduction

1.1 Overview and Motivation

With the prominence of lightweight structures for aerospace and automotive applications, for low fuel consumption and better performance, substituting steel components with aluminium parts is desirable. Aluminium is particularly the material of choice because it is nearly three times lighter than steel and alloyed aluminium can provide similar strength as steel. Another benefit of aluminium is its ability for casting in various shapes and sizes. It can also be extruded and rolled making it suitable for mass production. Compact and highly integrated casting process meets the demand for better performance, quality, and cost-efficient manufacturability.

Typically, commercial production of aluminium sheets for automotive applications encompasses several manufacturing processes. These include casting, homogenization of aluminium ingots, hot, cold rolling of the ingots to obtain required dimensions, followed by heat treatment to achieve desired mechanical properties. The casting process is particularly concerning because the majority of refining and recycling occur above the melting temperature. Casting process of aluminium can cause several solidification defects such as porosity, inclusions, hot and cold cracks which are detrimental to the quality of the cast and reduces product output. Also, the solidification of the grain structure determines the final material properties like strength, stiffness, ductility and creep behavior. Thus is it important to optimize the casting process for manufacturing high-quality aluminium at a minimum cost.

Over the past few years, there has been significant casting process improvements like continuous horizontal Direct Chill (DC) casting, Electromagnetic (EM) casting, air slip casting technology, melt level control, Electromagnetic stirring of liquid metal at advance solidification stage, casting with multiple alloy layers. These advancements in the process are largely attributed to computational analysis of the process. The semi-continuous vertical DC casting process is largely used to produce aluminium ingots (rectangular cross-section) and billets (circular cross-section) because of its robust nature and relative simplicity. This process is schematically shown in **Fig. 1.1**. Casting is performed by pouring the liquid metal in a bottom block and then the bottom block is withdrawn at a certain velocity with a certain level of molten metal maintained in the tundish or launder.

The liquid metal first undergoes primary cooling, which solidifies the outer shell of the ingot. The mechanism of heat transfer in primary cooling depends on casting technology. In conventional DC casting, the molten metal comes in contact with a water cooled mold, undergoing high contact heat transfer followed by the solidification of the shell and forming a gap between mold and ingot owing to contraction. In case of air slip technology, a mixture of air and oil is pumped through a porous graphite ring, causing cooling because of forced convection and avoiding contact with liquid metal with the mold. In EM casting, the liquid metal is contained by an electromagnetic mold using an electromagnetic field generated by the mold itself, causing heat transfer owing to radiation.

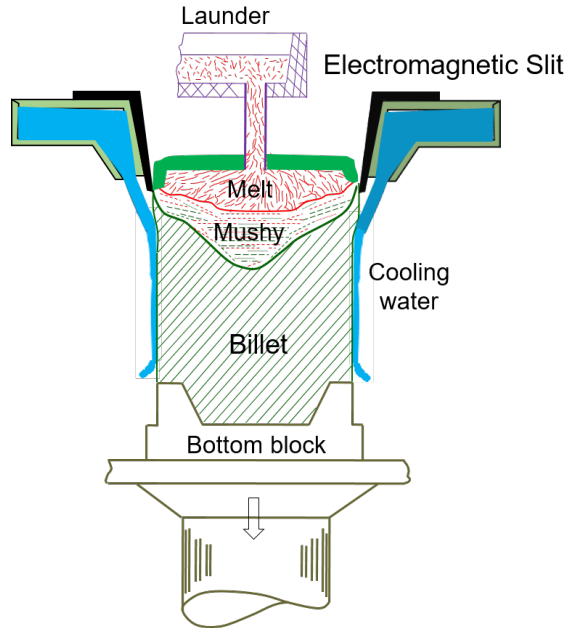


Figure 1.1: Schematic of vertical DC casting process

Secondary cooling in DC casting is caused because of direct impingement of water with an array of jets on the partially solidified shell as the ingot emerges from primary cooling. In secondary cooling, a major portion of the heat is extracted (80-90%) form the ingot. For this reason, heat transfer analysis in the secondary cooling region is crucial for process optimization.

1.2 Description of DC casting process for Aluminium Alloys

In industry, different casting parameters are used for different alloys and for different geometries. These parameters also vary from industry to industry and are proprietary to the industry. The normal length of the ingot is 8 - 10 m. Typically, the DC casting process can be divided into 3 phases.

First, the start-up phase. At the beginning of DC casting, the bottom block is placed inside the mold and liquid metal is poured into the bottom block at a low rate. Once a desired level of the melt is reached, the bottom block is lowered into a casting pit along with the casting ingot. Typically, there is a certain time delay between melt attaining certain hight and movement of bottom block, allowing metal in bottom block attain some strength. The level of molten metal in the mold is maintained constant with a reserve supply in launder. The casting speed and water flow rate are typically increased gradually in this start-up phase depending on the casting strategy. The start-up phase is complicated because of a lot of transient phenomenon. An accurate maintenance of several parameters such as melt pouring rate, water flow rate, casting speed is required to maintain product consistency.

During this phase, the water flow rate is kept low in order to decrease thermal gradients and thermal stresses by inducing partial or film boiling. For this purpose, in some industries, a pulsating water flow is used [1]. In this technology, a solenoid

valve is used to switch the water flow between drain and the mold at a certain frequency in a defined time cycle. The signal to the solenoid valve and the resultant water flow rate at mold is as described in **Fig. 1.2**. CO_2 injected water or water mixed with polymers is also used by some industries in order to reduce heat transfer in start-up phase [2]. As soon as the CO_2 injected water impinges on hot ingot, bubbles emerge promoting film boiling and water mixed with polymers will increase the surface tension of water reducing the surface heat flux.

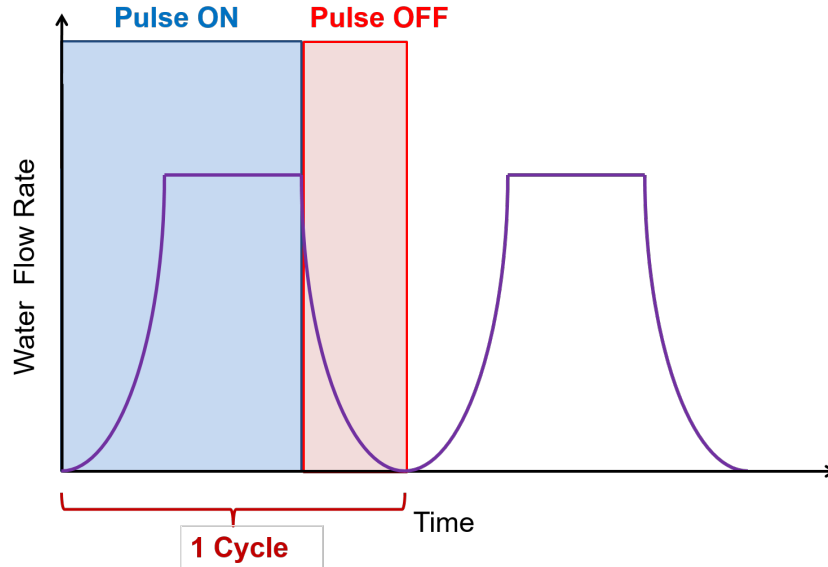


Figure 1.2: Water flow through the mold in the pulsating technology

Following the start-up phase, comes the steady state phase. In this phase, the transition phenomenon has reached an equilibrium and the casting parameters are maintained constant which means regulated constant water flow rate and casting speed is used. Steady state phase is usually achieved after a length of 0.5 - 1 m. This phase is the most productive stage but the duration of this stage is limited by the depth of casting pit. Followed by steady state phase is the end phase in which the casting speed is slowly reduced to stop the bottom block. At the end of this phase the ingot has reached its desired length and followed by this the ingot is removed from the casting pit as shown in **Fig. 1.3**.

1.3 Quality Issues in DC casting

As mentioned earlier, it is important to obtain a defect-free ingot from the casting process. A better understanding of the influencing parameter and techniques to control the process parameters is required to attain this goal. A large number of defects arise during the DC casting process. However, here the attention is focused only on the major defects which have a dominant influence on the quality of the cast.

1.3.1 Hot Tearing

Pure metal solidifies at a fixed temperature, whereas alloys solidify gradually over a wide temperature range. During the casting process, there is a considerable time



Courtesy: www.alibaba.com



Courtesy: NOVELIS INC.

Figure 1.3: DC casting of ingots and billets

during which the alloy consists of both solid and liquid phases. By definition, liquidus temperature (T_L) is the temperature above which a material is completely liquid and solidus temperature (T_S) is the temperature below which a material is completely solid.

Hot crack or pre-solidification cracks form in the mushy zone at a temperature between liquidus and solidus temperature. At high solid fraction, when the tensile stresses occur across partially solidified grains and the surrounding liquid cannot fill the gap between the dendrites is believed to be the origin of the hot tear. As concluded by Sigworth [3], a hot tear is initiated above the solidus temperature and this failure propagates in the interdendritic liquid film. Hence the crack always will be inter-granular. In some cases, the hot tear may run along the axial direction and in some other, it can extend in the lateral direction which can cause the liquid metal to pour out of the ingot. Because of hot tearing, the entire ingot has to be remelted, reducing the production of the plant.

The mechanism of hot tear formation in the DC casting is still not well understood. However, it is generally accepted that hot tear occurs in the mushy zone where the solidification shrinkage is not compensated by interdendritic melt flow due to insufficient liquid feeding in the presence of thermal stresses. Pure metals and the alloys with the eutectic composition are less susceptible to hot tear because of narrow solidification range. It is known that a fine grain structure and controlled casting 'recipe' avoiding high thermal gradients can reduce the hot tearing susceptibility. The hot tearing susceptibility depends on the composition of an alloy and their connection is many times established by Eskin et al. [4]. During the DC casting process, the formation of hot tear is critical during the start-up phase and if the casting speed is high in steady state phase. The ramping procedure is applied in the start-up phase for avoiding the hot tearing. Commonly, a hot tear is developed in the center of the ingot because the mushy zone is deepest there and stresses are tensile in nature. An example of the hot tear in the start-up is shown in **Fig. 1.4** and in steady state phase as shown in **Fig. 1.5**.

To address the hot tearing issue, it is important to understand the mechanism of solid growth in the mushy zone. Suytino et al. [5] categorized the alloy solidification process into four stages based on the permeability of the solid network :

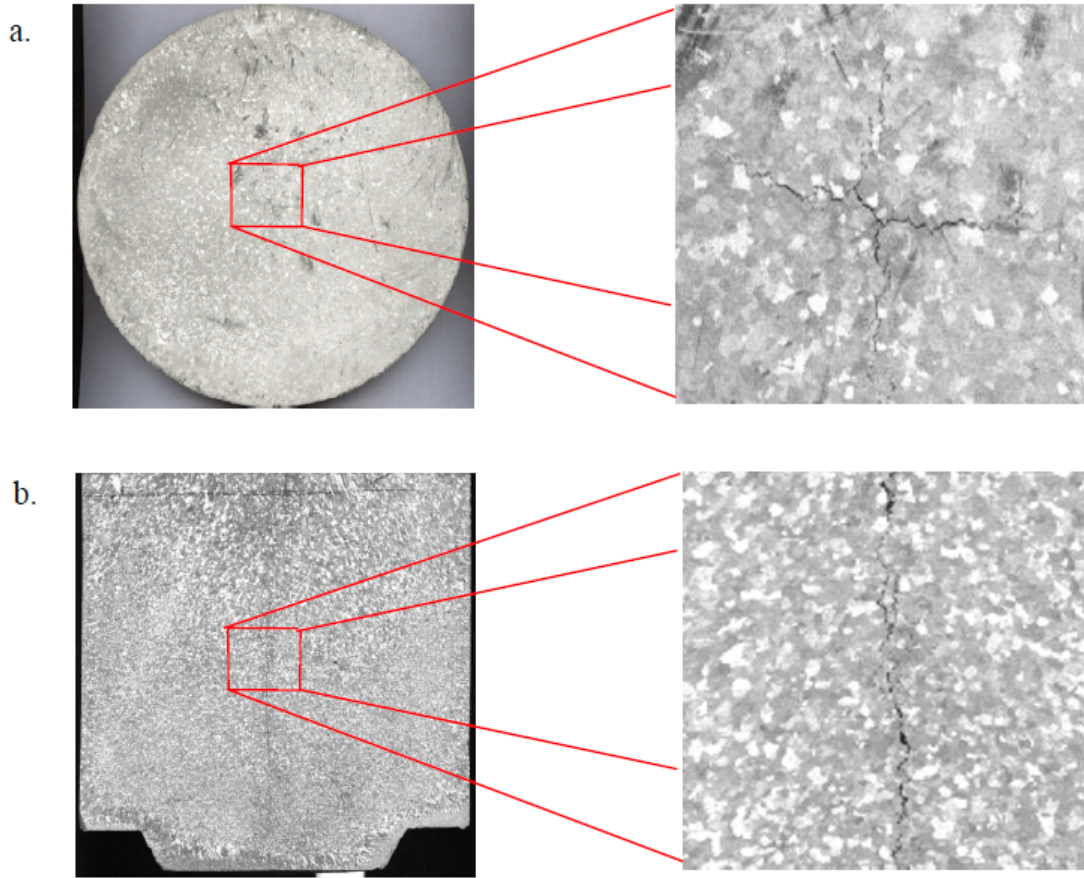


Figure 1.4: The hot tear in the start-up phase of 20 cm radius billet. a) radial and b) longitudinal cross section view. [5]

- Mass feeding, in which both liquid and solid are free to move.
- Interdendritic feeding, in which, after the dendrites have formed a coherent skeleton, the remaining liquid has to flow through the dendritic network. A pressure gradient (pressure drop) may develop across the mushy zone from solidification shrinkage occurring deeper in the mushy zone. However, at this stage, the permeability of the network is still large enough to prevent pore formation.
- Interdendritic separation, in which the liquid network becomes fragmented and pore formation or hot tearing may occur. With increasing solid fraction, the liquid is isolated in pockets or immobilized by surface tension. When the permeability of the solid network becomes too small for the liquid to flow, further thermal contraction of the solid will cause pore formation or hot tearing.



Figure 1.5: General hot cracking pattern observed in Al-Cu billet cast [5]

- Interdendritic bridging or solid feeding, in which the ingot has developed a considerable strength and solid-state creep compensates for further contraction. At the final stage of solidification ($f_s > 0.9$), only isolated liquid pockets remain and the ingot has considerable strength. Only solid-state creep can now compensate for solidification shrinkage and thermal stresses.

Generally, hot tearing occurs in the center of the ingot because of high tensile stresses. It is found that the circumferential stresses and inelastic strains are tensile at the solidus temperature near the center of the ingot. During the start-up phase, these values reach a maximum and this increases hot tearing susceptibility.

1.3.2 Cold Cracking

Cold cracking is a failure that occurs when the metal is fully solidified or when the temperature is below solidus temperature. Generally, cold cracks occur in high strength alloys due to the higher thermal stresses built up during the casting and cooling to the atmospheric temperature [6].

Thermally induced stress and strain developed during DC casting process can lead to the formation of micro-cracks at different locations in the ingot. Rapid propagation of such micro-cracks in tensile thermal stress fields can lead to catastrophic failure of ingots in the solid state after complete cooling. The 7xxx series aluminium alloys are more vulnerable to cold cracking mainly because of poor thermal and mechanical properties in the as-cast condition.

As depicted in **Fig. 1.6**, these cracks are dangerous as the ingot can potentially split into pieces. This not only limits the productivity of the plant but also creates a safety hazard. Cold cracks originate at center and at the surface of the ingot. Hence to prevent large temperature drops at the surface, cooling water can be stroked-off with separators or air impingement on the partially cooled surface, so that water film loses contact with the surface.

As mentioned in the hot tearing case, the stresses are tensile at the center of the ingot. At the surface of the ingot, on the other hand, stresses are tensile in the

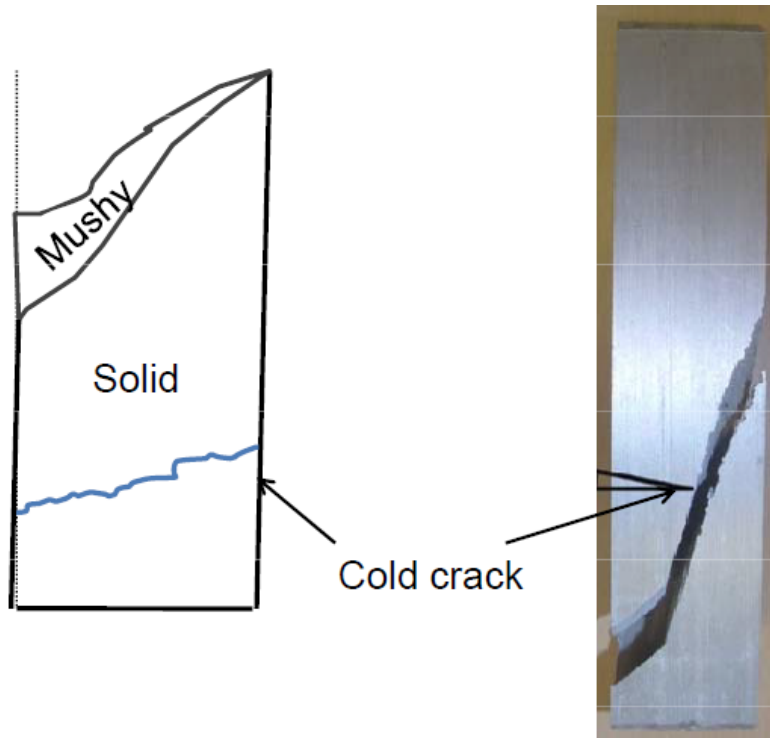


Figure 1.6: Cold crack in an ingot, breaking the ingot in parts[8]

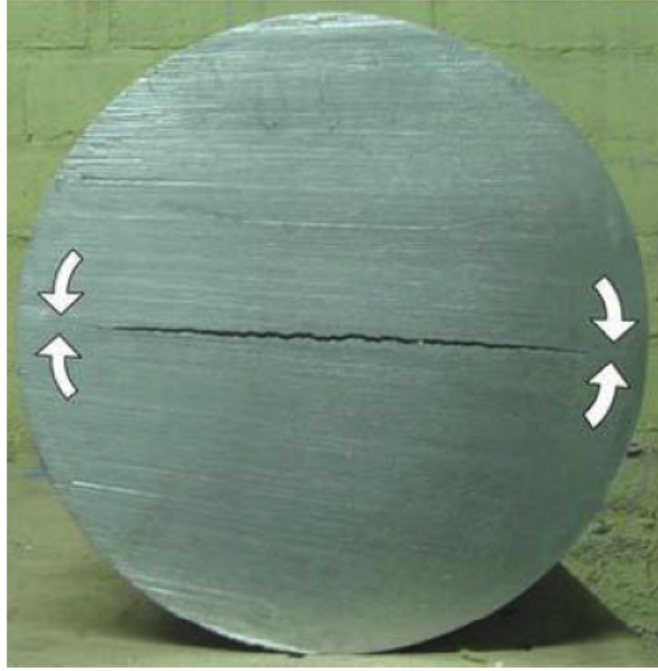
water impingement zone, but they turn to compressive in the free-falling zone. Even though there are chances of formation of cracks on the surface in the impingement zone, in the later stages due to excessive compressive stresses it can be healed. This is not possible at the center of the ingot. Because of this, similar to hot tearing, cold crack susceptibility is high at the center of the ingot. A typical cold crack which expands in the radial direction in the center of the billet is shown in **Fig. 1.7**. The arrow region indicates that the direction of circumferential compressive stress which arrests the crack expansion. Since this crack propagates after solidification of metal, it is trans-granular in nature.

1.3.3 Ingot Distortion

Because of temperature gradients in the ingot, large thermal stresses will develop in the solidifying metal causing deformation of the ingot. Butt curl is the major ingot distortion which occurs during the DC casting process. In the start-up stage, the solidified shell contracts inwards and the inhomogeneous cooling results the rectangular ingot deform into bone-shaped as shown in **Fig: 1.8**. In an attempt to compensate this effect, molding collars have to be designed in convex shape, usually with three segments per quadrant instead of a rectangular one. Butt curling also reduces the stability of the ingot because of decreasing contact area with the bottom block.

1.3.4 Macrosegregation

Macrosegregation refers to the variation of composition that occurs in alloy ingot and ranges in scale from several millimeters to centimeters. A typical variation of composition along the cross-section of the billet is as depicted in **Fig. 1.9**. It can



Courtesy: Lalpoor, Eskin & Katgerman

Figure 1.7: A typical cold crack at center of a billet [7]

be observed that there is negative segregation in the center, positive at center and a heavily depleted subsurface layer. These compositional variations have a detrimental impact on the subsequent processing behavior and property of the cast and can lead to rejection of casting product. Macrosegation is present in virtually all casting processes, because of the low diffusivity of the solute in the solid state and the large distances involved, macrosegation cannot be mitigated through heat treatment after solidification is completed.

Macrosegation can lead to nonuniform mechanical properties that affect the behavior of the metal during the subsequent processing and impair the quality of the final product [11]. Macrosegation is a really serious problem because it cannot be eliminated during the downstream processing, unlike microsegation, which can be removed relatively easily by high-temperature annealing. Macrosegation occurs due to the transport of segregated alloying elements at the scale of a casting by the relative movement of liquid and solid phases. It is caused by advective solute transport primarily due to the flow of segregated liquid in the mushy zone. This laminar flow is a result of convection in the liquid part, driven by buoyancy forces due to thermal gradients (thermal natural convection), buoyancy forces due to concentration gradients (solutal natural convection), and inlet flow (bulk convection). Additionally, a feeding flow due to the density difference between the two phases (solidification shrinkage) is induced in the mushy zone. Generally, the advancing solidification front pushes the liquid enriched in the solute (in the case of partition coefficient less than 1) towards the hotter part of the casting, e.g., the center. As a result, after solidification, the center of the casting will contain more solute than the periphery of the casting. In reality, the solute rich liquid should be transported toward the hot region of the casting (in the direction of solidification). The driving force behind such transport is either convection or shrinkage-driven flow.

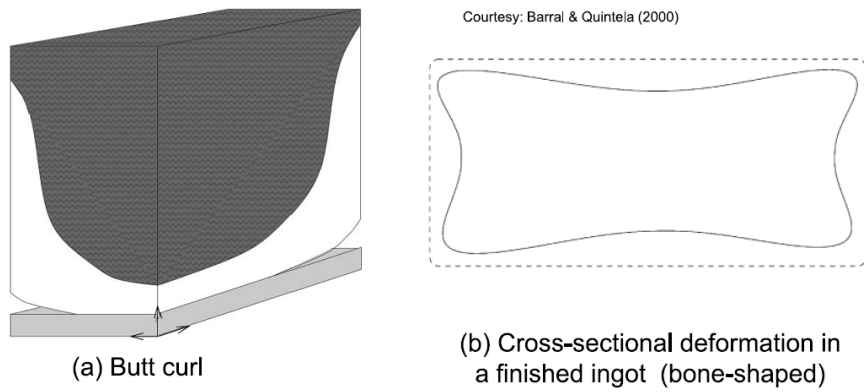


Figure 1.8: Butt curl and cross-sectional bone-shaped deformation of ingot [9]

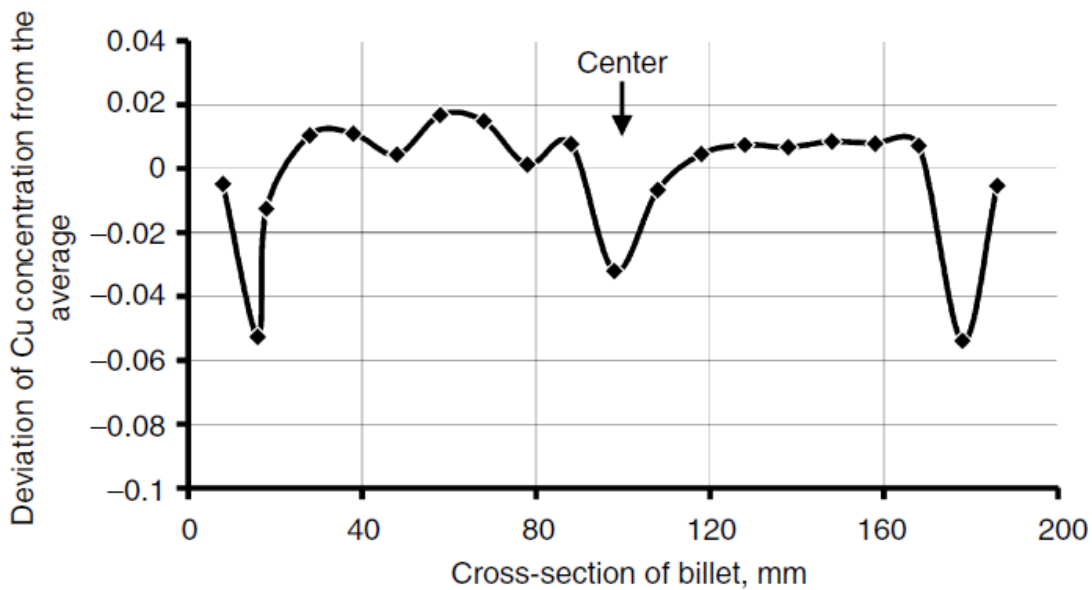


Figure 1.9: A typical pattern of macrosegregation in a 200 mm billet on a Al-4.2% Cu alloy cast at 120mm/min [10]

1.3.5 Other Defects

Some of the other defects that are non-progressive in nature but reduces the quality of the casting are depicted in **Fig. 1.10**. Flashing is the first defect that can occur during the DC casting process. This defect is caused when the melt flashes into the gap between the starting block and the mold or during casting when the metal bleeds-out through the weak solid shell. Another manifestation of the same problem is the separation of billet butt due to an insufficient degree of its solidification.

The opposite if the bleed-out is the hang-up of the casting in the mold in which the thick section of the billet is solidified inside the mold and gets stuck. This may cause damage to the mold assembly as well. Cold folding is caused by the freezing of the melt meniscus inside the mold, the solid meniscus then moves down and the melt flashes into the opening, filling the cavity. The process repeats with a periodicity that is a function of casting speed. Electromagnetic casting and air slip casting are much less prone to cold folding. The formation of the air gap because of thermal

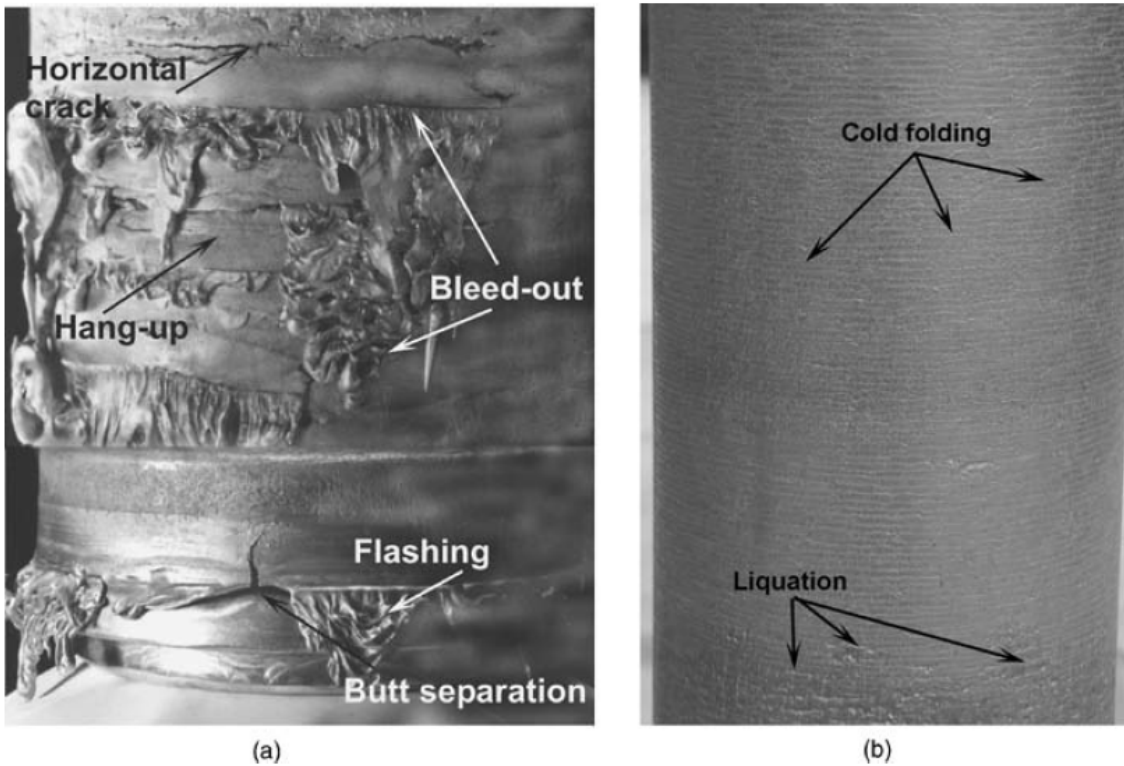


Figure 1.10: a) Flashing, bleed-out, hang-up, butt separation and cracking b) cold folding and liquation surface defect on a DC-cast aluminium alloy billet [10]

contraction and the corresponding reheating of the solid shell up to the point of its remelting is the main reason for the appearance of liquation marks on the billet surface.

1.4 Purpose

The failures, discussed in the previous section reduces the quality of product and the productivity of the plant as well. These failures are also potential safety hazards and need to be minimized. Hence an FE modeling of the DC casting process is required. An FE thermo-mechanical model can also be extended to improve the quality of the product by optimizing the process parameters.

The most critical stage of the DC casting process is the start-up phase, from a defects point of view. The start-up phase of DC casting process is complex to model because of its transient nature. Thermo-mechanical modeling of this phase is necessary for optimizing the casting parameters in order to minimize defects. For an FE model, the fundamental requirement is the thermal boundary condition. Many researchers have developed thermo-mechanical models but accurate thermal boundary conditions are required to derive implementable conclusions.

Experimental analysis of DC casting process for obtaining thermal data is very complicated and expensive. Hence it is important to conduct experimental analysis in the laboratory to quantify the influence of parameter on the boiling curve. For this, it is important to determine all the parameters that can influence the heat transfer process and minimize the dynamic parameters to conduct an experimental study.

The laboratory set-up also should be similar to the industrial casting process. Additionally, from the experiments, only the surface temperature data is obtained. Hence, a methodology to obtain heat flux or boiling curve is important for implementing the results in DC casting process simulation.

The experimental analysis can be conducted under two setups. Firstly, a moving sheet setup, in which the mold with water jets is kept stationary and the hot metal sheet is moved down at a controlled speed. The water jet first comes in contact with the bottom edge of the sheet and wetting front moves to the top of the sheet owing to the downward motion. Because of this, the water jet always comes in contact with hot metal and the hot metal sheet is cooled in the impingement zone. Second kind of setup is stationary setup, in which the water jet and hot metal sheet, both are kept stationary and the water jet impinges the top of metal sheet. The top portion of metal sheet is cooled first and then the wetting front propagates downstream of the sheet. In this case the cooling occurs when the water film is laminar and has only vertical momentum. It can be imagined that the heat transfer in these setups is different because of difference in turbulence in the water stream. Experimental analysis for these different zones is required in order to extend the understanding of thermal boundary conditions. In experimental analysis, transient phenomenon in which water is striking of the hot metal surface is observed and further experiments are conducted to understand this phenomenon.

Thermo-mechanical modeling of DC casting process needs to include the effects of phase-change, latent heat released, growing domain, dynamic boundary conditions and non-linear material properties. There are different physical fields coupled to each other such as thermal, metallurgical, and mechanical. It is tedious to solve the coupled field problem also since the solution domain is time dependent and it grows in the direction of casting.

The physical understanding of the transient start-up phase is analysed further with the thermal boundary conditions obtained from the experimental analysis. The respective physical parameters are identified and quantified by experimental analysis. Thermal measurements were also conducted in industrial DC casting process and the thermo-mechanical model and the thermal boundary condition are validated. This validated model is further analyzed to study the influence of stress evolution in different casting recipes.

1.5 Overview

The thesis deals with identifying the thermal boundary conditions in DC casting with a special emphasis on the transient start-up phase. The work consists of experimental analysis conducted in the laboratory at LTV, OvG University, Magdeburg to study the heat transfer mechanism during water impingement quenching. The goal of these experiments was to study the physics occurring during quenching of hot metal sheet and the influence of various process parameters on the heat transfer mechanism. The results from these experiments are used in a 2D FE thermo-mechanical model to match the temperature profiles obtained during electro-magnetic DC casting, hence validating the boundary conditions obtained from the experimental analysis.

Chapter 2 consists of a brief literature review and the state of the art. Experimental analysis conducted by various researchers is discussed to quantify the influence of

various parameters along with inverse models proposed to obtain heat flux from the thermal data. Various mathematical models for thermo-mechanical simulations are considered along with the considered thermal boundary conditions.

Chapter 3 explains the experimental setup used to conduct the experimental analysis and the methodology used to obtain the boiling curve. An infra-red thermography was used to record the thermal history during the quenching of hot metal sheet. This thermal history data is then further processed to obtain the boiling curve.

In **chapter 4** influence of various parameters on the heat transfer in the impingement region are studied and concluded and in **chapter 5** influence of casting parameters in the free-falling zone are analyzed.

A phenomenon of water ejection was observed in the startup region during quenching of moving, hot metal sheets. This phenomenon is analyzed further in **chapter 6**. A 2D FE model of the experimental setup is created to analyse this phenomenon further and experiments were conducted to validate the physical understanding of this phenomenon.

Chapter 7 elaborates the methodology used to extend the laboratory experimental results to DC casting in industry. Along with this, a 2D FE model for simulating the thermo-mechanical effects during DC casting is described along with the validation of thermal boundary conditions with experimental results from DC casting.

2. Literature Review

The rate of cooling for a metal product is dependent on many parameters. It also depends on the material properties of the cast. For instance, a metal with low thermal conductivity, if the cooling rate is too high, it will result in high thermal gradient and hence increasing strain in the product. This will result in failures or distorting the geometry causing rejection of the product. On the other side, slow cooling will reduce the productivity and deteriorate the material properties. Hence, controlling the rate of cooling is important in a process.

Typically, in case of non-ferrous metals, high heat transfer is desirable because of its high thermal diffusivity. For this reason, in the quenching of non-ferrous metals like aluminium, copper, bronze, etc. water jet impingement is commonly used. Another application of jet impingement quenching is the safety mechanism in a nuclear reactor to prevent the critical parts from overheating [12], [13]. The rewetting mechanism of the hot surface becomes critical as heat flux can reach a value over an order higher compared to the period before the wetting front starts to propagate. Other than that, a better understanding of jet impingement quenching will lead to better nuclear reactor safety [14].

2.1 Secondary Cooling

In the secondary cooling zone, the partially solidified metal surface is cooled by direct impingement with a vertical water film. The water film is formed by an array of water jets from a mold at a certain angle, with a certain velocity. Typically, the jet impingement angle of $15^\circ - 30^\circ$ [15]. The jet diameter and spacing, in case of rectangular ingots, may vary in the width and thickness direction and especially at the edges [16]. Various geometrical parameters of the water jet are as described in **Fig. 2.1**.

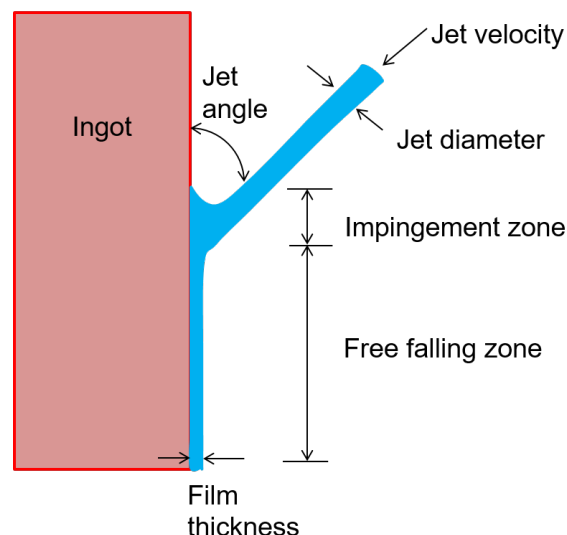


Figure 2.1: Geometry of the water jet, impinging on an ingot

The secondary cooling region can be divided in an impingement zone (IZ) and free falling zone (FFZ) [17]. Impingement zone can be described as the region where the water jets hit the ingot surface. In this region, the water stream is having horizontal and vertical momentum. Because of this, it can be imagined that the flow is turbulent. The turbulence will cause the bubbles formed at the surface to diffuse and the momentum or pressure in the horizontal direction will increase the heat transfer in this region.

In the free falling zone, the water stream has only vertical momentum and forms a laminar film along the surface. Because of this, the heat transfer will be less in this zone. Also, if the surface temperature in this zone is high, the formed bubbles in the water stream will throw away the water film from the surface. Because of this, there will be no contact between the water film and metal surface in the free falling zone, causing very less cooling in this region. The surface temperature at which the water film loses contact with the hot metal surface henceforth will be referred to as Re-wetting temperature (T_{RW}). This phenomenon is explored further in **Chapter 6**.

The impingement zone is present only in the vicinity of the mold and hence is small compared to the free falling zone. Though the heat transfer is high in the impingement zone, most of the heat is extracted in the free falling zone [18]. But the high heat transfer in the impingement zone increases the Biot number causing, high influence on the pre-cooling or upstream cooling of the ingot [19]. This width of pre-cooling if is not same as the location of formation of the meniscus, will cause poor surface quality [20].

At the start of DC casting process, the surface temperature at impingement point is high as compared to steady state phase. This is because, in steady state phase, there is a pool of cold quenched ingot, for heat to defuse increasing heat transfer in the axial direction. In the start-up phase, the heat transfer is dominant only in horizontal direction. This makes the cooling in the start-up phase complicated apart from heat transfer to the bottom block.

2.2 Boiling Water Heat Transfer

Since the ingot surface temperature is higher than the saturation temperature of water at atmospheric pressure, heat transfer will occur because of boiling. When water comes in contact with the hot metal surface, the heat flux can be defined as a function surface temperature. This plot of surface temperature vs. heat flux is referred to as boiling curve. A typical boiling curve is as shown in **Fig. 2.2**. In the figure, 4 boiling regions can be observed. In the film boiling region, because of high surface temperature a film of water vapor layer is formed on the metal surface, thus there is no contact between water and hot metal sheet, reducing the heat flux. This region is followed by transition boiling region, where there is partial contact between the metal surface and water. As the temperature decreases, the contact of cooling water and metal surface increases increasing the heat flux with decreasing temperature. Nucleate boiling region follows the transition boiling region, in which the water film is in contact with the hot metal surface but since the surface temperature is more than boiling temperature so bubbles are formed in water film. Because of this, the heat flux decreases with decreasing surface temperature. Beyond this, heat transfer is because of natural convection [22].

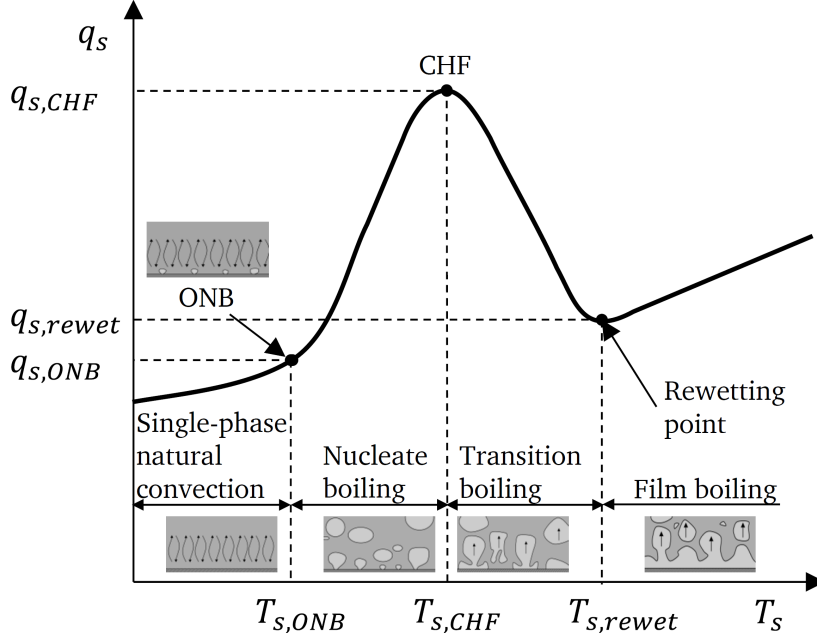


Figure 2.2: A schematic of boiling curve with bubble dynamics in the various boiling regimes [21]

In the impingement zone, Opstelten and Rabenberg [23] proposed an empirical relation for the heat flux as **Eq. 2.1**.

$$\begin{aligned}
 q &= 27.3 \times 10^3 T - 1.27 \times 10^6 & \text{for } T < 120^\circ\text{C} \\
 q &= 94.3 \times 10^3 T - 9.24 \times 10^6 & \text{for } 120^\circ\text{C} \leq T < 150^\circ\text{C} \\
 q &= 12.3 \times 10^3 T - 3.06 \times 10^6 & \text{for } T \geq 150^\circ\text{C}
 \end{aligned} \tag{2.1}$$

In 1982, Weckman and Niessen [24] proposed the following correlation from the estimation of nucleate boiling heat transfer coefficient as **Eq. 2.2**

$$h(T) = (-1.67 \times 10^5 + 704 \cdot \bar{T}) \left(\frac{Q}{\pi D} \right)^{1/3} + \frac{20.8}{T - T_{ref}} (T - 373.15)^3 \tag{2.2}$$

where T represents the surface temperature in Kelvin, T_{ref} is the bulk cooling water temperature, Q is the water flow rate in m^3/s and D is the billet diameter in meters.

Caron and Wells [18] modeled the film boiling average heat flux for secondary cooling for AA5182 vertical DC casting as **Eq. 2.3**

$$\Phi_{AVG,FB} = \frac{2}{\sqrt{3\pi}} \frac{\lambda_f}{L} \sqrt{\frac{(Pe^2 + 2Gn)^{3/2} - Pe^3}{Gn}} (T_{sat} - T_f) \tag{2.3}$$

where, λ_f is the thermal conductivity of cooling water in $(\text{W}/(\text{m} \cdot \text{K}))$, α_f is the thermal diffusivity of cooling water in (m^2/s) and L length of the vapor blanket

in meters. Pe is the dimensionless Peclet number and Gn is dimensionless gravity number defined as **Eq. 2.4** and **Eq. 2.5** respectively:

$$Pe = \frac{V_0 L}{\alpha_f} \quad (2.4)$$

$$Gn = \frac{gL^3}{\alpha_f^2} \quad (2.5)$$

Because of the high pressure in the impingement zone the length of the vapor blanket will be less because of which the heat flux will be high. In the free falling region, the water temperature will increase as the water film flows downstream. Sarler and Mencinger [25] presented a method to calculate the increase in water temperature as a function of height. Zuidema [26] also presented a method to determine the increase in water temperature. The experimental verification of water temperature with height is difficult to measure as the water film is thin and the ingot has limited access during DC casting process. Also, boiling water heat transfer is a 2-phase phenomenon, solving this in conjunction with surface heat flux is even more complicated.

2.3 Experimental Analysis

The analytical correlations, discussed in the previous section needs to be verified with experimental results to get a better understanding of boiling curve. This gives rise to the need for experimental analysis. A direct determination of heat flux through a surface is limited only to steady state condition with constant wall temperatures. Since this condition is not possible in DC casting process, an inverse heat transfer model has to be developed and implemented. But for this obtaining the temperature versus time history data is required.

Many researchers have conducted experimental analysis to record this temperature-time history data in various ways. One of the popular methods is to embed the thermocouples in the bottom block during the DC casting process. But maintaining the location of thermocouples, after they are submerged in metal and the metal solidifies is not possible so the location is determined by X-ray photography and ultrasound by many researchers [[24] , [27], [28]]. Another approach to obtaining heat flux is to record water film temperature distribution. This approach is a non-destructive method to obtain heat flux. [29] used an array thermocouples in a 7 mm diameter plastic cup, touching the ingot but avoiding contact with the metal surface. However, because of the high volume of the measurement system, the heat flux in the impingement zone cannot be determined with this approach.

Conducting in-situ experiments in the plant is expensive and also various casting parameters, like casting speed, water flow rate, initial temperature etc. cannot be varied much because of the occurrence of failures. Because of this, a majority of researchers [[30] [31] [32] [33] [34] [35]] have studied secondary cooling in DC casting by quenching of metal sample in laboratory. Typically, by these researchers, thermocouples are inserted into the sample at the sub-surfaces. The samples are then preheated and quenched with certain parameters with thermocouples recording the thermal history data.

2.4 Inverse code: Obtaining Boiling Curve

Using the experimental temperature data, an inverse 2-D heat conduction problem is solved to obtain the heat flux leaving on the quenched side. The ill-posed nature of the inverse problem demands sophisticated numerical techniques in order to avoid the numerical oscillations. Further, the inverse problem is highly sensitive to the experimental errors. A simple data noise filtering method is developed to reduce the level of error in the experimental measurements. Therefore many researchers have proposed various methodologies to obtain the boiling curve.

Inverse heat conduction techniques [36] can be used for estimating heat flux on the external surface of a conductive medium through the use of temperature measurements from experiments. Using the Laplace transform, Monde [37] obtained the solution for the one-dimensional inverse heat conduction problem. Ijaz et al. [38] have presented an adaptive state estimator for the estimation of input heat flux and measurement sensor bias in two-dimensional inverse heat conduction problem. A continuous-time analogue hop-field neural network based inverse solution algorithm has been proposed by Deng and Hwang [39]. Conjugate gradient method for the estimation of surface heat flux has been used by Huang and Wu [40] and by Xue and Yang [41]. Groß et al. [42] used conjugate gradient method along with temperature measurements from an infra-red camera to obtain heat flux in a falling film experiment. Gradeck et al. [43] used temperature data from the infrared camera to obtain transient heat flux with an inverse heat conduction problem formulated using an analytical solution of the direct problem expressed in Hankel space.

Elias and Yadigaroglu [44] developed an analytical one-dimensional model for the rewetting of a hot plate and predicted the wetting front velocity. They emphasized the importance of axial heat conduction. Wells and Cockcroft [45] applied an iterative two-dimensional FE inverse heat conduction model to estimate the surface heat flux. The experimental data obtained from thermocouples was smoothed and subsequently used for the inverse model. Nallathambi and Specht [46] applied a non-iterative finite element method for a two-dimensional inverse heat conduction problem, but it was observed that inverse FE model is very sensitive to experimental and numerical errors causing fluctuations in the results.

Mozumder et al. [47] studied the delay of wetting front propagation during jet impingement quenching and concluded that the value of maximum heat flux is 5 - 60 times higher than the heat transfer value just before the wetting front movement. Akmal et al. [48] studied the influence of initial surface temperature, water temperature and jet velocity on the curved surface exposed to an impinging water jet.

Investigations for heat flux under a condition where there is a relative motion between the array of jets and the hot surface has been reported by Caron and Wells [49]. They have characterized the boiling curve for magnesium alloy under different parameters. Opstelten and Rabenberg [23] used an inverse method to obtain the boiling curve for different parameters. Raudensky et al. [50] studied the impact of angle, pressure on cooling of a vertically moving hot steel sheet with an array of

sprays, to obtain the boiling curve for different spray pressures and angles with an upstream water spraying.

2.5 Thermo-Mechanical Aspect of DC casting

Mathematical modeling of DC casting process has evolved, especially with advancements in computational technology. A large number of researchers have published in this field, coupling the multiple physics involved in this process. But the fundamental, thermal boundary condition is not quantified completely. A thermo-mechanical model of the DC casting process is a basic requirement for process optimization. In this section, a brief literature review, studying the state of the art in this field is conducted.

Solidification is an important parameter that needs to be included in the simulation. During solidification, the liquid phase is transformed into a solid phase over a range of temperature, releasing latent heat, creating severe non-linearities and a local exchange of field variables [51]. Koric and Thomas [52] formulated the phase problem keeping the enthalpy as an independent variable and the nodal temperature derived from the enthalpy-temperature relation. Celentano et al. [53] proposed a temperature based FE method for the phase change problem which incorporates latent heat release by means of an additional phase-change matrix and a latent heat vector. They derived an approximate Jacobian matrix which maintains the numerical stability and gives a reasonable convergence rate.

Sengupta [54], presented a mathematical model for the evolution of thermal field during the start-up phase of the direct-chill casting process. He considered an aluminium alloy AA5182 for this analysis. In the start-up phase, the cooling is transient in nature, because of water ejection and reduced cooling in the bottom block because of butt curling. It is also possible that water enters the bottom block and the bottom of the ingot experiences water cooling. These effects are also considered in this work. Barral and Quintel [55] [9] presented a 3-D numerical model for accurate prediction of butt curl during the pseudo-steady phase. They used a time-space dependent heat transfer coefficient profile for the height of the ingot. Contact between the ingot and bottom block was modeled through the Lagrange multiplier method. To avoid non-linearities due to the contact condition and viscoplastic law, they introduced a maximal monotone operator technique involving a contact multiplier and a viscoplastic multiplier.

Kaymak [56] investigated the development of residual stresses in a solid material subjected to quenching. In this work, the curvature of the quenched object is treated as a measure of distortion. For this, a 2-D finite element model is developed using an elastoplastic material model with isotropic hardening. He concluded optimum cooling strategies to reduce distortion and residual stresses. With an enhanced cooling at the lumped mass region and reduce cooling at the edges, it is possible to reduce the residual stresses.

Nallathambi [57] studied the DC casting process with a thermomechanical model with a MATLAB model. In this work, the thermal, metallurgical and mechanical fields of DC casting process are modeled with attention on the mushy zone of the alloy for prediction of hot tear failures. An isothermal staggered approach is followed to couple the thermal and mechanical parts within a time step. He concluded that

the vulnerability of the start-up phase can be minimized through a proper ramping procedure. It is observed that increase in casting speed increases the steady state sump depth and mushy length increasing the probability of hot tearing. Penumakala [8] studied various casting processes like the continuous casting of steel, moving belt caster for copper and electromagnetic direct chill casting of aluminium alloy. He concluded mushy zone length of AA6061 is higher than AA5754 due to its large solidification interval. Also, the steady state deformation of AA6061 is higher than AA5754.

Williams et al. [58] simulated a 3-D DC casting of AA1201 alloy with ANSYS incorporating the liquid flow. They used a Perzyna type viscoplastic law for prediction of the mechanical behavior of solid and mushy phase. They reported extremely higher values of stresses due to the inappropriate material model. Magnin et al. [59] performed the tensile test on an Al-4.5% Cu alloy in order to determine the rheology and ductility over a wide range of temperature from room temperature to the dendritic coherency temperature. From the experimental observations, they proposed an elasto-viscoplastic law as **Eq. 2.6**

$$\sigma = K(\dot{\epsilon}_p + \dot{\epsilon}_{po})^u (\epsilon_p + \epsilon_{po})^n \quad (2.6)$$

where, K , u and n are material parameters which are dependent on temperature, ϵ_p and $\dot{\epsilon}_p$ are the plastic strain and plastic strain rate ($10^{-4} s^{-1}$) and ϵ_{po} and $\dot{\epsilon}_{po}$ are the small constant plastic strain and strain rate ($10^{-2} s^{-1}$) respectively.

Suyitno et al. [60] use the following constitutive equation for the mushy zone **Eq. 2.7**

$$\sigma = \tilde{\sigma}_0 \exp(\tilde{\alpha} f_s) \exp\left(\frac{mQ}{RT}\right) (\dot{\epsilon})^m \quad (2.7)$$

where Q is the activation energy of the solid phase deformation behavior, m is the strain rate sensitive coefficient, R is the gas constant, σ_0 and α are material constants and $\dot{\epsilon}$ is the strain rate.

3. Eulerian Steady State Solution of Boiling Curve for Impinging Water Jet on Moving and Stationary Hot Metal Plate

3.1 Introduction

This chapter proposes a method for obtaining boiling curve from experimental temperature measurement for an impinging water stream on the moving and stationary hot plate without using the inverse method. Inverse method is typically sensitive to numerical and experimental errors and implementing an inverse method is time-consuming and requires a lot of expertise. Another method to obtain boiling curve is using a 1D model. This model assumes the same temperature profiles at the quenching side and measuring side of the metal sheet and gives heat flux based on 1D energy balance equation. But it is important to quantify the temperature difference between the quenching side and measuring side. Hence this model is proposed in which analytical expression for temperature profile is obtained using a Boltzmann function. The heat flux obtained from 1 energy balance equation is applied as a boundary condition to a 2D FDM model to quantify the temperature difference between the quenching side and measuring side.

During a moving front, there will be temperature drop before heat transfer to cooling water. This temperature drop will be more significant in case of metals with high thermal conductivity like aluminium. Hence the proposed model also distinguishes between quenching region and pre-cooling region **Fig. 3.3**.

Using infrared thermography, temperature profiles on the back side of the moving hot metal sheet were measured. On the front side, water impinges on the hot region and induces pre-cooling in the dry region. This experimental setup can be treated as an impinging region of the DC casting. Once the Eulerian steady state is reached, temperature profiles can be approximated as a single curve using the Boltzmann function. With this function, energy balance is conducted, including the advection term to obtain the boiling curve. It is observed that the obtained boiling curve is similar to the boiling curve obtained from inverse solution.

3.2 Experimental Method

3.2.1 Setup

A small section of a real mold was used for these experimental works in order to mimic the secondary cooling process of real DC casting. It consists of an array of jets that creates a water curtain along the hot surface during the quenching process. The dimension of the mold used was $120 \text{ mm} \times 120 \text{ mm} \times 90 \text{ mm}$. It has 11 small orifices at its base, each of 2 mm in diameter, **Fig. 3.1**. The experimental setup of



Figure 3.1: Mold with array of 11 jets replicating the secondary cooling

this moving sheet analysis is shown in **Fig. 3.2**. The heated plate is shifted immediately from the electric furnace to the quenching chamber once the required initial temperature was reached. A 2 phase-stepper motor with an IT 116 flash controller, which actuates the axial movement. This controller has 128 micro steps for one full step by which a very smooth motion is possible for the connected 2 phase stepper motor. This movement is similar to the real DC casting process, where the ingot or billet is the moving part instead of the plate. The casting speed depends on the experimental requirements, which is completely controlled by the motor.

The cooling water was delivered by a centrifugal pump from the top of the mold and flow out through the array of orifices which produce water jets. These jets impinge on the quenching side of the metal sample. In this cooling process, the metal sheet is cooled from the bottom to the top.

For analysis of quenching of stationary sheet, the mold is shifted vertically so that the first water contact with the metal sheet is at the top region. In order to avoid contact of cooling water with the hot metal sheet, till the desired temperature is reached, a metallic separator is placed between the mold and hot sheet. Once the plate is positioned and the desired temperature is reached, the barrier is dropped at high speed and the quenching water comes in contact with the hot metal sheet. In order to illustrate the analysis method, an example of moving 5 *mm* thick aluminium sheet, sheet moving speed of 20 *mm/s* with a fixed jet velocity of 3 *m/s* and a jet angle of 45° is considered.

3.2.2 Experimental Sample

A rectangular sheet of aluminum alloy AA6082, with length and width as 250 *mm* and 90 *mm* respectively and a thickness of 5 *mm* was used for experimental investigation. The samples were painted black on the measuring side in order to increase the emissivity, for a more accurate measurement. From the emissivity calibration

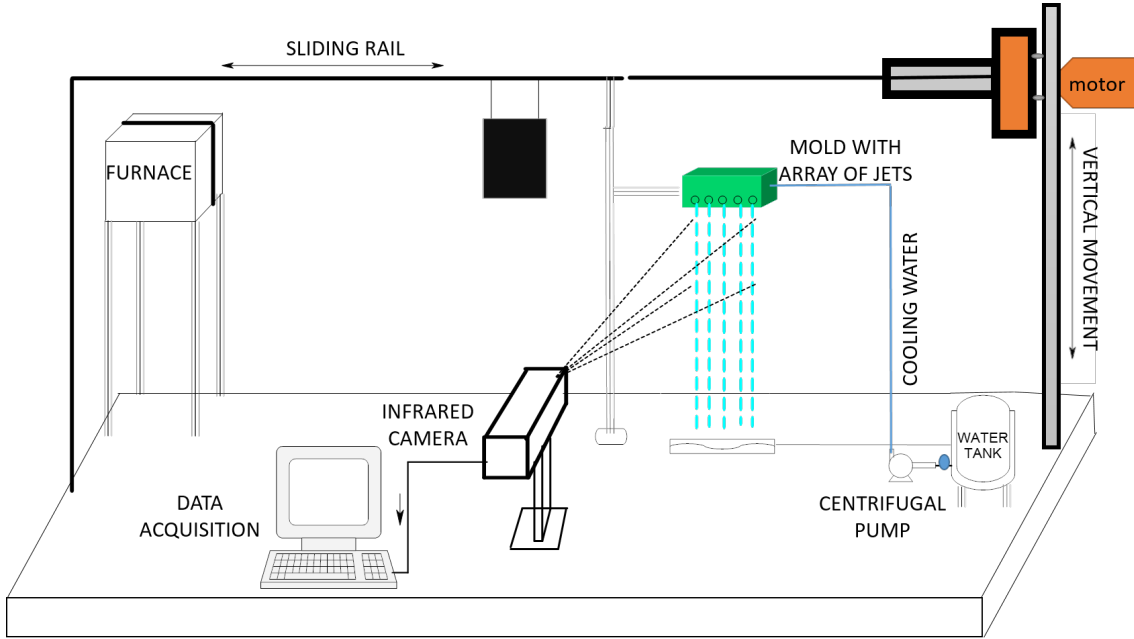


Figure 3.2: Moving sheet mechanism experimental setup

process, it was found that the emissivity of the coating was stable in the range of 0.90 to 0.92 and independent from surface temperature. A detailed review is available in another work by Alam et al. [61].

Table 3.1: Material property of Aluminium Alloy AA6082

| | |
|------------------------------------|------------------------------------|
| Density (ρ) | 2770 kg/m^3 |
| Thermal Conductivity (λ) | $170 \text{ W/m} \cdot \text{K}$ |
| Specific Heat Capacity (c) | $1050 \text{ J/kg} \cdot \text{K}$ |

3.2.3 Experimental Results

For the purpose of accuracy, the thermal images were captured and stored at an extremely high frame rate of 50 images per second with the resolution of 320×240 pixels. Therefore, a temperature analysis can be done for every 0.53 mm and to an accuracy of $\pm 0.1 \text{ K}$. The temperature measurement range of $100^\circ\text{C} - 500^\circ\text{C}$ was used for this experimental setup. The results along the center line are considered for analysis in order to minimize the errors because of end effects.

Fig. 3.3 shows an example of a thermal image from the infrared camera during the quenching process. This acquired thermal history data was processed further in order to obtain the temperature data as a function of time and position. x_e is the eulerian position recorded by the infrared camera.

3.3 Analysis Method

An analytical approach is presented here, with less sensitivity to experimental and numerical errors. In metals with high thermal conductivity, a lot of heat will diffuse

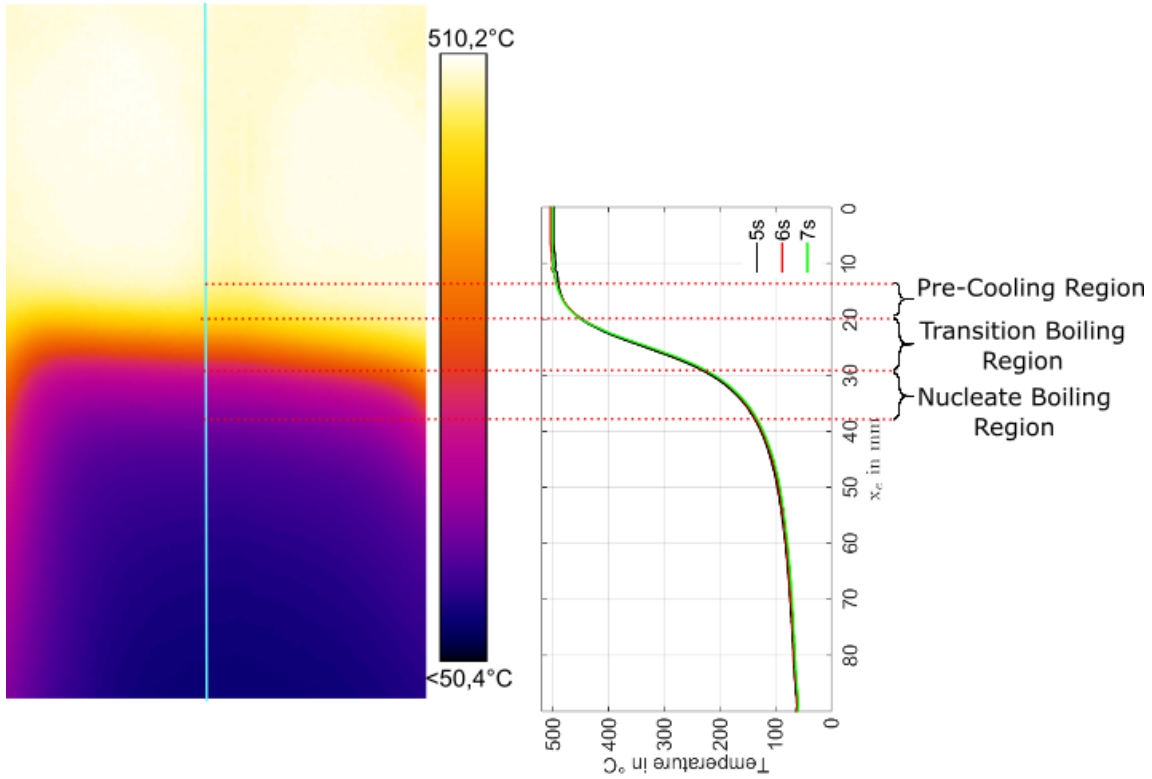


Figure 3.3: Infrared image and temperature profiles at different times

in the axial direction before the start of cooling in quenching region. In other words, there is a significant temperature gradient even before the material point experiences water cooling. Henceforth, this region will be referred to as pre-cooling region and the region in which there is a heat transfer to the cooling water from the hot metal plate is referred as quenching region. An analytical expression for temperature profile in quenching region, when it has attained Eulerian steady state is determined by curve fitting. This analytical expression is used in conjecture with energy equation to determine the heat flux. The simplified governing differential equations are solved in a two-dimensional finite difference model in order to obtain the heat flux as a function of temperature on the quenching side and measuring side of the plate.

3.3.1 Advection

Firstly, it is required to distinguish between the pre-cooling region and the quenching region as seen in Fig. 3.4. This is done by identifying the interface temperature between these regions or the temperature drop because of diffusion in the pre-cooling region. The interface temperature ($T_{z=0}$) is the temperature at the material point transitioning from pre-cooling region to quenching region, this is the temperature where the heat transfer with quenching water begins. Experimentally, it is difficult to distinguish between these regions as there is spluttering when the jet hits the plate. In the pre-cooling region, the thermal gradient along the thickness is not very strong as there is no heat flux on the boundary in this region. Hence, a solution of one-dimensional heat conduction equation will provide a reasonable temperature profile. Since the plate thickness is small, in the quenching region entire cooling is completed within the impingement zone. Hence distinguishing between free falling

zone and impingement zone is not required.

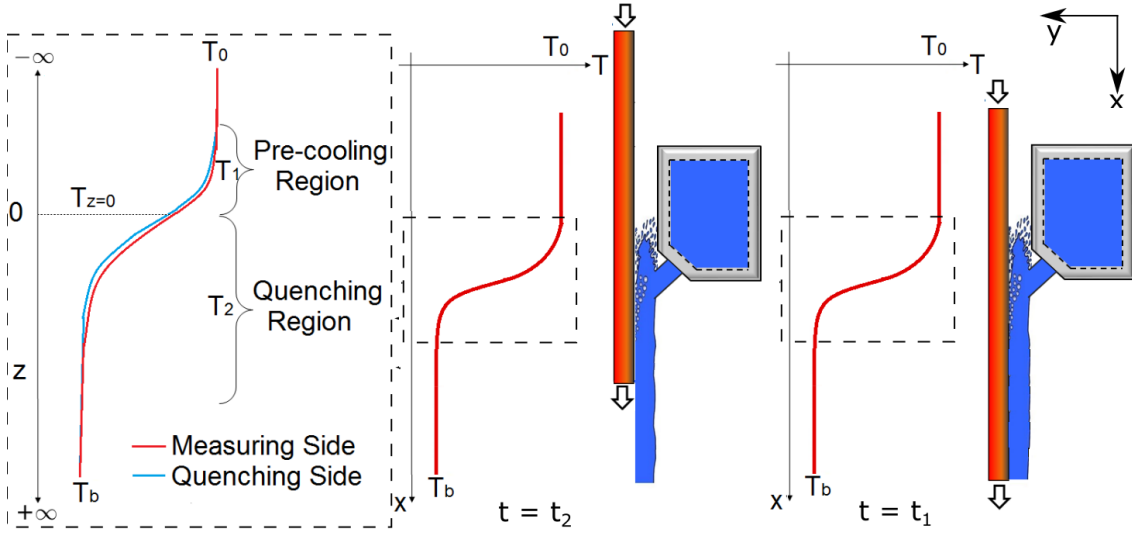


Figure 3.4: Temperature profiles in different regions in quenching process under moving sheet setup

An one-dimensional conduction equation for solid can be written as:

$$\lambda \frac{\partial^2 T}{\partial z^2} - \frac{\dot{q}}{s} = \rho C \frac{DT}{Dt} \quad (3.1)$$

where λ, ρ, C, s are thermal conductivity, density, specific heat capacity and thickness of the slab respectively. Also, T and \dot{q} are the temperature and heat flux on quenching side of the sheet.

In case of stationary sheet setup, the first wetting occurs at the top of the sheet and the wetting front propagates down. Near the wetting front, the above region is in contact with cooling water and the below region the water is thrown away from the surface. Because of this the lower region experiences no water cooling. In the above region of the wetting front first cooling is because of convection followed by nucleate boiling and transition boiling, as shown in Fig. 3.5. In the lower portion of the wetting front, the density of bubbles will increase and at a point, the water will be thrown away from the surface since the water film has no momentum in the horizontal direction. Referring to this region as film boiling region is not correct as the water film is thrown away from the surface and there is no contact between the water film and metal surface. The cooling in the bottom region will be because of advection and radiation and convection with air. The advective heat transfer will be dominant near the wetting front causing the wetting front to propagate.

3.3.2 Eulerian Steady State

For a constant casting velocity V_c , in the spacial vicinity of the mold, the space and time derivatives are then related by:

$$\frac{DT}{Dt} = V_c \frac{\partial T}{\partial z} + \frac{\partial T}{\partial t} \Big|_z \quad (3.2)$$

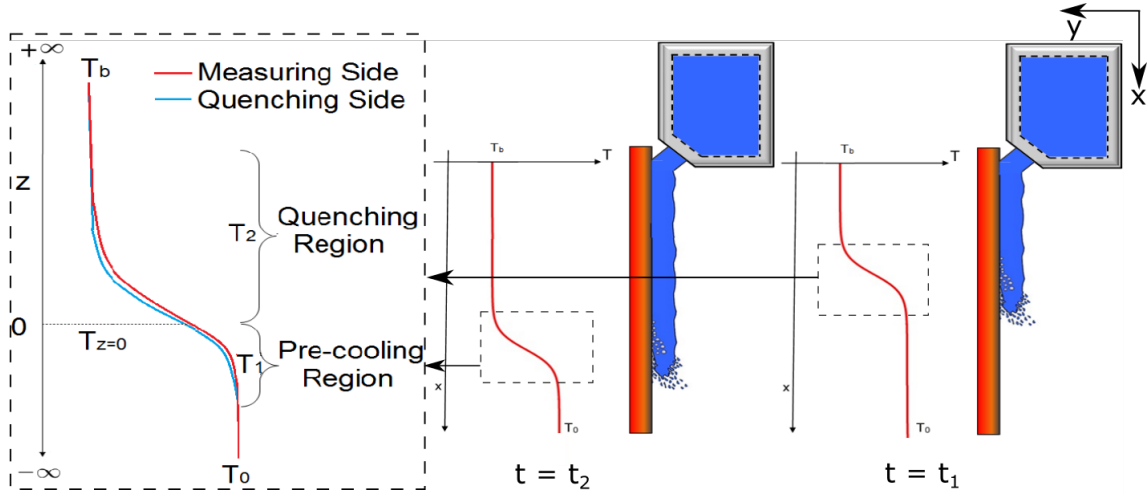


Figure 3.5: Temperature profiles in different regions in quenching process under stationary sheet setup

As the metal plate moves, the temperature profile in the Eulerian region in the vicinity of the mold is nearly independent of time.

$$\left. \frac{\partial T}{\partial t} \right|_z = 0 \quad (3.3)$$

This can also be verified with the experimental results when the temperature profile for 20 mm/s casting velocity for 5, 6, 7 seconds, as shown in **Fig. 3.6** are superimposed. Since the profiles match well, the Eulerian steady state assumption is valid. The cooling of the plate because of radiation and natural convection can be neglected, as the heat loss by radiation and natural convection is very small compared to heat loss by cooling water.

In case of stationary sheet setup, the wetting front velocity cannot be controlled. Hence, it is required to determine the position of wetting front. Visually, tracking the wetting front is not possible because of splattering of water. To track the wetting front with the temperature profile, Filipovic et al. [14] proposed the wetting front will be positioned where the second derivative of temperature will reach a minimum value, as shown in **Fig. 3.7**. This approach is used to get wetting front velocity as it can be observed from **Eq. 3.8** below the wetting front, the second derivative will be negative as the Peclet number will be negative and the thermal gradient will be positive. The magnitude of second temperature derivative will increase as it approached wetting front as the temperature gradient will increase. In the pre-cooling region, from **Eq. 3.9** the positive Biot number and temperature term is added to the negative Peclet number term decreasing the magnitude of the second temperature derivative. Hence, it can be concluded that the second temperature derivative will reach a minimum value at the wetting front.

Based on this approach the location of the wetting front and hence the wetting front velocity can be determined. It was observed that after the impingement region, the wetting front velocity was nearly constant can be determined, discussed further in **Ch. 5**. Based on this it can be observed that the sheet attains an Eulerian steady state in the vicinity of the wetting front and obey the condition described in **Eq. 3.3**.

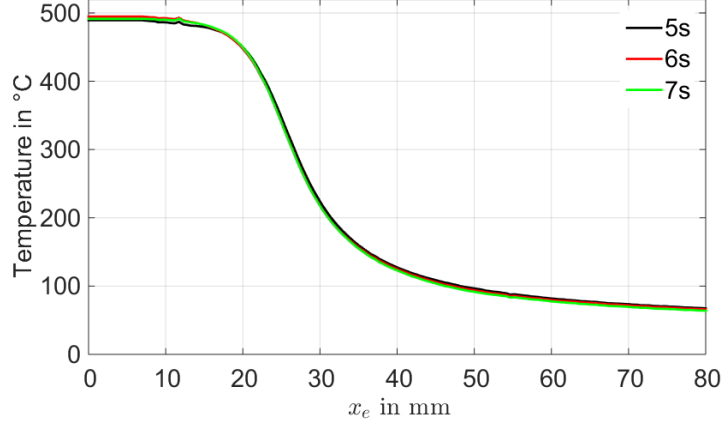


Figure 3.6: Temperature profiles of 20 mm/s casting velocity during Eulerian steady state

Using this condition **Eq. 3.2**, **Eq. 3.3** can be simplified as,

$$\frac{DT}{Dt} = V_c \frac{\partial T}{\partial z} \quad (3.4)$$

This condition is referred to as quasi steady state condition by Agrawal and Sahu [62]. Using this condition **Eq. 3.4**, **Eq. 3.1** can be written as:

$$\lambda \frac{\partial^2 T}{\partial z^2} - \frac{\dot{q}}{s} = \rho C V_c \frac{\partial T}{\partial z} \quad (3.5)$$

The advection term from **Eq. 3.4** will incorporate the movement of the plate. To solve this governing differential equation **Eq. 3.5**, we can define the following normalized variables

$$\theta_1 = \frac{T_1 - T_w}{T_0 - T_w} \quad \theta_2 = \frac{T_2 - T_w}{T_0 - T_w} \quad \theta_{z=0} = \frac{T_{z=0} - T_w}{T_0 - T_w} \quad \bar{z} = \frac{z}{s} \quad (3.6)$$

where T_1 and T_2 are the temperatures in pre-cooling region and quenching region, T_w is the water temperature, T_0 is the initial temperature of the plate and $T_{z=0}$ is the temperature at the interface between pre-cooling and quenching region. Biot number and Peclet number are defined as

$$Bi = \frac{hs}{\lambda} \quad Pe = \frac{V_c s \rho c}{\lambda} \quad (3.7)$$

So **Eq. 3.5** will be transformed to as following for the pre-cooling region where there is no heat flux to water

$$\frac{d^2 \theta_1}{d\bar{z}^2} - Pe \frac{d\theta_1}{d\bar{z}} = 0 \quad (3.8)$$

and for the quenching region as

$$\frac{d^2 \theta_2}{d\bar{z}^2} - Pe \frac{d\theta_2}{d\bar{z}} - Bi \theta_2 = 0 \quad (3.9)$$

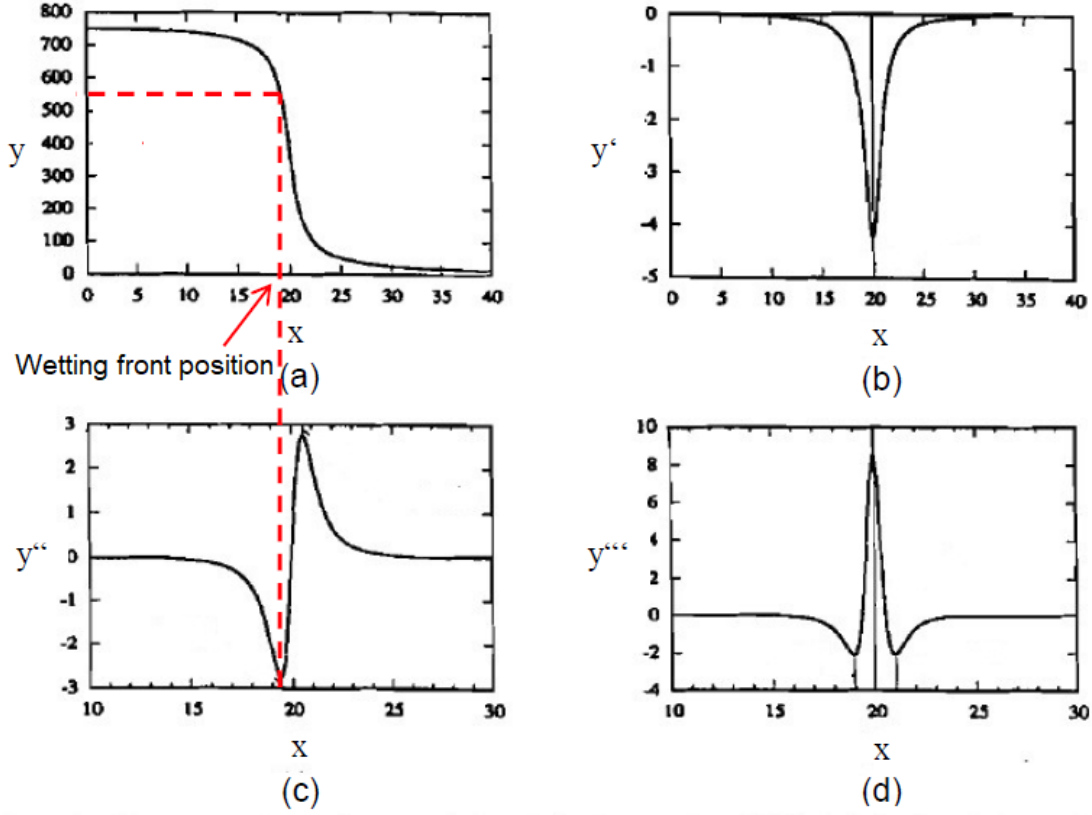


Figure 3.7: The idealized quenching curve: a) analytical expression of temperature profile b) first derivative c) second derivative d) third derivative [14]

So by assuming a constant Biot number in the quenching region with Sparrow and Siegel approach as used by Yamanouchi [63] we obtain the following solution:

$$\theta_1 = 1 + (\theta_{z=0} - 1) \exp(Pe \cdot \bar{z}) \quad (3.10)$$

$$\theta_2 = \theta_{z=0} \cdot \exp \left[-\frac{Pe}{2} \left(\sqrt{1 + \frac{4 \cdot Bi}{Pe^2}} - 1 \right) \cdot \bar{z} \right] \quad (3.11)$$

where $\theta_{z=0}$, the normalized temperature at interface is,

$$\theta_{z=0} = \frac{2}{1 + \sqrt{1 + \frac{4 \cdot Bi}{Pe^2}}} \quad (3.12)$$

With this approach, we can determine $T_{z=0}$ for a constant Biot number in the quenching region and hence distinguish between the pre-cooling region and quenching region.

3.4 Heat flux as a function of position

Since we have quantified the quenching region, the temperature profile in the quenching region can be obtained. An analytical expression for this temperature profile can

be obtained by curve fitting. For this *Origin* software was used. It was observed that a Boltzmann function provides the best fit to the experimental temperature profile. The temperature only in the transition region is considered in order to increase the accuracy of the curve fitting. The equation for the Boltzmann function is as follows:

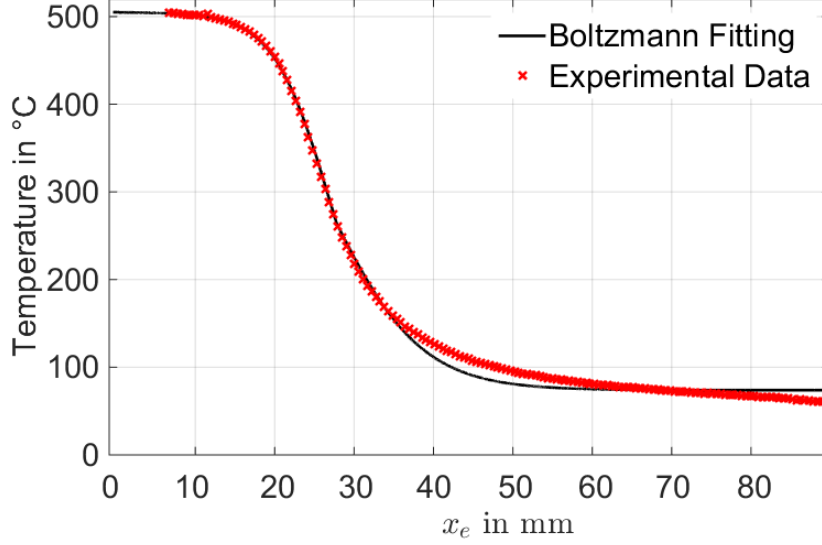


Figure 3.8: Fitting Boltzmann function with experimental temperature profile

$$T = A_2 + \frac{A_1 - A_2}{\left[1 + \exp\left(\frac{z-z_0}{dz}\right)\right]} \quad (3.13)$$

From **Fig. 3.8**, it can be observed that the experimental data matches well with the Boltzmann curve. Hence we can assume this analytical expression for temperature profile as a function of position. Since we have the analytical expression for the temperature distribution, the distribution of the Biot number can be determined:

$$Bi = \left(\frac{d^2\theta}{dz^2} - Pe\frac{d\theta}{dz}\right) \times \frac{1}{\theta} \quad (3.14)$$

Since the analytical solution is for a constant Biot number, the Biot number is averaged over the region where the Biot number has a non-zero value. Since we have the analytical expression for the temperature distribution, the first and second spatial derivatives can be obtained to get heat flux as a function of position. So from **Eq. 3.5** we obtain :

$$\dot{q}(z) = s\lambda\frac{\partial^2 T}{\partial z^2} + sV_c\rho C\frac{\partial T}{\partial z} \quad (3.15)$$

By this method, we can obtain an analytical expression of heat flux as a function of position. But in order to obtain the boiling curve, it is required to determine heat flux as a function of temperature on quenching side.

3.5 Heat flux as a function of temperature

Even though a thin aluminium sheet is used for experimental analysis, the temperature on the measuring side will be different from the temperature on the quenching side. The difference will be higher especially at DNB temperature since the heat flux is maximum. Hence, a 2-D analysis where the temperature on the quenching side and that on measuring side will be different is required. So considering the Eulerian steady state **Eq. 3.5** in global coordinates, the 2-D conduction equation to be solved will be:

$$\rho CV_c \frac{\partial T}{\partial z} = \lambda \left(\frac{\partial^2 T}{\partial z^2} + \frac{\partial^2 T}{\partial y^2} \right) \quad (3.16)$$

This equation can be solved with a 2D-Finite Difference Model using central difference discretization and by adding ghost points along the boundaries with Neumann boundary condition. On the quenching side, the heat flux as a function of the position must be applied as a boundary condition and on the measuring side and the bottom boundary, an insulated boundary condition is considered. On the top boundary the initial temperature is defined.

Boundary condition on the measuring side:

$$\frac{\partial T}{\partial y} = 0$$

on Quenching side:

$$\frac{\partial T}{\partial y} = -\frac{\dot{q}}{\lambda}$$

on the bottom side:

$$\frac{\partial T}{\partial z} = 0$$

on the top side:

$$T = T_0$$

Solving this model we obtain temperature on measuring side and temperature on quenching side and a plot of heat flux vs. temperature on measuring side and temperature on quenching side can be obtained.

3.6 Results and discussion

3.6.1 Boiling Curve

A 5 mm thick aluminium alloy AA6082 plate with length and width of 250 mm and 90 mm respectively was used. This plate painted black on the measuring side is placed in an oven and heated to an initial temperature of 500°C and moved to the quenching apparatus, with IR camera recording the temperatures. Temperature profiles over the position during the cooling process with a casting velocity of 20 mm/s are depicted in **Fig. 3.6**.

So analyzing the temperature profiles, following values are obtained for the constants in the Boltzmann function via curve fitting:

$$A_1 = 517.24 \quad A_2 = 75.83 \quad z_0 = 20.2 \quad dz = 5.15$$

With the analytical solution for temperature profile, a Biot number can be obtained as a function of position according to **Eq. 3.14**. This plot can be seen in **Fig. 3.9**. It can be seen that at the Biot number beginning of the pre-cooling region and at the end of the quenching region is tending to zero. To find the average value, the region where the Biot number is more than 1% of the maximum value. In this case, the average Biot number is obtained as 0.3683. Assuming this constant Biot number, the analytical solution for the 1D equation, the interface temperature from **Eq. 3.12** and **Eq. 3.6** $T_{z=0}$ as $451.25^\circ C$.

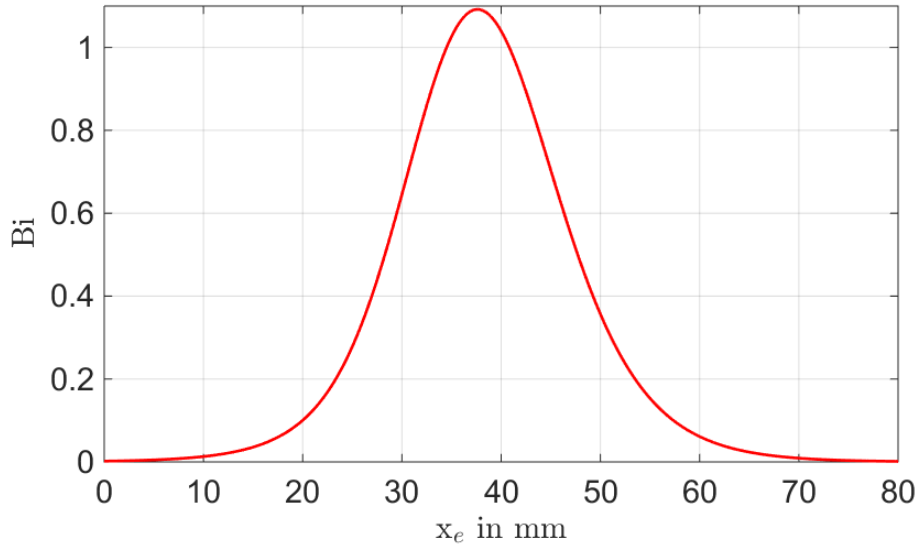


Figure 3.9: Biot number distribution

Filipovic et al. [14] proposed an approach considering that the second derivative of temperature with respect to time will reach a minimum when the heat transfer mechanism changes from axial conduction to heat transfer to cooling water. It was observed that this approach leads to similar interface temperature, but is not used for analysis because it is sensitive to experimental error.

With these values of constants, we obtain heat flux as a function of position as depicted in **Fig. 3.10** obtained from a 1D model. Using this heat flux as a function of position as a boundary condition in 2D FD model we obtain heat flux as a function of temperature on quenching side and measuring side, as seen in **Fig. 3.11**. So at the interface temperature, the surface heat flux is $\sim 2 MW/m^2$. The maximum heat flux i.e. heat flux at DNB temperature is $\sim 6.67 MW/m^2$. At maximum heat flux, it can be observed that the temperature at measuring side is $\sim 286^\circ C$ and that at the quenching side is $\sim 195^\circ C$. It can be seen that there is a difference of nearly $91^\circ C$ between measuring side and quenching side at maximum heat flux. So the observed DNB temperature obtained for AA6082 is nearly $195^\circ C$. Similar DNB temperature

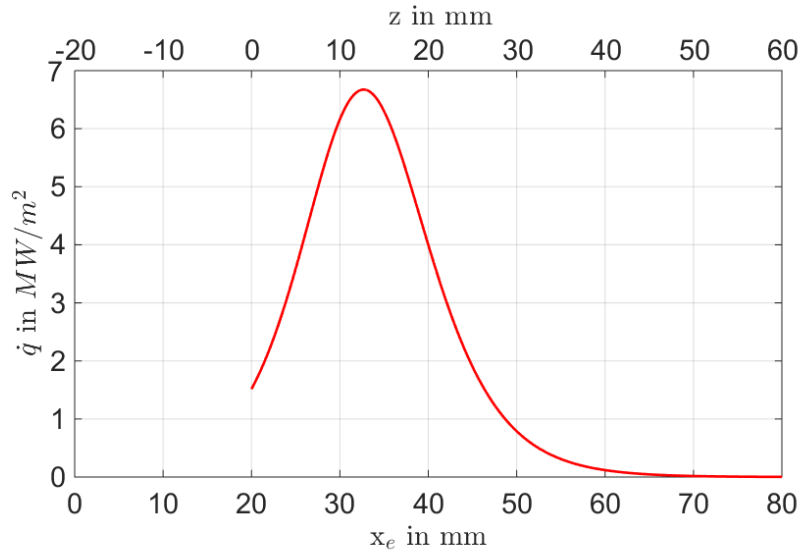


Figure 3.10: Heat flux as a function of position

is also reported by various authors in industrial and laboratory setup. Kraushaar et al. [64] reported a DNB temperature between 200°C to 250°C for aluminium. Grandfield et al. [65] conducted experiments with various parameters for aluminium alloy and reported DNB temperature in the range of 150°C to 200°C . Wiskel et al. [66] reported a DNB temperature of 180°C and Watanabe et al. [67] reported DNB temperature of 150°C . The value of maximum heat flux will depend in principle on the quenching apparatus hence may vary from researcher to researcher.

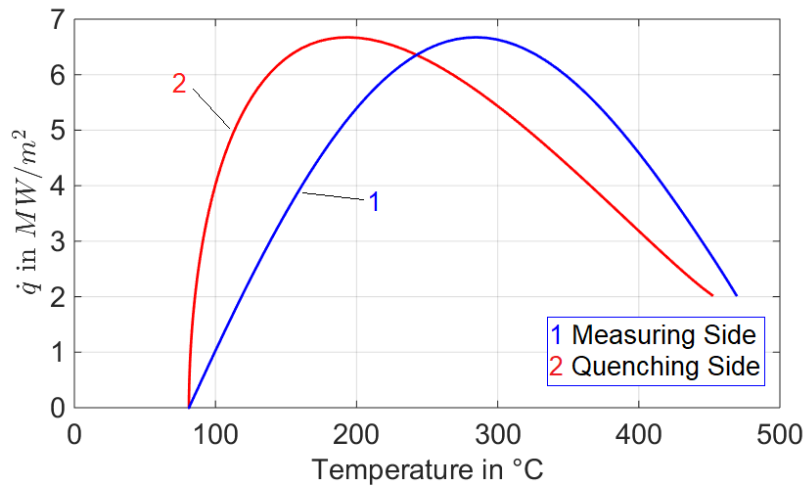


Figure 3.11: Heat flux as a function of temperature on measuring side and quenching side

The distinction between the pre-cooling region and quenching region cannot be made based on the position of the mold as the water hits the metal sheet, it will splatter and cooling starts above the mold position. Hence, a temperature-based approach that can distinguish between these region needs to be considered. In **Fig. 3.12**, it can be seen that the temperature profile on the measuring side obtained from the 2-D FD model matches with the experimentally obtained data. The proposed

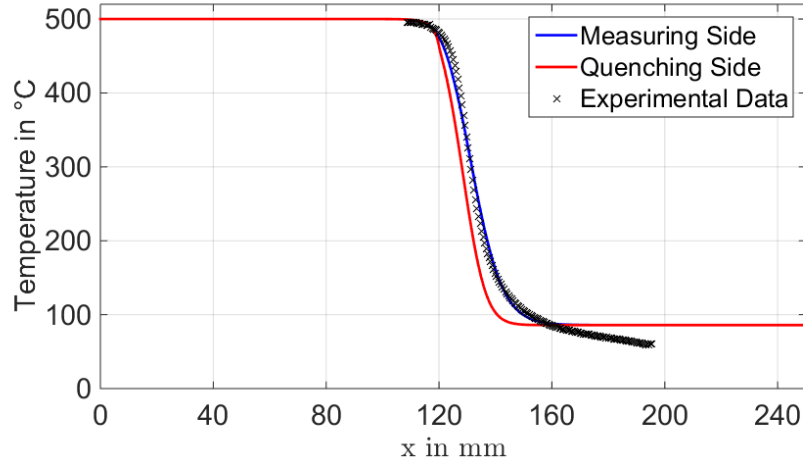


Figure 3.12: Comparison of experimental and 2D-FD model

models present a preliminary approach for determining these variables. It can also be observed that the temperature difference between the quenching side and measuring side is less in the pre-cooling region, it increases till the DNB temperature and decreases till the final equilibrium temperature.

3.6.2 Comparison with Inverse Model

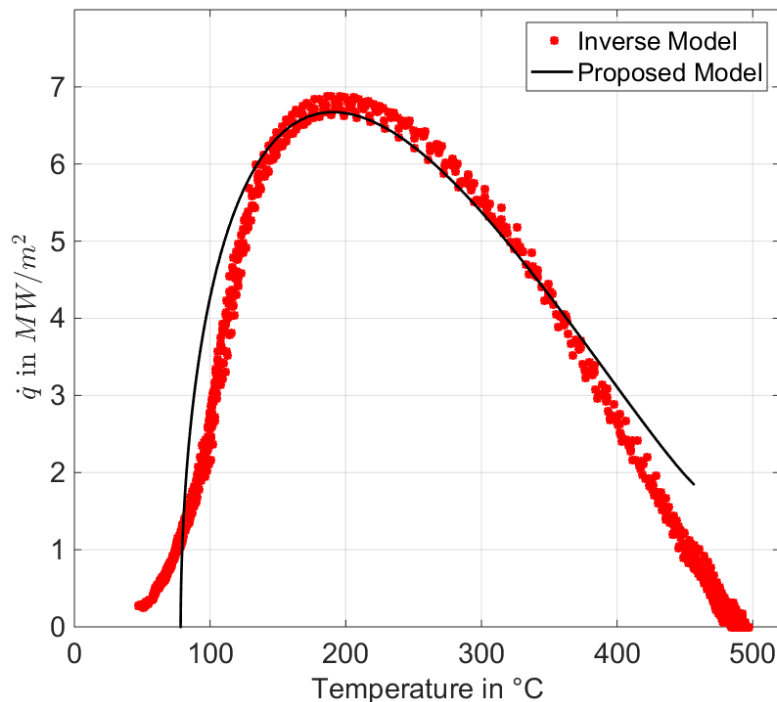


Figure 3.13: Comparison of 2D-inverse model with the proposed model

As mentioned in Nallathambi and Specht [46], a non-iterative inverse FE model is used to obtain the 2D inverse solution. While using 9 noded quadrilateral elements, the dependence of the solution on the number of elements in the thickness direction

is minimized. However, inverse method demands rigorous smoothing of experimental temperature profiles and regularization methods.

Fig. 3.13 shows the solution obtained from this algorithm compared with the proposed Boltzmann approximation solution. It is obvious that the transition and nucleate boiling region slopes and maximum heat flux vary slightly. However, it is promising to use the proposed method which significantly reduces the expertise knowledge of the inverse method.

3.6.3 Front Width

From the experimental data, we can observe that the cooling process can be classified mainly in 3 regions. Firstly, a pre-cooling region, this is a region where cooling occurs because of heat transfer in the axial direction to the cool region. The start of this region can be considered when the temperature reaches 99% of initial temperature i.e. $T_s = 99\%$ of T_0 on the quenching side. End of this region can be considered when the temperature on the quenching side reaches the interface temperature $T_{z=0}$.

Secondly, transition boiling region, this is the region where the heat flux to quenching water increases with cooling of the metal sheet. In this region, the heat flux is because of partial contact between quenching water and hot metal sheet. The start of this region can be considered when the temperature on the quenching side is interface temperature $T_{z=0}$ and the end will be when the heat flux reaches a maximum at DNB temperature T_{DNB} .

Thirdly, nucleate boiling region, this is the region where heat flux decreases with cooling of the metal sheet. Physically this region can be identified by intensive bubble formation on the surface of the metal sheet. The start of this region can be considered when the temperature on the quenching side is DNB temperature T_{DNB} and the end can be considered when the temperature reaches $100^\circ C$.

In **Fig. 3.3**, various regions are pointed out on the infrared image and also on the analyzed quenching side temperature. Since the infrared camera provides a full field temperature data, these regions can be distinctly visualized. From **Tab. 3.2** it can be seen that the transition boiling region has the maximum width followed by pre-cooling region and nucleate boiling region. In pre-cooling region the temperature drop of $\sim 40^\circ C$ is spanned over 6.89 mm , in transition boiling region the metal sheet experiences a temperature drop of $256^\circ C$ over a region of 11.07 mm and in nucleate boiling region the temperature drop of $95^\circ C$ occurs over a length of 7.28 mm . Hence it can be observed that the cooling rate in the pre-cooling region is low, which causes deterioration in the metallurgical quality of metal. Because of which minimizing this region is required in metal processing industries.

Table 3.2: Width of various regions

| Width of | |
|---------------------------|-------------------|
| Pre-Cooling Region | 6.89 mm |
| Transition Boiling Region | 11.07 mm |
| Nucleate Boiling Region | 7.28 mm |

4. Heat Transfer Analysis of Moving Metal Sheet with an Array of Jets

4.1 Introduction

Quenching with a fixed array of jets and moving hot metal parts, is a widely used application as a means of rapid cooling with water in metal processing and casting industries as this kind of setup can be integrated on a production line for a continuous quenching process.

This chapter comprises of the results and discussion on the influence of various parameters on heat transfer of moving metal sheet with an array of jets. The results are first compared by superimposing the temperature profiles obtained from the experiments. These temperature profiles are recorded with an infrared camera on the back side or the measuring side of the plate. The comparison of these profiles gives us a qualitative idea of the influence of the parameter under investigation from the raw data, without the use of any numerical model. The interface temperature is obtained from the 1D analytical solution for energy balance equation with constant Biot number in the wet region and used for superimposition of the data. The obtained temperature profiles are then analyzed further to obtain the boiling curve that is the plot of heat flux vs. temperature on the quenching side. This boiling curve provides us with the maximum heat flux and the temperature at which the maximum heat flux is occurring i.e. DNB temperature. Comparison of the boiling curve for the parameter provides us an understanding of influence on the parameter on the cooling process. The physical understanding of these parameters is used further in **Ch. 7** for process optimization in the industrial casting process.

4.1.1 Mechanism of Heat Transfer

A water jet has horizontal momentum as well as vertical momentum in the impingement zone and only vertical momentum in the free-falling region. Hence, it can be understood that the water jets have a very turbulent flow in the impingement zone as the horizontal momentum is completely diminished in this region. It is possible that a portion of water jet will bounce off the hot metal surface. This phenomenon is particularly observed when the jet angle and jet velocity are high. This complicates defining the impingement region as a part of the bounced off water stream comes in contact with water film in the lower portion because of surface tension between the array of jets.

From an energy balance point of view, it can be imagined that when the water first comes in contact with a very hot surface, the water will evaporate and the vapors will form a film on the metal surface. This vapor film will act as a barrier and restrict the contact of water and hot surface. This vapor film will create a resisting energy in the direction of the surface normal. As the surface cools the energy of this film

barrier will decrease and at Leidenfrost temperature, the energy of the barrier will become less than that of water. This will cause the water to penetrate the barrier and come in contact with the hot metal surface and increasing heat flux. With this understanding, it can be imagined that if the energy or momentum of the water stream in the direction normal to the metal surface is higher, the temperature at which the water stream can penetrate the film barrier will be higher.

The horizontal momentum for array jets is very high compared to sprays. In case of sprays water droplets are used to cool the surface. This will reduce the momentum of cooling water. In case of jets, a water stream at high velocity is used for quenching or a water stream with high momentum. Hence, jets will wet the surface at a higher temperature compared to sprays. Because of high turbulence in the impingement zone, it is expected that the heat flux will be higher as the turbulence will help the bubbles diffuse.

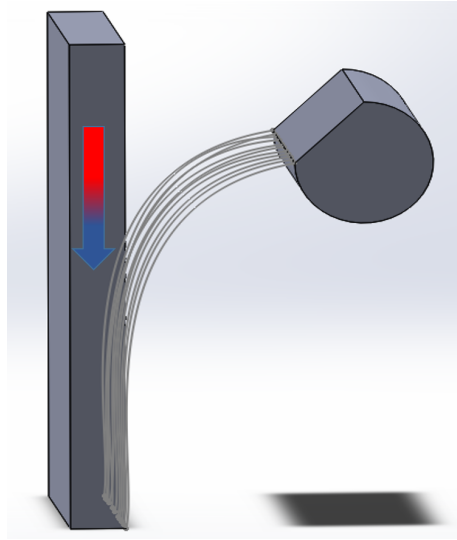


Figure 4.1: Moving mold mechanism in moving sheet experimental setup

Whereas, in the free falling zone the water stream has no horizontal momentum. The flow in the free falling zone will be smooth and the turbulence will be less. This will reduce the diffusivity of bubbles formed in the water stream, lowering the heat flux. Also, if the surface temperature is more than the re-wetting, the water stream is pushed away from the metal surface, causing water ejection. This phenomenon is discussed further on **Ch. 6**.

In the hot metal sheet, the heat will diffuse in the thickness direction to the quenching surface and also diffusion of heat will be strong in the axial direction from the dry region to the wet region. This diffusion will be high at the wetting front because of high thermal gradient present and hence needs to be considered.

In the experiments conducted with a moving metal sheet, initially, the water jet comes in contact at the very bottom of the sample and goes up along the surface as the sample moves down. This type of cooling lead to diffusion of heat before coming into contact with cooling water, as illustrated in **Fig. 4.1**. This phenomenon is also observed by other researchers, defined as temperature drop which takes place before water cooling [24] [15] [68]. Caron and Wells [69] integrated this phenomenon in an inverse heat conduction problem. It is important to incorporate cooling because of

advection in an inverse model as the domain of boundary condition for the governing differential equations is different. This phenomenon will be particularly higher in case of aluminium because of high thermal conductivity. This situation is also similar to the DC casting process where hot molten is supplied continuously from the top, diffusing the heat in the axial direction.

4.2 Results and Discussion

The moving metal sheet setup can be compared to the general phenomena of the real DC casting process, in which instead of the metal sheet a partially solidified layer of metal impinges with cooling water. The experiments were conducted on aluminium alloy AA6082 and the temperature data is measured with an infrared camera. A 1D analytical solution with constant Biot number in the quenching region is used to obtain the interface temperature $T_{z=0}$ as described in **Eq. 3.12**. The experimentally measured temperature profiles are superimposed with this interface temperature, to obtain a basic idea of the trend of cooling curves that can be expected. These superimposed temperature profiles are directly obtained from the raw experimental data without the use of any numerical model. Hence are immune to computational errors. The temperature profiles are further analyzed to obtain the boiling curve, considering the temperature difference between quenching side and the measuring side of the plate. Further description of the analysis method is provided in **Ch. 3**.

Since an infrared camera is used to record the temperature history data, a full field thermal data is available. The temperature data at every pixel point is recorded for the entire time span. With thermocouples, the temperature only at the thermocouple position is recorded. Since a full field thermal data is available the width of various wetting fronts can also be determined. The width of the wetting front in different regions during quenching experiments are also quantified with the use of temperature profile on quenching side. This is done to improve the understanding of the physical mechanisms during quenching of high-temperature surface.

The investigated parameters can be classified into 2 categories:

- Quenching setup: These are the parameters which are related to quenching apparatus and the process of controlling. These parameters are external to the casting process and have only influence on the thermal boundary condition in the process. Following are the quenching setup parameters investigated:
 - Quality of water
 - Temperature of water
 - Jet velocity (or water flow rate)
 - Jet impingement angle
- Metal sheet: These parameters depend on the casting process and controlling them in the casting process is relatively difficult. Following are the parameters investigated related to the metal sheet:
 - Thickness of metal sheet
 - Casting speed

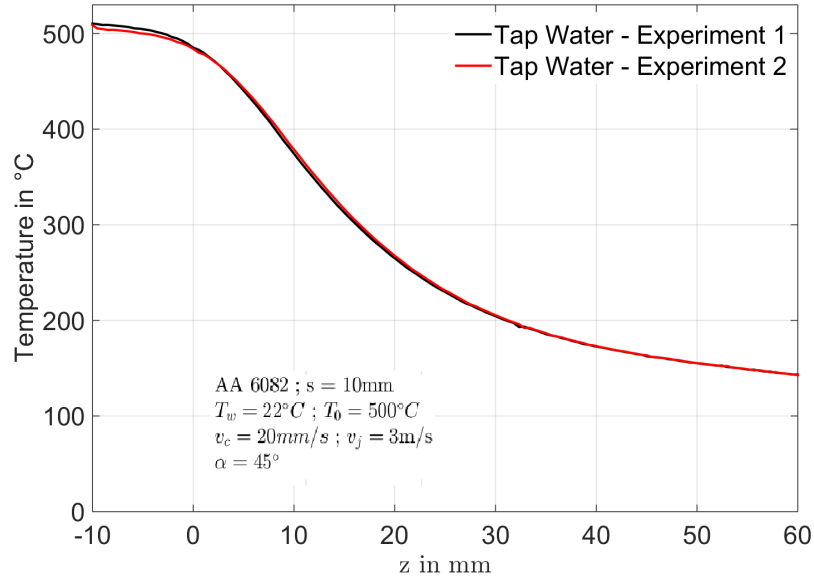


Figure 4.2: Superimposed temperature profile of repeated experiments with tap water

- Initial temperature of metal sheet
- Kind of metal

Before proceeding with the experimental investigation it is important to verify the repeatability of the experimental procedure. The deposition of salts on the metal surface or change in material properties may have an influence on results if the experiments are repeated. Hence, an experiment if conducted with the same parameters on the same metal sheet multiple times, it needs to be verified if the results obtained are identical. In case of spray quenching it was observed that the experiments were not repeatable for tap water. In case of mold quenching in moving sheet setup, it can be observed from **Fig. 4.2** that the temperature profile is identical for both the cases. The experiments were conducted on a 10 mm AA6082 sheet at an initial temperature of around 500°C , jet angle of 45° , jet velocity of 3 m/s , water temperature of 22°C and a casting speed of 20 mm/s . Since the experimentally observed temperature profiles are identical, we can conclude that the experiments are repeatable and the sample can be reused for analysis.

During the quenching of thinner sheets, it was observed that the quenching process induces significant distortions. Hence the sample cannot be reused directly and needs to undergo a straightening process followed by application of black coating on the measuring side. From these results of repeatability, it can be concluded that there is no need for any surface treatment between consecutive experiments. Prior to the experiments, it is insured that the geometry and the coating are as desired. In experimental analysis, the experiments were repeated a couple of times to insure that the obtained results are consistent. With these results, it can be concluded that the metal sheets can be reused to investigate a wide range of parameters.

4.2.1 Influence of Water Quality

Sabariman [70] has studied the influence of salinity on the heat transfer during spray cooling of hot metals. He has conducted an extensive study on determining the influence water quality and salt content on the Leidenfrost and DNB temperature, maximum heat flux, and heat transfer coefficient in the film boiling region. It is observed that in spray quenching, the quality of water has a large influence on the boiling curve. More the salt content, larger is the maximum heat flux, Leidenfrost and DNB temperature.

Quality of water is an important parameter to control as it can change over the duration of time. Quality of water depends on the source of water also and can change from region to region. Variation in this parameter can cause different product quality for same casting recipe, from region to region.

Electrical conductivity (EC), which is often used as an index of the total dissolved solids, is used as a measure to estimate the salinity level of the cooling water. Salinity depends on the ions dissolved in water. The dissolved ions can be positively charged ions like Na^+ , Mg^{2+} or negatively charged like Cl^- , SO_4^{2-} which comes from the dissolved salts in water. Electrical conductivity depends on the presence of charged ions and its concentration. Hence, electrical conductivity is used as an indicator of quality of water in this work. The quality of water, will also change the thermal properties of the quenching medium and the influence of this on boiling curve needs to be explored.

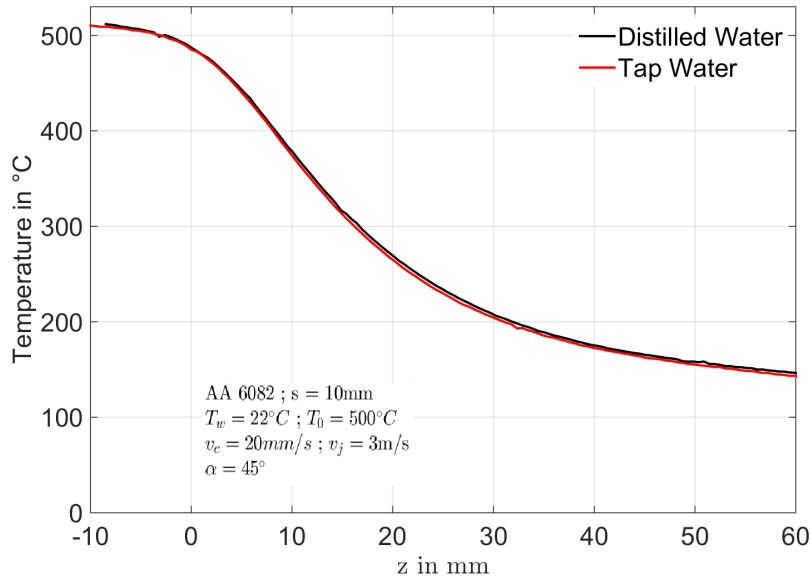


Figure 4.3: Superimposed temperature profile for different water quality

The experiments were performed with both distilled water and tap water, to identify the influence of water quality on heat transfer during quenching process. The tap water used for experiments is the water in Magdeburg, Germany. The electrical conductivity of this tap water is measured to be $0.58 mS/cm$. The distilled water is obtained from distillation of tap water to remove salts and impurities in water. Because of this, the electrical conductivity of distilled water is $0 mS/cm$. This additional distillation process, increases the cost of water.

The experiments are conducted to quantify the influence of the salt content on the heat transfer during the quenching process with a moving sheet mechanism. For this quenching experiment were conducted with water at 22°C , jet velocity of 3 m/s , jet angle of 45° and an 10 mm thick, AA6082 sheet, heated to an initial temperature of around 500°C and moving at 20 mm/s . The **Fig. 4.3** shows the superimposed temperature profiles for distilled water and tap water. It can be observed that the temperature profiles are identical. This means that the change in water quality has no influence on heat transfer in the impingement zone. This can be because of high turbulence in the impingement zone. Hence it can be expected that the boiling curve in **Fig. 4.4** and the width of various fronts **Tab. 4.1** are also identical. The final temperature at the bottom of the sheet was observed to be above 100°C . This means that the bottom of the sheet is still in the nucleate boiling region. For this reason, the width of nucleate boiling region is greater than 30 mm .

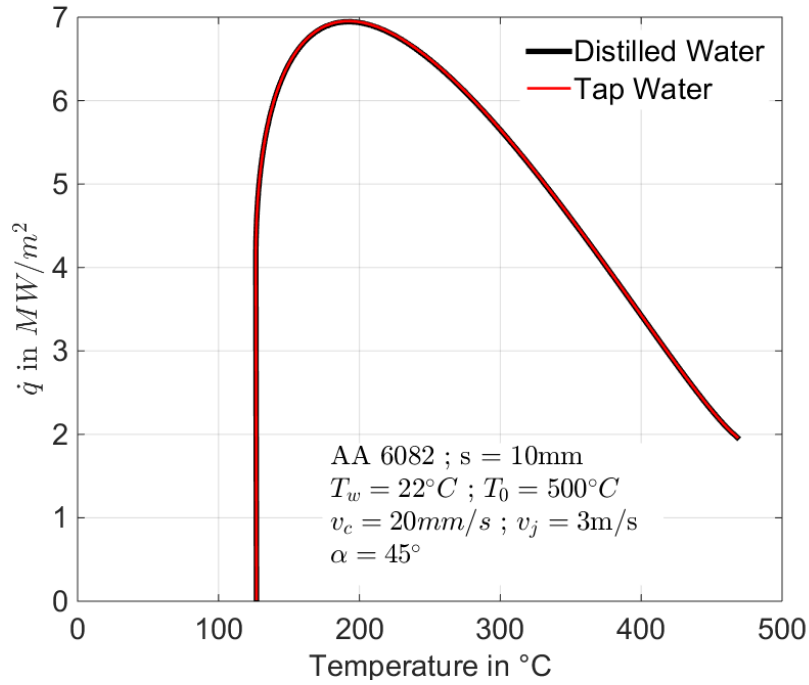


Figure 4.4: Boiling curve for different water quality

From these results, it can be concluded that the quality of water has no significant influence on cooling in the impingement zone. Because of this, for further experiments tap water is used to investigate the influence of other parameters.

Table 4.1: Width of various regions for different water quality

| | Distilled water | Tap Water |
|---------------------------|-----------------------|-----------------------|
| Pre-Cooling Region | 5.20 mm | 5.20 mm |
| Transition Boiling Region | 26.52 mm | 26.52 mm |
| Nucleate Boiling Region | $>30\text{ mm}$ | $>30\text{ mm}$ |
| $T_s = 0.99 * T_0$ | 509.3°C | 509.3°C |
| $T_{z=0}$ | 485.2°C | 485.2°C |
| T_{DNB} | 193.6°C | 193.6°C |

4.2.2 Temperature of Water

During the DC casting process, temperature of water needs to be controlled as this might change during the process. Typically, in a casting plant, the cooling water is recycled. After quenching the water temperature increases. So the water has to be cooled in the cooling towers before recycling it. The temperature of water can also change based on the atmospheric temperature. Basically, by using cooler water for quenching will result in higher heat extraction because of higher cooling capacity. But because of high turbulence in the impingement zone, the effect of increasing cooling capacity can be diminished as the time of contact between the water drop and metal surface will be short.

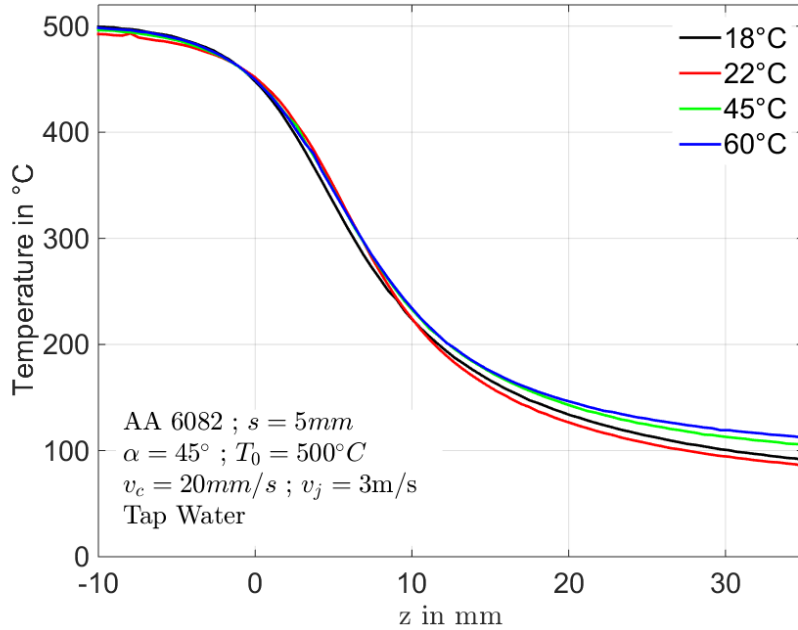


Figure 4.5: Superimposed temperature profile for different water temperature

To quantify the influence of different water temperature on the heat transfer during quenching of hot aluminium metal sheet (AA6082), the experiments were conducted for different water temperature of 18°C , 22°C , 45°C , and 60°C . A 5 mm thick sheet is used at a casting speed of 20 mm/s and the jet angle and velocity as 45° and 3 m/s respectively. The initial temperature of the sheet was maintained constant at around 500°C and tap water was used for quenching. The generated temperature profiles for different water temperature are superimposed as shown in **Fig. 4.5**. A constant cooling trend is observed for all the water temperatures during quenching and a constant interface temperature ($T_{z=0}$) of 449.8°C is observed. In the nucleate boiling region, the difference in cooling is observed owing to the reduced cooling capacity of water. The change in temperature profile in the bottom region, gives an idea that in the free falling zone, water temperature can have significant influence on heat transfer.

The width of the wetting front in various regions of quenching is shown in **Tab. 4.2**. It can be observed that the interface temperature is same for different water temperatures but the front width in the pre-cooling region decreases with increase

in water temperature from, 6.92 mm to 5.88 mm. Whereas, the front width during transition boiling decreases with increase in water temperature from, 12.11 mm to 10.03 mm. At the end of transition boiling region the DNB temperature increases with increase in water temperature from, 193.5°C to 209.9°C. From the **Fig. 4.6**, it can be seen that the maximum heat flux (\dot{q}_{max}) for all water temperatures lies in the range from 6.60 MW/m² to 6.73 MW/m². With this we can conclude that the maximum heat flux remains constant irrespective of water temperature. The final temperature of the sample also varies for water temperature. It can be observed that for water temperature of 45°C and 60°C the sheet has not cooled beyond 100°C. Which means that the sheet is in the nucleate boiling region, at end of the field of view of the infrared camera. This sharp increase in the nucleate boiling region occurs when the cooling is not completed in the impingement zone and enters the free falling zone, where the heat flux is lower. From these results, water temperatures of 22°C were used during quenching experiments to quantify the influence of different metal thickness, jet velocity, the angle of jet impingement and casting speed.

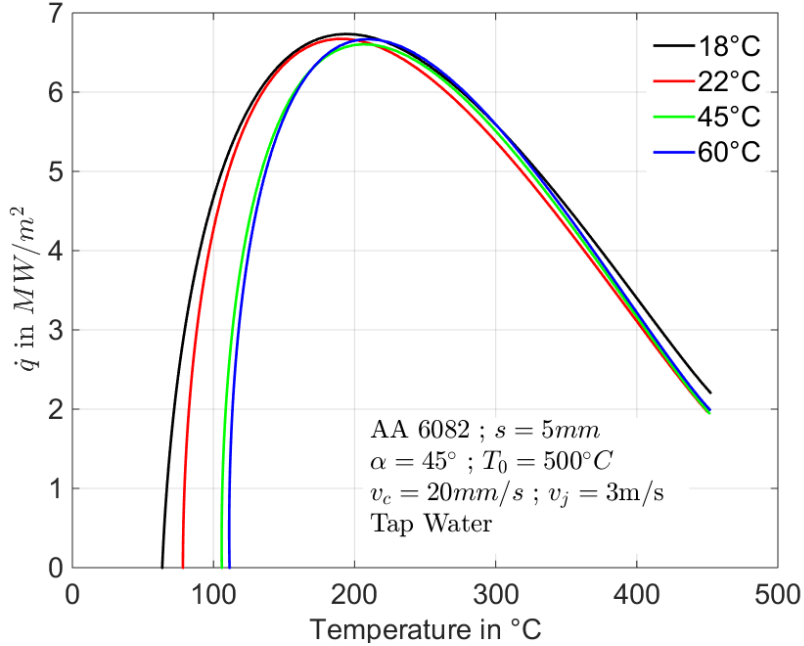


Figure 4.6: Boiling curve for different water temperature

Table 4.2: Width of various regions for different water temperature

| | 18°C | 22°C | 45°C | 60°C |
|---------------------------|----------|----------|----------|----------|
| Pre-Cooling Region | 6.92 mm | 6.89 mm | 5.88 mm | 5.96 mm |
| Transition Boiling Region | 12.11 mm | 11.07 mm | 10.38 mm | 10.03 mm |
| Nucleate Boiling Region | 7.92 mm | 7.28 mm | > 30mm | >30 mm |
| $T_s = 0.99 * T_0$ | 496.3°C | 489.9°C | 494.8°C | 497.3°C |
| $T_{z=0}$ | 449.8°C | 449.8°C | 449.8°C | 449.8°C |
| T_{DNB} | 193.5°C | 194.7°C | 206.5°C | 209.9°C |

4.2.3 Jet Velocity

Increasing the jet velocity will increase the water flow through the mold. The increase in jet velocity will increase the supply of coolant but also will increase the momentum of water jet. The increase in supply of water would increase the cooling capacity of water. At higher jet velocities, it is possible that the water stream will bounce from the surface. This can reduce cooling even though the mass flow rate of coolant is increases. During the casting process, the position where the cooling water comes in contact with the ingot will also change slightly. This is because at lower jet velocity the water stream is weak and the angle at which it comes in contact with ingot decreases. At higher jet velocity the water stream touches the ingot at angle closer to jet angle in mold. The typical distance between mold and ingot in around 20 mm, so the change in point of contact is not high but will contribute to change in boundary conditions. Increase in jet velocity translates to increase in pressure in the mold. This will also make the flow through the array of jets in the mold to be more uniform, specially at distance away from the mold inlet. In case of quenching with sprays, [70] has found strong influence of water flow rate on the boiling curve. The maximum heat flux and the Leidenfrost temperature increased significantly with increase in water flow rate, for spray quenching.

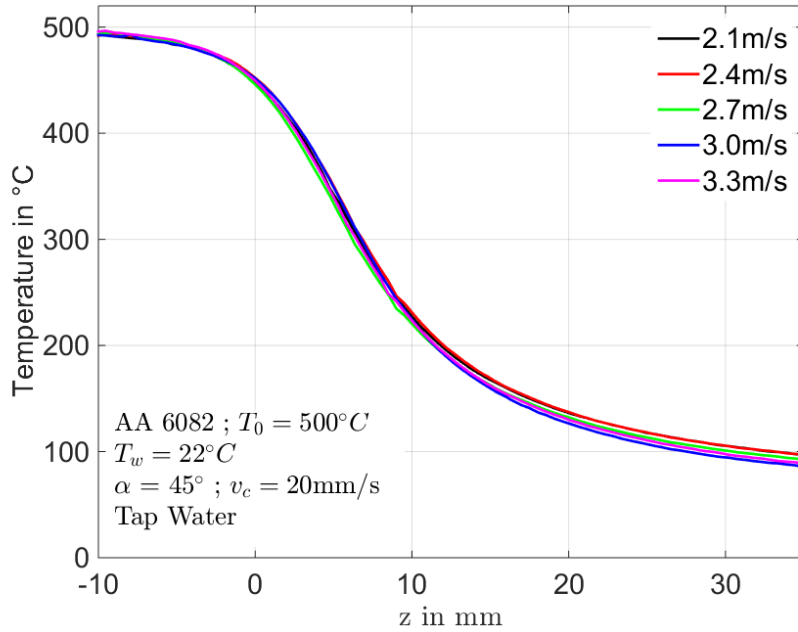


Figure 4.7: Superimposed temperature profile for different jet velocity

To quantify the influence of water jet velocity or water flow rate on the quenching of hot metal sheet, experiments are conducted at different jet velocities of 2.1 m/s, 2.4 m/s, 2.7 m/s, 3.0 m/s, 3.3 m/s. Tap water at 22°C, jet angle of 45°, metal plate of thickness 5 mm and casting speed at 20 mm/s are used. **Fig. 4.7** and **Fig. 4.8** shows the superimposed temperature profiles with different jet velocities and boiling curves of different jet velocities. From these figures, it can be seen that a constant interface temperature ($T_{z=0}$) was observed for all jet velocities at 449.8°C. It can be observed that the cooling behavior is almost same at different jet velocities in the impingement zone. The DNB temperature decreases slightly with increase in the jet

velocity from 201.1°C to 194.7°C . The maximum heat flux increases with increase in jet velocity from 6.57 MW/m^2 to 6.67 MW/m^2 , from these observations we can say that jet velocities at 3 m/s gives maximum heat flux during quenching process. At the jet velocity of 3.3 m/s , it was observed that the jet stream was reflecting off the surface. This will lead to a change in the trend of cooling characteristics in the impingement zone.

Tab. 4.3 shows the front width of various regions during quenching process. It can be observed that the width of the pre-cooling region increases with increase in jet velocity from 4.15 mm to 6.89 mm and the width of transition boiling region increases with increase in jet velocity from 10.72 mm to 11.07 mm . However the width of nucleate boiling region oscillates around 8.3 mm . From these results, jet velocity of 3 m/s was used to quantify the influence of jet impingement angle and casting speed during quenching experiments.

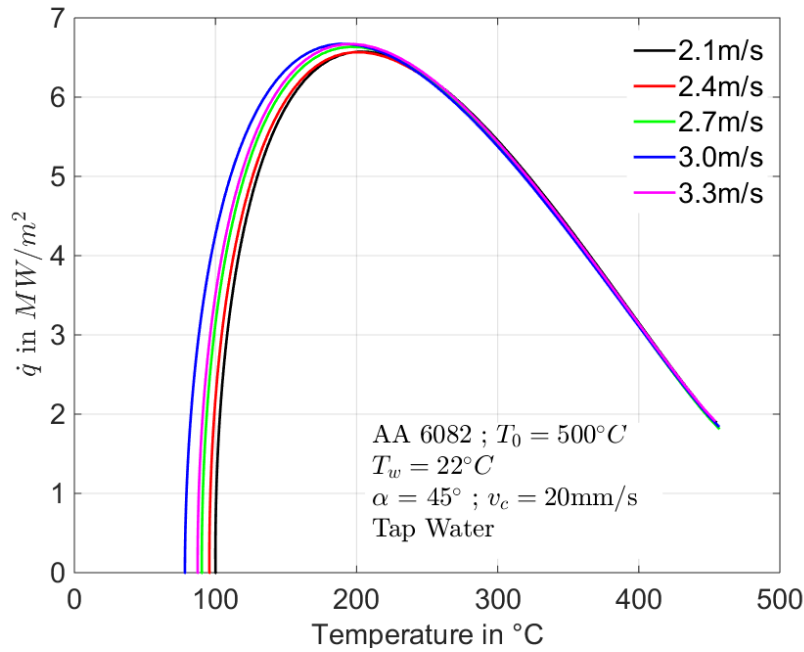


Figure 4.8: Boiling curve for different jet velocity

Table 4.3: Width of various regions for different Jet Velocity

| | 2.1 m/s | 2.4 m/s | 2.7 m/s | 3.0 m/s | 3.3 m/s |
|---------------------------|-------------------------|-------------------------|-------------------------|-------------------------|-------------------------|
| Pre-Cooling region | 4.15 mm | 4.15 mm | 5.19 mm | 6.89 mm | 6.19 mm |
| Transition Boiling region | 10.72 mm | 11.07 mm | 10.72 mm | 11.07 mm | 10.72 mm |
| Nucleate Boiling region | 8.3 mm | 7.96 mm | 8.25 mm | 7.28 mm | 8.3 mm |
| $T_s = 0.99 * T_0$ | 490.3°C | 490.7°C | 492.2°C | 489.9°C | 493.1°C |
| $T_{z=0}$ | 449.8°C | 449.8°C | 449.8°C | 449.8°C | 449.8°C |
| T_{DNB} | 201.1°C | 197.9°C | 195.8°C | 194.7°C | 197.5°C |

4.2.4 Jet Impingement Angle

Typically in industry, jet angle is a part of mold design and it cannot be varied. Jet angle is designed by the requirement of distance between the primary cooling and secondary cooling regions. During the DC casting process, the water first cools the primary cooling mold and then impinges on the ingot from the array of holes located at the bottom of the mold. Also by changing the jet angle, the ratio of horizontal and vertical momentum can be changed. Also, at higher jet angle the water stream tends to bounce off the surface, changing the cooling trend. Jet angle will also change the width of the impingement zone as the geometry and fluid dynamics of jet is completely altered. Higher jet angles might lead to maintenance issues because of clogging of jet holes. During the experimental analysis, it was observed that water flow is uneven from the array of jets, specially at lower water flow rates. The flow tends to be stronger at the location near to main supply pipe.

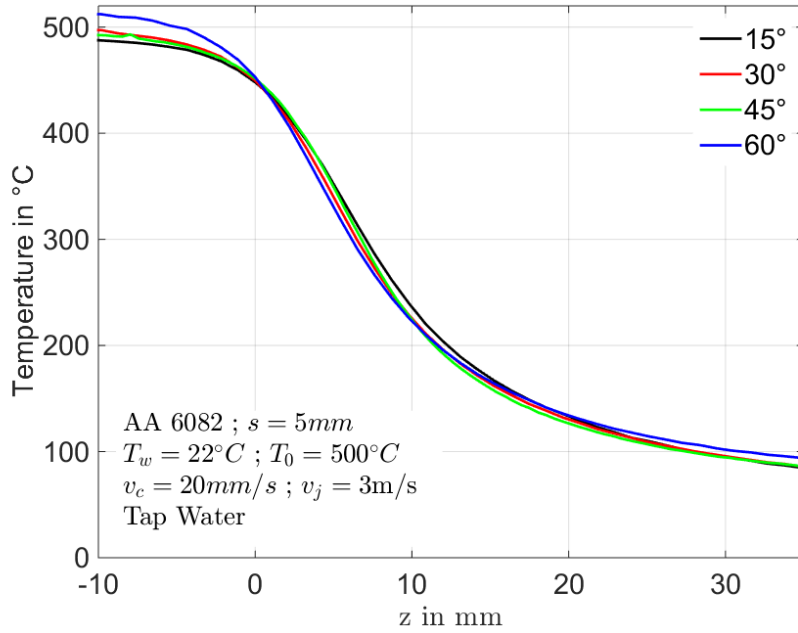


Figure 4.9: Superimposed temperature profile for different jet angle

The dependence of heat transfer on jet impingement angle during quenching process is evaluated with this set of parameters. For which experiments were conducted with a 5 mm AA6082 sheet, heated to initial temperature of around 500°C, tap water at 22°C, a jet velocity of 3 m/s and casting speed of 20 mm/s was maintained for different angles. The water jet angles of 15°, 30°, 45°, 60° impinge on the hot metal sheet. The influence of jet impingement angle on the interface temperature ($T_{z=0}$), with superimposed temperature profiles is depicted in **Fig. 4.9**, in which a constant interface temperature at 449.8°C is observed for all jet angles. From this figure, it can be observed that the cooling characteristics changes with the jet angle. **Fig. 4.10** shows the boiling curves of different jet impingement angles, from this figure it can be observed that the maximum heat flux increases with increase in the angle from 15° to 60°, the highest value of heat flux, 6.79 MW/m² is observed with an angle of 60°. The DNB temperature decreases with increase in angle of jet

impingement, a decrease of 17.4°C was observed, the DNB temperature decreases from 199.9°C for 15° angle to 182°C for 60° angle.

The width of the pre-cooling region increases with increase in jet impingement angle from 4.85 mm to 6.22 mm , the width of the transition boiling region decreases with increase in jet angle from 13.84 mm to 11.42 mm and the width of the nucleate boiling region decreases significantly with increase in jet angle from 12.11 mm to 5.19 mm . This is because of higher heat flux and lower DNB temperature for higher jet angles. **Tab. 4.4** shows the front widths during pre-cooling, transition boiling and nucleate boiling during quenching with different angles of jet impingement. From these results it can be observed that at any angle of water jet impinging the metal surface has no change in interface temperature ($T_{z=0}$) and the jet angle has influence on heat flux during quenching process, it was observed that the heat flux increases from 6.19 MW/m^2 to 6.79 MW/m^2 .

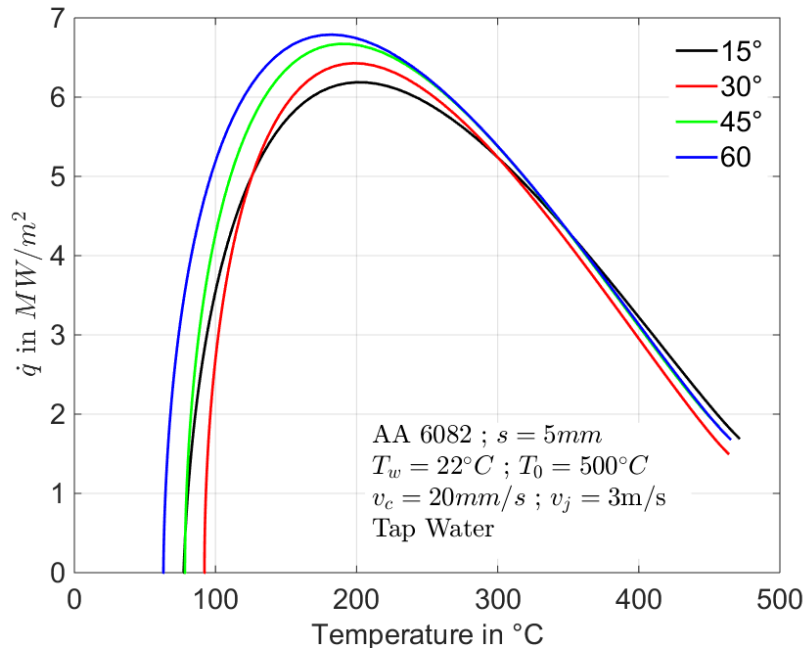


Figure 4.10: Boiling curve for different jet angle

Table 4.4: Width of various regions for different Jet angles

| | 15° | 30° | 45° | 60° |
|---------------------------|-------------------------|-------------------------|-------------------------|-------------------------|
| Pre-Cooling Region | 4.85 mm | 5.89 mm | 6.89 mm | 6.22 mm |
| Transition Boiling Region | 13.84 mm | 11.42 mm | 11.07 mm | 11.42 mm |
| Nucleate Boiling Region | 12.11 mm | 9.34 mm | 7.28 mm | 5.19 mm |
| $T_s = 0.99 * T_0$ | 493.3°C | 502.1°C | 489.9°C | 495°C |
| $T_{z=0}$ | 449.8°C | 449.8°C | 449.8°C | 449.8°C |
| T_{DNB} | 199.9°C | 197.6°C | 194.7°C | 182.5°C |

4.2.5 Thickness of Metal Sheet

The thickness of ingot depends on the final geometry of the ingot. The thicker ingots will increase the output of the casting process but might increase further processing

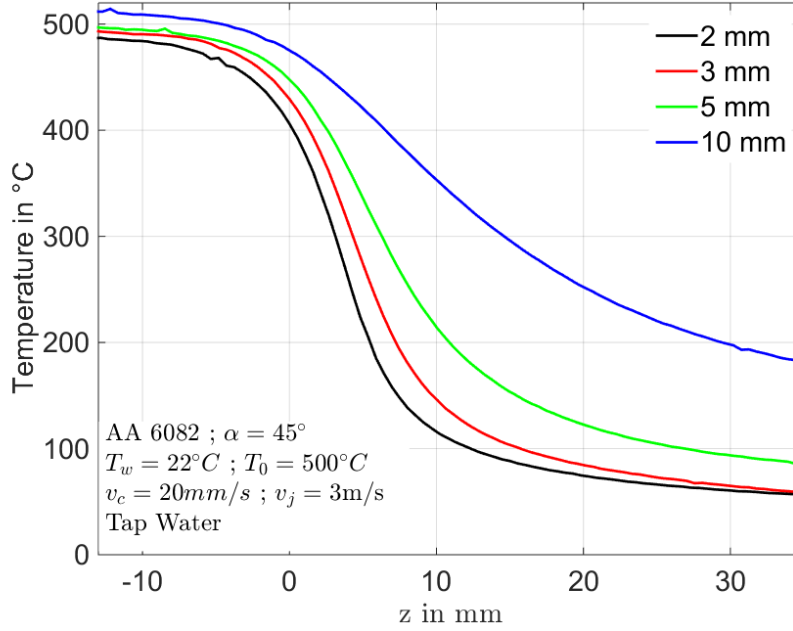


Figure 4.11: Superimposed temperature profile for different thickness

to obtain the final product. The thicker ingots will increase the heat capacity of the ingot and increases the time required for the center of ingot to cool. With an increase in thickness, the Biot number will also increase. A higher Biot number implied that the internal thermal resistance is dominant in heat transfer process compared to the surface heat flux. This means the sump depth at the center of the ingot will increase with an increase in thickness and will not change much after a point [10].

Since surface temperatures are obtained from the infrared camera, the temperature measurements for thicker plates is further away from the quenching surface. As the analysis method compensates for the temperature difference between quenching side and measuring side, this model can be used to determine boiling curve for different thickness. The temperature difference between both sides of the sheet will increase with increasing thickness. In order to study the heat transfer changes during quenching process for different thickness of the metal sheet, experiments were conducted with water at 22°C , jet velocity and angle of 3 m/s and 45° respectively. An AA6082 alloy heated to an initial temperature of around 500°C and casting speed of 20 mm/s metal sheet with different thickness of 2 mm , 3 mm , 5 mm , and 10 mm are used for analysis. **Fig. 4.11** shows the superimposed temperature profiles for different thickness of the metal sheet. It can be observed that as expected the cooling trend is highly dependent on the thickness of the metal sheet. The interface temperature ($T_{z=0}$) increases with increase in metal sheet thickness as the ratio of Biot number to Peclet number squared decreases with increasing thickness **Eq. 3.12**. Compared to 2 mm , 3 mm and 5 mm sheet, with the same cooling capacity applied through the same jet velocity and casting speed, it takes a longer time to cool the metal plate with 10 mm thickness. This is typically observed when the sheet is not completely cooled in impingement zone. **Fig. 4.12** shows the boiling curves of different metal sheet thickness, in which the DNB temperature decreases with increase in metal thickness from 199.5°C to 193.6°C and the maximum heat flux is

observed with 10 mm sheet (6.95 MW/m^2) compared to 5 mm (6.67 MW/m^2), 3 mm (6.39 MW/m^2) and 2 mm (5.03 MW/m^2) sheet. From these, it can be seen that the metal plate with more thickness experiences higher heat flux and lower DNB temperatures compared with the metal sheet with lower thickness.

Tab. 4.5 shows the front widths of various regions during quenching of metal sheet. The width of the pre-cooling region decreases with increase in metal sheet thickness, from 11.42 mm to 5.20 mm and the width of the transition boiling region increases with increase in metal sheet thickness, from 5.54 mm to 26.52 mm. From these observed results the metal sheet of 5 mm thick was used for the experiments with different metal thickness, varying jet velocity, an angle of impingement, and casting speed.

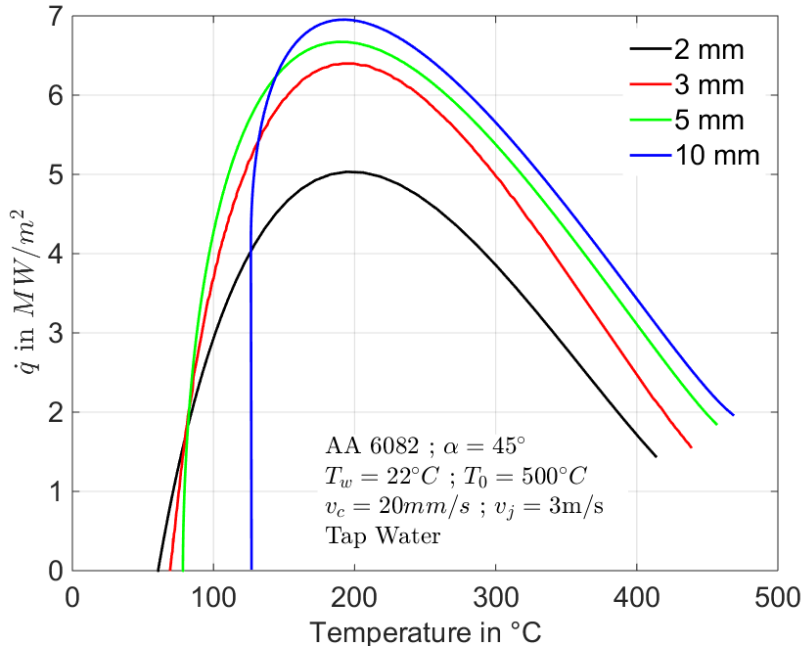


Figure 4.12: Boiling curve for different thickness

Table 4.5: Width of various regions for different thickness

| | 2 mm | 3 mm | 5 mm | 10 mm |
|---------------------------|----------|---------|----------|----------|
| Pre-Cooling Region | 8.3 mm | 7.42 mm | 6.89 mm | 5.20 mm |
| Transition Boiling Region | 5.54 mm | 7.27 mm | 11.07 mm | 26.52 mm |
| Nucleate Boiling Region | 6.76 mm | 5.53 mm | 7.28 mm | >30 mm |
| $T_s = 0.99 * T_0$ | 495°C | 498.7°C | 489.9°C | 509.3°C |
| $T_{z=0}$ | 407.41°C | 426.3°C | 449.8°C | 485.2°C |
| T_{DNB} | 194.2°C | 199.5°C | 194.7°C | 193.6°C |

A 2 mm thick metal sheet experience a drastically different cooling characteristic compared to a 3 mm sheet. This phenomenon is typically observed when the interface temperature drop bellow 420°C . Similar results were also observed by Caron and Well [18] during the experimental investigation. With these results it can be concluded that the boiling curve depends not only on the surface temperature but also on interface temperature. In order to explore this hypothesis, further experimental investigation is carried out in following sections.

4.2.6 Casting Speed

During a casting process, increasing the casting speed will increase the productivity of the process, but it leads to lesser cooling time of the ingot. This changes the dynamics of the process and arises need to study the influence of casting speed on the heat transfer process. Basically, by changing the casting speed, the Peclet number is changed for a constant thickness. Increasing the casting speed also translates to less time spent by the ingot in the impingement zone.

In this work casting speed is represented by the moving speed of the metal sheet. The temperature at which cooling water comes in contact with hot ingot i.e. interface temperature $T_{z=0}$ depends on the ratio of Biot number and Peclet number squared as described in **Eq. 3.12**. Based on this, for sheets with different thickness, the casting speed can be changed to obtain a similar interface temperature. A thicker sheet moving at a lower velocity will have lower interface temperature.

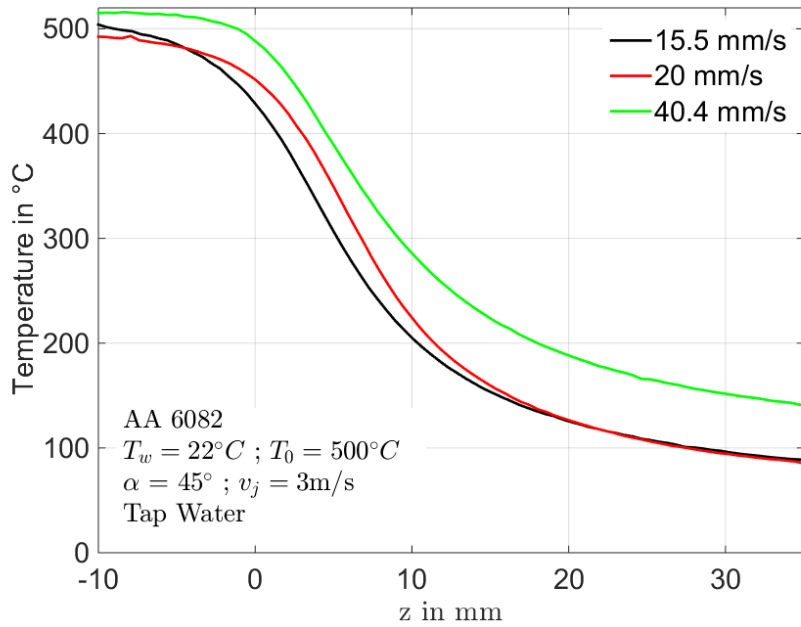


Figure 4.13: Superimposed temperature profile for different casting speed

To explore the influence of casting speed on the cooling characteristics, a 5 mm AA6082 sheet heated to an initial temperature of around 500°C is used. Tap water at 22°C is used for quenching with jet velocity and angle of 3 m/s and 45°. The casting speed is decided in such a way that the interface temperature will be same as that for a 3 mm and 10 mm sheet at 20 mm/s.

The superimposed temperature profiles during quenching of a 5 mm AA6082 sheet with different casting speed are depicted in **Fig. 4.13**, along with the respective interface temperature for each varying casting speeds. From this figure, it can be observed that the higher casting speed results in higher interface temperature ($T_{z=0}$).

Fig. 4.14 shows the boiling curves of different casting speeds, from this figure it was observed that, the DNB temperature decrease with increase in casting speed. For casting speed of 15.5 mm/s it is 201.7°C and at casting speed of 40.4 mm/s it is 192.6°C. Whereas, the maximum heat flux increase with increasing casting speed,

for 15.5 mm/s it is 6.37 MW/m^2 and for casting speed of 40.4 mm/s it is at 7.03 MW/m^2 . This result agrees with other researchers [70], [69].

Tab. 4.6 shows the front width of various regions during quenching process. Where the front width in the pre-cooling region decreases with increase in casting speed, for 15.5 mm/s it is 10.73 mm and for casting speed of 40.04 mm/s it is 3.48 mm . the front width in the transition boiling region increases with increase in casting speed, for 15.5 mm/s it is 7.95 mm and at 40.4 mm/s it is at 23.72 mm . These results support the hypothesis that the boiling curve depends on the interface temperature as for same interface temperature with different thickness, the same boiling curve is obtained.

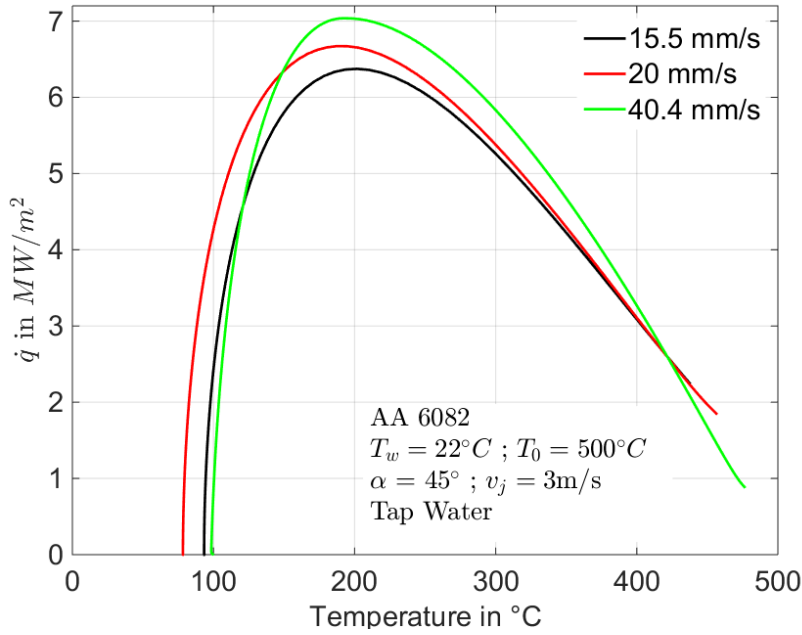


Figure 4.14: Boiling curve for different casting speed

Table 4.6: Width of various regions for different casting speed

| | 15.5 mm/s | 20 mm/s | 40.4 mm/s |
|---------------------------|-----------|----------|-----------|
| Pre-Cooling Region | 10.73 mm | 6.89 mm | 3.48 mm |
| Transition Boiling Region | 7.95 mm | 11.07 mm | 23.72 mm |
| Nucleate Boiling Region | 9.01 mm | 7.28 mm | >30 mm |
| $T_s = 0.99 * T_0$ | 506.2°C | 489.9°C | 509.3°C |
| $T_{z=0}$ | 426°C | 449.8°C | 485.1°C |
| T_{DNB} | 201.7°C | 194.7°C | 192.6°C |

It can be observed that with increase in casting speed, the width of pre-cooling region is reduced. This is very important for metal processing industry, where the metal once it crosses a critical temperature (like eutectic temperature in case of steel) a lower rate of cooling will lead to deterioration in material properties. Hot metal will cross the critical temperature in the pre-cooling region and will experience slow cooling. Hence to avoid this, the casting speed of metal sheet moving speed should be increased. This will increase the length of the quenching setup but will provide a higher rate of cooling.

4.2.7 Initial Temperature of Metal Sheet

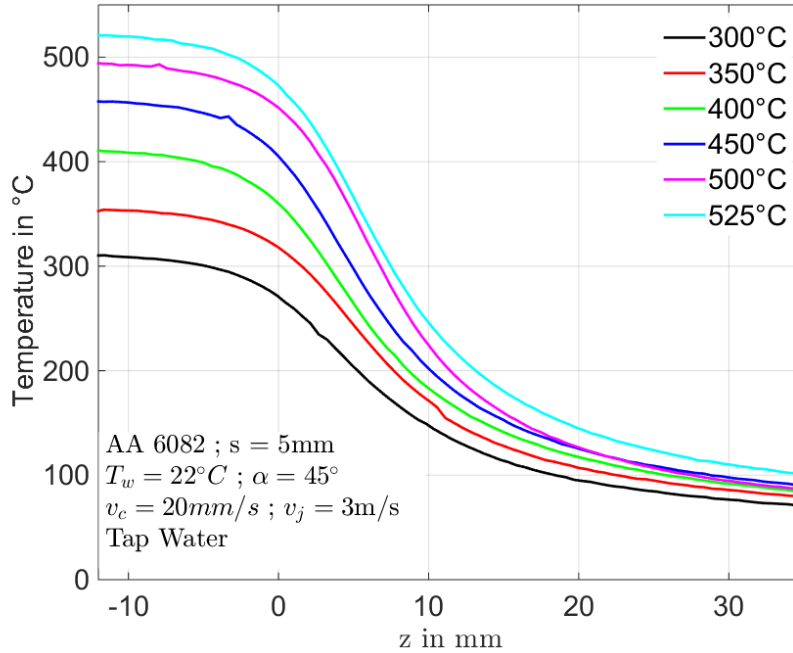


Figure 4.15: Superimposed temperature profile for different initial temperature

It can be thought that the initial temperature of the metal sheet will have a very significant effect on cooling of the metal sheet as the total heat capacity of the system will change with the initial temperature. Even though in boiling curve heat flux is obtained as a function of surface temperature, the internal energy stored in the metal sheet will be different with different initial temperature. This is expected to have an influence on the boiling curve. The change in initial temperature will also change the interface temperature which is also hypothesized to have an influence on the boiling curve. The initial temperature of the metal sheet also has an effect on the boiling curve with different quenching apparatus like spray cooling and full jet nozzle. The influence of initial temperature on heat transfer during quenching process is quantified by comparing the initial temperature of metal sheet in a range of 300°C to 525°C . The experiments were conducted with tap water at 22°C temperature 2.1 m/s jet at an angle of 45° , AA6082, 5 mm thick metal sheet moving at a speed of 20 mm/s .

The superimposed temperature profiles during quenching of AA6082 sheet with different initial temperature are depicted in **Fig. 4.15**, along with respective interface temperature for each initial temperature. From this figure, it can be observed that the initial temperature results in higher interface temperature $T_{z=0}$ and the temperature profiles are converging to final temperature without intersecting with each other. It can also be observed that the maximum temperature gradient is smaller for a lesser temperature of the metal sheet.

Fig. 4.16 shows the boiling curve for the different initial temperatures of metal sheet, from this figure it can be observed that the maximum heat flux depends strongly on the initial temperature of the metal sheet. The maximum heat flux increases with increasing initial temperature and after an initial temperature of

Table 4.7: Width of various regions for different thickness

| | 300°C | 350°C | 400°C | 450°C | 500°C | 525°C |
|---------------------------|----------|----------|----------|----------|----------|----------|
| Pre-Cooling Region | 5.9 mm | 5.53 mm | 5.88 mm | 5.88 mm | 5.88 mm | 5.88 mm |
| Transition Boiling Region | 11.11 mm | 10.83 mm | 10.73 mm | 10.03 mm | 11.77 mm | 11.42 mm |
| Nucleate Boiling Region | 2.1 mm | 4.15 mm | 4.5 mm | 5.89 mm | 6.93 mm | >30 mm |
| $T_s = 0.99 * T_0$ | 297°C | 346.5°C | 396°C | 445.5°C | 495°C | 519.8°C |
| $T_{z=0}$ | 272.9°C | 317.1°C | 361.3°C | 405.4°C | 449.5°C | 472.9°C |
| T_{DNB} | 123°C | 146.3°C | 153.5°C | 173.1°C | 188°C | 210.6°C |

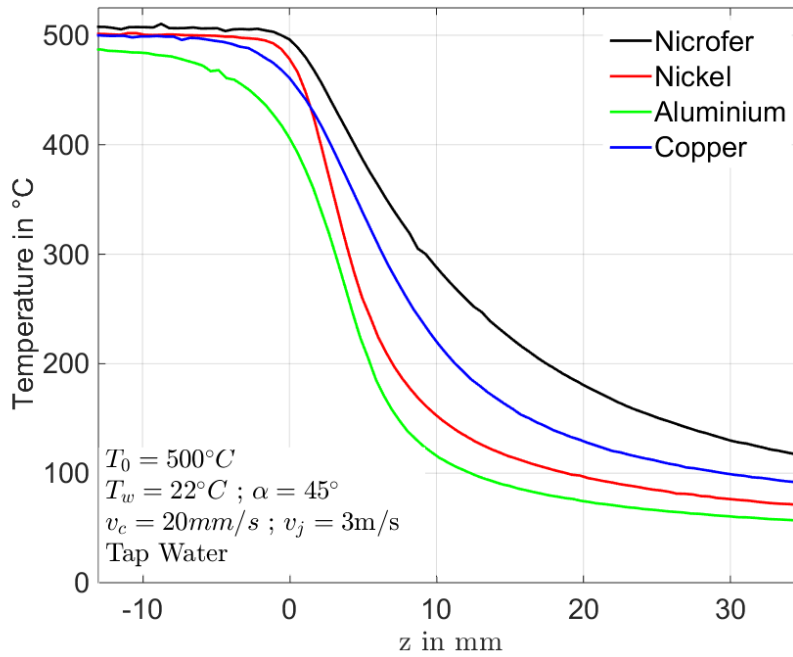


Figure 4.17: Superimposed temperature profile for different metals

with higher thermal conductivity, the interface temperature is lower. It should be noted that the interface temperature for copper is much higher than aluminium also because of the thickness of the copper sheet. From these profiles it can be seen that the thermal gradients are very high in case of nickel. In case of nicrofer the gradients are small and the cooling length is high.

Fig. 4.18 shows the boiling curve for different metals. It can be clearly seen that the boiling curve strongly depends on material properties. As expected from the temperature profiles and also from **Fig. 4.17**, the maximum heat flux for nickel is higher than other metals. The DNB temperature for nickel, aluminium, and copper is nearly same $\sim 200^\circ\text{C}$ and in case of nicrofer the DNB temperature is lower $\sim 175^\circ\text{C}$. For metals with low thermal conductivity, a 2D model is necessary as the temperature difference between the quenching side and the measuring side will be high.

Table 4.8: Material properties for different metals

| | Aluminum | Nickel | Copper | Nicrofer |
|--|----------|--------|--------|----------|
| Density (kg/m^3) | 2700 | 8908 | 8940 | 8400 |
| Thermal Conductivity ($W/m \cdot K$) | 170 | 65 | 120 | 17 |
| Specific Heat Capacity ($J/kg \cdot K$) | 1050 | 500 | 390 | 510 |
| Thickness (mm) | 2 | 2 | 4 | 2 |

Tab. 4.9 shows the widths of various fronts during the quenching process of different metals. It can be observed that the width of pre-cooling region for metals with low thermal conductivity and high heat capacity is smaller. Hence, during the heat transfer analysis of metals with high thermal conductivity, it is important to quantify the temperature drop because of diffusion of heat. The width of transition boiling region also increases with heat capacity and with decreasing thermal conductivity whereas, the width of nucleate boiling region is nearly same for aluminium, nickel and nicrofer.

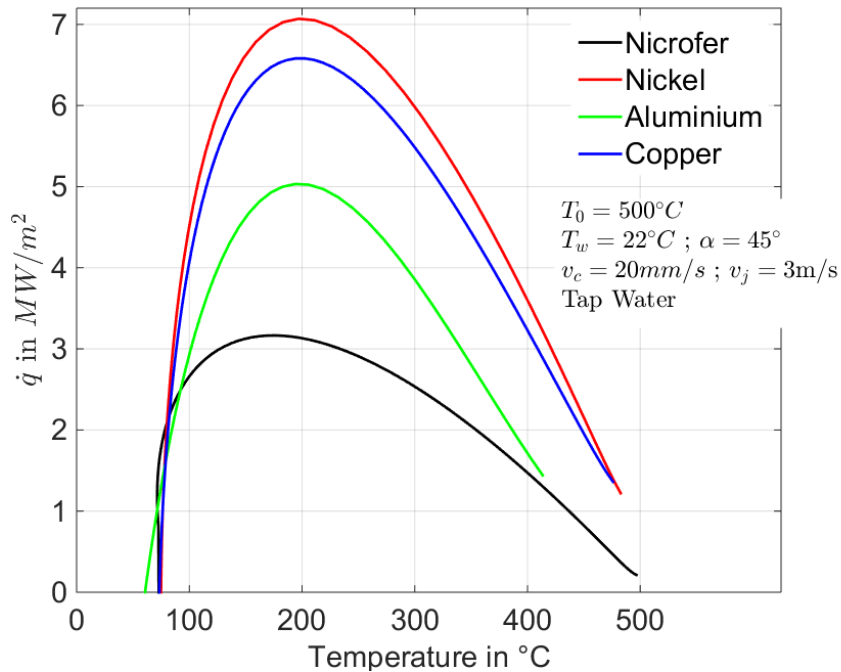


Figure 4.18: Boiling curve for different initial metals

Table 4.9: Width of various regions for different metals

| | Copper | Aluminum | Nickel | Nicrofer |
|---------------------------|---------|----------|---------|----------|
| Pre-Cooling Region | 3.8 mm | 8.3 mm | 1.03 mm | 0.17 mm |
| Transition Boiling Region | 11.9 mm | 5.54 mm | 7.96 mm | 22.06 mm |
| Nucleate Boiling Region | 6.67 mm | 4.15 mm | 3.81 mm | 4.85 mm |
| $T_s = 0.99 * T_0$ | 495°C | 495°C | 495°C | 495°C |
| $T_{z=0}$ | 462.2°C | 407.4°C | 477.5°C | 493.1°C |
| T_{DNB} | 198.2°C | 194.2°C | 197.1°C | 176°C |

5. Heat Transfer Analysis of Stationary Metal Sheet with an Array of Jets

5.1 Introduction

In this chapter, a brief overview of the heat transfer during the quenching of stationary sheet is provided. Followed by this, results from various experiments are discussed along with influence of various process parameters is provided. The results are first compared by superimposing the temperature profiles obtained from the experimental analysis. The wetting front velocity is determined with a second derivative approach to obtain the interface temperature $T_{z=0}$. A comparison of these temperature profiles provides an idea of influence of the parameter on the cooling process. The data is further processed to obtain the boiling curve for each case in order to study the exact influence of the parameter on heat transfer process.

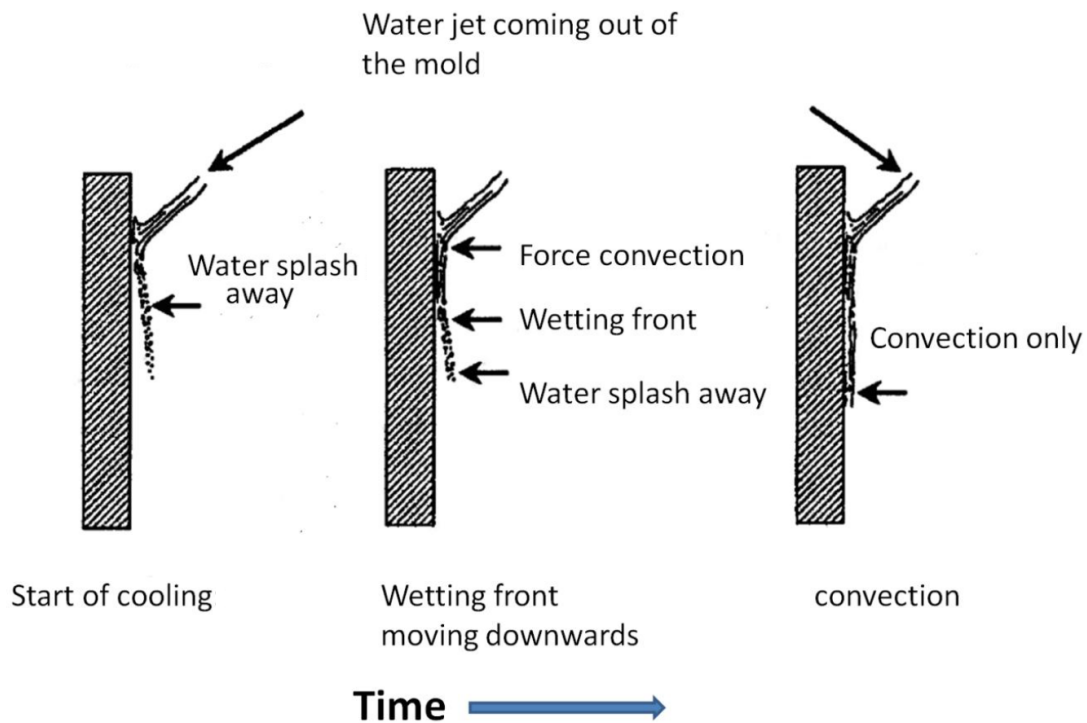


Figure 5.1: Evolution of wetting front during quenching in stationary setup

Rapid cooling with an array of jets on a stationary hot metal is a widely seen application. In this setup, the cooling occurs in the downstream region, away from first impingement point. The top portion i.e. the point of first impingement cools first and then the wetting front progresses downstream, because of which the water temperature is nearly same as initial water temperature, at the wetting front. In

the wet region, the cooling is by convective heat transfer with coolant. This cooling process is further described in **Fig. 5.1**. The turbulence at the wetting front is also less, because of this the cooling characteristics will be different.

5.1.1 Mechanism of Heat Transfer

During the experiments, the mold and the hot metal sheet are stationary and the water jet is impinged on the top of the metal sheet **Fig. 5.2**. In this top region the wetting front collapses and the wetting front propagates downstream. Because of this, the hot metal is in the lower portion and the upper portion is cooled first. Mathematically, the primary difference between the moving metal sheet experiments and the stationary experiments is that, in the former case, the wetting front velocity is same as the casting speed or the sheet movement speed, which can be controlled according to experimental requirements. In case of stationary analysis, the wetting front velocity cannot be controlled and needs to be determined experimentally. It is observed experimentally that the wetting front velocity in the middle region of metal sheet remains constant and the temperature reaches an Eulerian steady state.

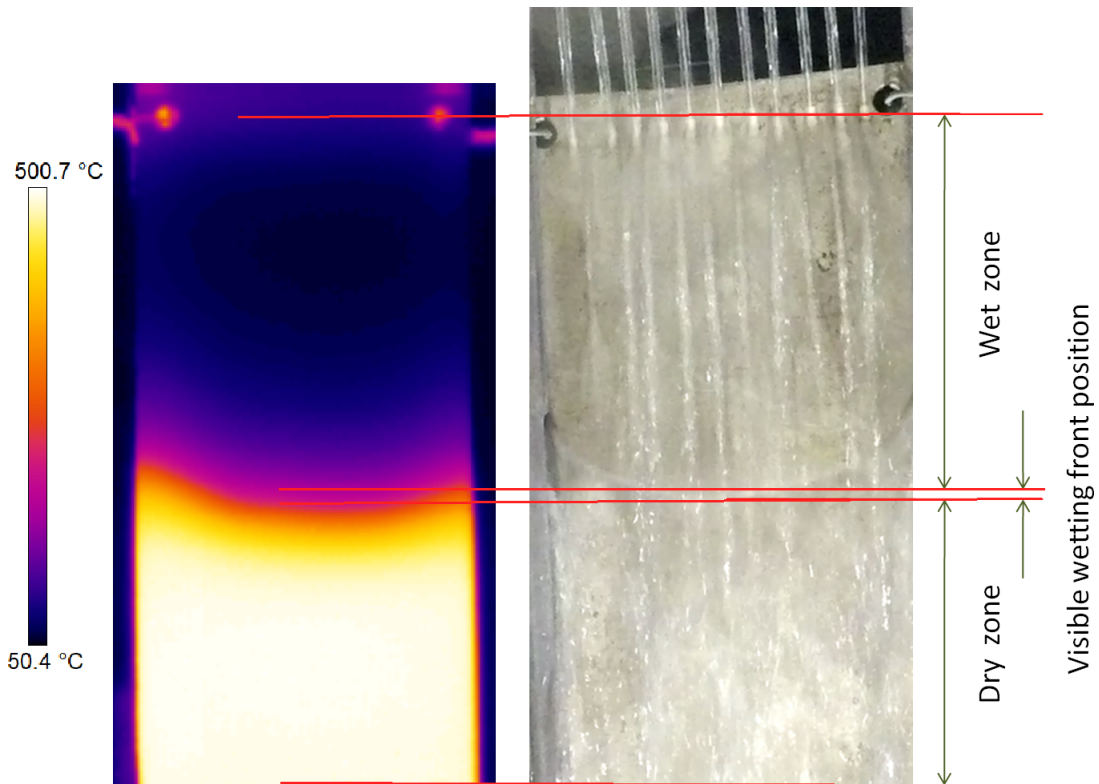


Figure 5.2: Wetting front during quenching with stationary metal sheet

The impinging water during steady state will first come in contact with cooled metal, where the heat transfer is less and occurs because of forced convection. Then the water jet flows downstream, near the wetting front, where the surface temperature is high and the heat transfer occurs because of nucleate boiling, followed by transition

boiling region. The pre-cooling region is downstream further. This phenomenon is opposite to moving mold experiments and is further illustrated in **Fig. 3.5**.

The heat transfer in the downstream of the wetting front will be because of advection. This will reduce the downstream temperature in the vicinity of wetting front. Once the temperature drops below the rewetting temperature T_{rw} the wetting front will propagate, wetting the new region. Visually, it is difficult to determine the exact location of the wetting front. This is because of the transient phenomenon occurring and the water stream splashing away from the metal surface. Hence, the location of wetting is determined from the temperature history data from the infrared camera, as described in **Sec. 3.3.2**. Although this approach creates errors to determine the interface temperature, it was observed that the wetting front velocity, obtained with this approach provides stable results. With this method the wetting front velocity can be determined and incorporated in **Eq. 3.12**, to determine the rewetting temperature.

The wetting front velocity for different positions is as seen in **Fig. 5.3**. 50 mm from the top region is neglected from analysis because the jet impingement point is at a distance from the topmost edge and the cooling occurring in the impingement zone is not the focus of this analysis. From the infrared camera image **Fig. 5.2**, it can be seen the wetting front is not completely horizontal. This is because of the end effects near the edges. Hence the temperature at the centreline is considered for analysis, to avoid these effects. Since in the lower region there is a significant time delay for the wetting front to reach, there is slight cooling because of radiation and convection with air. This reduces the temperature of the sheet slightly and because of this, a slight acceleration in the wetting front velocity is observed. This change in velocity is very small and can be neglected.

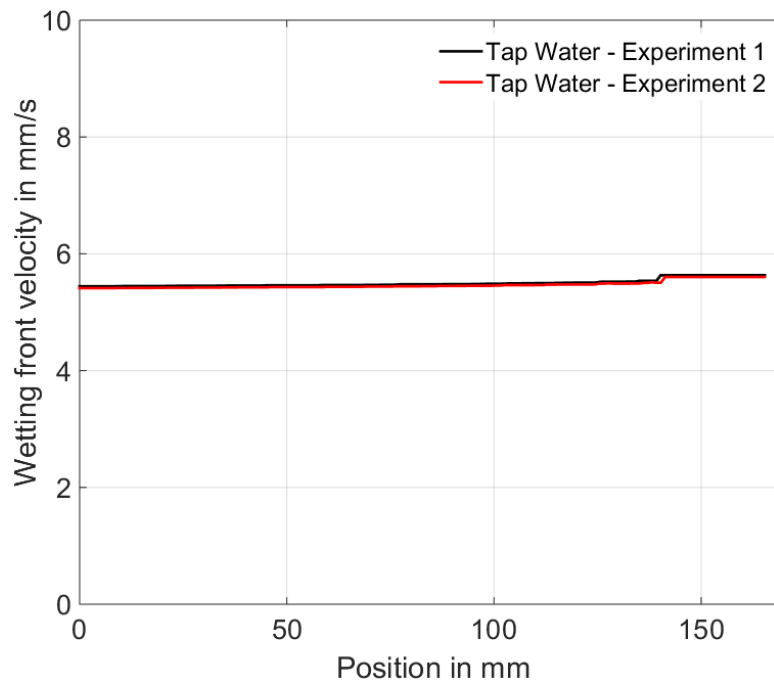


Figure 5.3: Wetting front velocity at different positions during quenching with stationary mechanism

Since the pre-cooling region is downstream, the heat will diffuse from bottom to top. The direction for diffusion of heat is further illustrated in **Fig. 5.4**. This is opposite from moving sheet experiments where the diffusion of heat is from top to bottom. Because we can control the casting speed and hence the Peclet number in moving sheet experiments, the temperature at which cooling with water starts can be controlled. In case of stationary sheet, the wetting front velocity cannot be controlled and Peclet number needs to be determined from experimental results. Hence, the wetting temperature needs to be determined analytically.

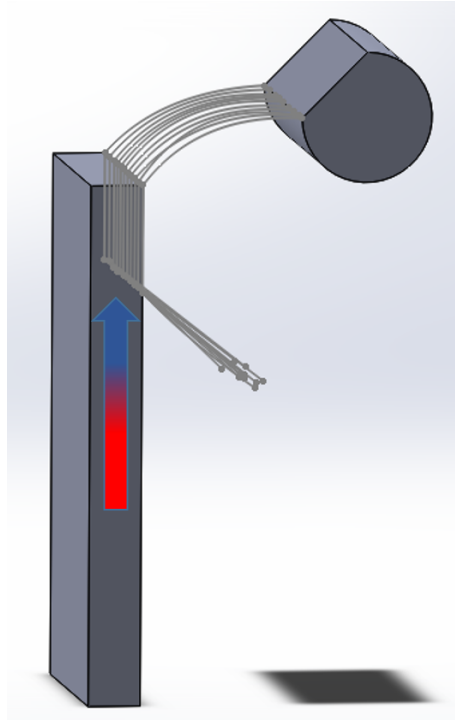


Figure 5.4: Heat transfer mechanism during quenching with stationary sheet

5.2 Results and Discussion

The stationary sheet mechanism can be compared to the free-falling zone of DC casting process. In this free-falling zone the water jet has only vertical momentum and the flow is less turbulent. But in stationary experiments, the water temperature near the wetting front is nearly same as the initial temperature as the water undergoes heat transfer only because of forced convection, whereas in case of DC casting the cooling water undergoes heat transfer because of transition boiling and nucleate boiling in impingement zone before flowing downstream in free falling zone. Because of this, the temperature of the water is more when it enters the free falling zone. This physical change needs to be incorporated while implementing these results to industrial process simulations.

For the experimental analysis, it needs to be ensured that the experiments are repeatable. If the experiments are conducted multiple times on a metal sheet with same parameters, the temperature results are identical. The results may vary because of inconsistent or unaccounted experimental parameters. In the impingement zone it is observed that the experiments are repeatable. It can be seen that the

experimental results do not change when the experiments are repeated. The superimposed temperature profiles for repeatability of the experiments are as shown in **Fig. 5.5**. The experiments are performed on a 10 mm AA6082 sheet initially of around 500°C , with tap water jets at an inclination of 45° and velocity on 3 m/s at 22°C . It can be seen that the obtained temperature profiles show good repeatability.

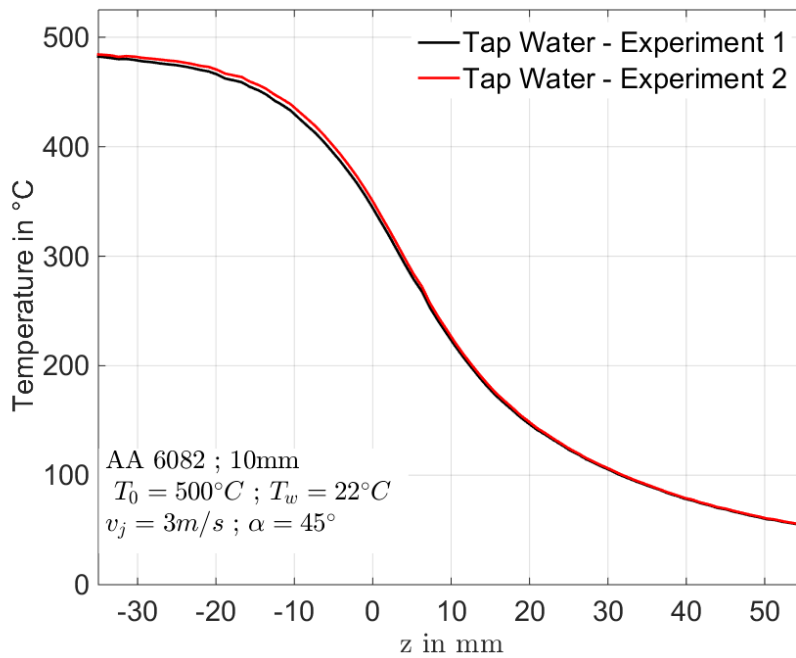


Figure 5.5: Superimposed temperature profiles during quenching experiments

Also, the wetting front velocity for repeating these experiments, are also consistent **Fig. 5.3**. For the repeated experiments, a consistent wetting front velocity was obtained. Since the temperature profiles and the wetting front velocities are repeatable, it can be concluded that the experiments are repeatable and will provide identical boiling curve if the experiment is repeated. Hence, a metal sheet can be reused to perform quenching analysis.

5.2.1 Influence of Water Quality

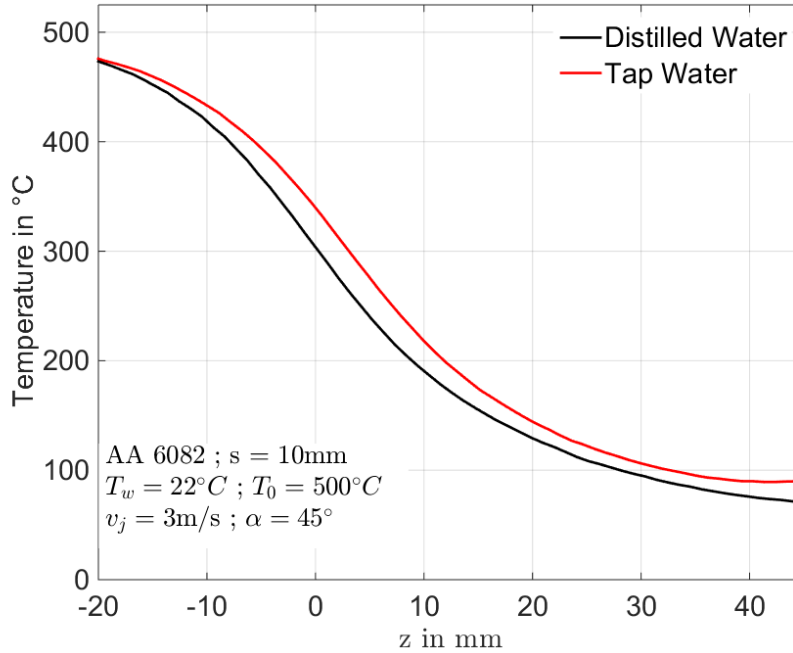


Figure 5.6: Superimposed temperature profiles for different water quality

Water quality is an important parameter when most industrial cooling water consists of different kind of contaminants such as lubricants, chemicals, salty, organic matter, solid particulates, etc. Therefore, it is important to do research on the effect of water quality on heat transfer in metal quenching process.

To quantify this influence, experiments were conducted on 10 mm AA6082 metal sheet at initial temperature of around 500°C jet velocity of 3.0 m/s , jet angle of 45° . Distilled water is obtained from the distillation of tap water to remove salts and impurities. Because of this, the electrical conductivity of distilled water is 0 mS/cm . The tap water used is the water in Magdeburg, Germany. The electrical conductivity of this tap water is measured to be 0.58 mS/cm . These experiments were conducted to quantify the influence of salt content on the heat transfer process during the quenching of stationary metal sheet.

The **Fig. 5.6** shows the superimposed temperature profile for distilled water and tap water. It can be observed from the temperature profiles for tap water and distilled water is distinctly different and the slopes of the profiles are also different. Because of this it can be expected that the quality of water will have significant influence on the heat transfer and the rewetting temperature. The boiling curves for different water quality can be seen in **Fig. 5.7**. It can be seen that the boiling curves are distinct for different water quality. For distilled water, it can be seen that the rewetting temperature is lower but the maximum heat flux and the DNB temperature are higher. The DNB temperature with distilled water is $\sim 235^{\circ}\text{C}$, which is higher than any case observed during other experiments.

The width of the various wetting front and front velocity can be seen in **Tab. 5.1**. The wetting front velocity in case of quenching with distilled water is observed to

be 5.79 mm/s and of 5.48 mm/s in case of tap water. It can be seen that the transition boiling region for distilled water is nearly half the width in case of tap water. The nucleate boiling region is greater in case of distilled water. The width of the pre-cooling region also depends on water quality. Though there is not much change in maximum heat flux with the water quality ($1.98 \text{ MW/m}^2 - 2.2 \text{ MW/m}^2$), the change in rewetting and DNB temperature changes the cooling characteristics changes significantly with water quality.

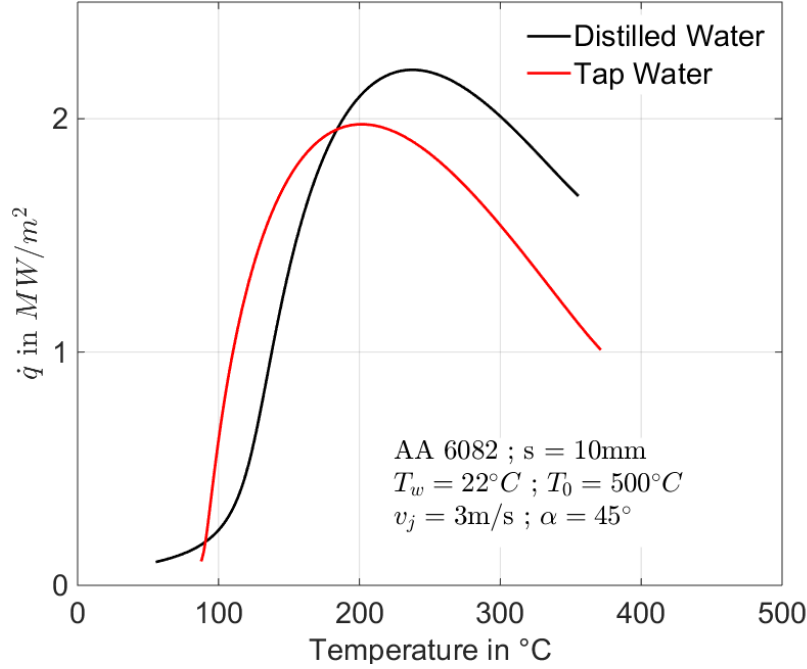


Figure 5.7: Boiling curve for different water quality

Table 5.1: Width of various fronts for different water quality

| | Distilled water | Tap Water |
|---------------------------|-----------------------|-----------------------|
| Pre-Cooling Region | 33.33 mm | 31.18 mm |
| Transition Boiling Region | 5.02 mm | 11.83 mm |
| Nucleate Boiling Region | 33.69 mm | 22.58 mm |
| Wetting front velocity | 5.79 mm/s | 5.48 mm/s |
| $T_s = 0.99 * T_0$ | 482.6°C | 476.8°C |
| $T_{z=0}$ | 296.1°C | 338.9°C |
| T_{DNB} | 236.4°C | 198.8°C |

In the impingement zone it is observed that water quality does not influence the heat transfer, as described in **Sec. 4.2.1**. But in case of free falling zone, it can be concluded that the water quality has influence on cooling process. Hence, it can be concluded that in case of DC casting process, the quality of cooling water will play a role in heat transfer process.

5.2.2 Temperature of Water

Water temperature is also thought to have an influence on heat flux during quenching of metal sheet as the cooling capacity of water will change with water temperature.

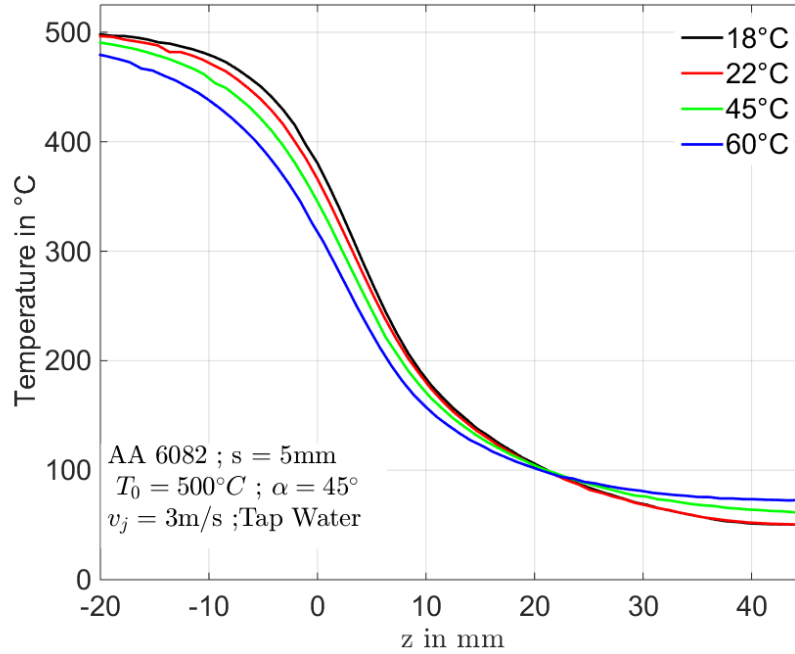


Figure 5.8: Superimposed temperature profiles for different water temperature

Water at a higher temperature will be more prone to bubble formation affecting the heat transfer. In this experimental work, 5 mm AA6082 metal sheet, heated to initial temperature of around 500°C , with a jet velocity of 3.0 m/s and jet angle of 45° is quenched with tap water. During the experiments, it was observed that at higher water temperature the quenching time was higher because of slower wetting front velocity.

The superimposed temperature profiles **Fig. 5.8**. It can be observed that the cooling characteristics depend significantly on water temperature. It can be observed that the rewetting temperature lower for higher water temperature. It can also be seen that the temperature gradients are lesser for warmer water. Hence, it can be expected that the maximum heat flux will be lesser for higher water temperature. The final temperature of metal sheet in case of 60°C water temperature is higher than water at 18°C .

The boiling curves, obtained from the experimental analysis are as shown in **Fig. 5.9** and front widths **Tab. 5.2** were analysed. It can be observed that with increase in water temperature, the interface or rewetting temperature, wetting front velocity and maximum heat flux decrease from 380.2°C , 9.95 mm/s and 3.27 MW/m^2 for the water temperature of 18°C to 316.1°C , 6.66 mm/s and 2.02°C for water at 60°C . But it is observed that the water temperature does not have any influence on the DNB temperature.

The width of pre-cooling region keeps increasing with the increase of water temperature from 16.48 mm to 27.32 mm , owing to the change in wetting front velocity. While the transition boiling region is shortened from 9.68 mm to 7.53 mm , though the thermal gradient in transition boiling region is not changing much. For nucleate boiling region, the width increases till water temperature of 45°C and decreases for higher temperature.

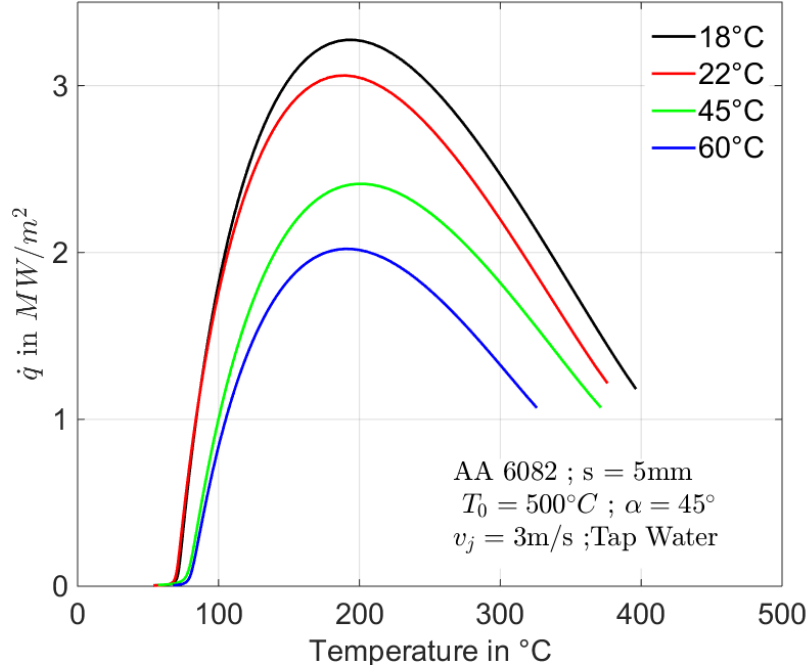


Figure 5.9: Boiling curve for different water temperature

Table 5.2: Width of various fronts for different water temperature

| | 18°C | 22°C | 45°C | 60°C |
|---------------------------|-----------|-----------|-----------|-----------|
| Pre-Cooling Region | 16.48 mm | 19.72 mm | 22.58 mm | 28.32 mm |
| Transition Boiling Region | 9.68 mm | 8.24 mm | 8.25 mm | 7.53 mm |
| Nucleate Boiling Region | 8.60 mm | 8.25 mm | 11.83 mm | 11.47 mm |
| Wetting front velocity | 9.95 mm/s | 9.14 mm/s | 8.24 mm/s | 6.66 mm/s |
| $T_s = 0.99 * T_0$ | 482°C | 482.9°C | 477.2°C | 466.1°C |
| $T_{z=0}$ | 380.2°C | 367.9°C | 347.1°C | 316.1°C |
| T_{DNB} | 190.6°C | 190.1°C | 198.4°C | 190.1°C |

With increase of water temperature, the wetting front velocity decrease. Such difference becomes larger when the water temperature continue to rise. It can be observed that the cooling characteristics changes drastically for water temperature of 45°C. This phenomenon was also observed by Caron [18]. They reported higher heat flux only in convection region for sub-cooled quenching water and above water temperature of 40°C promoted bubble formation reducing the overall heat flux. Akmal et al. [48], Wells et al. [45], Sabariman [70] also concluded that lower water temperature enhances heat transfer and the wetting front velocity.

In case of Impingement zone, as described in **Sec. 4.2.2**, a slight influence of water temperature is observed in the cooling process. Whereas, in case of free falling zone the water temperature plays significant role. It can be concluded that the turbulence in the impingement minimizes the effect of reduced cooling capacity in impingement zone.

5.2.3 Jet Velocity

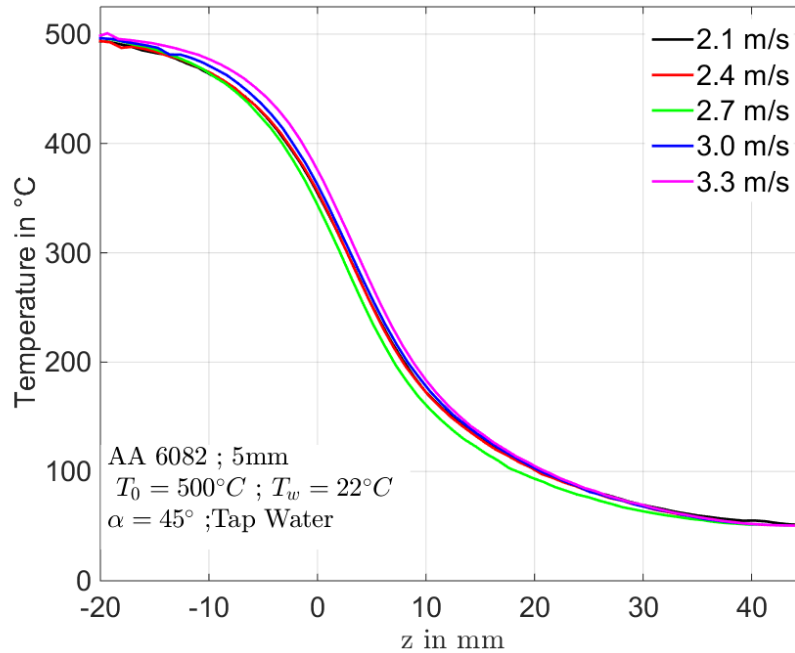


Figure 5.10: Superimposed temperature profiles for different jet velocities

Jet velocity will change the mass flow rate of the coolant, but it will also alter the momentum of the water stream and hence the fluid dynamic behaviour. This can have an influence on the cooling characteristics of the quenching process. In general, it can be imagined that higher the water flow rate, more will be the cooling. But the exact relationship between the boiling curve and the jet velocity needs to be studied. For this experiments were conducted on a 5 mm thick AA6082 sheet at an initial temperature of around 500°C, with tap water at 22°C and a jet angle of 45°. Experiments were conducted with jet velocities of 2.1 m/s, 2.4 m/s, 2.7 m/s, 3.0 m/s and 3.3 m/s.

The superimposed temperature profiles during the quenching of AA6082 sheet with different jet velocity are depicted in **Fig. 5.10**. From this figure, it can be observed that the interface temperature or the rewetting increases with the increasing water flow rate. The thermal gradients are not changing significantly, but the change in rewetting temperature will influence the cooling characteristics.

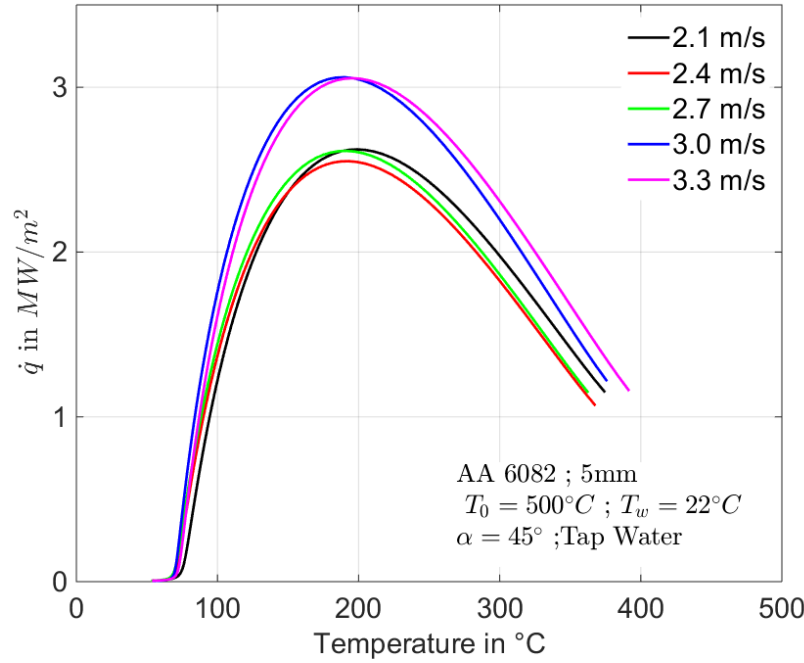


Figure 5.11: Boiling curve for different jet velocities

The boiling curve and the width of wetting front are showed in **Fig. 5.11** and **Tab. 5.3**. It can be observed that the maximum heat flux does not change much for jet velocity from 2.1 m/s to 2.4 m/s . But further increasing the jet velocity to 3.0 m/s and above leads to a increase of heat flux from $\sim 2.6 \text{ MW/m}^2$ to $\sim 3.06 \text{ MW/m}^2$. The DNB temperature remains in the range of 190°C to 200°C for the range of jet velocities. The wetting velocity for the jet velocity of 3 m/s and 3.3 m/s is higher than the other jet velocities.

The width of the pre-cooling region shows a similar trend as the DNB temperature. From jet velocity of 2.1 m/s to 2.7 m/s pre-cooling region increases and beyond that, a decreasing trend is observed. The width of transition region remains stable at $\sim 8.24 \text{ mm}$ for different jet velocities. On the other hand, the nucleate boiling region decreases with increasing jet velocity. Further increasing the jet velocity has prolonged the nucleate boiling and transition boiling region and lead a decrease of a pre-cooling region. It can be observed that the width of wetting front i.e. the sum of the pre-cooling region, transition boiling region and nucleate boiling region together remains almost constant for different jet velocities. Hence the thermal gradients in the metal sheet will remain same irrespective of the jet velocity. In case of impingement zone, jet velocity is not having a significant influence on the boiling curve, as discussed in **Sec. 4.2.3**.

A similar trend of relationship of jet velocity and boiling curve is also reported by Sabariman [70]. He observed that increasing jet velocity from 1.2 m/s to 1.5 m/s increased the heat transfer, however further increase to 1.8 m/s had no influence on heat flux. Mozumder et al. [71] concluded that maximum heat flux increases gradually with increasing jet velocity and is proportional to $v_j^{\frac{1}{3}}$.

Table 5.3: Width of various fronts for different jet velocities

| | 2.1 m/s | 2.4 m/s | 2.7 m/s | 3.0 m/s | 3.3 m/s |
|---------------------------|-----------|-----------|-----------|-----------|-----------|
| Pre-Cooling Region | 21.51 mm | 22.23 mm | 22.23 mm | 19.72 mm | 17.92 mm |
| Transition Boiling Region | 8.24 mm | 8.24 mm | 8.24 mm | 8.24 mm | 8.96 mm |
| Nucleate Boiling Region | 10.75 mm | 9.68 mm | 9.32 mm | 8.25 mm | 9.32 mm |
| Wetting front velocity | 8.61 mm/s | 8.30 mm/s | 8.30 mm/s | 9.14 mm/s | 9.84 mm/s |
| $T_s = 0.99 * T_0$ | 480.7°C | 476.5°C | 478.2°C | 482.9°C | 482.4°C |
| $T_{z=0}$ | 353.2°C | 348°C | 348.4°C | 361.9°C | 373.9°C |
| T_{DNB} | 199°C | 193°C | 191.4°C | 190.1°C | 195.5°C |

5.2.4 Jet Impingement Angle

By changing the jet angle, the vertical momentum of the water stream can be increased. This will have effect on the heat transfer which quenching of sheet. To quantify the influence of jet angle on boiling curve in free falling region, experiments were conducted on a 5 mm thick AA6082 sheet, initially heat to a temperature of around 500°C, with tap water at 22°C and a jet velocity of 3 m/s. Experiments were conducted by adjusting the angle of mold to 15°, 30°, 45°, 60°.

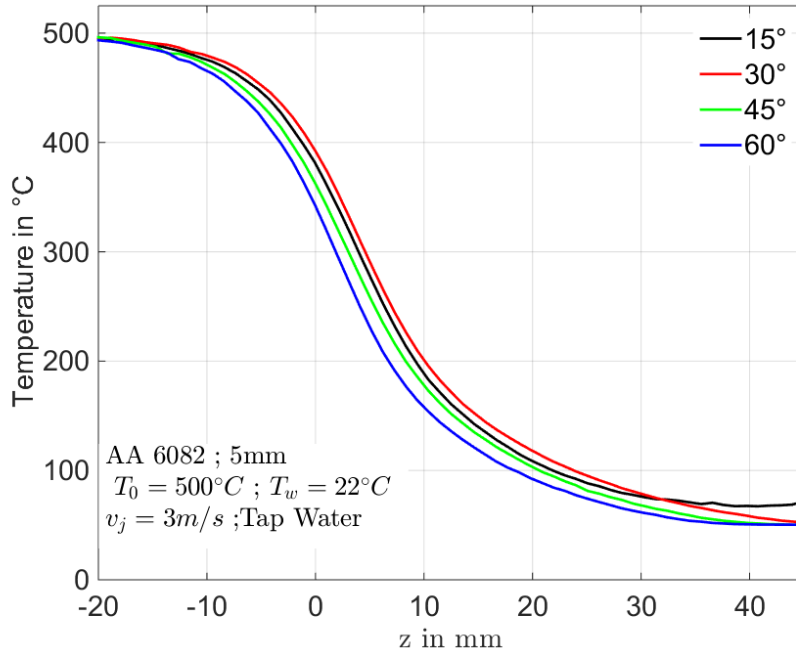


Figure 5.12: Superimposed temperature profiles for different jet angles

Fig. 5.12 shows the superimposed temperature profile for different jet angles. In this figure, it can be observed that for a jet angle of 30° the interface temperature is highest and as the angle increases, the interface temperature decreases. It can also be observed that the thermal gradients decrease with increasing jet angle.

The boiling curve and the width of wetting fronts are as shown in **Fig. 5.13** and **Tab. 5.4**. It can be observed that the maximum heat flux decreases, from 3.4 MW/m^2 to 2.6 MW/m^2 with increasing jet angle. However the DNB temperature and the rewetting temperature are maximum for jet angle of 30° of 201.7°C and 387°C respectively. The wetting front velocity is also maximum for 30° jet angle at 11.3 mm/s . Thereafter, the wetting front velocity decreases with increasing jet angle.

The width of the pre-cooling region is smallest for the jet angle of 30° and the width of transition boiling and nucleate boiling region is highest. Based on this, it can be concluded that a 30° has the fastest cooling characteristics. In case of impingement zone, a linear relationship between jet angle and the boiling curve is observed, as discussed in **Sec. 4.2.4**.

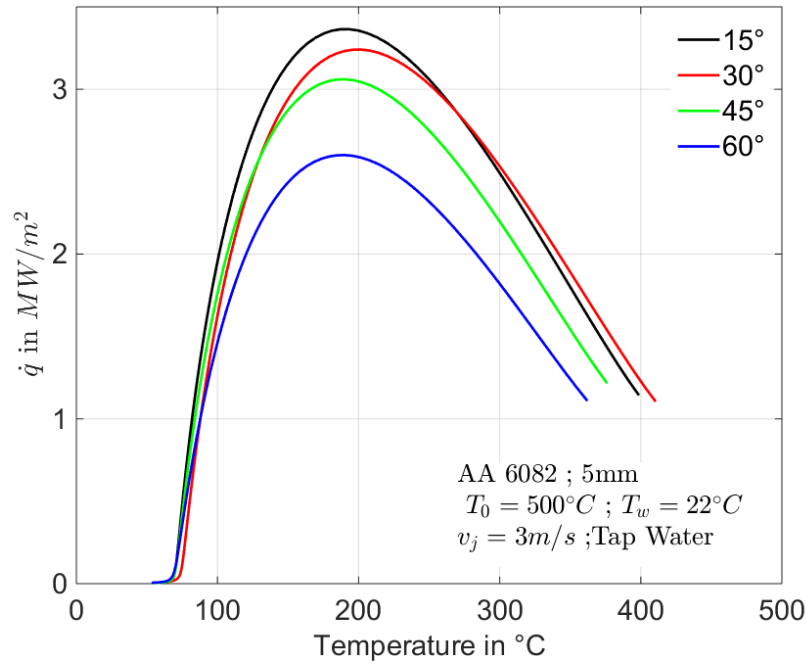


Figure 5.13: Boiling curve for different jet angles

Table 5.4: Width of various fronts for different jet angles

| | 15° | 30° | 45° | 60° |
|---------------------------|-----------------------|-----------------------|-----------------------|-----------------------|
| Pre-Cooling Region | 16.48 mm | 15.42 mm | 19.72 mm | 22.23 mm |
| Transition Boiling Region | 9.32 mm | 9.67 mm | 8.24 mm | 8.24 mm |
| Nucleate Boiling Region | 7.89 mm | 10.4 mm | 8.25 mm | 8.96 mm |
| Wetting front velocity | 10.7 mm/s | 11.28 mm/s | 9.14 mm/s | 8.46 mm/s |
| $T_s = 0.99 * T_0$ | 482.9°C | 480.9°C | 482.9°C | 476.2°C |
| $T_{z=0}$ | 378.4°C | 387°C | 361.9°C | 346.4°C |
| T_{DNB} | 187°C | 201.7°C | 190.1°C | 189.8°C |

Caron [18], reported that for low jet velocities $\sim 2 \text{ m/s}$, jet angles has influence only in the forced convection region. However, for higher jet velocities maximum heat flux was found at jet angle of 30° . El-Genk et al. [72] reported that while in transition boiling region, heat flux increased, in the nucleate boiling region heat flux decreases as the jet angle increased.

5.2.5 Thickness of Metal Sheet

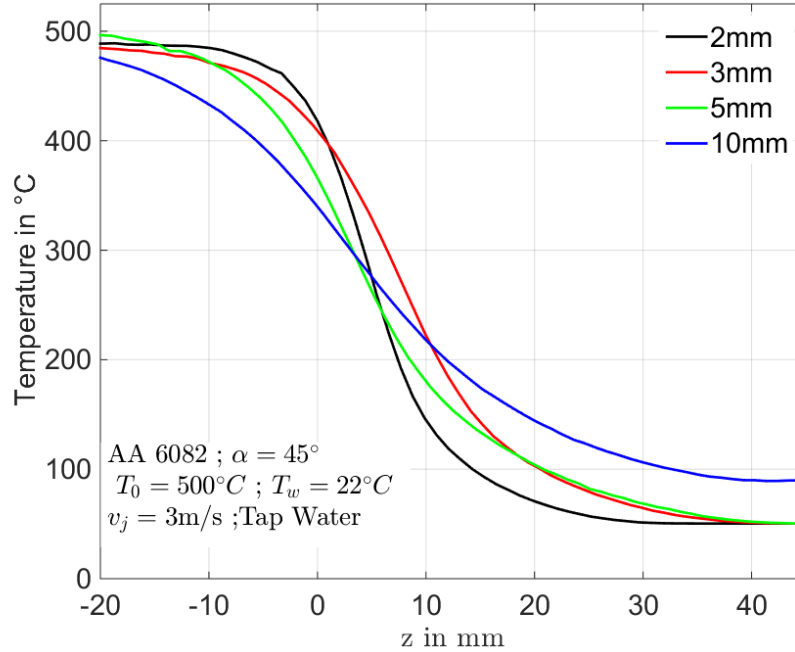


Figure 5.14: Superimposed temperature profiles for different thickness

With increasing thickness of the metal sheet, the heat capacity of the system will change. The heat transfer along the thickness direction will be dominant for higher thickness. Since, in the simulation model, the temperature difference between the quenching side and the measuring side is considered, the heat flux as a function of temperature on the quenching side can be determined. This is important as with an infrared camera, the temperature on the back side of sheet is obtained. This temperature difference between the quenching side and the measuring side will increase for thick sheets.

In order to study the influence of thickness on heat transfer during quenching in the free falling zone, experiments were conducted with tap water at $22^\circ C$, jet velocity and angle of 3 m/s and 45° respectively. AA6082 sheets with different thickness like 2 mm , 3 mm , 5 mm and 10 mm , were heated to a initial temperature of around $500^\circ C$ before quenching.

The superimposed temperature profiles **Fig. 5.14**. From this figure, it can be observed the thickness of the metal sheet has a significant influence on the heat transfer characteristics. The interface temperature decreases highly with an increase in thickness. Even the thermal gradients can be observed to decrease with increasing thickness.

Boiling curves **Fig. 5.15** and the front widths **Tab. 5.5** are also analysed. It can be observed that the maximum heat flux is highest for 2 mm sheet at 4.3 MW/m^2 and decreases with increasing thickness to 1.9 MW/m^2 for 10 mm sheet. It was also observed that the time required for cooling of the 10 mm sheet was significantly longer than for 2 mm sheet. This is because the wetting front velocity and the rewetting temperature were observed to be higher at 21.5 mm/s and 411.5°C for a 2 mm thick sheet and at 5.5 mm/s and 338.9°C for a 10 mm sheet.

The width of pre-cooling region increases with increasing thickness from 7.17 mm for a 2 mm sheet to 31.18 mm for a 10 mm sheet. The transition boiling region and the nucleate boiling region also increases with increasing thickness for 6.45 mm , 6.45 mm respectively for a 2 mm sheet to 11.83 mm and 22.58 mm respectively for a 10 mm sheet. From these results, it can be observed that the thermal gradients are highest for a thin sheet and decrease with increasing thickness.

The width of the pre-cooling region significantly increases with the increase of plate thickness. For transition boiling and nucleate boiling region, the widths of these area were mainly prolonged by increasing the metal thickness from 2 mm to 10 mm. But considering the thickness of 3 mm and 5 mm, the width slightly decrease. For a 2 mm sheet a change of 21.5°C/m is observed and for a 10 mm sheet the thermal gradient is only 6.9°C/m in the wetting front. Because of this higher induced distortions were observed for thinner sheets.

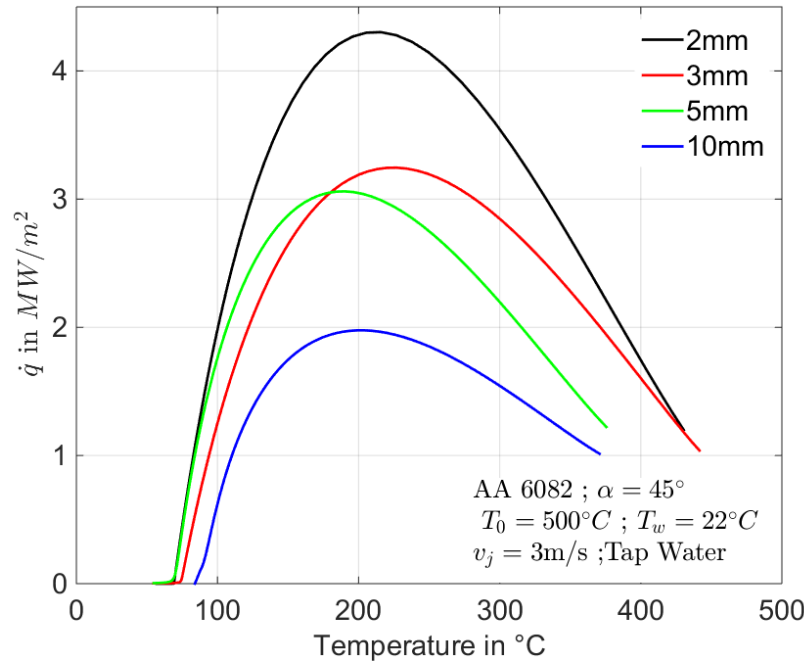


Figure 5.15: Boiling curve for different thickness

The influence of thickness on boiling curve for stationary setup was studied by Westwater et al. [73]. They reported maximum heat flux will decrease with increasing thickness. A theory by Sharp [74] predicted that heat transfer coefficient should decrease with decreasing thickness, while Magrini and Nannei [75] hypothesized that the effect would be reverse i.e. heat transfer coefficient should increase with decreasing thickness. From the experimental analysis, it can be observed that in the

Table 5.5: Width of various fronts for different thickness

| | 2mm | 3mm | 5mm | 10mm |
|---------------------------|------------|------------|-----------|-----------|
| Pre-Cooling Region | 7.17 mm | 9.32 mm | 19.72 mm | 31.18 mm |
| Transition Boiling Region | 6.45 mm | 8.96 mm | 8.24 mm | 11.83 mm |
| Nucleate Boiling Region | 6.45 mm | 11.1 mm | 8.25 mm | 22.58 mm |
| Wetting front velocity | 21.49 mm/s | 17.21 mm/s | 9.14 mm/s | 5.48 mm/s |
| $T_s = 0.99 * T_0$ | 483°C | 483.2°C | 482.9°C | 476.8°C |
| $T_{z=0}$ | 411.5°C | 409.2°C | 361.9°C | 338.9°C |
| T_{DNB} | 215.9°C | 227°C | 190.1°C | 198.8°C |

impingement zone heat flux decreases with decreasing thickness, as discussed in **Sec. 4.2.5** and in free falling zone heat flux increases with decreasing thickness.

5.2.6 Initial Temperature of Metal Sheet

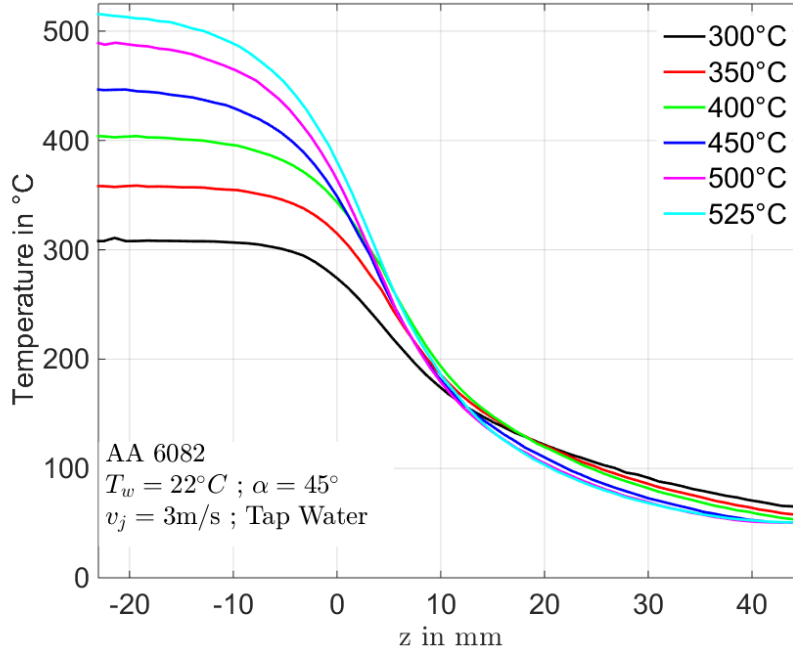


Figure 5.16: Superimposed temperature profiles for different initial temperature

The initial temperature of the metal sheet is also expected to have an influence on the cooling characteristics during experiments with stationary mechanism. With changing the initial temperature of the metal sheet, the heat capacity of the system changes. Because of this, it can be imagined that the heat transfer character will change. Because of change in the initial temperature, the thermal gradients in the sheet can also change, which can have an effect on the boiling curve.

For this reason, experiments were conducted on a 5 mm thick AA6082 sheet quenching with tap water at 22°C with a jet angle of 45° and a jet velocity of 3 m/s. The initial temperature of the metal sheet is changed in the range of 300°C to 525°C. The superimposed temperature profiles during quenching of AA6082 sheet with different initial temperature are depicted in **Fig. 5.16**. From this figure, it can be

observed that the interface temperature decreases with the decrease in initial temperature. This is expected as with a change in the initial temperature, the thermal gradient will decrease, reducing the heat transfer because of diffusion. It can also be observed the thermal gradient for the sheet at higher temperature is higher than for lower temperature.

Fig. 5.17 shows the boiling curves for different initial temperature for the free falling zone. From this figure, it can be observed that the maximum heat flux and the DNB temperature strongly depends on the initial temperature. The DNB temperature increases with increasing initial temperature from $161.8^{\circ}C$ to $215.5^{\circ}C$. But the maximum heat flux is increasing till the initial temperature of $450^{\circ}C$ and is remaining constant there after. This phenomenon is also observed in the impingement zone **Sec. 4.2.7**.

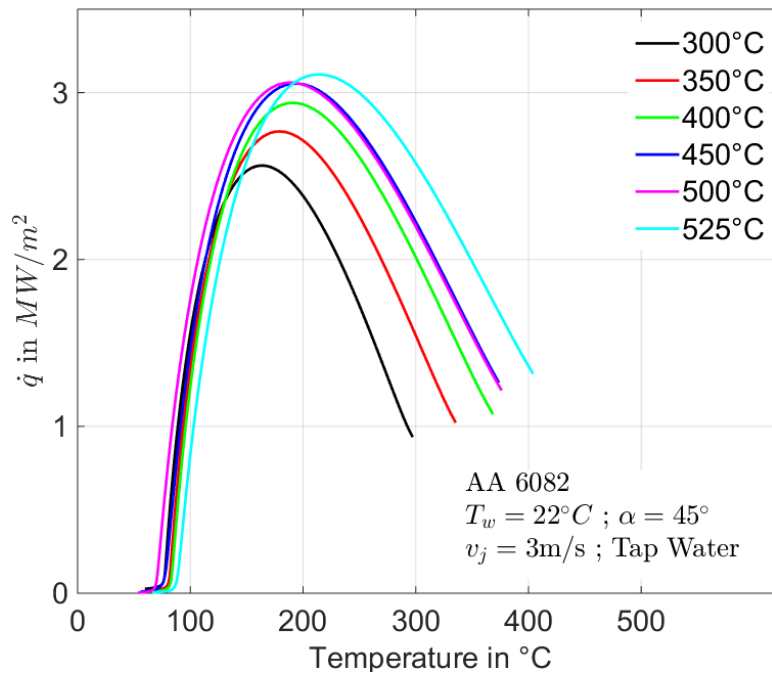


Figure 5.17: Boiling curve for different initial temperature

Table 5.6: Width of various fronts for different initial temperature

| | $300^{\circ}C$ | $350^{\circ}C$ | $400^{\circ}C$ | $450^{\circ}C$ | $500^{\circ}C$ | $525^{\circ}C$ |
|------------------------------------|----------------|----------------|----------------|----------------|----------------|----------------|
| Pre-Cooling Region(mm) | 6.63 | 8.96 | 11.83 | 17.21 | 19.72 | 19.36 |
| Transition Boiling Region(mm) | 13.8 | 11.47 | 10.39 | 8.60 | 8.24 | 8.24 |
| Nucleate Boiling Region(mm) | 11.11 | 12.19 | 12.19 | 10.04 | 8.25 | 14.34 |
| Wetting front velocity(mm/s) | 21.75 | 16.63 | 12.84 | 9.24 | 9.17 | 9.42 |
| $T_s = 0.99 * T_0$ ($^{\circ}C$) | 310 | 360.36 | 412.24 | 461 | 482.82 | 511.83 |
| $T_{z=0}$ ($^{\circ}C$) | 276.41 | 311.62 | 343 | 354 | 361.87 | 386.94 |
| T_{DNB} ($^{\circ}C$) | 161.8 | 179 | 190.02 | 190.02 | 190.01 | 215.5 |

Tab. 5.6 shows the front widths of various regions during the quenching process. It can be seen that the wetting front velocity decreases strongly with increasing initial temperature. Also the width of pre-cooling region increases with increasing initial temperature. The transition boiling regions shrinks and the nucleate boiling region fluctuates with initial temperature. It can also be observed that the width of wetting front i.e. nucleate boiling region and transition boiling region together is shrinking with increasing initial temperature. This can also be observed in **Fig. 5.16** where, the sheet at initial temperature of 525°C cools in a shorter duration than the sheet at 300°C . This phenomenon is also observed in the research of Sabariman [70] and needs to be investigated further.

5.2.7 Kind of Metal

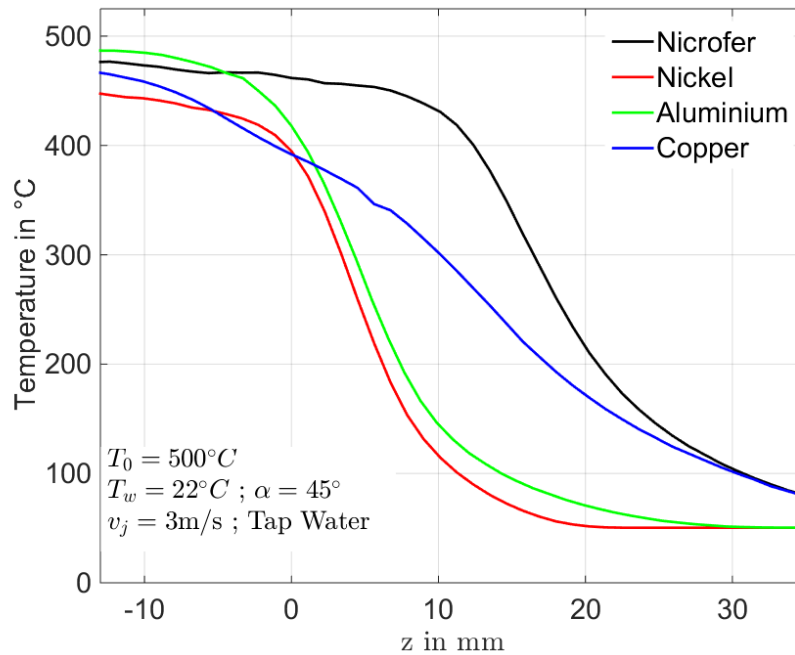


Figure 5.18: Superimposed temperature profiles for different metals

The difference in material property of the metal sheet is also belied to have an influence on the cooling during the quenching process. To quantify the influence on material properties sheets of different metals like Copper, Nickel, Nicrofer and Aluminium are used at an Initial temperature of around 500°C quenching with a tap water jets at 22°C and a jet velocity and inclination of 3 m/s and 45° . The material properties are these difference metals is as given previously in **Tab. 4.8**.

The superimposed temperature profiles for quenching of these different metals is as depicted in **Fig. 5.18**. It can be seen that the temperature gradient for aluminium is highest and less in case of nicrofer. The boiling curve is as shown in **Fig. 5.19**. It can be seen that the maximum heat flux for Aluminium is highest. The widths of various wetting fronts are as depicted in **Tab. 5.7**.

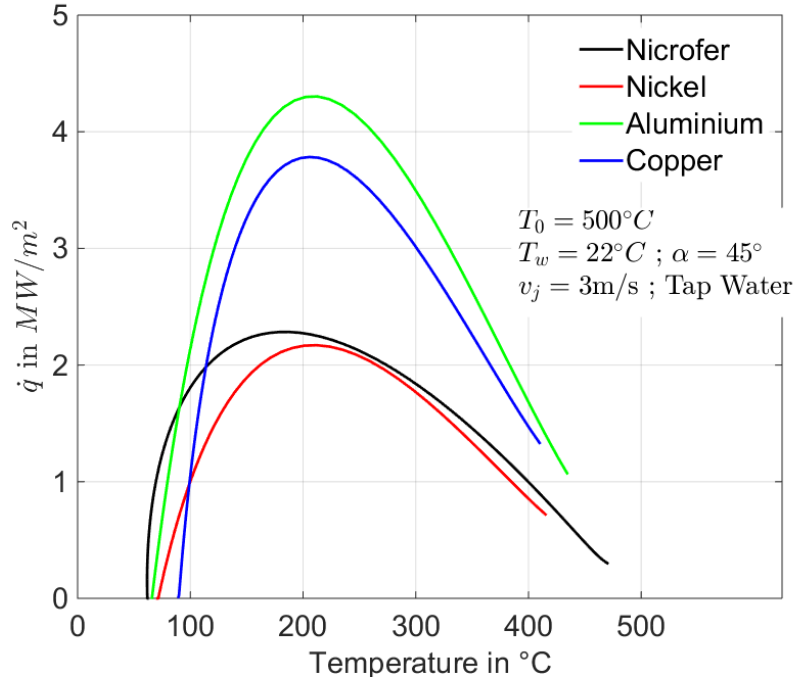


Figure 5.19: Boiling curve for different metals

Table 5.7: Width of various fronts for different metals

| | Copper | Aluminium | Nickel | Nicrofer |
|---------------------------|-----------|------------|-----------|------------|
| Pre-Cooling Region | 14.4 mm | 8.6 mm | 6.63 mm | 1.24 mm |
| Transition Boiling Region | 7.35 mm | 6.81 mm | 5.54 mm | 14.17 mm |
| Nucleate Boiling Region | 10.47 mm | 6.09 mm | 5.94 mm | 4.66 mm |
| Wetting front velocity | 9.86 mm/s | 21.49 mm/s | 7.07 mm/s | 11.71 mm/s |
| $T_s = 0.99 * T_0$ | 495°C | 485°C | 460.35°C | 475°C |
| $T_{z=0}$ | 395.35°C | 415.6°C | 391.18°C | 462.01°C |
| T_{DNB} | 205.7°C | 212.7°C | 212°C | 187.8°C |

6. Water Ejection - Phenomenon and Physical Understanding

6.1 Introduction

During the course of experimental analysis, a phenomenon was observed because of which the lower region of the metal sheet experience slower cooling for a prolonged period of time. Because of this, the lower portion of the metal sheet is at a higher temperature than the middle portion as depicted in **Fig. 6.1**. Upon further investigation, it was observed that this was caused because water film was ejected away from the surface of the metal sheet. Hence, there was no contact of water with the hot metal sheet in the bottom region. During the course of experiments, the front was observed to collapse and propagate downstream to wet and cool the bottom region. In some cases, this phenomenon was observed for a long time till the end of the experiment. The film collapse occurred at the end of the experiment when the plate moment stops. The film was then observed to propagate downstream rewetting the surface.

In this case was observed to be similar to quenching in case of stationary sheet mechanism **Ch. 5** with the sheet at a lower temperature than initial temperature. **Fig. 6.2** shows the infrared image of water ejection. It can be observed that the bottom region is at a higher temperature compared to the middle region. Also, it can be observed that the wetting is occurring only near to the center line. First wetting is not symmetric along the width of the hot metal sheet. Because of this, it can be concluded that wetting front propagation will be a 3D phenomenon and will have extra variables like the width of the wetting region at first collapse. These parameters are difficult to determine hence a qualitative thermal analysis of ejection phenomenon is conducted.

This phenomenon resulted in different cooling characteristics with the same quenching parameters, hence this phenomenon needs to be quantified and investigated further. For this reason, this chapter describes the experiments conducted under various parameters to quantify the influence of parameters like:

- Temperature of Water
- Thickness of Metal Sheet
- Casting Speed
- Jet Velocity
- Jet Impingement Angle
- Initial Temperature of Metal Sheet
- Quality of Water

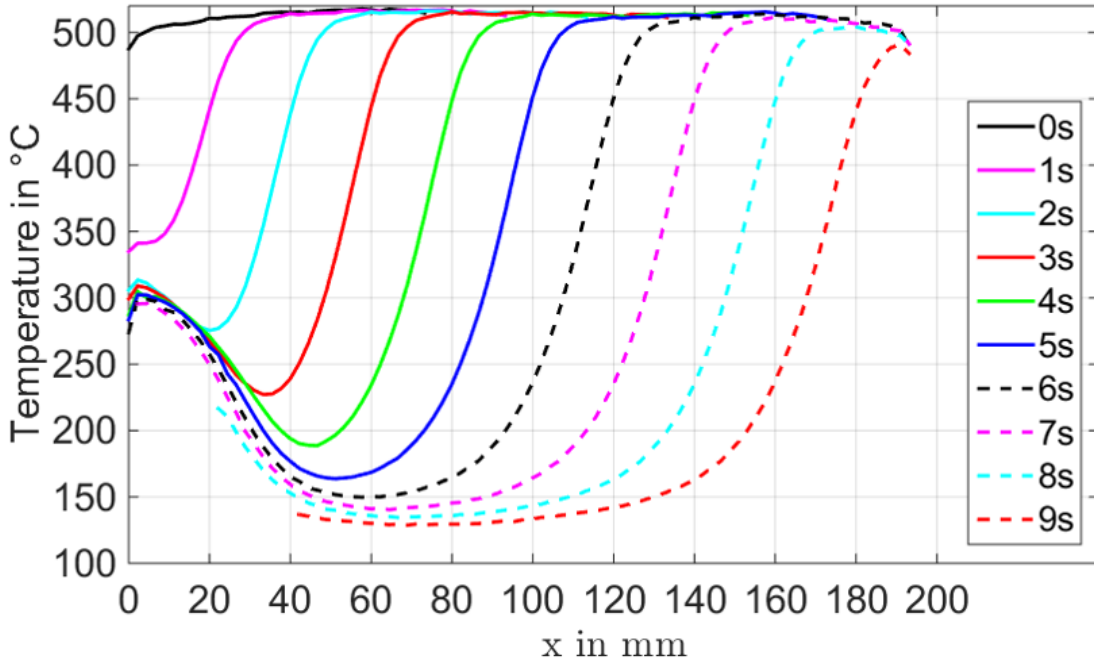


Figure 6.1: Temperature profile of water ejection observed during quenching of a 10 mm, AA6082 sheet at an initial temperature on 500° with tap water jets at an angle of 45°, velocity of 2.1m/s and water temperature of 30°

This phenomenon is expected to occur because of different heat transfer mechanisms in the impingement zone and in the free falling zone during metal quenching. In the impingement zone, as discussed in **Ch. 4**, the water jet impinges with horizontal and vertical momentum. Because of this, the water film has high Reynolds number and experiences a turbulent flow. Because of turbulence, it can be imagined that the bubbles produced near the metal surface can quickly move away from the surface creating space for fresh cold water for further cooling. Because of this the metal will experience high heat flux in the impingement region. Also, because of horizontal momentum, the water jet has the energy to breach the film layer to cool the metal surface. This will result in higher Leidenfrost temperature or temperature at which the hot metal experiences water cooling.

In the free falling zone, the water sheet has only vertical momentum and no horizontal momentum. The flow in the free falling zone is observed to be smooth and laminar. Because of this, it can be imagined that the heat transfer characteristics will be different. In this free falling zone, the water jet has no horizontal momentum, if the bubbles in the water film increases, it can through the water film away. This results in a dry region below the wet region. The temperature at which the water cooling starts in the free falling zone can be referred to as wetting temperature T_{wet} .

During the quenching of hot moving metal sheet, if the cooling in impingement zone is not sufficient then the surface temperature at the exit of impingement region will be higher. Is this temperature is more than the wetting temperature T_{wet} in the free falling zone, it can be imagined that the water stream will be thrown away from the metal surface, causing water ejection phenomenon. This ejection phenomenon

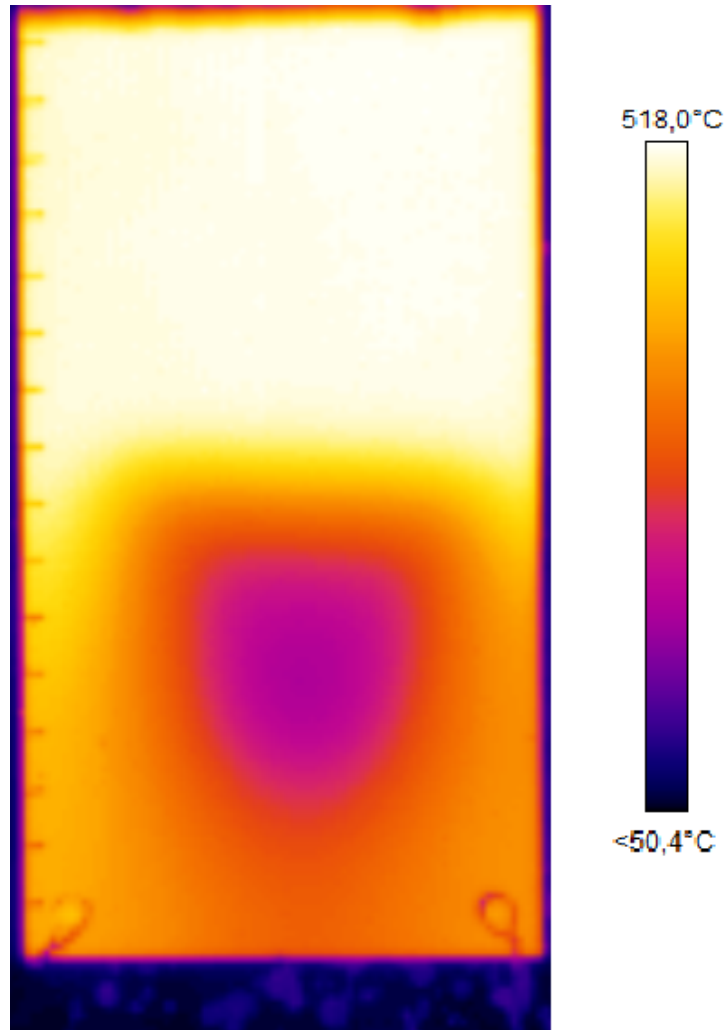


Figure 6.2: Infrared image of water ejection observed during quenching of a 10 mm, AA6082 sheet at an initial temperature on 500° with tap water jets at an angle of 45°, velocity of 2.1m/s and water temperature of 30°

is observed predominantly in the bottom region of the metal sheet, as temperature drop because of diffusion of heat is not present in this region. In some cases, the film collapses gradually because of additional cooling caused by diffusion of heat.

To replicate this phenomenon in FE simulations, following additional parameters are required for applying the thermal boundary conditions:

- Boiling curve in impingement zone
- Boiling curve in free falling zone
- Width of impingement zone

The boiling curve for impingement zone can be considered as obtained from quenching of the moving metal sheet, as the cooling occurs in a small region where water has momentum in the horizontal direction. The boiling curve and influence of various parameters on the boiling curve are studied and quantified in previous chapter **Ch. 4**.

The free falling zone, where cooling occurs when water stream has only vertical momentum, is similar to cooling occurring in stationary sheet quenching. Where water first impinges on the top portion of the hot metal sheet and the wetting front propagates downwards. The boiling curve and influence of various parameters on the boiling curve are studied and quantified in previous chapter **Ch. 5**. But to distinguish between the impingement zone and free falling zone, the width of impingement zone is required.

6.2 Boiling Curve

The thermal boundary condition for the impingement zone and the free falling zone are transient in nature and are dependent on various parameters. So a boiling curve is used to determine the surface heat flux. A quadratic interpolation between the heat flux and the surface temperature is considered in the transition and nucleate boiling region. It is observed that a quadratic interpolation provides better approximation compared to a linear approximation. Depending on the casting parameters, the points of the boiling curve will change, changing the heat transfer characteristic. Following are the boiling curve parameters:

- \dot{q}_{max} , maximum heat flux
- \dot{q}_{100} , saturation heat flux
- \dot{q}_{Le} , Leidenfrost heat flux
- T_{DNB} , departure from nucleate boiling temperature
- T_{100} , saturation temperature i.e. 100°
- T_{Le} , Leidenfrost temperature

The heat flux on these boiling regions can be determined with these boiling parameters.

Forced Convection Regime

For both, the impingement zone and free falling zone when the ingot surface temperature is less than the saturation temperature, $T \leq T_{100}$, the heat flux q can be given by the following equation:

$$\dot{q} = (14.6 \times (T + 273) + 68.5 \cdot (T_f + 273) - 21500) \times \sqrt[3]{Q} \times (T - T_f) \quad (6.1)$$

where, Q is the water flow rate in $L/(m \times min)$, T_f is the final water temperature in °C.

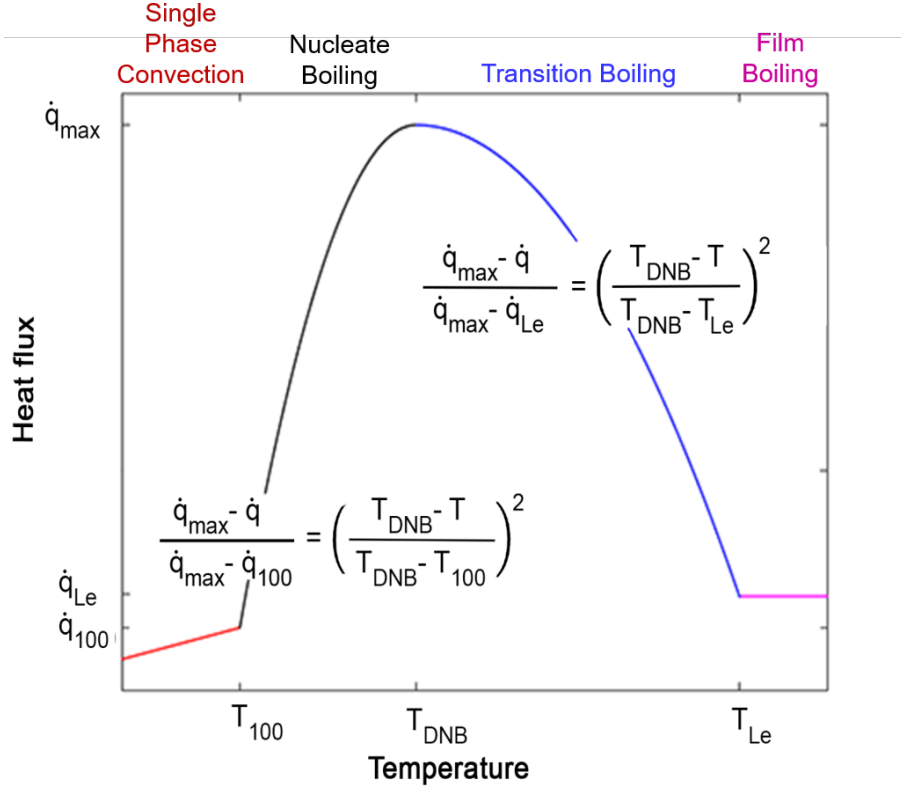


Figure 6.3: Quadratic function of boiling curve

Nucleate Boiling Regime

The nucleate boiling region exists above a surface temperature of 100° and temperature less than DNB temperature. In the nucleate boiling region there is contact between cooling water and the hot surface. Since the surface temperature is above the boiling temperature, it will result in the formation of bubbles. The heat flux increases with increasing surface temperature. The heat flux in this region can be determined with the following equation:

$$\dot{q} = \dot{q}_{max} - \left(\frac{T_{DNB} - T}{T_{DNB} - T_{100}} \right)^2 \times (\dot{q}_{max} - \dot{q}_{100}) \quad (6.2)$$

Transition Boiling Regime

Transition boiling region exists above a surface temperature of DNB temperature and less than the Leidenfrost temperature or the rewetting temperature. There is partial contact between the hot metal surface and cooling water, because of this heat flux reduces with increasing temperature. The heat flux in this regime for impingement zone can be determined with the following equation:

$$\dot{q} = \dot{q}_{max} - \left(\frac{T_{DNB} - T}{T_{DNB} - T_{Le}} \right)^2 \times (\dot{q}_{max} - \dot{q}_{Le}) \quad (6.3)$$

and for the free falling region, the heat flux can be determined with following equation:

$$\dot{q} = \dot{q}_{max} - \left(\frac{T_{DNB} - T}{T_{DNB} - T_{Le}} \right)^2 \times (\dot{q}_{max} - \dot{q}_{RW}) \quad (6.4)$$

Film Boiling or Ejection Regime

For higher surface temperature, the heat flux remains constant. In impingement zone, at a higher surface temperature a vapor film is formed on the surface and hence heat flux remains constant at \dot{q}_{Le} . For the free falling region, when the surface temperature is higher than rewetting temperature, water splashes away from the surface, causing less heat flux on the surface of \dot{q}_{RW} .

6.3 Width of Impingement Zone

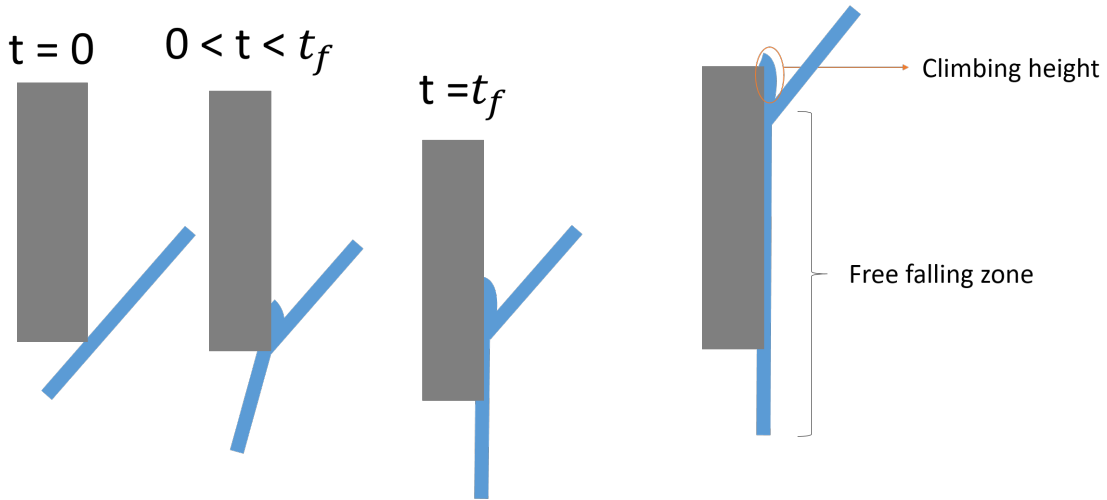


Figure 6.4: Methodology used to determine width of impingement zone

As discussed previously, the heat transfer in the impingement zone and the free falling zone will be different. In case of DC casting, the dimensions of the casted ingot are high and the cooling is not completed in the impingement zone. Hence, it is required to distinguish between the impingement zone and the free falling zone. For this reason, it is important to determine the width of the impingement zone. This is particularly important during the transient start-up phase because of high temperature phenomena like film boiling in impingement zone and water film ejection in the free falling zone.

By definition, the impingement zone is the zone where the water stream has horizontal momentum. The water jet will split when it impinges metal sheet, once stream will climb above the point of impingement and the second part will travel down in direction of gravity. Numerically it is difficult to determine the width if these two streams because of the high number of variables. Hence, a visual experimental method to obtain a rough estimate of the width of impingement zone is required.

In order to determine the width of impingement zone, the climbing height and the width of the downward stream are determined separately. The metal sheet at room temperature is placed in the experiential setup and is lowered in small steps. The first point of contact between the water jet and metal sheet can be observed and is noted. At this point, the water jet starts to splash and just after this point the jet comes in contact with the metal plate but at the jet stream is not vertical at the bottom edge of the sheet. In other words, the water jet has horizontal momentum at the bottom edge hence the bottom edge is still in the impingement zone. As the sheet moves downwards, the water stream starts to become vertical and beyond this point, the stream remains vertical. As the water stream is vertical, at the bottom edge the water jet has no horizontal momentum and the impingement zone has ended. This point can be observed and considered as an endpoint for the downward stream. With these two points, the width of the downward stream can be determined.

The metal sheet will be lowered further and at a point, it can be observed that the water is coming in contact with the top edge of the metal sheet and touches the top surface and measuring side of the sheet. The first point where the water jets touches the top surface is observed and noted. From this the distance the metal sheet has displaced from the first contact with the bottom edge to contact of water jet with the top edge can be determined and the climbing height will be the difference between the height of the plate and this displace of the plate.

With this, the width of the downward stream and climbing height can be determined to get the width of impingement zone. This width of impingement zone is also verified by taking the metal sheet of height same as the width of impingement zone determined by this experimental methodology. When these small sheets were placed in the experimental setup, it is observed that at one position the downward stream is vertical and the water is not touching the top surface of the plate. From this position, if moved upward, the downward stream is not vertical and if lowered, the water is climbing the sheet and exiting from above. Hence the dimension of the metal sheet is the width of impingement zone. The width of impingement zone is determined experimentally for various jet velocities and jet angles. It can be imagined that the width of impingement zone will also depend on the bore diameter, but the influence of this is not studied as this will depend on mold design.

Table 6.1: Width of impingement zone for jet angle of 45°

| Jet Velocity | Climbing Hight | Down Stream Impingement zone | Width of Impingement zone |
|----------------|----------------|------------------------------|---------------------------|
| 2.1 <i>m/s</i> | 5 <i>mm</i> | 10 <i>mm</i> | 15 <i>mm</i> |
| 2.4 <i>m/s</i> | 8 <i>mm</i> | 10 <i>mm</i> | 18 <i>mm</i> |
| 2.7 <i>m/s</i> | 10 <i>mm</i> | 9 <i>mm</i> | 19 <i>mm</i> |
| 3.0 <i>m/s</i> | 12 <i>mm</i> | 11 <i>mm</i> | 23 <i>mm</i> |
| 3.3 <i>m/s</i> | 14 <i>mm</i> | 8 <i>mm</i> | 22 <i>mm</i> |

6.4 Mechanism of Heat Transfer

The heat transfer because of water ejection is dynamic and nonuniform. Hence it is required to investigate the heat transfer further. It is observed that ejection is

Table 6.2: Width of impingement zone for jet velocity of 3.0 m/s

| Jet angle | Climbing Hight | Down Stream Impingement zone | Width of Impingement zone |
|-----------|----------------|------------------------------|---------------------------|
| 15° | 7 mm | 15 mm | 22 mm |
| 30° | 10 mm | 11 mm | 21 mm |
| 45° | 12 mm | 11 mm | 23 mm |
| 60° | 13 mm | 8 mm | 21 mm |

predominately observed in the lower portion of the hot metal sheet. During the DC casting process, similar ejection is observed during the start-up region. This causes uncontrolled cooling in the bottom region, causing failures like hot tearing.

When the film collapse the upper portion has not experienced any cooling and the bottom region, experiences water ejection causing slow cooling. Because of this, there is diffusion of heat that occurs from the lower portion and upper portion as shown in **Fig. 6.5**.

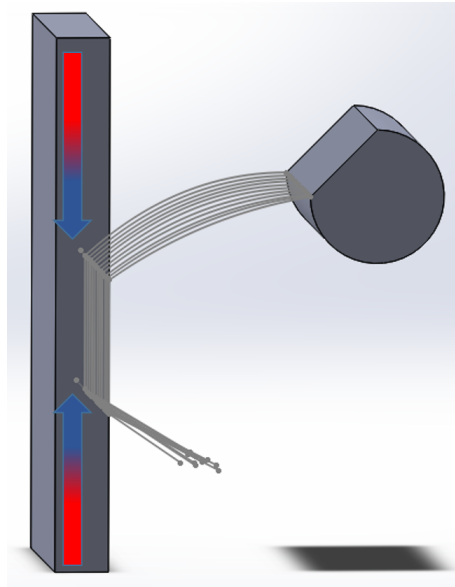


Figure 6.5: Heat transfer mechanism during water ejection

6.5 Simulation of Water Ejection

Simulating the physics behind the water ejection phenomenon will help validate the hypothesis and provide a better understanding of this phenomenon. For this a FE model in *COMSOL MULTIPHYSICS* is developed. This model consists of metal sheet at the required initial temperature and the thermal boundary condition growing with time, depending on casting velocity v_c . The quenching region is further divided into 2 zones, namely impingement zone, and free falling zone. In the impingement zone, the boiling curve from the moving sheet analysis and in the free falling zone the boiling curve from stationary sheet analysis is applied. This model is described in **Fig. 6.6**.

The simulation is conducted for a 10 mm AA6083 sheet at 500°, with 30°C tap water jets at an angle of 45° at a velocity of 2.1 m/s. In this case water ejection was

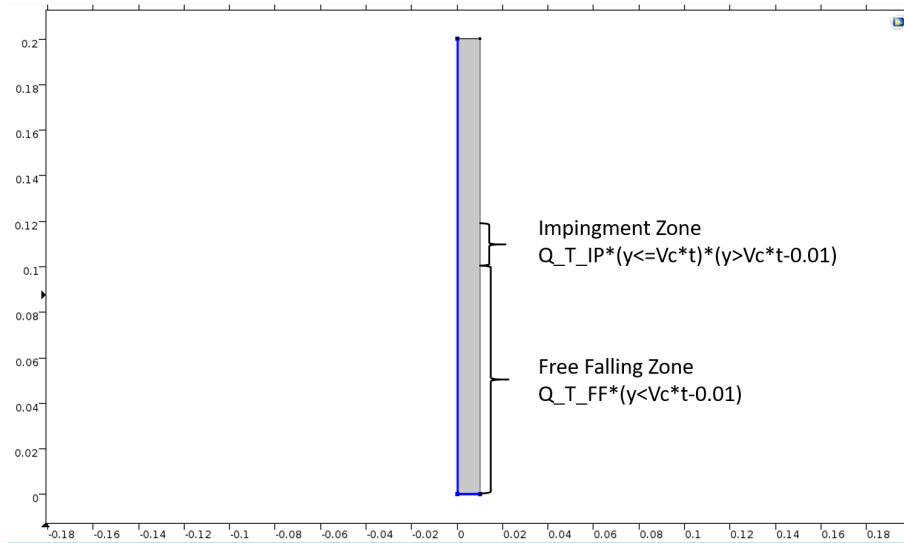


Figure 6.6: Model for simulating the water ejection phenomenon.

observed and the temperature profile is depicted in figure **Fig. 6.1**. The boiling for impingement zone is as obtained from the experimental results, as depicted in **Fig. 6.7**. As it is seen during the experimental analysis, change in water temperature and jet velocity does not have significant influence on the boiling curve in impingement zone. So this boiling curve should provide correct heat flux for the experimental parameters.

In the free falling zone, there is one physical difference in stationary sheet analysis and water ejection experiments. In case of stationary sheet analysis, the impingement zone is cooled and there is no significant change water temperature till it reaches the wetting front. But in case of water ejection experiments, the quenching water first comes in contact with hot metal in impingement zone and the temperature of the water is higher than the initial water temperature in the free falling zone. From the experiments it can be observed that the water temperature has a strong influence on heat transfer in the free falling zone. Hence this physical effect also needs to be incorporated, by modifying the boiling curve in the free falling region. Because of this, the boiling curve used in the free falling zone is as depicted in **Fig. 6.7**.

The temperature profiles from the simulation are as depicted in figure **Fig. 6.8**. It can be seen that the temperature profile is similar to water ejection as in **Fig. 6.1**. Hence it can be validated that the hypothesis for dividing the quenching region into 2 zones with distance boiling curves is acceptable.

6.6 Results and Discussion

During the casting process, it is critical to control the water ejection. Sengupta et al. [54] has concluded that during hot casting i.e. when the water is completely ejected from the surface, but-curling is reduced significantly. But the slow cooling in the bottom region might result in other failures like hot tearing can occur. Hence it is important to control the water ejection in order to avoid these failures. The influence of various parameters can be simulated using the FE model and this influence is also validated experimentally.

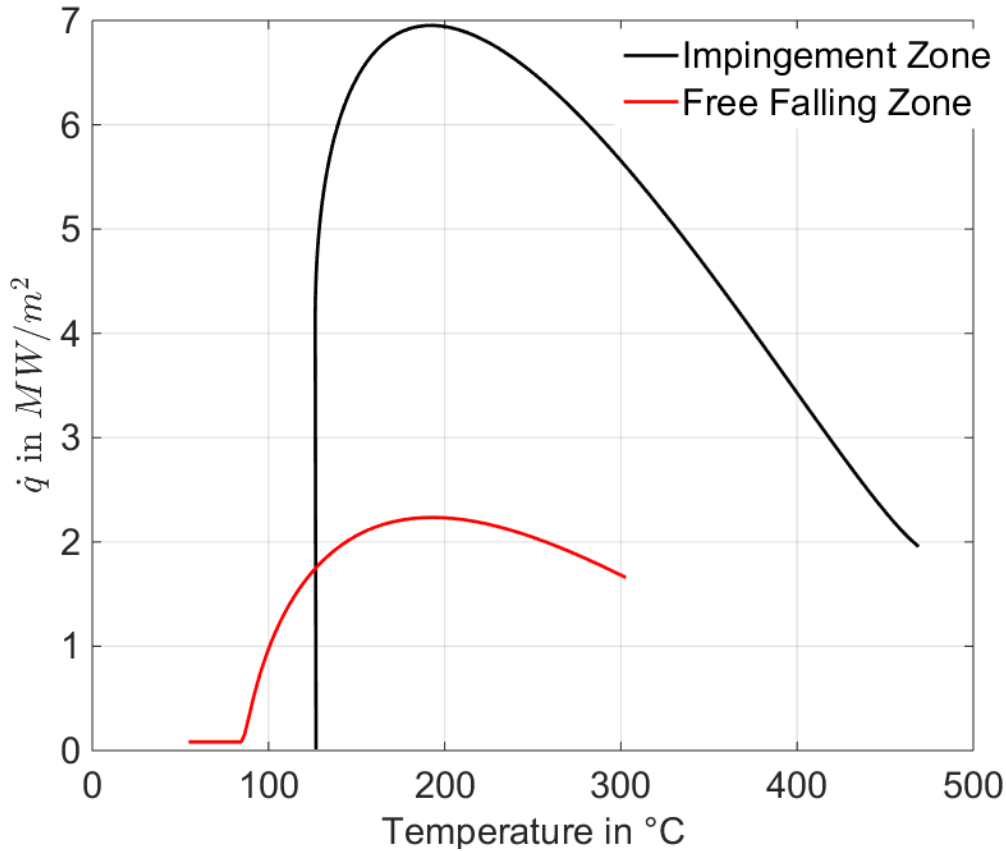


Figure 6.7: Boiling curve for impingement zone for simulating 10 mm AA6083 sheet at 500°, with 30° tap water jets at an angle of 45° at a velocity of 2.1 m/s

6.6.1 Temperature of Water

It is observed that the temperature of the water has a strong influence on the occurrence of water ejection. This phenomenon is also observed during investigation of water temperature in free falling zone. With increase in water temperature, the rewetting temperature is lower and the maximum heat flux along with wetting front velocity is also significantly lower. Water temperature is found to have not much effect on cooling in impingement zone.

Since water temperature has minimal effect in impingement region and lowers the boiling curve in free falling region significantly, it can be imagined that increasing the water temperature increases the occurrence of water ejection. Similar results were also obtained from simulations. During the experimental analysis, it is observed that a 10 mm AA6082 sheet at initial temperature of 500°C moving at casting speed of 20 mm/s quenching with tap water jets at an incline of 45° with a jet velocity of 2.1 m/s, demonstrated no ejection at lower temperatures till 30°C water temperature. At water temperatures above 30°C water ejection was observed.

From this, it can be concluded that temperature of water has significant influence on water ejection phenomenon. During industrial casting, if it is required to increase the wetting front velocity in the ejection region, lowering the water temperature temporarily will speed up the cooling in the bottom region.

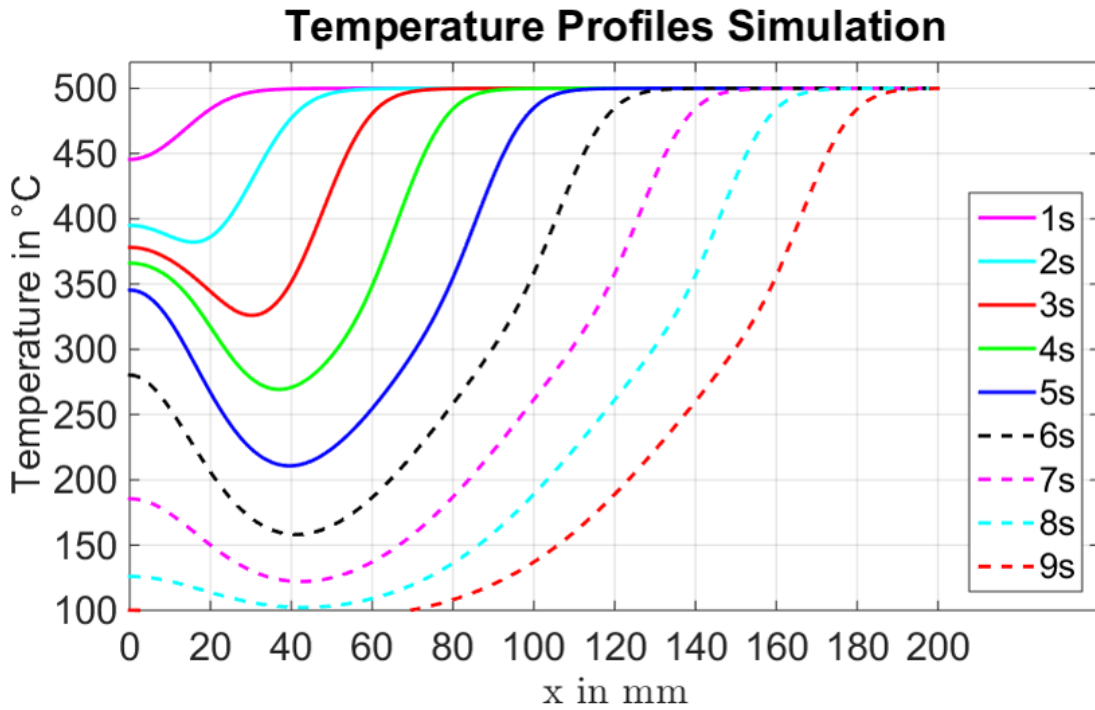


Figure 6.8: Simulated Temperature profile of water ejection observed during quenching of a 10mm, AA6082 sheet at an initial temperature of 500° with tap water jets at an angle of 45° , velocity of $2.1m/s$ and water temperature of 30°

6.6.2 Thickness of Metal Sheet

It can be imagined that the thickness of metal sheet will have strong influence on the water ejection, as with changing thickness the heat capacity of the system also changes. A thicker metal plate with more heat capacity will have lesser cooling in the impingement zone resulting in more water ejection. The maximum heat flux in impingement zone also depends on the thickness of sheet. It was observed during the experimental investigation that thicker sheet has slightly higher maximum heat flux beyond 5 mm thickness. In the free falling zone also it can be observed that the maximum heat flux, re-wetting temperature, and wetting front velocity decreases strongly with increasing thickness.

Since the effect of thickness beyond 5 mm in the impingement zone is slight and significant in the free falling zone and also the change in heat capacity of the system, it can be imagined that thickness has a strong influence on water ejection. Similar results were also obtained from simulation. In the impingement width, the 5 mm sheet is cooled to a fairly lower temperature than 10 mm sheet and the temperature at end of impingement zone is lower than wetting temperature, no water ejection can be observed. During experimental analysis also no ejection was observed for 5 mm sheet even for higher water temperatures.

6.6.3 Casting Speed

By varying the casting speed, the Peclet number will change. This will change the diffusion of heat in the pre cooling region. Also, by changing the casting speed,

the time spent by metal sheet in the impingement zone will change, changing the cooling in this region. If the casting speed is lower, the sheet will experience cooling in impingement zone longer and if the surface temperature is lower than the rewetting temperature, the sheet will experience no water ejection.

In the impingement zone, from the experimental investigation, it can be concluded that by decreasing the casting speed, the metal sheet has more time for diffusion of heat in the quenching region. This lowers the interface temperature and decreases the maximum heat flux slightly. By decreasing the casting speed, there will be more heat transfer between water and hot metal sheet in the impingement zone. This will increase the water temperature, reducing the rewetting temperature. But it can be imagined that the effect of more cooling is stronger than the increase in water temperature. Because of this, it can be observed from simulation results, that water ejection decreases with decreasing casting velocity. This can also be observed from experimental investigation. For a 10 mm AA6082 sheet, initially at 500° when quenched with water at 30°, with jet velocity of 2.1 m/s and an angle of 45°. When the casting speed was maintained at 20 mm/s water ejection was observed and when the casting speed was reduced to 16 mm/s no ejection was observed. For casting velocities higher than 25 mm/s complete ejection was observed. At a casting speed of 17 mm/s as critical velocity was observed at which only slight ejection was observed.

6.6.4 Jet Velocity

The water jets are inclined to vertical plane, because of which by changing the jet velocity, the vertical momentum in the free falling zone also changes. Because of this, the wetting front velocity increases in the free falling zone which increases the maximum heat flux and the wetting front velocity also. This is discussed previously. In the impingement zone, it is observed from the experimental investigation that there is no significant change in boiling curve.

The width of impingement zone will also change with changing jet velocity. By increasing the jet velocity the width of impingement zone will increase. Because of this the metal sheet will experience high heat flux for a longer time, reducing the temperature at the end of impingement zone, hence reducing water ejection. Also by increasing the jet velocity, the water flow rate also increases, which will reduce the increase of water temperature at beginning of free falling zone. This will increase the wetting front velocity and wetting temperature, hence reducing water ejection.

From simulations also it can be observed that increasing the jet velocity, decreases water ejection. Similar influence was also observed in experimental investigation conducted on a 10 mm AA6082 sheet at an initial temperature of 500° moving at a casting speed of 20 mm/s, cooled with tap water jets at an angle of 45° at a temperature of 30°. At a jet velocity of 2.1 m/s significant ejection was observed as shown in figure **Fig. 6.1**. At a jet velocity of 2.4 m/s just a slight ejection was observed making this casting speed critical for this water flow rate and when the jet velocity was increased further, no water ejection was observed.

6.6.5 Jet Impingement Angle

In the impingement zone, the jet angle has an influence on the boiling curve. By decreasing the angle, it is observed that the heat flux also decreases and the DNB

temperature increases. Whereas, in the free falling zone the effect is opposite. By decreasing the jet angle, the vertical momentum increases, which leads to increase in wetting front velocity, increasing maximum heat flux. The rewetting temperature also increases with decreasing angle.

The width of impingement zone also changes with changing the jet angle. Because of this quantifying the water ejection for different jet angles is complicated. From simulations, the net influence of jet angle is that by increasing angle, the water ejection decreases slightly. Because of opposite influence factors, the jet angle is observed to not have a strong influence on water ejection. From experimental analysis also, it is observed that for a 10 mm AA6082 sheet initially at a temperature on 500° moving at a casting speed of 20 mm/s, quenching with 30° tap water jets at a velocity of 2.1 m/s. At a jet angle of 45° water ejection was observed as depicted in **Fig. 6.1**, when the jet angle was increased to 60° very slight ejection was observed and when the jet angle was decreased to 30° complete ejection was observed.

6.6.6 Initial Temperature of Metal Sheet

As discussed previously that beyond an initial temperature of 450°, the maximum heat flux does not change significantly in impingement zone and free falling zone as well. But since the heat capacity of the system changes, the temperature of the metal sheet is lower while exiting the impingement zone for lower initial temperature. Because of this ejection decreases significantly with decreasing initial temperature. Similar results can be observed from simulations and from experimental analysis. When the experiments were conducted on a 10 mm AA6082 sheet, moving with a casting speed of 20 mm/s, quenching with tap water at 30° with a jet velocity of 2.1 m/s at an inclination of 45°. At an initial temperature of 500° water ejection was observed as seen in figure **Fig. 6.1**, but when the initial temperature was reduced to 450° there was no water ejection observed. With this, it can be concluded that the initial temperature of the metal sheet has a strong influence on water ejection.

6.6.7 Quality of Water

In impingement zone it is observed from the experimental analysis, water quality has no significant influence on the heat flux in the impingement zone whereas, as discussed previously, water quality has a significant influence on heat flux in the free falling zone. In free falling zone, for distilled water, the heat flux and DNB temperature are higher. The wetting temperature is higher in case of tap water. Because of this from simulations, it can be concluded that the water ejection is more for distilled water compared to tap water. This means with more salt content water ejection decreases.

Similarly from the experimental analysis when the experiments were conducted on a 10 mm AA6082 sheet initially at 500°, moving with a casting speed of 20 mm/s, quenching with water at 22° with a jet velocity of 2.1 m/s at an inclination of 45°, slight ejection was observed in case of distilled water, whereas no ejection is observed in case of tap water. At 27° water temperature in case of tap water, slight ejection was observed and very significant ejection was observed in case of distilled water. With this, it can be concluded that quality of water has an influence on water ejection.

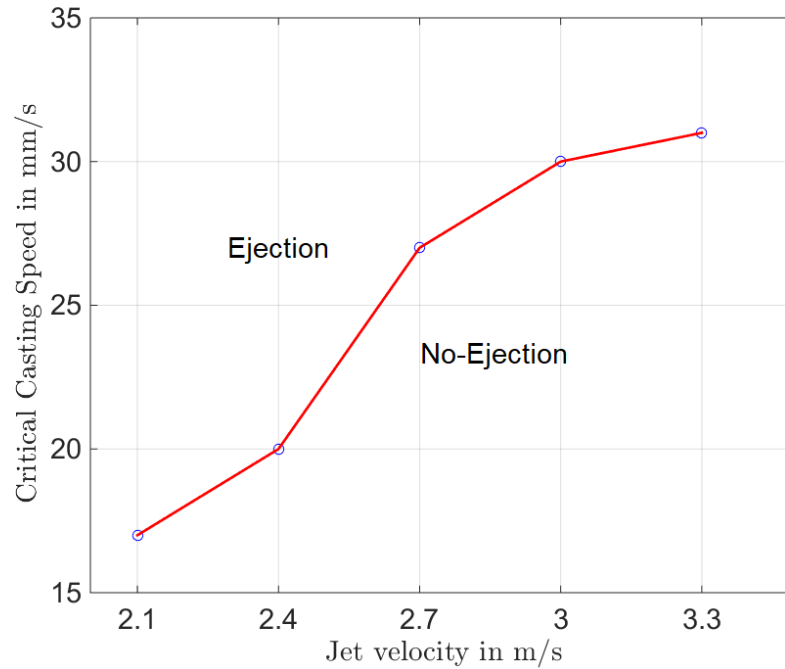


Figure 6.9: Plot of critical velocity and water flow rate during quenching of an 10 mm, AA6082 sheet at an initial temperature on 500° with tap water jets at an angle of 45° and water temperature of 30°

6.7 Critical Casting Speed

During industrial casting, controlling casting parameters like the temperature of metal cannot be varied as it influences various other factors. Jet impingement angle is also determined by various factors in mold designing. The thickness of casting also cannot be varied during the casting. The temperature of water can be controlled to some degree but it is very expensive considering the energy required for cooling the water.

So the parameters that can be controlled are primarily casting speed and the jet velocity. Hence it is important to find critical casting velocity for different water flow rate. For this experiments were conducted on a 10 mm AA6082 sheet at an initial temperature of 500° , quenching with tap water at 30° with a jet at an inclination of 45° . The jet velocity was varied from 2.1 m/s to 3.3 m/s and a critical casting speed was determined by conducting a number of experiments for each jet velocity. The results from this critical casting speed for different jet velocities is as shown in figure **Fig. 6.9**.

From this figure, it can be seen that with increasing the jet velocity the critical casting speed also increases. The increase is very strong at 2.7 m/s jet velocity. It can be seen that the plot grows asymptotic to the horizontal axis. Which means that beyond a certain casting speed, no matter how much water flow increases, ejection cannot be avoided. This means that water flow rate can influence water ejection only in a certain range.

The importance of this figure is that with this figure, we can determine if ejection will occur or not. If for a jet velocity and casting speed lies above this curve, water ejection will occur and if it lies below this curve there will be no ejection.

7. Implementing Laboratory Results to Industrial DC Casting Process Simulation

Simulation of DC casting process is crucial for process optimization and for process improvement. In the previous chapters, an effort has been made to understand the heat transfer mechanism in the DC casting process. The main focus is the start-up phase because of its transient nature and higher susceptibility to failures. For this, transferring the results from laboratory experimentation to the industrial process simulation is necessary.

In order to simulate the process, an FE model capable of simulating thermal, mechanical and metallurgical field is developed. The temperature scale is initially from a molten phase to room temperature, because of which non-linear temperature dependent material properties along with a non-isothermal solidification model. In order to simulate the growth of the ingot, new elements are added along the casting direction, depending on the casting speed.

The thermal boundary conditions, applied to the model needs to be validated. For this temperature measurements are conducted in the casting process, by inserting thermocouples in the molten metal. These thermal boundary conditions can be applied to the FE model in order to study the evolution of stresses.

7.1 Extending Laboratory Results for DC Casting

From the experiments performed in the laboratory, transfer the results and the physical understanding to industrial DC casting is an important step. The heat transfer during the quenching process is sensitive to the quenching apparatus. Also in the experiential analysis, solidification is neglected. The solidification of alloy will release latent heat causing the heat capacity of the ingot to increase. This will also effect on the boiling curve and needs to be compensated. But the results obtained from the experimental results provide an initial approximation for fitting the data obtained from the in-situ experiments.

From the various experiments performed to study the heat transfer characteristics in the impingement following important observations can be made:

- The maximum heat flux and DNB temperature depend on the interface temperature $T_{z=0}$. When the casting speed was changed for the 5 mm sheet to get the same interface temperature as for 10 mm and 3 mm sheet, the resultant boiling curves are similar. Hence it can be said that the boiling curve depends on the interface temperature. Although, it can be observed that when the interface temperature is above 420°C the change in the boiling curve is not very significant.

- The initial temperature also significantly changes the boiling curve. This is an expected influencing parameter as the heat capacity of the system changes. But it is interesting to note that beyond the initial temperature of 450°C , the maximum heat flux remains constant, though the DNB temperature changes slightly. Once again it can be seen that when the interface temperature is above 428°C , the boiling curve does not change significantly.
- The boiling curve also depends on the material properties. Because of this, it can be seen that the boiling curve changes significantly for different metals.
- Quenching parameters like quality of water, water flow rate, jet impingement angle and temperature of the water does not have a very significant influence on the boiling curve. Surface properties like surface rough also resulted in identical cooling characteristics.

Hence, a boiling curve where the maximum heat flux is around $7\text{ MW}/\text{m}^2$ and a DNB temperature of 180°C is a suitable assumption for boiling curve in impingement zone. In the start-up phase, the pulsating water jet is used. This will increase the transient nature of the boundary condition. This also places strong constraints on the time step and the meshing for the simulation. Simulating the exact pulsating water flow is neglected. But the physical effect of this is considered by incorporating film boiling in the thermal boundary condition. This assumption will decrease computational effort significantly, will avoid fluctuations in the solution and consider the physical effect involved as well. During industrial casting, to change the cooling in the impingement zone, water flow rate can be changed to vary the width of impingement zone or the mold design with 2 rows of jets can be used to increase the width of impingement zone. The width of impingement zone will also influence the upward conduction distance i.e. the distance from which the diffusion of heat in the axial direction is significant, In order to obtain better surface quality and less macrosegregation, it is important that the upward conduction distance should be the meniscus position. If this distance is lesser, the solidified meniscus can be remelted causing various failures as described in previous chapter **Ch. 1**.

The heat transfer characteristics in the free falling zone are complicated as the wetting front velocity is also a variable. The heat transfer characteristics will change because of laminar flow of the stream. But the following conclusions can be made from the experimental analysis.

- Water quality has a significant influence on the boiling curve. The wetting front velocity and the rewetting temperature changes with water quality.
- Jet angle and jet velocity also influences the vertical momentum and hence wetting front velocity and boiling curve.
- Water temperature is having a high influence on the wetting characteristics. Increase in water temperature reduces the wetting front velocity and maximum heat flux.
- For tap water the DNB temperature is in the range of $180\text{-}200^{\circ}\text{C}$ for all the cases.

- The maximum heat flux remains constant for initial temperature above 450°C . Although the temperature of the casting is lower than this, the maximum heat flux does not change significantly.

7.2 Mathematical Modeling of DC Casting Process

In industrial DC casting process, the bottom block is withdrawn with casting velocity and the mold is fixed. The ingot grows because liquid melt is continuously added from the top. However, in the FE model, the bottom block and ingot are kept fixed and the primary and secondary cooling is incorporated by moving the thermal boundary condition with casting velocity. Addition of melt is considered by adding new elements on top of the ingot, along with the casting direction. This way of modeling eliminates the continuous change in spatial coordinates of the material point. The liquid phase is treated as a fictitious solid, neglecting its flow.

The DC casting model is divided in to two parts:

- Thermal model
- Mechanical model

The thermal model consists of solidification model and an interface heat transfer model. The change in temperature will induce phase transformation, releasing latent heat will affect the thermal field. Hence the heat conduction and phase field have to be modeled simultaneously. From the knowledge of temperature change at every instant, the thermal strain can be computed. An in-house developed FE model by Nallathambi [57] is extended to simulate the DC casting process. In this section, a brief overview of the model is provided.

7.2.1 Thermal Modeling

The objective of thermal modeling problem is to find the temperature evolution inside the ingot. To achieve this, the phase-change phenomenon has to be modeled which strongly influence the heat conduction of the domain. Further, the primary and secondary cooling, thermal boundary conditions has to be defined properly. The heat transfer with the bottom block is considered based on a gap dependent model. Due to the transient nature of the DC casting process, the thermal model of the casting process is time dependent and account for temperature dependencies in thermophysical properties of the materials employed in the casting process. The assumptions of thermal modeling are considered as follows:

- Material is treated as an isotropic rigid heat conductor.
- Fluid flow in the liquid phase is neglected. Therefore, the liquid phase is treated as a fictitious solid.
- The dissipation due to mechanical deformation is negligible when compared to the latent heat released during solidification. Therefore, the solidification and mechanical problems are decoupled within the time step.

- The liquid convection is accounted in form of increasing the thermal conductivity above the liquidus temperature.
- There is no pore formation, i.e. $f_s + f_l = 1$, where f_s and f_l are solid and liquid phase fractions respectively.

Considering the above mentioned assumptions, the energy balance is obtained based on the first law of thermodynamics. The latent heat phenomena is incorporated in the balance equation through the definition of the specific internal energy. This way of incorporating the latent heat is commonly known as temperature-based fixed grid method. The moving phase-front boundary condition is automatically satisfied and gets cancelled once deriving the weak form of energy equation. A linear phase-change function is employed to capture the latent heat release. Based on this, the governing differential equation for the thermal problem can be written as:

$$\lambda \left(\frac{\partial^2 T}{\partial z^2} + \frac{\partial^2 T}{\partial y^2} \right) + Q = \rho C \frac{\partial T}{\partial t} \quad (7.1)$$

where, ρ is density, C is specific heat capacity, λ is the thermal conductivity, $\frac{\partial T}{\partial t}$ is the cooling rate and Q is the latent heat released during the phase change. Latent heat released during the phase change is proportional to the rate of solid fraction f_s according to the following relation:

$$Q = \rho L \left(\frac{\partial f_s}{\partial T} \right) \cdot \left(\frac{\partial T}{\partial t} \right) \quad (7.2)$$

where L is the latent heat released.

7.2.2 Solidification Model

A model considering the heat conduction and the change of phase simultaneously is known as a solidification model. Phase change is one of the critical phenomena that needs to be considered in modeling the DC casting process. A phase change model can be of two types as follows:

- Isothermal phase change
- Non-isothermal phase change

During the isothermal phase change, the domain of the heat conducting body Ω can be divided into liquid region Ω_l and a solid region Ω_s , as shown in **Fig. 7.1**. This kind of a phase change function is commonly observed during solidification of pure metals where solidification occurs at one temperature. In a non-isothermal phase change apart from solid and liquid region, there exists a mushy region Ω_m , as shown in **Fig. 7.2**. This kind of phase change function is observed during solidification of alloys. Because of alloying elements, the metal mixture solidifies over a range of temperature. Between the liquidus temperature T_l and solidus temperature T_s , the melt will exist as a partially solid and liquid mush. Phase front is the line that divides these regions where latent heat is released. The phase front temperature is

equal to the corresponding temperature and the Stefan condition should be satisfied as:

$$k_s \nabla \theta_s \cdot \vec{n}_s + k_l \nabla \theta_l \cdot \vec{n}_l - \rho L \vec{v}_p \cdot \vec{n}_l = 0 \quad (7.3)$$

where, k_s , θ_s and \vec{n}_s are the solid thermal conductivity, solidus temperature and the unit outward normal vector on the solid domain respectively. Similarly, k_l , θ_l and \vec{n}_l are the same field for the liquid domain and \vec{v}_p is the phase front velocity.

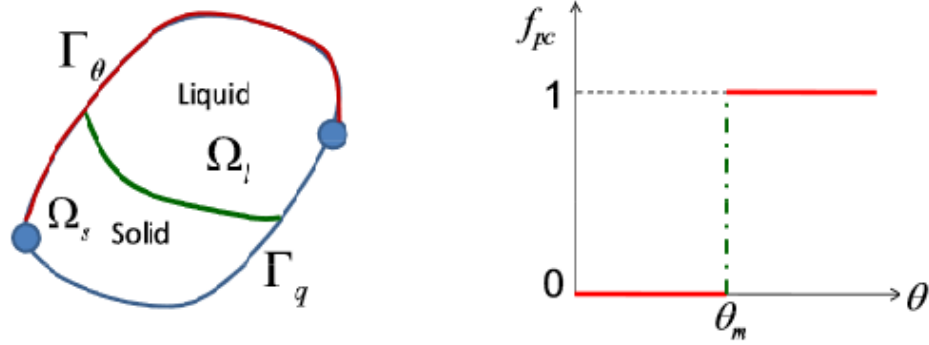


Figure 7.1: Domain and phase change function for isothermal phase change.

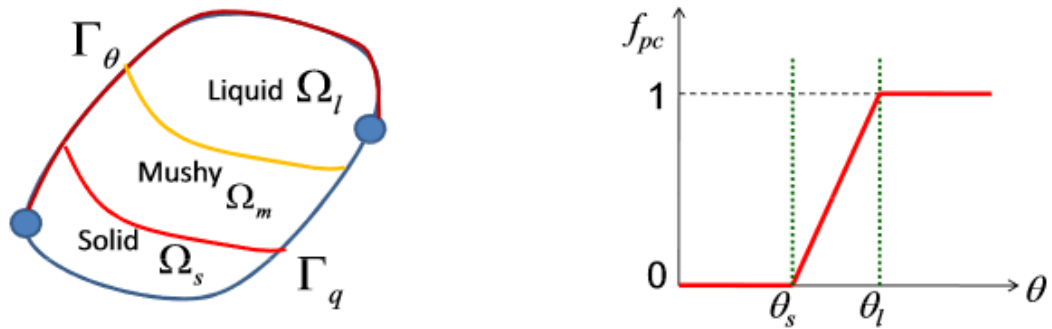


Figure 7.2: Domain and phase change function for non-isothermal phase change

The numerical phase change function for isothermal phase case can be written as follows:

$$f_{pc}(\theta) = \begin{cases} 1 & : \theta > \theta_m \quad \text{on } \Omega_l \\ 0 & : \theta \leq \theta_m \quad \text{on } \Omega_s \end{cases} \quad (7.4)$$

and for non-isothermal case as:

$$f_{pc}(\theta) = \begin{cases} 1 : & \theta > \theta_l \quad \text{on} \quad \Omega_l \\ 0 < g(\theta) \leq 1 : & \theta_l < \theta \leq \theta_s \quad \text{on} \quad \Omega_s \\ 0 : & \theta \leq \theta_s \quad \text{on} \quad \Omega_s \end{cases} \quad (7.5)$$

where, $g(\theta)$ is the phase change function. A simple linear approximation for phase change function is a linear one by the equation as:

$$g(\theta) = \frac{\theta - \theta_s}{\theta_l - \theta_s} \quad : \quad \theta_s < \theta \leq \theta_l \quad (7.6)$$

7.2.3 Mechanical Modeling

In DC casting process, the material is subjected to thermal stresses and strain due to strong thermal gradient during solidification. In order to model the mechanical fields of DC casting process, a displacement field should be derived from the momentum equation.

The equilibrium equation which yields the displacement solution \vec{u} is given as:

$$\nabla \cdot \mathbf{T} = \vec{0} \quad (7.7)$$

where \mathbf{T} is the stress tensor, which is given by:

$$\mathbf{T} = T_{ij} \vec{e}_i \otimes \vec{e}_j \quad (7.8)$$

The total deformation is assumed to be less than 4% and therefore small deformation theory is employed and total strain tensor \mathbf{E} can be decomposed into three components as thermal strain \mathbf{E}^t , elastic strain \mathbf{E}^e and inelastic strain \mathbf{E}^{ie} tensors as below,

$$\mathbf{E} = \mathbf{E}^T + \mathbf{E}^e + \mathbf{E}^{ie} \quad (7.9)$$

The thermal strain is a reversible strain which occurs in the solidification process in the absence of external mechanical load. The thermal strain is volumetric in nature. It can be computed using the coefficient of thermal expansion as:

$$\mathbf{E}^T = \alpha(\theta - \theta_{ref})\mathbf{I} \quad (7.10)$$

where, α is the coefficient of thermal expansion and θ_{ref} is the reference temperature at which thermal strain is zero.

Inelastic strain tensor \mathbf{E}^{ie} might be either rate dependent plastic or rate dependent viscoplastic strain tensor based on the material property and intensity of residual thermal stress.

The plastic strain occurs when the equivalent stress exceeds the yield stress. Plastic strain rate tensor \dot{E}_p can be estimated from the stress rate as follows,

$$\dot{\mathbf{T}} = C : (\dot{E} - \dot{E}^t - \dot{E}^P) = C^{ep} : \dot{E} \quad (7.11)$$

where, C^{ep} is the tangent elasto-plastic operator. The viscoplastic strain is a permanent deformation, which occurs after the application of load and continues to undergo a creep flow as a function of time under the influence of the applied load. \dot{E}^{vp} is the viscoplastic strain rate tensor and $\dot{\epsilon}^{vp}$ is the scalar viscoplastic strain rate. The equivalent viscoplastic strain rate can be formulated by the following two laws.

Garafalo Law

Garafalo law portrays the behavior of the solidified metal with no concept of yield surface. Equivalent viscoplastic strain rate $\dot{\epsilon}^{vp}$ can be defined as,

$$\dot{\epsilon}^{vp} = A \left[\sinh \left(\frac{\sigma_{eff}}{\tilde{\sigma}_0} \right) \right]^{\tilde{n}} \exp \left(-\frac{Q}{RT} \right) \quad (7.12)$$

where, A , $\tilde{\sigma}_0$ and \tilde{n} are the material dependent constants and Q is apparent creep activation energy and R is the universal gas constant. The values for the constants are as described in **Tab. 7.1** as used by [76].

Table 7.1: Garafalo law constants

| | |
|--------------------|-------------------------------|
| A | $28.2 \times 10^{25} [1/sec]$ |
| Q | $400 [kJ/mol]$ |
| R | 8.31 |
| \tilde{n} | 7.13 |
| $\tilde{\sigma}_0$ | $1 [Mpa]$ |

Norton-Hoff Law

Norton-hoff law is one of the simplest viscoplastic model, which is used in modeling the behavior of the mushy region and it is defined as,

$$\dot{\epsilon}^{vp} = \tilde{k} \left(\frac{\sigma_{eff}}{\tilde{\sigma}_0} \right)^{\tilde{n}} \quad (7.13)$$

where, \tilde{k} , $\tilde{\sigma}_0$ and \tilde{n} are temperature dependent material constants. The values for these constants, at different temperatures are as described in **Fig. 7.3** and **Fig. 7.4**.

Garafalo law is used to determine viscoplastic strain rate for the solid phase and Norton-Hoff law for the mushy phase.

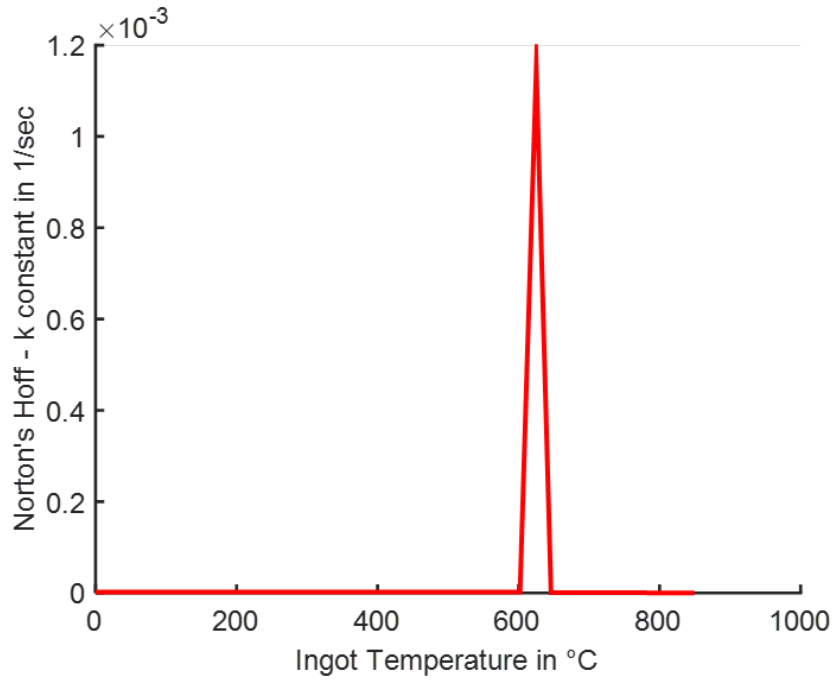


Figure 7.3: Norton-Hoff law - k constant

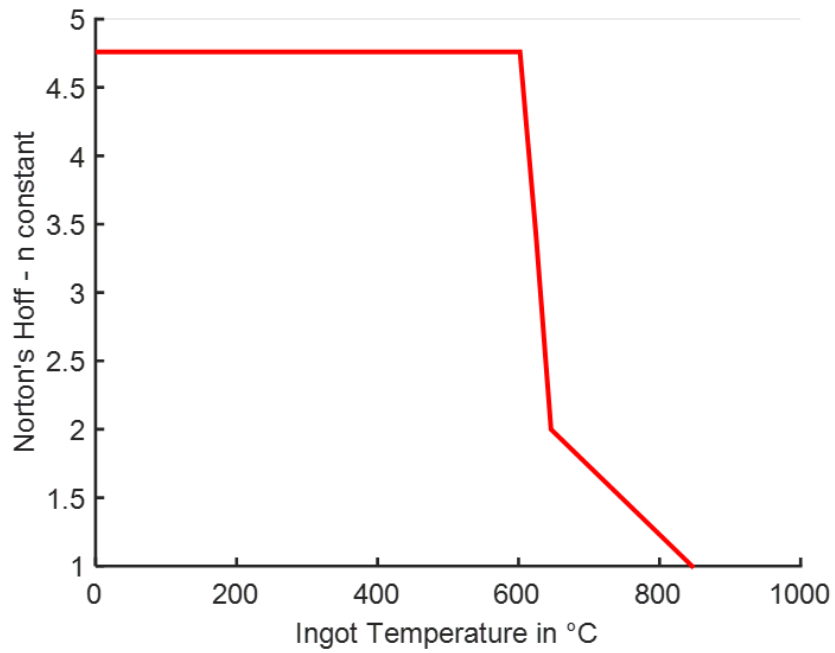


Figure 7.4: Norton-Hoff law - n constant

Stress tensor \mathbf{T} can be estimated from the elastic part of strain tensor \mathbf{E}^e by using the constitutive law of the material as

$$\mathbf{T} = \mathbf{C} : \mathbf{E}^e \quad (7.14)$$

where \mathbf{C} is the fourth order elasticity tensor, defined as follows,

$$\mathbf{C} = 3k\mathbf{P}_1 + 2\mu\mathbf{P}_2 \quad (7.15)$$

where k is the bulk modulus, μ is the shear modulus and \mathbf{P}_1 and \mathbf{P}_2 are the fourth order volumetric and deviatoric projectors as:

$$\mathbf{P}_1 = \frac{1}{3}(I \otimes I) \quad (7.16)$$

$$\mathbf{P}_2 = \mathbf{I} - \frac{1}{3}(I \otimes I) \quad (7.17)$$

where, I is second order symmetric identity tensor and \mathbf{I} is the fourth order symmetric identity tensor.

7.3 Thermal and Mechanical Boundary Condition

The boundary of the computational domain Γ is divided into various segments depending on the boundary condition in the region. As shown in **Fig. 7.5**, it can be seen that the bottom boundary Γ_1 heat transfer is considered through convection. At the interface of ingot and the bottom block, the heat transfer is determined by conditions of contact, gap formation and water intrusion between the ingot and bottom block.

Once the ingot height reaches H_{int} (initial height of the ingot above the bottom block before domain starts growing), water starts to impinge on the surface of the ingot, therefore bottom of the ingot contracts due to solidification and formation of gap occurs in between the bottom block and ingot bottom boundary. In this case, the heat transfer coefficient will be very low. The values of the heat transfer coefficients depend on temperature or gap distance.

At the boundary Γ_2 , cooling is considered by radiation, in the EM casting this will be the length of the EM slit. For the case considered, the length of this zone is 33 *mm*. This is the primary cooling region in this case. The secondary cooling region can be divided into two regions: Impingement zone Γ_3 and Free Falling zone Γ_4 . Different boiling curves are used in the impingement zone and free falling zone to apply thermal boundary conditions respectively.

At boundary Γ_5 , the temperature is constant and the boundary moves in the axial direction with casting velocity. At the boundary Γ_6 , a symmetric boundary condition is considered i.e. the heat flux is zero. Since it is a plane strain model 2D, the width direction is neglected and mechanical boundary conditions is considered as on the boundary Γ_1 is hinged at the bottom, so the vertical and horizontal movements are not possible and on the boundary Γ_6 is hinged, since it is a symmetry plane of the ingot.

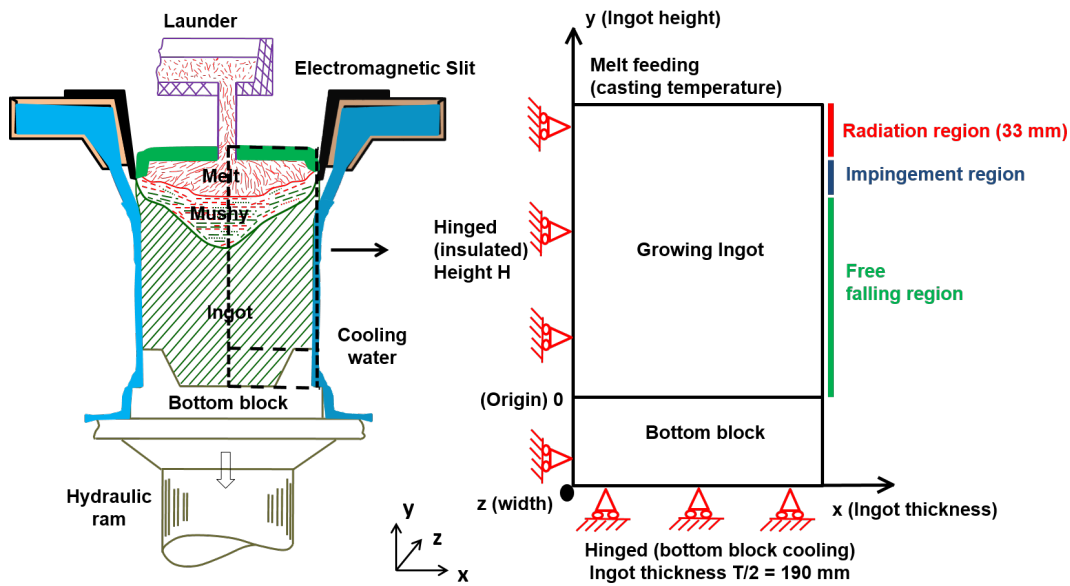


Figure 7.5: Computational domain of the DC casting process with thermal and mechanical boundary conditions

7.4 Casting Parameters

To conduct in-site temperature measurements and validate the thermal boundary conditions, electromagnetic DC casting process is used. The temperature measurements were conducted with experimental parameters. Thermocouples were fixed to the bottom block and then the bottom block was filled with molten metal and lowered in the casting pit.

7.4.1 Material Properties

The thermal and mechanical properties of the aluminium alloy are crucial. In the model to determine the boiling curve constant thermal properties are used to reduce the non-linearities involved. Because of this constant thermal properties are used to simulate the DC casting process. The thermal material properties for the aluminium alloy are as described in **Tab. 7.2**

Table 7.2: Thermal material properties for the aluminium alloy

| | |
|-------------------------------|---|
| Thermal Conductivity | $134 \text{ W}/(\text{m} \cdot \text{K})$ |
| Density | $2677 \text{ (kg/m}^3\text{)}$ |
| Liquidus Temperature | 646°C |
| Solidus Temperature | 602°C |
| Coherence Temperature | 625°C |
| Latent heat of Solidification | 358 MJ/kg |

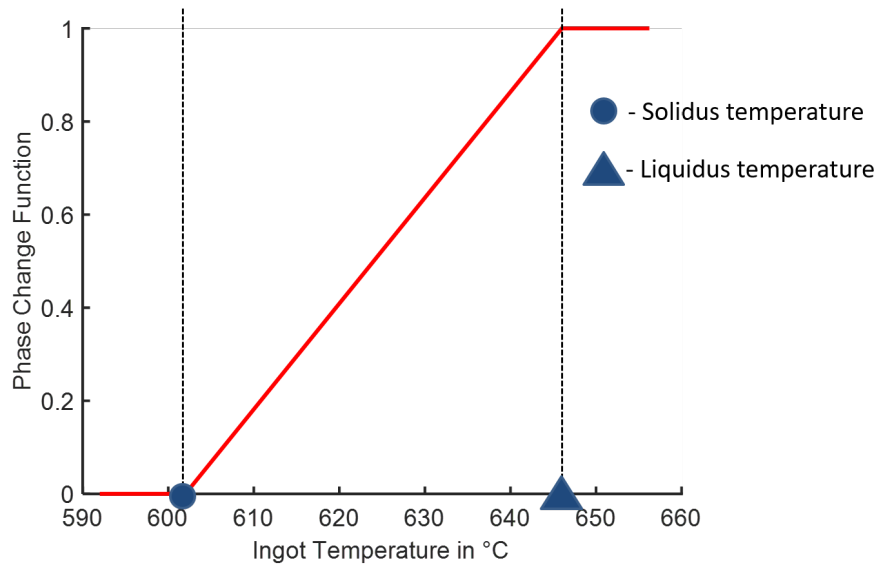


Figure 7.6: Phase change function for the aluminium alloy

As shown in **Fig. 7.6**, a linear phase change function be approximated between the liquidus and solidus temperature. At temperatures above liquidus temperature, the metal will be in complete liquid phase and at temperatures below solidus temperature, the metal will be completely solidified.

The mechanical properties of the aluminium alloy will also vary strongly with temperature. The mechanical properties are adapted form Drezet el al. [76]. This needs to be considered in the model. For this Young's modulus as shown in **Fig. 7.7** is considered along with the Poisson's ration as shown in **Fig. 7.8**.

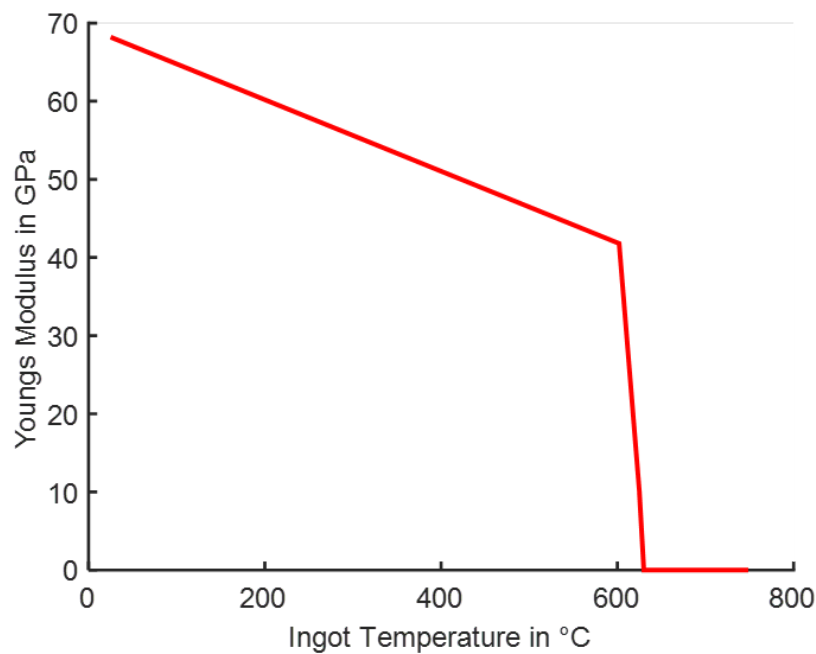


Figure 7.7: Young's modulus for different temperatures

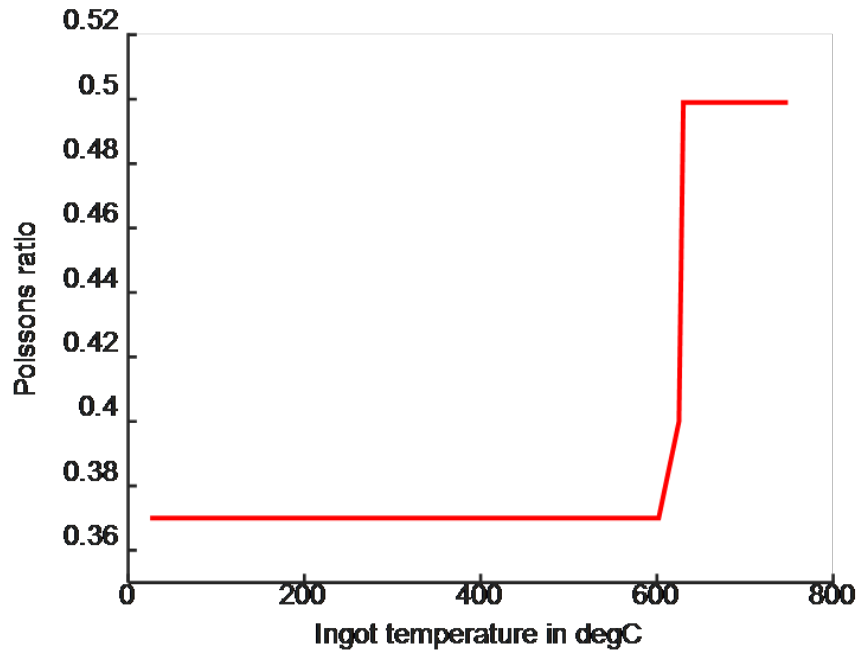


Figure 7.8: Poisson's ratio for different temperatures

The coefficient of thermal expansion will also depend strongly on temperature. In the liquid phase, there will not be any expansion. During solidification, the change in volume will be high and will decrease with decreasing temperature as shown in **Fig. 7.9**. The yield strength of the metal will decrease with increase in temperature as shown in **Fig. 7.10**.

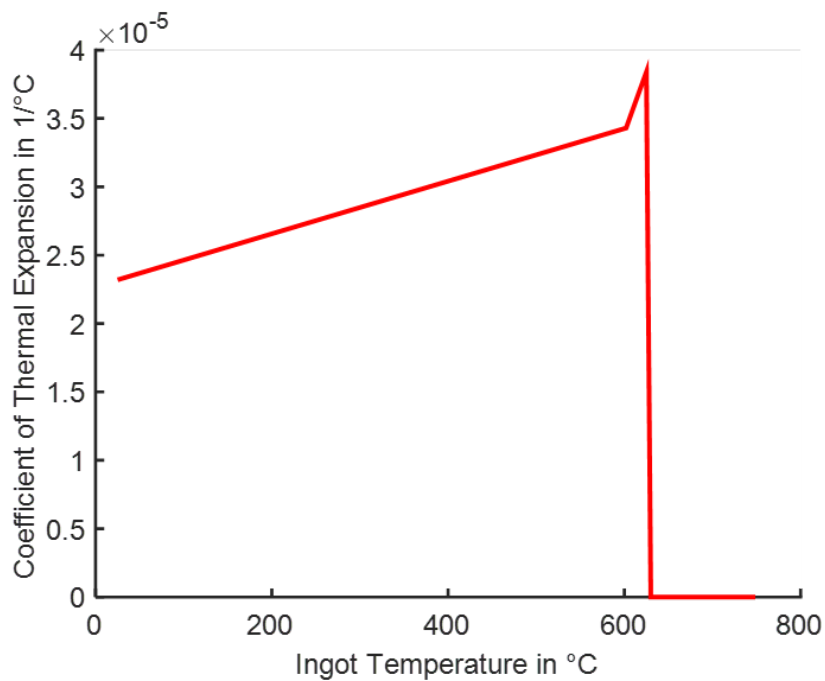


Figure 7.9: Coefficient of thermal expansion for different temperatures

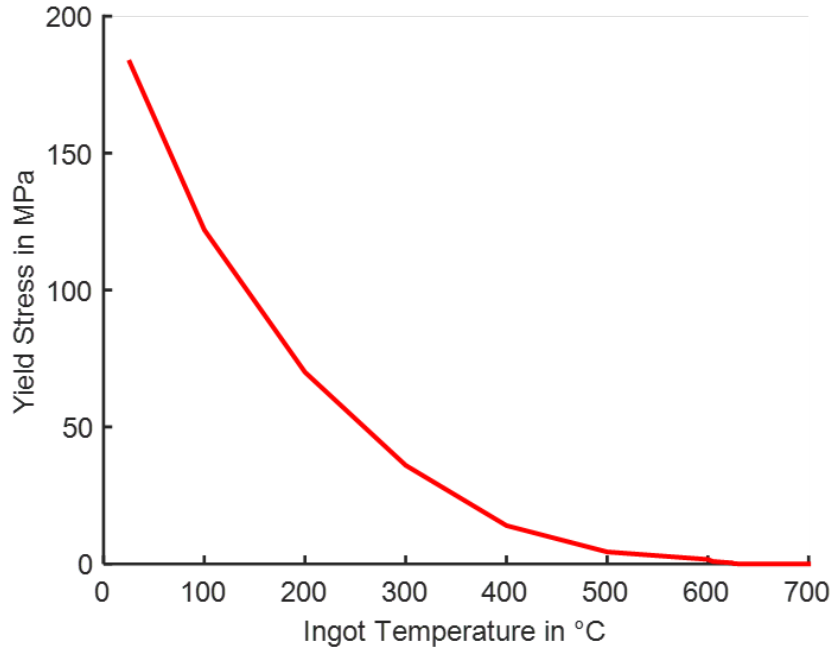


Figure 7.10: Yield strength for different temperatures

7.4.2 Casting Speed

Initially, bottom block is filled with liquid melt in a stationary position for 40 seconds. The height of bottom block filling is 68 mm. After 40th second, the ingot start grows up to 33 mm from the bottom block with the casting speed without any water cooling. In this start-up phase, as discussed earlier, the casting speed is gradually increased so that the ingot can gain strength. The casting speed with respect to the growing ingot height is shown in **Fig. 7.11**.

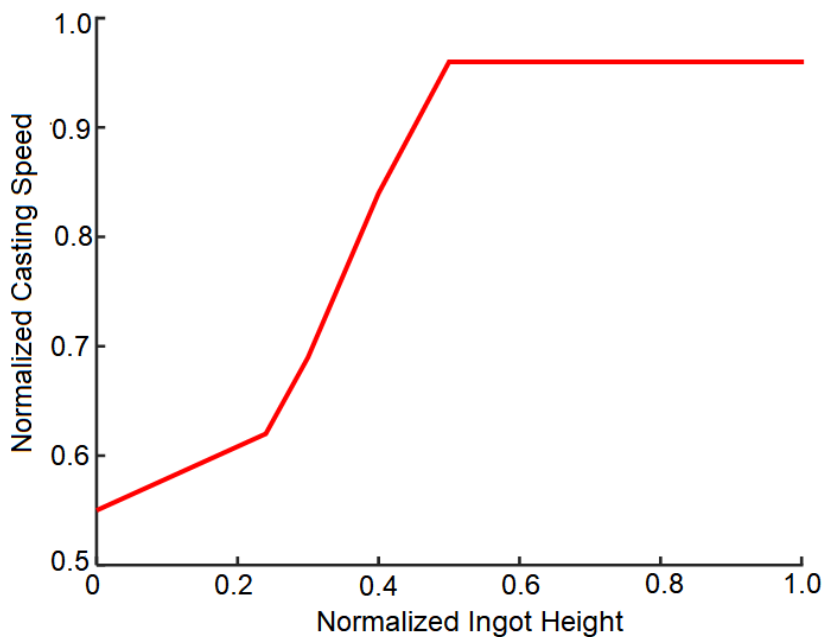


Figure 7.11: Casting speed with increasing ingot height

7.4.3 Water Flow Rate

For the in-situ experimental case, pulsed water flow rate is used from 60 *mm* to 160 *mm* of the ingot height from the bottom. The cycle time period for the pulsed water is 1.5 *s*, in which pulsed water is shut down for first 36% of the cycle (ie., 0.54 *s*) and the water flow is allowed for remaining 64% of the cycle (ie., 0.96 *s*) to strike the ingot surface. To find out the influence of pulsed water, results are obtained without pulsed water flow from 60 *mm* to 160 *mm*. Water flow rate without pulsed situation with respect to ingot height also shown in **Fig. 7.12**. For the pulsed water situation, the water flow rate for the initial start-up phase is around 60 *L/m/min* at 60 *mm* and increases rapidly to 100 *L/m/min* at 160 *mm*. whereas for without pulsed water flow situation, water flow rate is 90 *L/m/min* at 60 *mm* and gradually increased to 100 *L/m/min* at 160 *mm*.

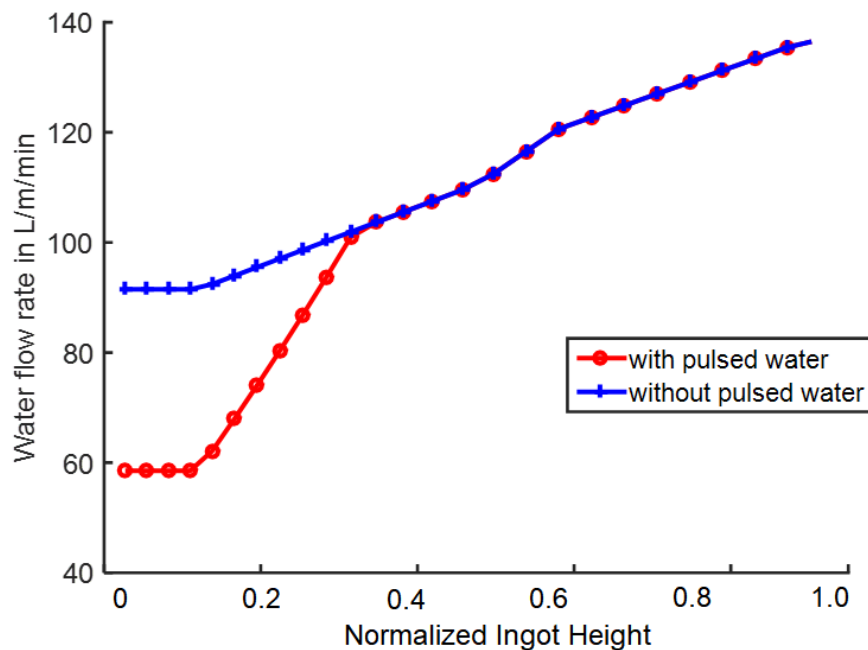


Figure 7.12: Water flow rate with increasing ingot height

7.5 Analysing Experimental Results from DC Casting

Experiments conducted during the Electro-magnetic DC casting with thermocouples inserted in the cast. The thermocouples were positioned at 15 *mm* from the surface and at a height of 20 *mm*, 50 *mm*, 100 *mm* and 150 *mm* from the top edge of the bottom block. The positions of the thermocouples are as shown in **Fig. 7.13**. The thermocouples are position inside the surface as contact of thermocouples with cooling water will result in incorrect temperature readings. At the start of the experiment, the thermocouples are not in contact with hot metal and as gradually the bottom block is lowered and the casting domain grows, the thermocouples are submerged in molten metal. This point can be observed by a sudden increase in temperature. The molten metal around the thermocouple then solidifies because of

surface cooling. The entrapped thermocouple continues to give temperature profile in the solidified ingot.

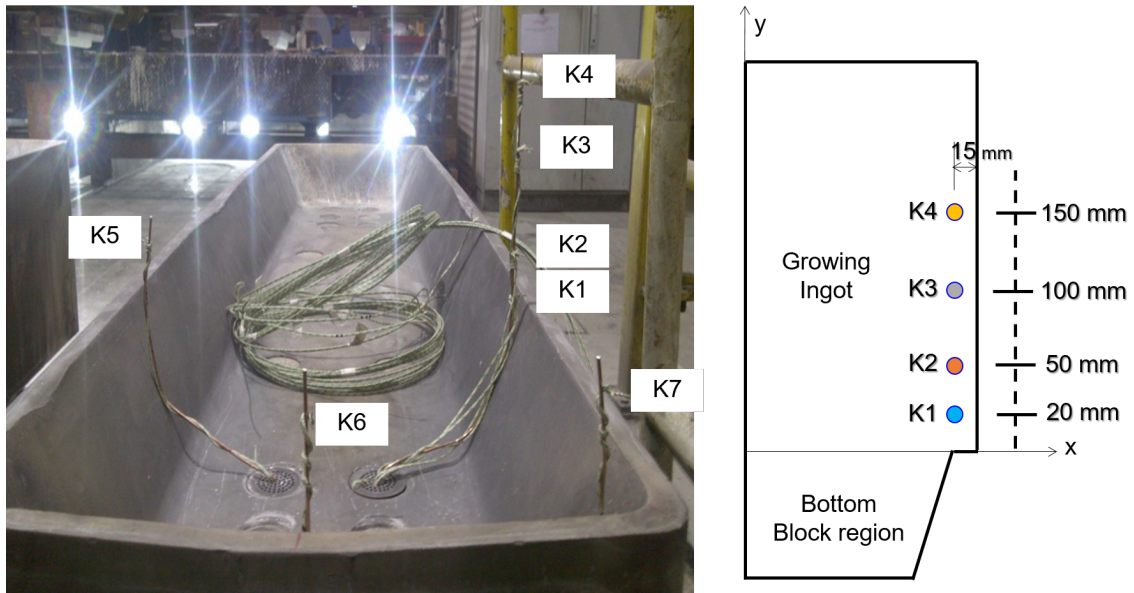


Figure 7.13: Bottom block and position of thermocouples during casting experiment.

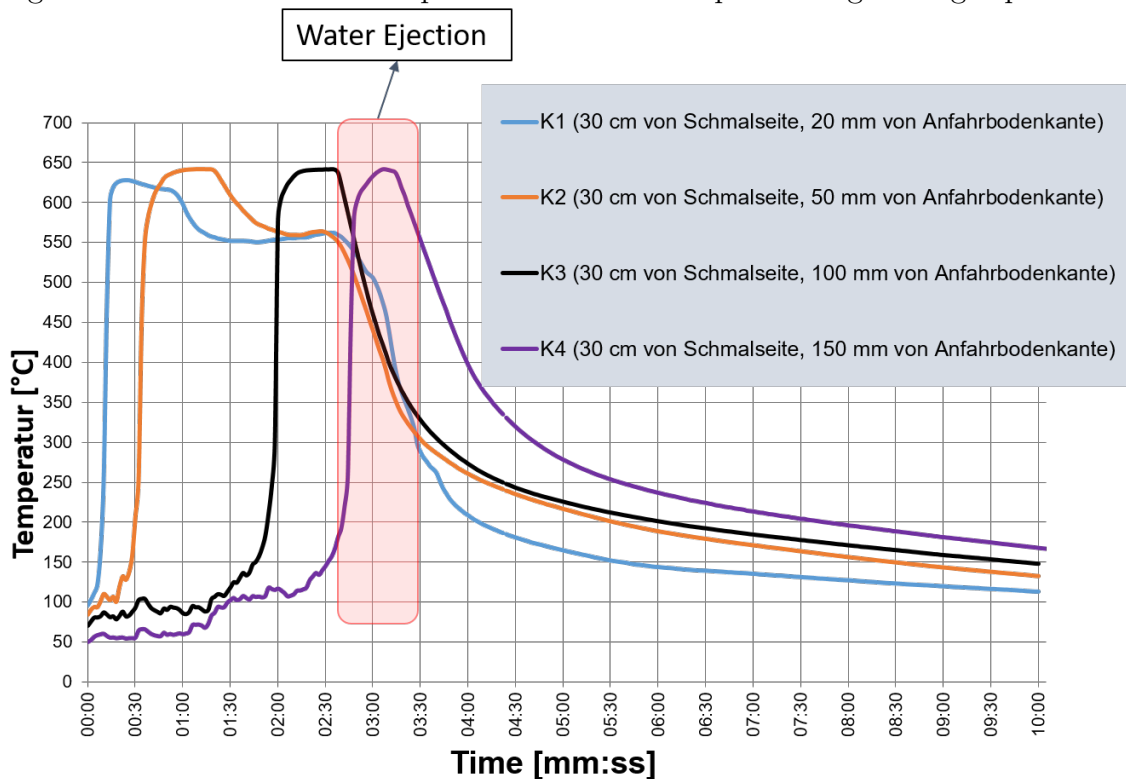


Figure 7.14: Temperature profile for the experimental measured during DC casting.

Since the thermocouples are at different positions, they come in contact with molten metal at a different time. The thermocouple K_1 submerges after 67s, K_2 after 206s,

K_3 after 168s and the thermocouple K_4 after 227s. The casting velocity and the water flow rate also changes with increasing height of the casting.

The measured temperature profiles during casting are as shown in **Fig. 7.14**. It can be seen in the highlighted region, the temperature at the material point K_1 is warmer than K_2 and K_3 . This is because of water ejection occurring during casting. The wetting front collapses after material point K_2 . This can also be observed by a change in the temperature profiles.

Fig. 7.15 shows the thermocouple K_1 temperature measurement. At 40 s, the thermocouple starts heating and reaches a maximum temperature at 64 s (A). As per the ingot growth curve, at 67 s, the melt level reaches thermocouple K_1 region. From A-B (96s) slight temperature decrease indicates that the thermocouple is in above the water impinging region. Water first strikes the ingot at 33 mm from the top of the ingot. When the thermocouple K_1 stays in this region, cooling is mainly due to radiation and natural convection. From B to C (116s), a moderate temperature drop of 610 to 540°C indicates that the thermocouple is in the water jet impinging region. From C to D (196s), there is no temperature change. At this time, thermocouple reaches the free falling region. Later, from D-E intensive cooling indicates that the typical water boiling occurs on the surface of the hot surface. It is quite interesting to understand that why the temperature remains constant from 116 – 196s and what is the heat transfer mechanism at the surface of the ingot.

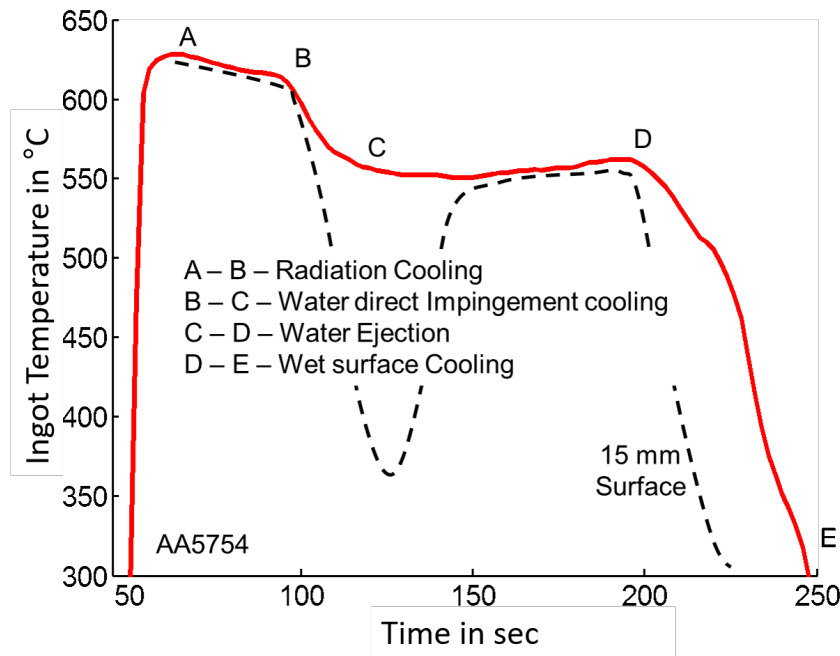


Figure 7.15: Thermocouple K_1 - Surface and Measurement region temperature.

The thermocouples are located 15mm from the ingot surface. Therefore, it is curious to know what happens at the surface of the ingot. One possible guess based on the assumed theory which is explained later is shown in **Fig. 7.15**. Once the K_1 reaches water impingement region, the surface temperature drops drastically due to the impact of the jet. In the water jet direct hitting the ingot surface region, the

surface temperature reaches lowest possible temperature. While entering into the water free falling region, surface temperature should increase and reaches as close to C-D. This phenomena clearly indicates the important physical mechanism of heat transfer in water ejection.

7.6 Thermal Boundary Condition during Secondary Cooling

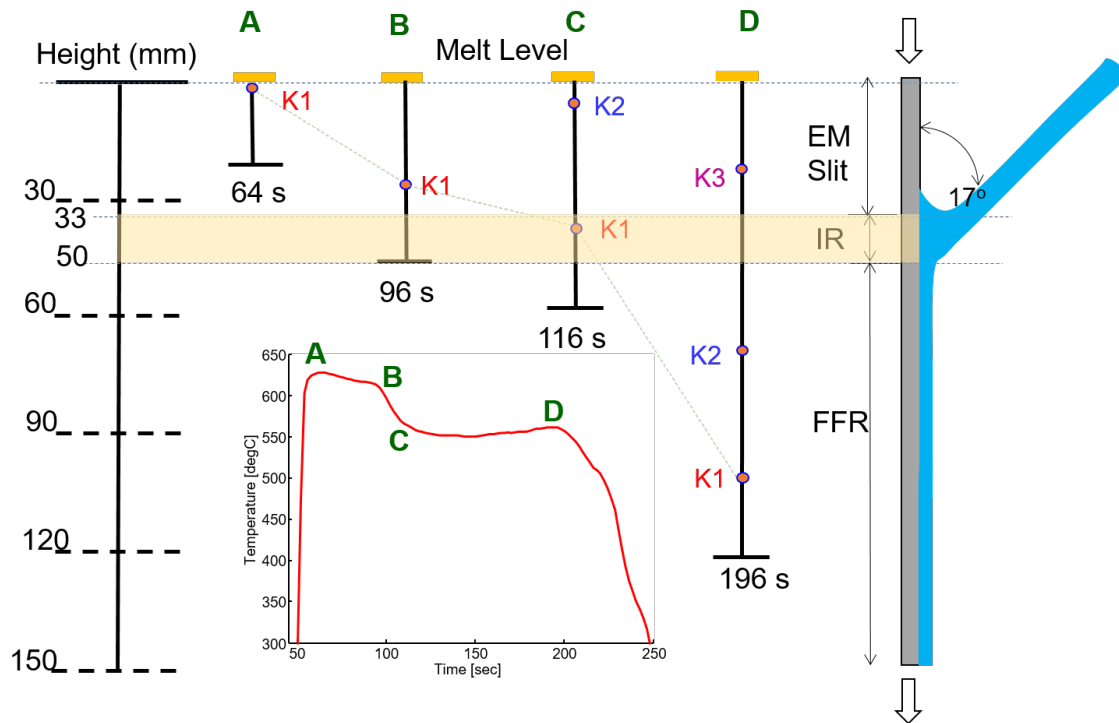


Figure 7.16: Cooling regimes in Secondary water cooling.

As the jet hits the ingot surface at an angle, the horizontal momentum is balanced by the vapor film pressure. This deflects the jet to move away from the surface. Therefore, the jet keeps a certain distance from the surface. Due to this phenomena, there is no possibility of boiling associated heat transfer. Further, the surface is still dry in the free falling region, there is no possibility of single phase heat transfer.

From **Fig. 7.16** one can perceive that the water jet striking region and the growth of ingot. Keeping melt inlet position as a reference, the change in position of the thermocouple K_1 and the different cooling regions can be identified. The cooling mechanisms in electromagnetic slit region, water impinging region and free falling regions are distinct.

In the free falling region, it is perceived that the vapor film exists at the early stage. Due to this water get ejected from the surface. When the temperature drops below the rewetting temperature, the wetting front starts propagating. Finally, the complete wet surface is established in the entire cooling region.

Based on the experimental temperature measurements which are explained before, the secondary cooling regions can be classified as:

- (a) Impingement region
- (b) Free falling region

In the EM-slit region, radiation and natural convection are the dominant modes of heat transfer. In the bottom block region, a gap dependent heat transfer coefficient is assumed. The bottom block temperature is assumed as $120^{\circ}C$. Once the water wets the ingot surface and the front reached the bottom edge of the ingot, there is a possibility of water incursion in the gap. Therefore, the heat transfer coefficient is increased 4 times higher than the gap case.

7.6.1 Boiling Curve

The heat flux as a function of surface temperature is applied based on a quadratic interpolation between the Leidenfrost, DNB and $100^{\circ}C$ point, as shown in **Fig. 6.3**.

As explained earlier, 2 distinct boiling curves for impingement zone and for the free falling zone are used. Depending on the results from laboratory experimental investigation, the maximum heat flux in the impingement zone is considered to be $7 MW/m^2$ at $180^{\circ}C$ and a high heat flux in the film boiling region of $2.5 MW/m^2$ to compensate for the cooling because of pulsating water jet is considered. The width of impingement zone is considered as obtained from the experimental analysis.

In the free-falling zone, the maximum heat flux of $3 MW/m^2$ is considered at $180^{\circ}C$ and a very small heat flux above the rewetting temperature of $0.25 MW/m^2$ is considered. The boiling curves for the impingement zone and free falling zone are as shown in **Fig. 7.17**.

At the beginning of the casting, a pulsating water jet is used. Because of this, the thermal gradients are relieved as the heat flux is lowered and heat can diffuse to the cooler outer surface. To simulate the pulsating water jets a very small time step will be required, which will increase the computational time. So in order to compensate for this phenomenon, a lower Leidenfrost temperature is used and the resultant temperature matches with the experimental profile. The Leidenfrost temperature is considered dependent on the water flow rate as similar dependency is also observed in spray quenching. The plot of Leidenfrost temperature and water flow rate considered is as shown in **Fig. 7.18**. The slop of relation between Leidenfrost temperature and water flow rate is determined by curve fitting. It is found that the Leidenfrost temperature can be related to water flow rate with the following relation:

$$T_{LF} = 100 + 32.2\sqrt{Q} \quad (7.18)$$

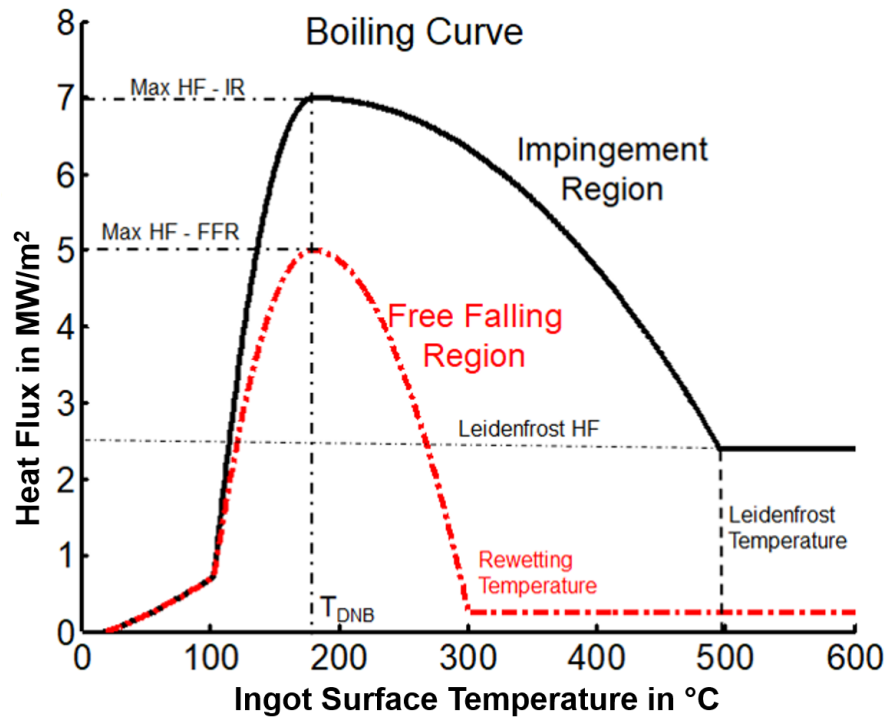


Figure 7.17: Quadratic function of boiling curve in impingement zone and free-falling zone

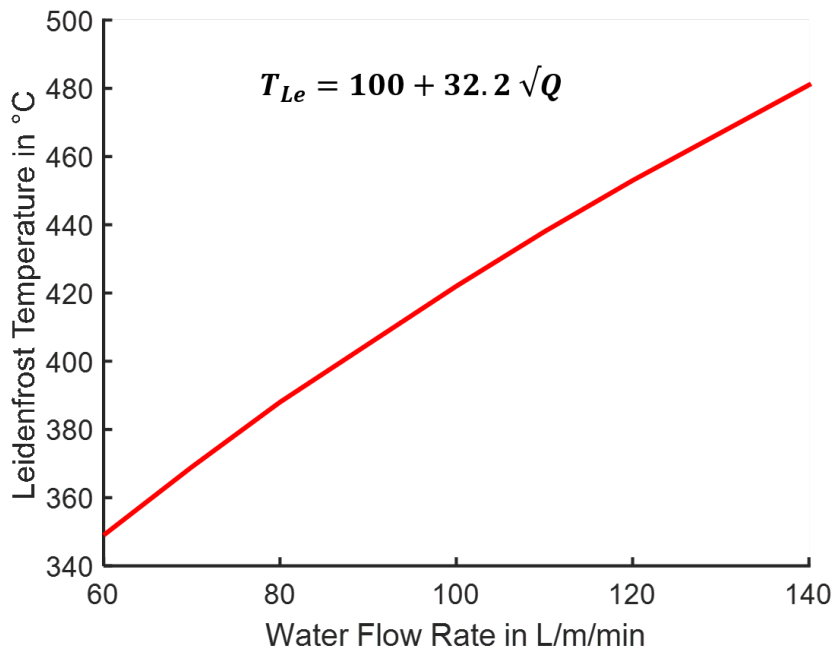


Figure 7.18: Leidenfrost temperature in the impingement zone

During the experimental analysis, it is observed that in the free falling zone the rewetting temperature strongly depends on water temperature. With increasing water temperature the rewetting temperature decreases. During DC casting, the cooling water first comes in contact with hot metal in impingement zone and flows

downstream in free-falling zone. Because of this, the water temperature in the free falling zone is higher than the initial temperature of water. To get the exact water temperature and hence the rewetting temperature in the free falling zone, a 2 phase model which can predict the water temperature also can be used, but this will be computationally very expensive. Because of this, in order to compensate for the increase in water temperature, the rewetting temperature depending on the impingement point temperature is considered. At higher impingement point temperature, film boiling farther region of transition boiling will be dominating and the resultant heat flux will be lower. Because of this, the increase in water temperature will be lower and the resultant rewetting temperature will be higher. At lower impingement point temperature, the heat transfer will be closer to maximum heat flux and the resultant heat flux will be higher and hence the water temperature will be higher. Because of this, the rewetting temperature will also be lower. The plot of rewetting temperature and impingement point temperature is as shown in **Fig. 7.19**.

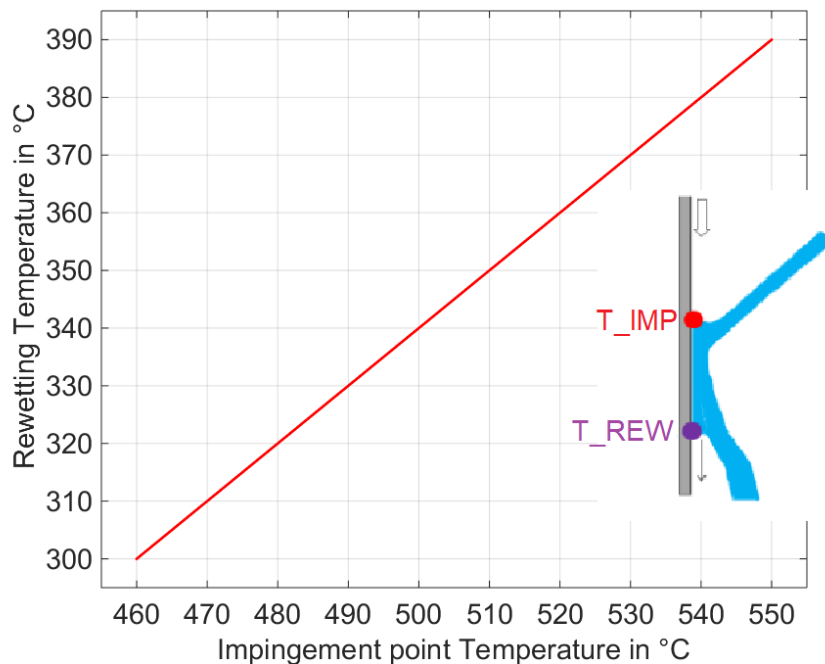


Figure 7.19: Rewetting temperature in the free falling zone

The Leidenfrost temperature and the rewetting is determined based on these relationships. With these points, the boiling curve in the transition boiling region is altered based on the quadratic interpolation as described in **Eq. 6.3** and **Eq. 6.4**. The altered boiling curves are as depicted in **Fig. 7.20**.

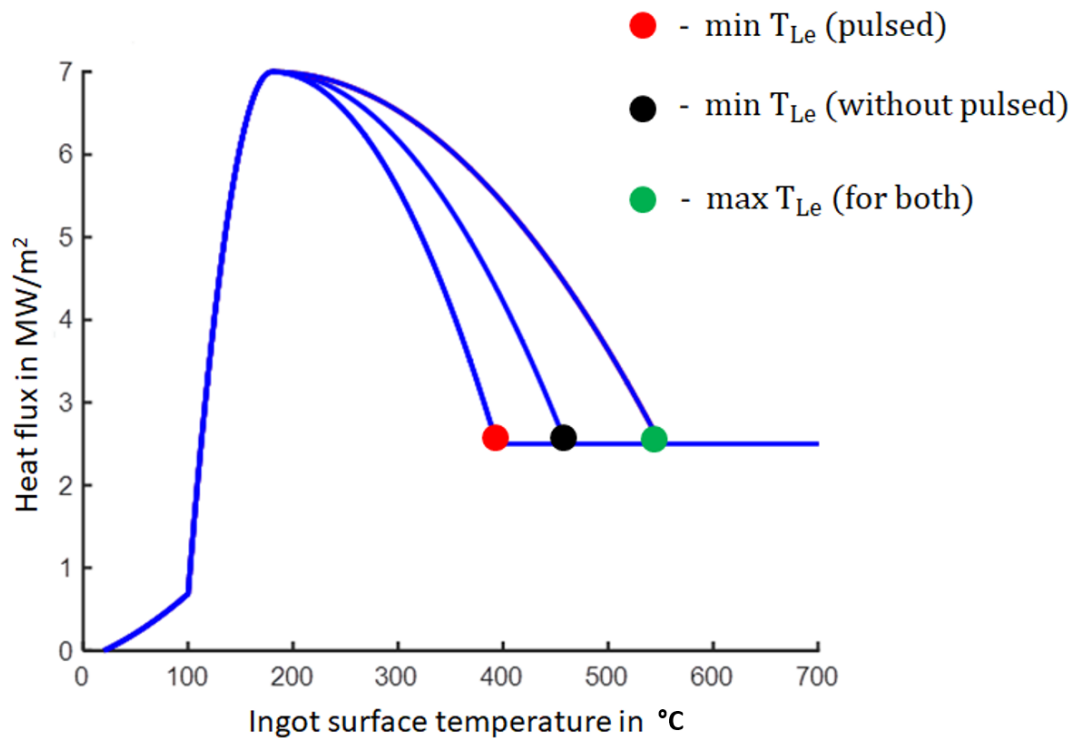


Figure 7.20: Boiling curve in the impingement zone changing according to the Leidenfrost temperature

7.7 Simulation of DC Casting

7.7.1 Computational Domain

A 2-D thermal model is developed in *MATLAB* and *COMSOL* and the experimental temperature profiles are compared with the simulated one. It is found that film boiling at the early stages of start-up phase is the dominant mode of heat transfer in DC casting. Due to this, water ejection occurs after the impingement region of water jet which depends on rewetting temperature. A stable film boiling persists for certain period of time and the film collapses at the Leidenfrost temperature which is assumed to be a function of cooling water flow rate. Film collapsing criteria and the movement of wetting front after the collapse of vapour film are the challenging aspects of the simulation of the temperature profile. This Leidenfrost phenomenon is also considered to compensate for the pulsating water jets at the beginning of casting process.

Due to symmetry in boundary condition, only half of the ingot is considered for the analysis. Heat conduction along the thickness direction is neglected. The bottom block is not considered for the analysis.

Fig. 7.21 shows the heat transfer domain considered for the analysis. Bottom block filling is simulated using a fixed domain. The filling time is 40 *seconds*. After the filling time, the height of the domain grows with time. It is assumed that the

domain is fixed with respect to spacial coordinate, and the corresponding boundary conditions are shifted along the height. 4 thermocouples aligned at 15 mm from the ingot surface along the ingot height is shown in **Fig. 7.13**. The positions of the thermocouples are 20, 50, 100, and 150 mm from the bottom block which attains melt at 67, 106, 168, and 227 s.

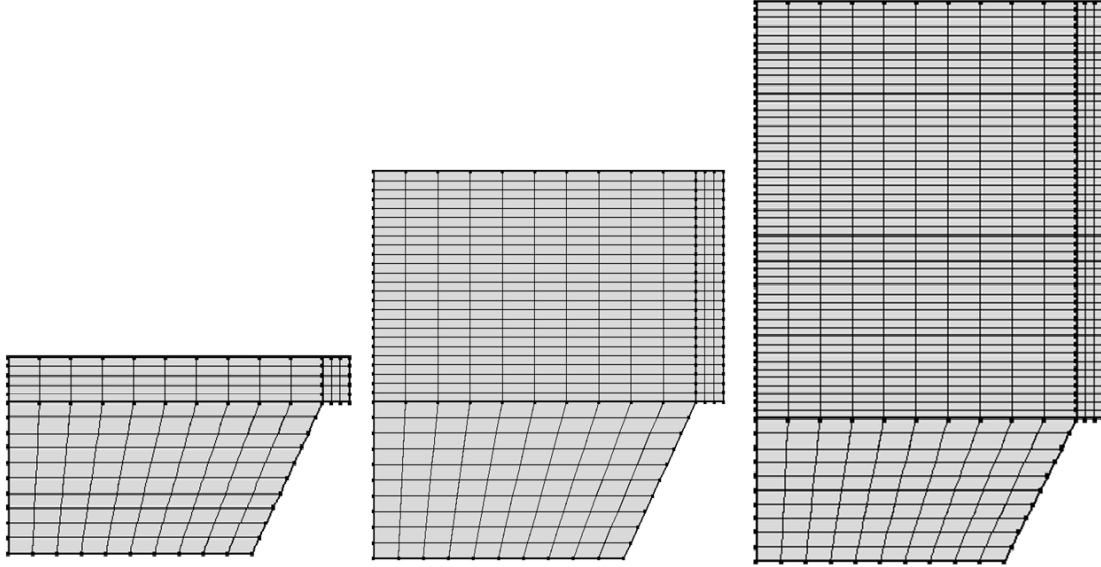


Figure 7.21: Computational domain and ingot growth curve to simulate DC casting

To understand the physical influence of various parameters *COMSOL MULTIPHYSICS* software is used. In *COMSOL* the growing domain is simulated with a combination of *deformed geometry* function. In *MATLAB* the growing domain is simulated by adding new layers of mesh for every time step, depending on the casting velocity.

7.8 Results

7.8.1 Thermal Results

Simulation for the thermal field is conducted on the model with the pre-described boundary conditions. The simulation results are compared with the in-situ thermal measurements in order to validate thermal boundary conditions. The temperature profiles for the material points for the position of the thermocouples are analyzed. The plot of the temperature profiles is described in **Fig. 7.22**. Since the thermocouples are 15 mm inside the ingot position, the temperature at the surface for the location is also determined from the simulation. The surface temperature is important as the heat flux will be dependent on this surface temperature.

In the simulation thermal model, it can be seen that in the starting region water is ejected and the film collapses. The collapsed film then propagates downstream wetting the casting surface. It can be observed from this figure that the temperature profile matches well for the thermocouple positions. With this, it can be concluded that the applied thermal boundary condition is accurate. Hence, the thermal boundary can be used for further analysis of the DC casting process.

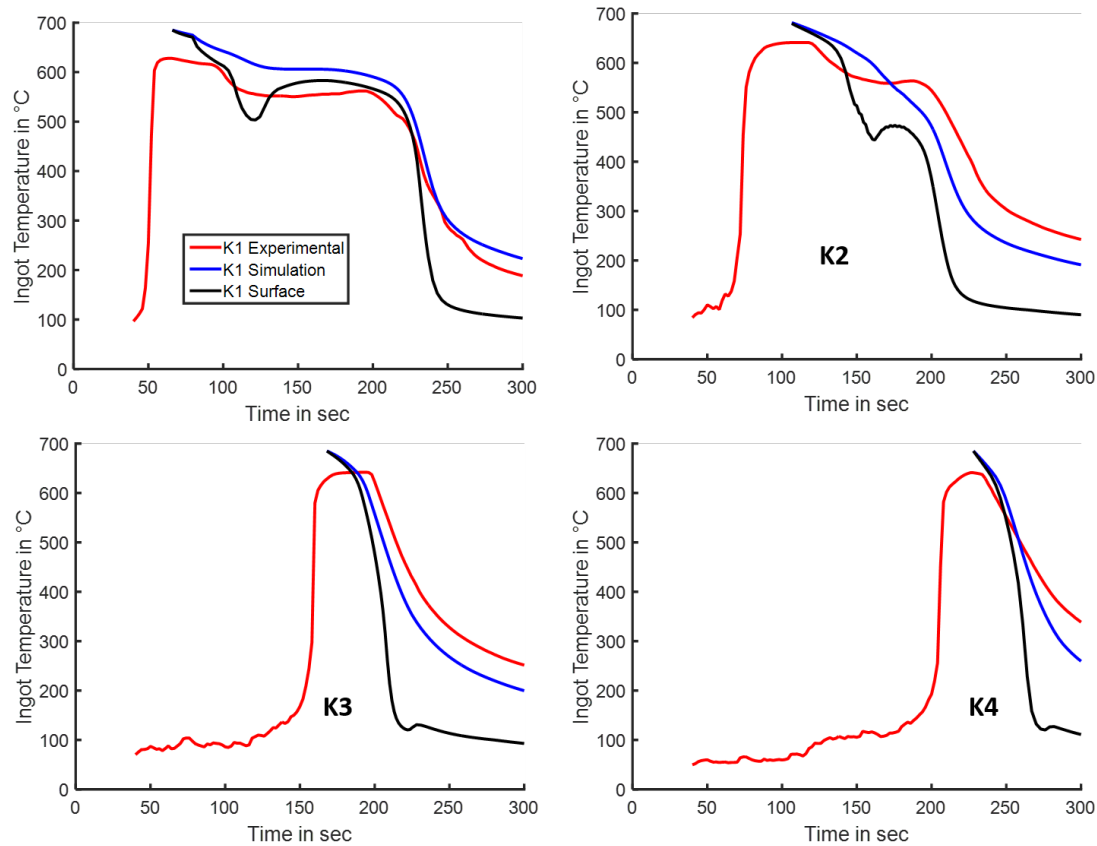


Figure 7.22: Temperature profiles from simulation

Temperature Counter

Fig. 7.23 shows the counterplot of the ingot during DC casting process. The solidus and liquidus temperature counters are also highlighted in these figures. The region between these temperature will be the mushy zone. It can be observed that the mushy zone is narrow near the surface and has maximum depth at the center of the ingot. This is expected as the heat flux boundary condition is applied on the surface of the ingot. The top of the ingot is at the highest temperature because of the molten metal at the initial temperature being added. The surface of the ingot in the bottom block cools slowly even after the wetting front has propagated to the bottom because of the effect of incursion of water in the bottom block is neglected. In reality, water will flow inside the bottom block, depending on the design of the bottom block. This effect will make the thermal boundary condition even more complex as a boundary condition incorporating butt curl and water ejection will be required.

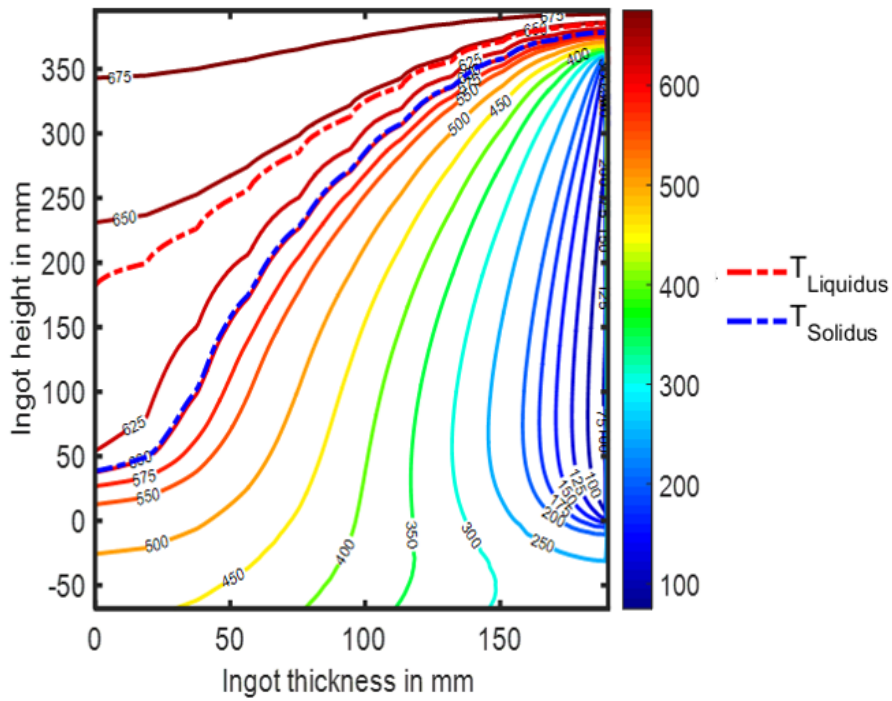


Figure 7.23: Temperature contour plot from simulation

Temperature at Bottom Block

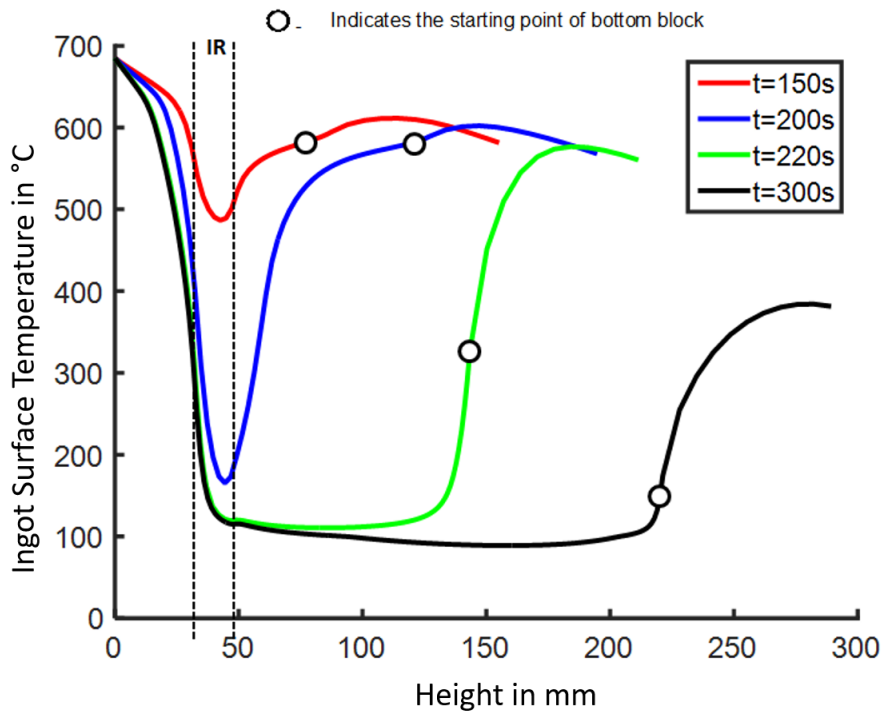


Figure 7.24: Bottom block position on the surface temperature and ingot height

Water ejection is also observed in the simulation. As illustrated in the previous chapter, water ejection will cause slow cooling in the bottom region. **Fig. 7.24**

shows the position of the top of the bottom block on the temperature and ingot height plot. It can be observed that this region experience slow cooling. When water is ejected from the surface the temperature of the bottom region changes very slightly.

Increase of Water Temperature

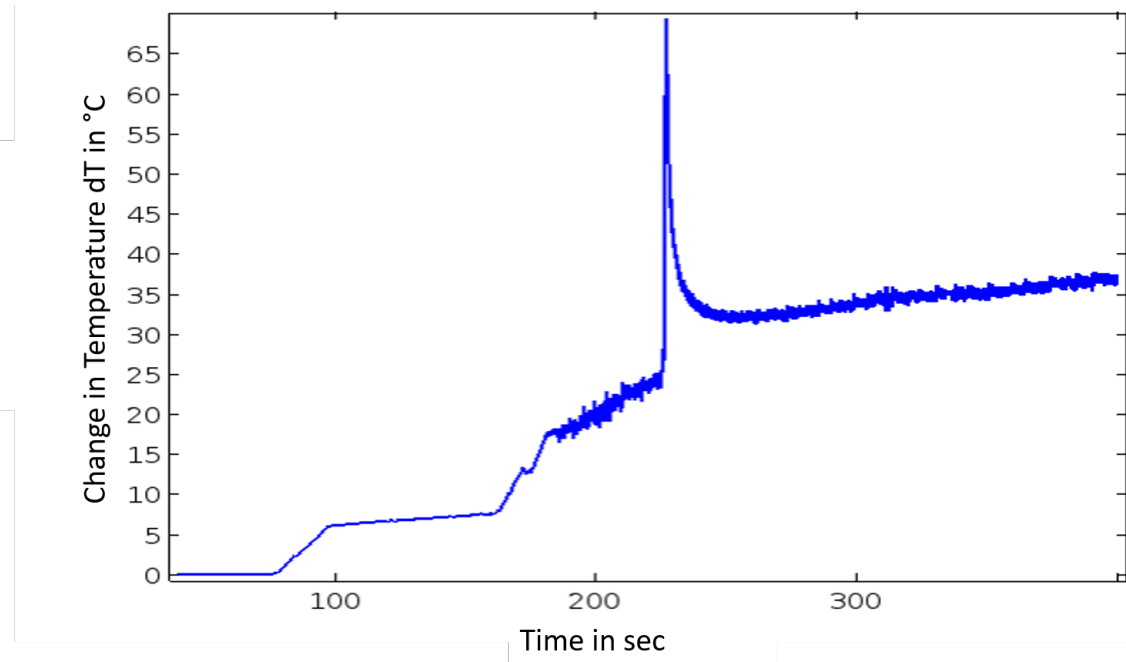


Figure 7.25: The increase in water temperature during DC casting

The rise of water temperature during DC casting simulation is obtained by energy balance between hot metal and cooling water. For this analysis evaporation of water is also neglected. The cooling water will always come into contact with hot metal because of the ingot moving downwards. This will cause a significant increase in water temperature as the water stream flows downwards. When the water stream enters the free-falling region, the temperature of the water is significantly higher than the initial water temperature. During the DC casting process, the cooling water is first used to cool the mold or EM slit in case of EM casting. This will also cause an increase of water temperature on it enters secondary cooling. This will have an influence in the heat transfer characteristics as observed in the experimental analysis.

Since a simple energy balance approach is considered to obtain the rise in water temperature, no thermal gradient is considered along the thickness of water film. In reality, there will be a thermal gradient in the water film. The rise in water temperature will change because of changing water flow rate and casting speed. The increase in water temperature is as shown in **Fig. 7.25**. From this figure, it can be observed that initially the increase in water temperature negligible because there is no contact between the cooling water and ingot. The cooling water is impinging on the bottom block in this region. The increase in water temperature increases slowly

to $\sim 20^{\circ}\text{C}$ with changing casting speed and water flow rate. A sudden increase in water temperature is observed at the instance when the film collapses and the wetting front propagates downstream. Followed by this spike, once again a steady increase in water temperature is observed of nearly $\sim 35^{\circ}\text{C}$ in the steady state region.

With these results, it can be concluded that outlet water temperature can be used to determine the existence of water ejection and the instance of film collapse. When water ejection is occurring, there is only heat transfer in the impingement zone, in the free falling zone, there is no contact between cooling water and ingot. Because of this, the increase in water temperature is not high. At the instance of film collapse, cooling water in free falling zone comes in contact with hot ingot and very high increase in water temperature is observed. In the steady state region, the bottom region is moderately cooled and the heat transfer reaches a steady value.

During the laboratory experimental analysis, a similar trend for an increase in water temperature was observed. During ejection, the increase in water temperature was not high. The point of film collapse and wetting front propagation was marked with a very high increase in water temperature and high water evaporation. This observation can be used to determine the exact instance of film collapse.

The validated thermal boundary conditions are used in a thermo-mechanical model to determine the stresses during DC casting process. This can be extended to incorporate hot tearing criteria to investigate the influence of casting parameters.

Ingot Temperature for Different Water Flow

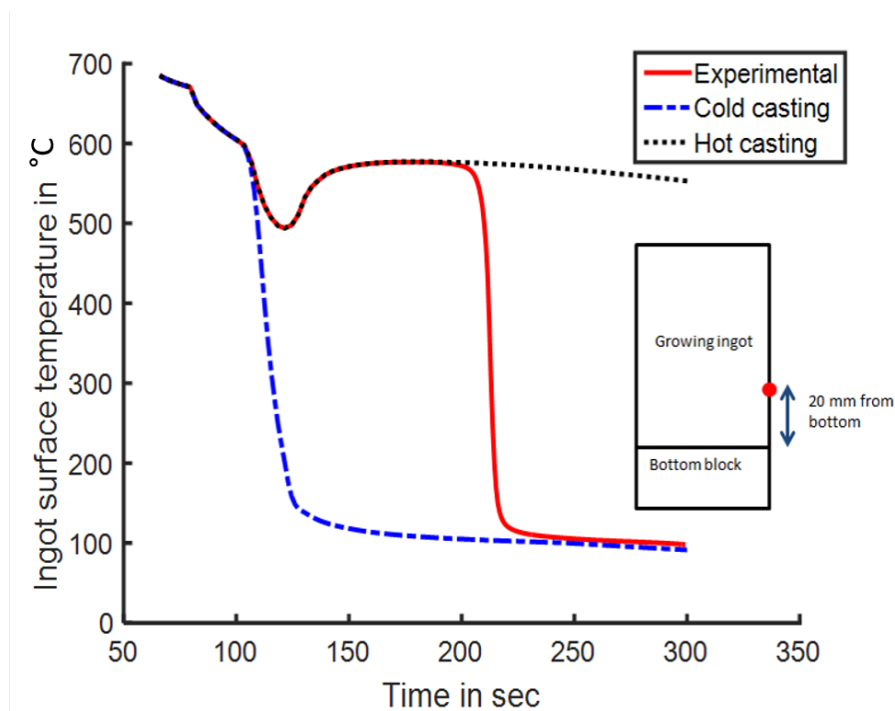


Figure 7.26: Temperature at 20 mm from the bottom block for different cases

In order to study the influence of water ejection on the DC casting process, two extreme cases are considered. These extreme cases are compared with the experimental case, where real parameters are used. The first extreme case considered

is when a high water flow rate is used. In this case there will be no ejection will occur because of increased water flow rate. This case is referred to as cold casting by Sengupta [17]. For this case, a constant water flow of $140 L/(m \cdot min)$ is used. The second extreme case considered is when the water flow rate is very low. In this case, there will be complete ejection till the end of the casting process. For this, a low water flow rate of $60 L/(m \cdot min)$ is considered. The temperature profile at a point located $20 mm$ from the top of the bottom block is shown in **Fig. 7.26**. It can be observed that in the cold casting case because of high water flow rate, the surface temperature drops immediately. For the hot casting and experimental case, there is strong cooling in the impingement zone followed by ejection. Though in experimental case the film collapses and the wetting front propagates downstream, cooling the ingot. In case of hot casting, there will be complete ejection of water and the ingot will remain at high temperature. Similarly, the temperature at the point of impingement for these case can be observed in **Fig. 7.27**. It can be observed that in case of cold casting the impingement point temperature drops immediately and for hot casting, the temperature remains high for a long time.

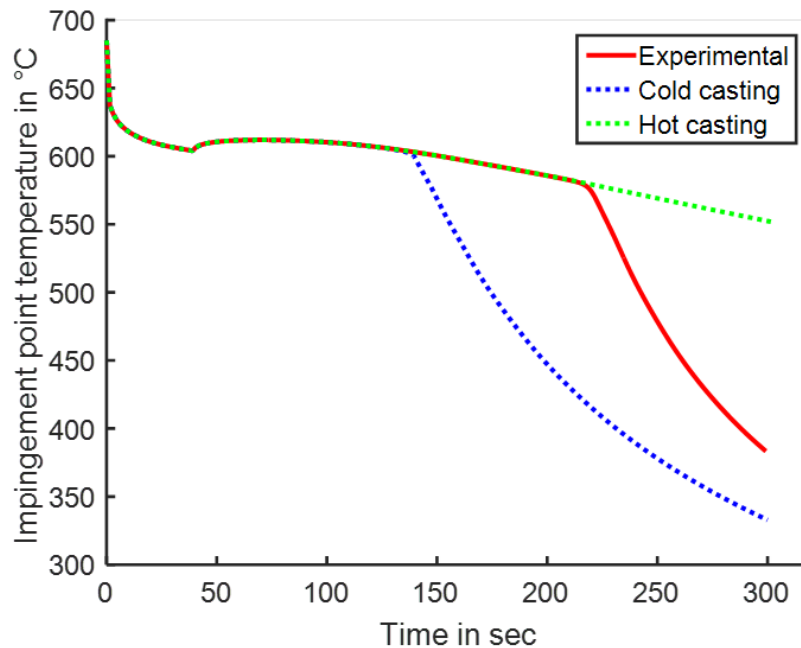


Figure 7.27: Temperature at impingement point for different cases

7.8.2 Mechanical Results

Stress Components on Ingot Surface

The validated thermo-mechanical model can be used to study the evolution of stress during the DC casting process. The mechanical field is modeled by using a 2D plane strain model. **Fig. 7.28** shows the plot of various components of stresses with the experimental case at end of simulation or 300 seconds. From this figure, it can be observed that the trend of different stress components is same but the magnitude of the out of plane stress is maximum. For this reason, the out of plane stress is used as critical parameter for failures. Also, the out of plane stress will be responsible for cracks formation along the axial direction.

The maximum stress occurs in the impingement zone as the thermal gradients are maximum in this region. A maximum value of 150 MPa is observed in this region. The stresses are relieved in the free falling region as the thermal gradients reduce.

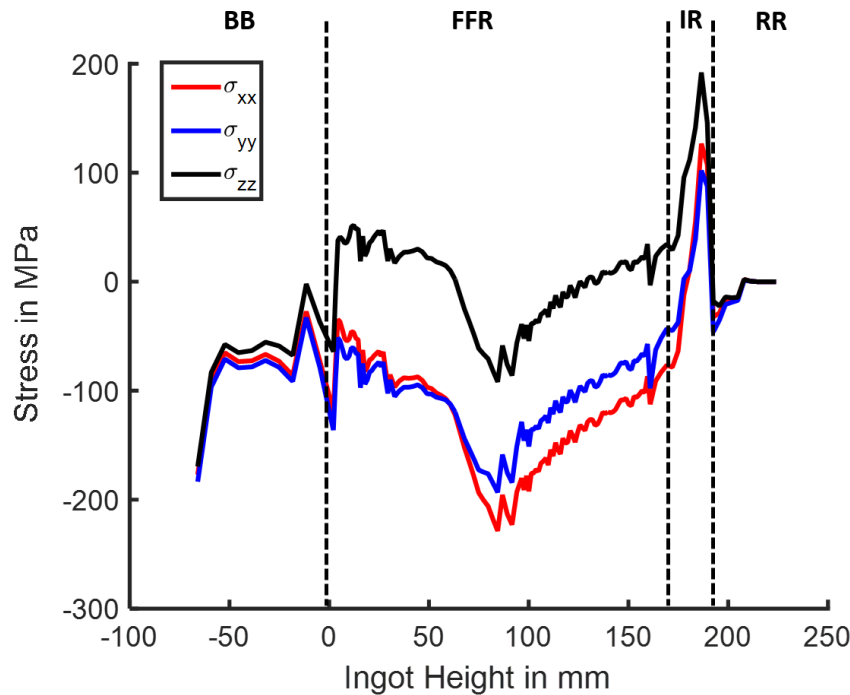


Figure 7.28: Stress at surface of the ingot for experimental casting case

Stress and Temperature on Ingot Surface

In order to study the stresses, the out of plane stress and the temperature are plotted with time for various positions. The corresponding surface locations of the thermocouple positions are selected for this. From **Fig. 7.29** it can be observed that, when the point comes in impingement zone, there is a sharp decrease in temperature, owing to high heat flux in the impingement zone. Correspondingly, the stress can be observed to drop in the compressive nature. This is because when the point enters in the impingement zone the temperature is higher than the solidus temperature as seen in **Fig. 7.27**.

Once again there is a spike in stresses when the wetting front propagates and comes to this location. Since the surface is cooler and has gained strength, a sharp rise in stresses is observed. Followed by the wetting front the thermal gradient reduces and hence the magnitude of stresses. The induced plastic strain, however, will continue to exist creating residual stresses in the ingot at the end of casting.

A similar trend is observed in case of a point 50 mm from the bottom block, on the surface of the ingot, as shown in **Fig. 7.30**. When the water is ejected from the surface, the stresses remains constant and the stresses spike when the wetting front comes to this location.

For position of 100 mm and 150 mm, it can be observed from figure **Fig. 7.31** and **Fig. 7.32** respectively, that there is no water ejection occurring. The ingot surface is cooled largely at one point. Because of this, it can be observed that the stresses spikes at a point, in the impingement zone.

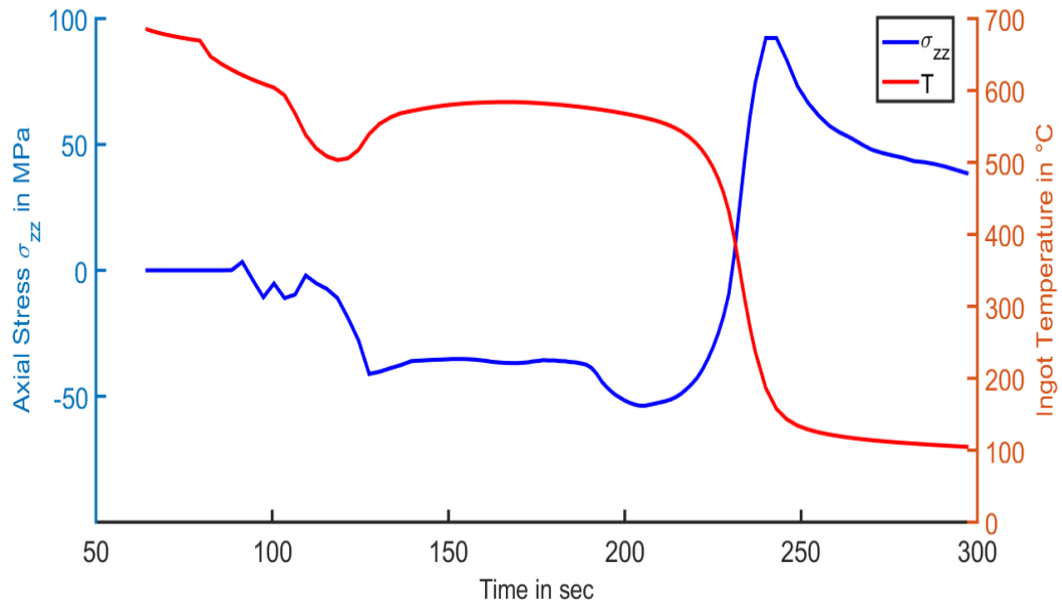


Figure 7.29: Surface temperature at thermocouple position K1 and axial stress vs time

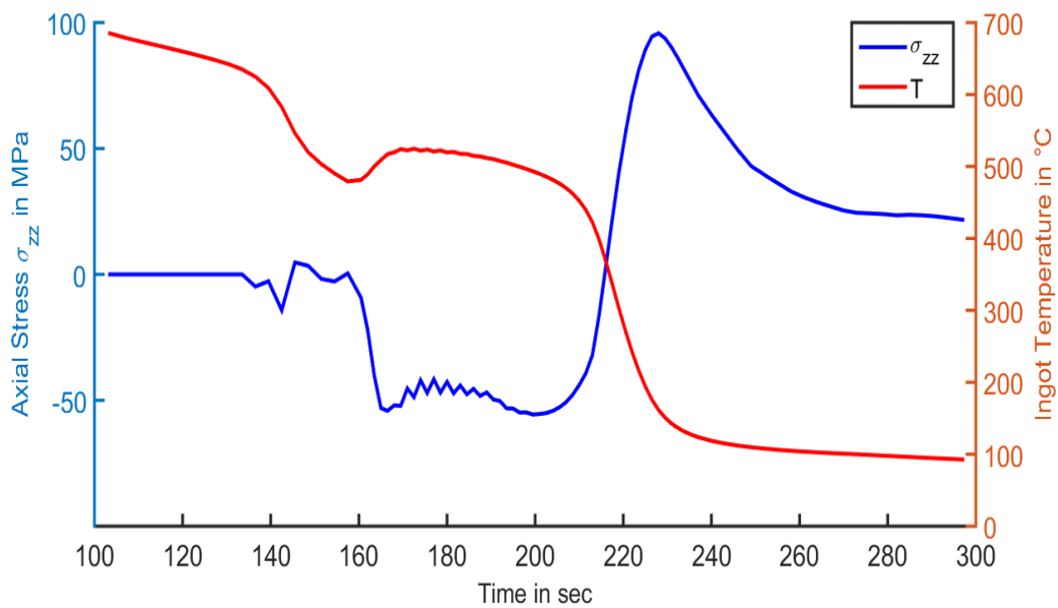


Figure 7.30: Surface temperature at thermocouple position 2 and axial stress for different time steps

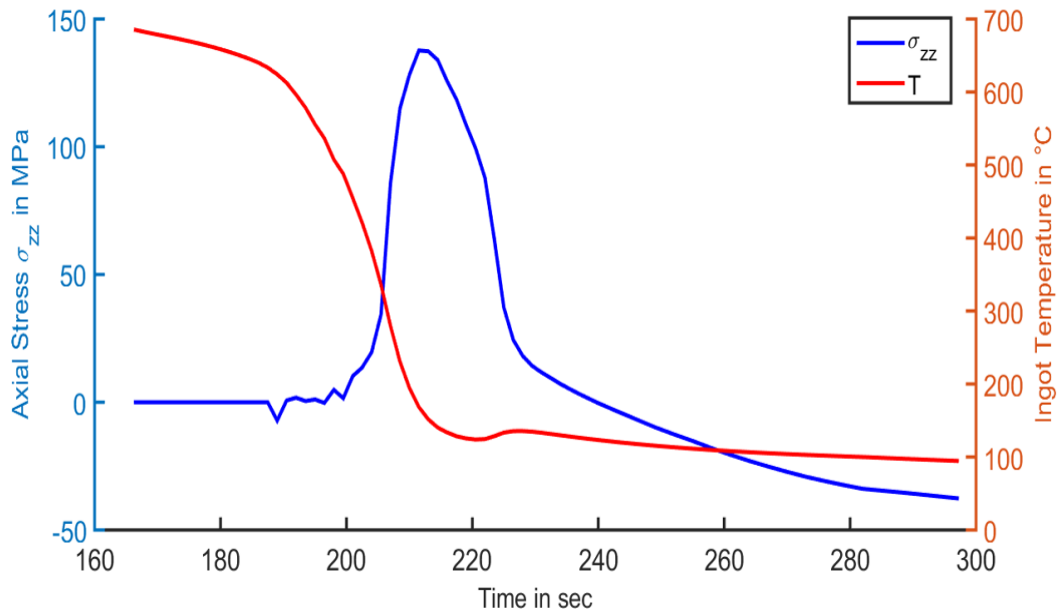


Figure 7.31: Surface temperature at thermocouple position K3 and axial stress for different time steps

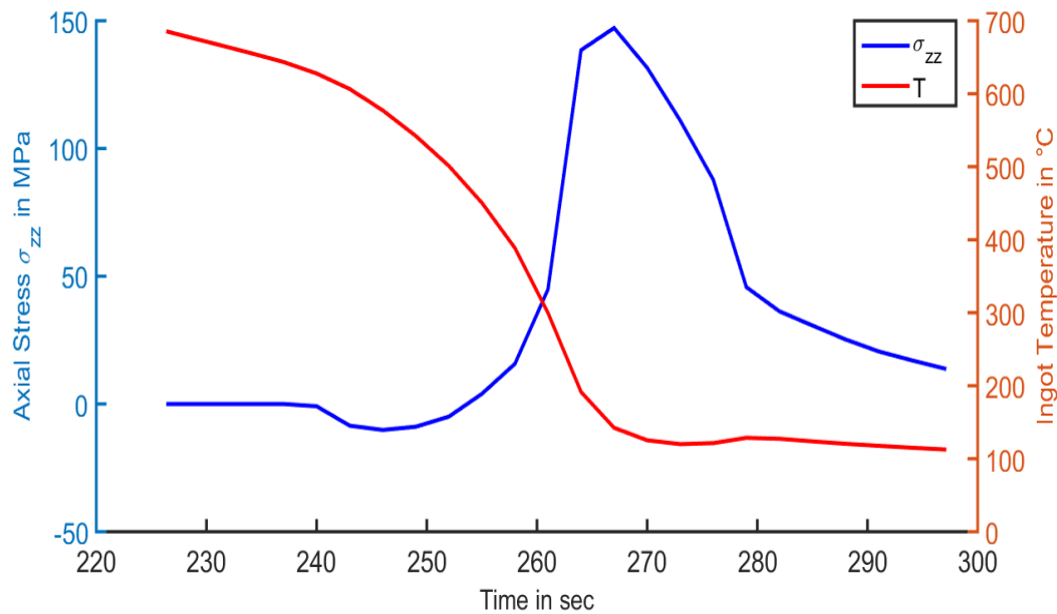


Figure 7.32: Surface temperature at thermocouple position K4 and axial stress for different time steps

Thus it can be concluded that because of occurrence of water ejection, in the starting time range the stresses are lesser and compressive. When the film collapses the stress increases. Following the collapse, the stresses are very high in the impingement zone and near the wetting front region. In other words, when the film collapses spike of stresses propagates in both the directions. This can be observed in **Fig. 7.35**.

Thus if there are any cracks formed in the bottom region cannot propagate in the upward direction because of compressive stresses upstream. The formed cracks have a possibility of healing because of compressive stresses.

Axial Stress and Strain for Different Cases

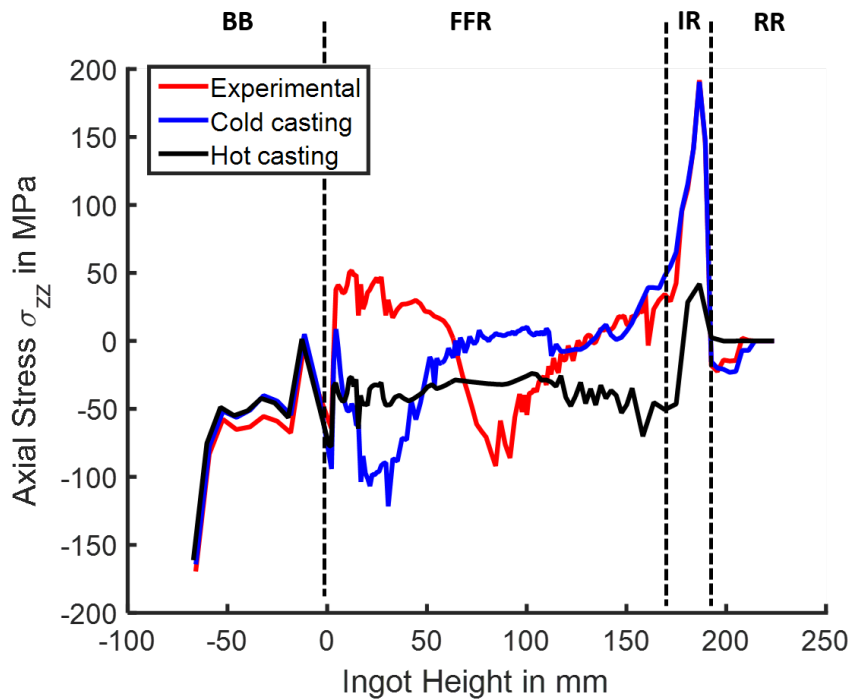


Figure 7.33: Final axial stress for different ingot height for different cases

To study the stresses for different extreme cases, stress analysis is conducted. In **Fig.7.33** it can be observed that at time 300 seconds, the stresses in the bottom block region are same for all the cases. This is understandable as the secondary cooling has no significant influence in this region. The stresses are maximum in the impingement zone and are nearly same for experimental and cold casting case. In the bottom region, the stress profile is mirrored for these two cases. Near to the bottom block, the stresses are higher for the experimental case as the cooling occurs in the impingement zone and when the wetting front travels downstream. In case of hot casting, the water is ejected from the surface during the entire process. This reduces the rate of cooling and hence the stresses. This is not a desirable case as this will reduce the productivity of the process but also lead to other failures.

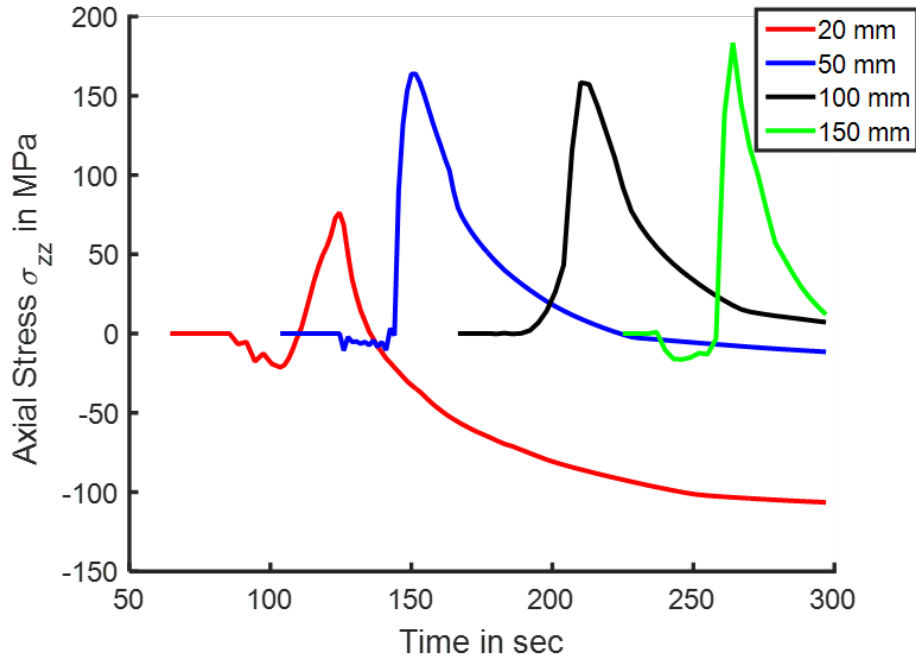


Figure 7.34: Axial stress at different locations for cold casting

In order to illustrate the evolution of stresses at different locations, stresses are plotted with time for different locations. These stresses are studied for cold casting case, as depicted in **Fig. 7.34** and for experimental case as in **Fig. 7.35** in order to quantify the influence of water ejection. From these figures, it can be observed that the maximum stress in cold casting case, at a lower position, occurs at an early stage. The peak then propagates upstream in cold casting case. So any cracks formed in the bottom region will propagate in the axial direction because of propagation of peak maximum stress.

Whereas in case of experimental case, as depicted in **Fig. 7.35**, during the start the stresses are compressive because of which any cracks formed in the bottom region can heal. But when the front collapses and the wetting front propagates downstream. High thermal gradient occurs when the ingot is at a lower temperature. Also, the experimental case plastic stresses are accumulated from the impingement zone. So it can be observed that the magnitude of stresses is higher. So it is possible that cracks can be formed in the bottom region but because of water ejection the cracks are localized to the bottom region and will not propagate in the casting direction.

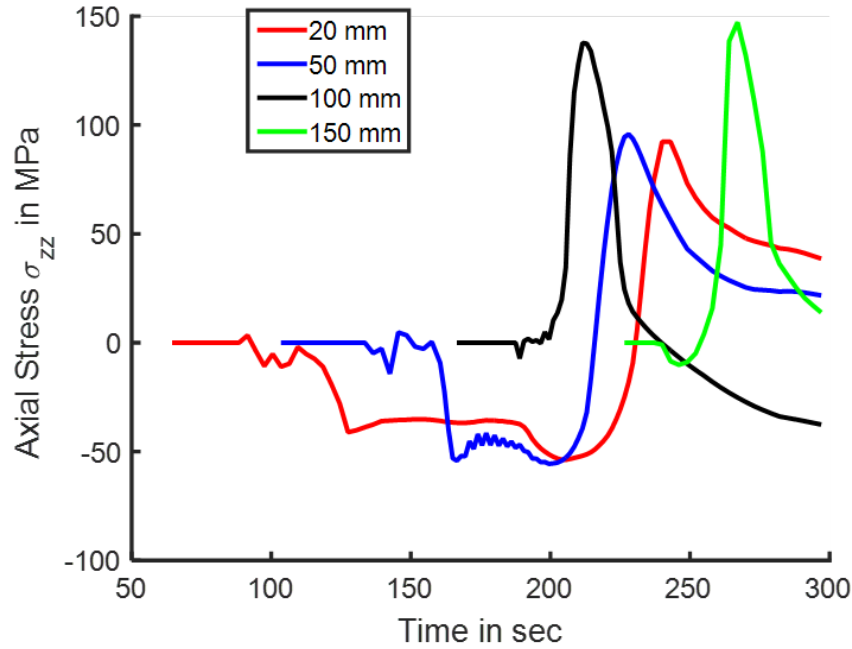


Figure 7.35: Axial stress at different locations for experimental casting case

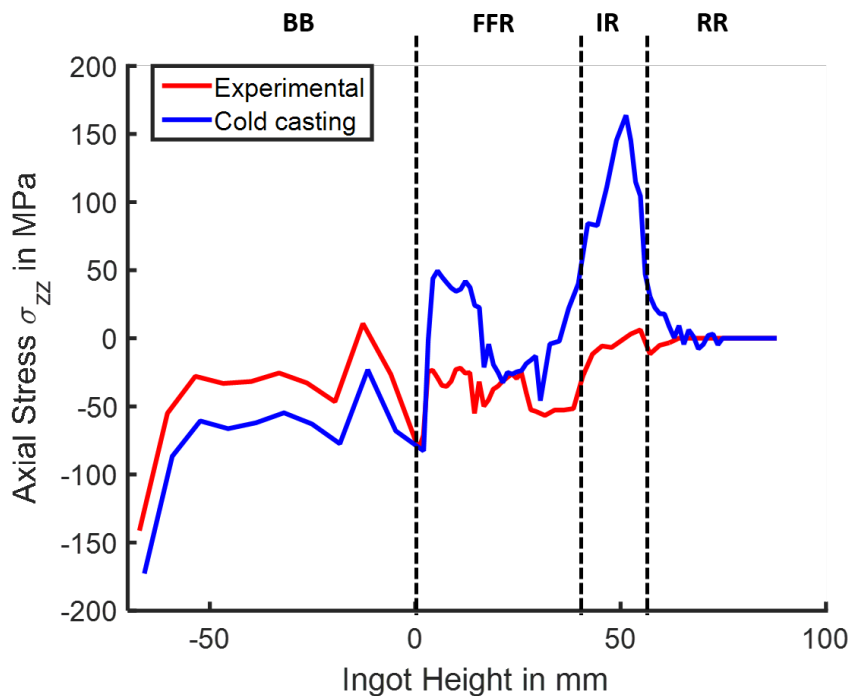


Figure 7.36: Axial stress at different ingot height for experimental casting case at 150 seconds

In order to understand the evolution of stress and the influence of presence of water ejection in an ingot, axial stress is plotted for different time steps as seen in **Fig. 7.36**, **Fig. 7.37** and **Fig. 7.38** for time 150, 200 and 250 *seconds* respectively. From **Fig. 7.36**, it can be observed that because of ejection, the stresses in the impingement region are significantly reduced.

In **Fig. 7.38**, it can be observed that the film has collapsed after 250 *seconds*. The impingement point temperature also has dropped, as observed in **Fig. 7.27**. Because of this, the heat transfer in the impingement zone is similar for cold casting and experimental case, because of which a similar stress profile is observed for both the cases.

Comparing the impingement point temperature for 150 *seconds* from start of the casting, it can be observed that the impingement point temperature is above solidus temperature. At this time, the material is in the mushy zone and not completely solidified. In absence of ejection, a very high heat flux is applied to this region causing very high stresses as seen in **Fig. 7.36**. In case of presence of ejection, the heat flux and hence stresses are low. It can be imagined that this will reduce the susceptibility of the bottom region to failures.

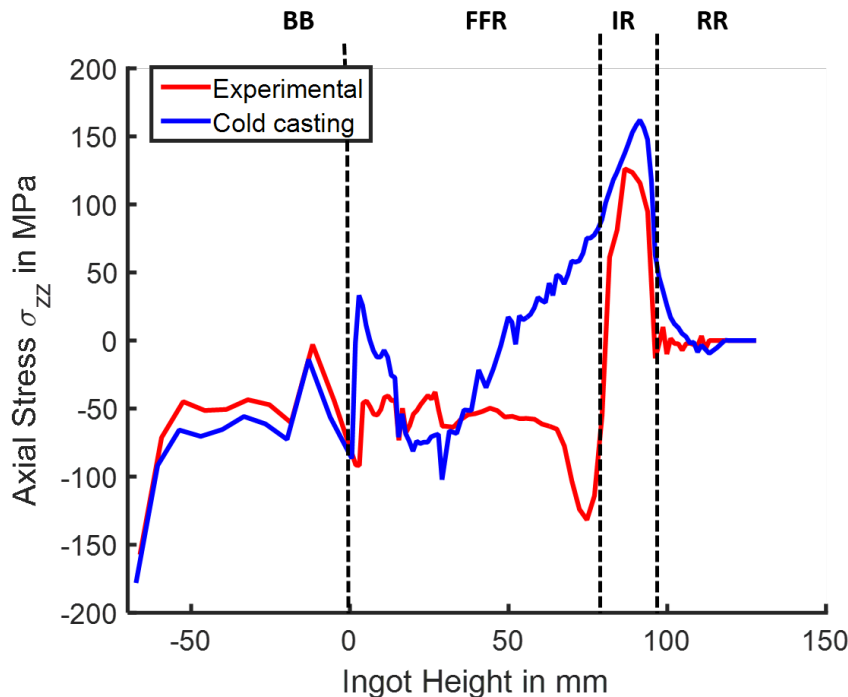


Figure 7.37: Axial stress at different ingot height for experimental casting case at 200 seconds

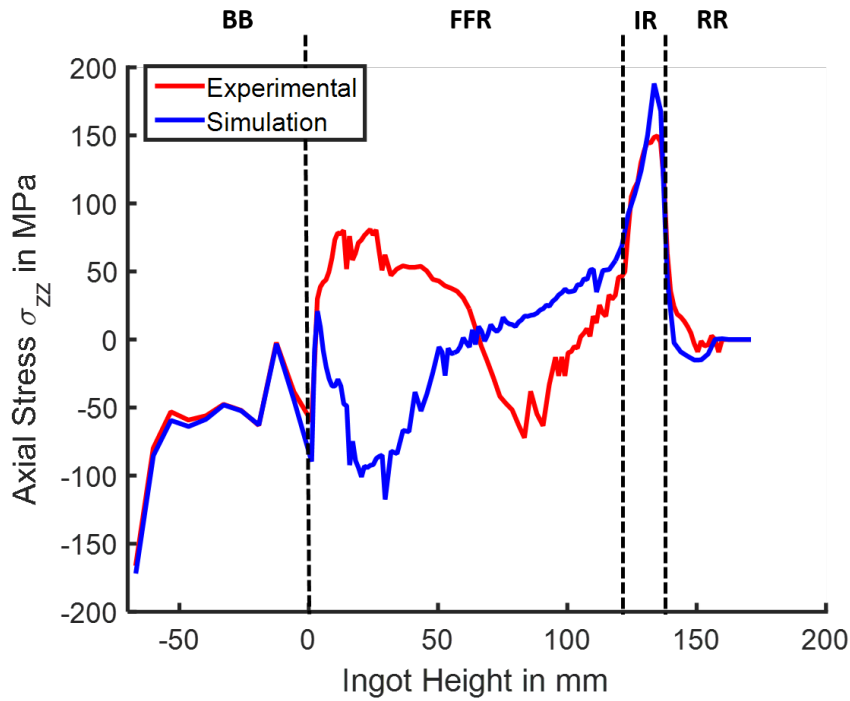


Figure 7.38: Axial stress at different ingot height for experimental casting case at 250 seconds

7.9 Critical Casting Speed

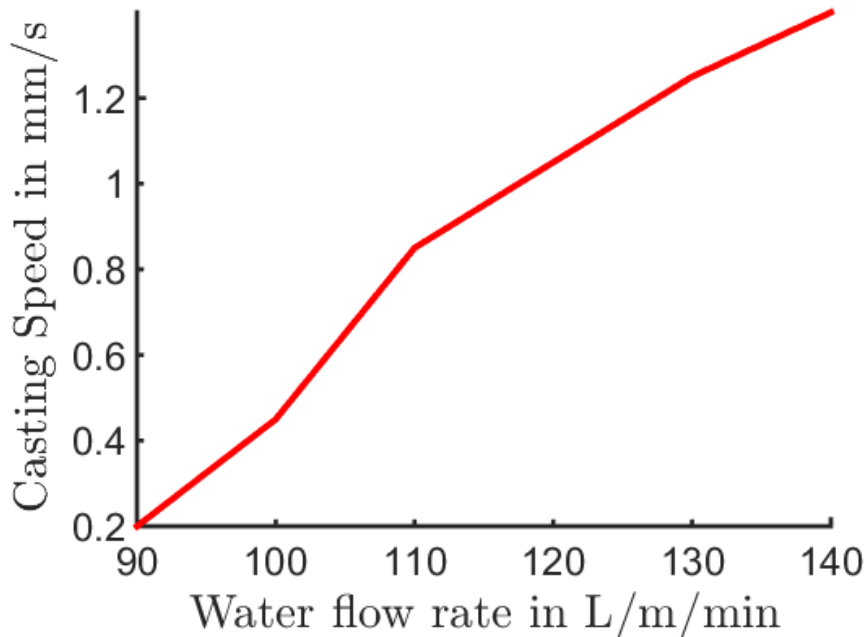


Figure 7.39: Critical casting speed for simulation

Critical casting speed is the speed above which water will get ejected from the surface and below the critical casting speed there will be complete wetting of the surface.

At critical speed, there will be a slight ejection. It is understood that for a casting speed, increasing the water flow rate will increase the width of the impingement zone and increase the rewetting temperature, reducing the occurrence of ejection. Hence, if the water flow rate is increased at a casting speed, the susceptibility of ejection will decrease.

For a constant water flow rate, if the casting speed is increased, the time ingot will spend in the impingement zone will decrease. Hence, the temperature at which ingot enters free-falling zone will increase, increase the susceptibility of ejection.

The geometry of the ingot, the validated thermal boundary conditions are used for this analysis. This plot of critical casting speed provides a strategy for controlling the occurrence of ejection. The region in which ejection is required the water flow rate can be reduced or increased the casting speed to cross the critical casting speed. Similarly, water flow can be increased to reduce the susceptibility of ejection.

7.10 Formation of Meniscus

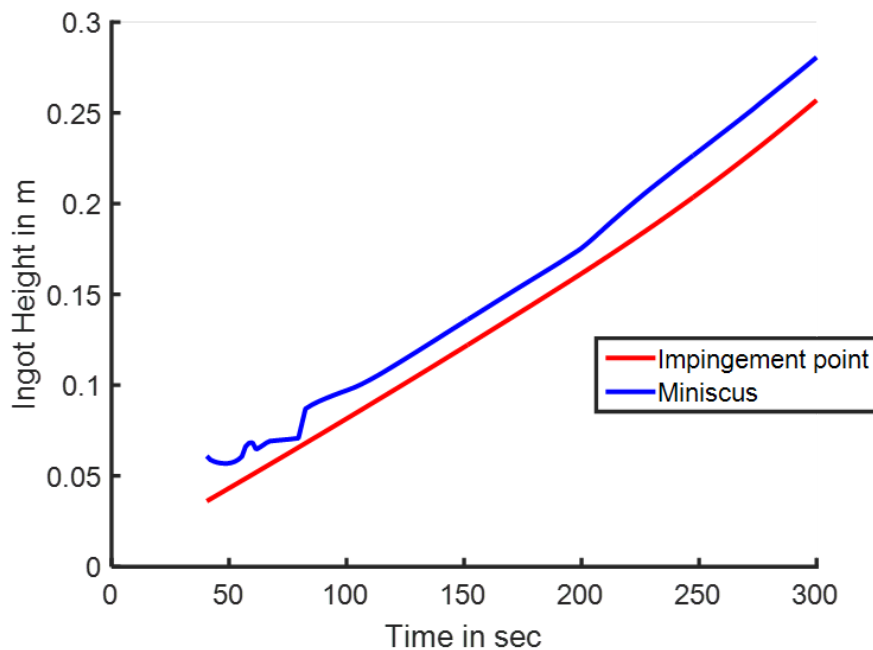


Figure 7.40: Distance between meniscus and impingement point for experimental case

A meniscus is the point at which the liquid metal starts to solidifies or when the metal is at liquidus temperature. The formation of the meniscus has to be in the primary cooling region as if the liquid metal comes in contact with cooling water will cause an explosion. **Fig. 7.40** shows the plot of hight at which meniscus is formed and point of impingement against time. It can be observed during water ejection, the meniscus and the impingement point are closer. Followed this the distance between the meniscus and impingement point increase and reaches a steady value of 23.5 mm. In case of absence of water ejection, the trend of the location of the meniscus is different, but the steady state distance between the two cases is the same. It is

important to study the distance between the meniscus and impingement point as if this distance is large, it might cause remelting of the meniscus and deteriorate surface quality and cause some failures as discussed in **Ch. 1**.

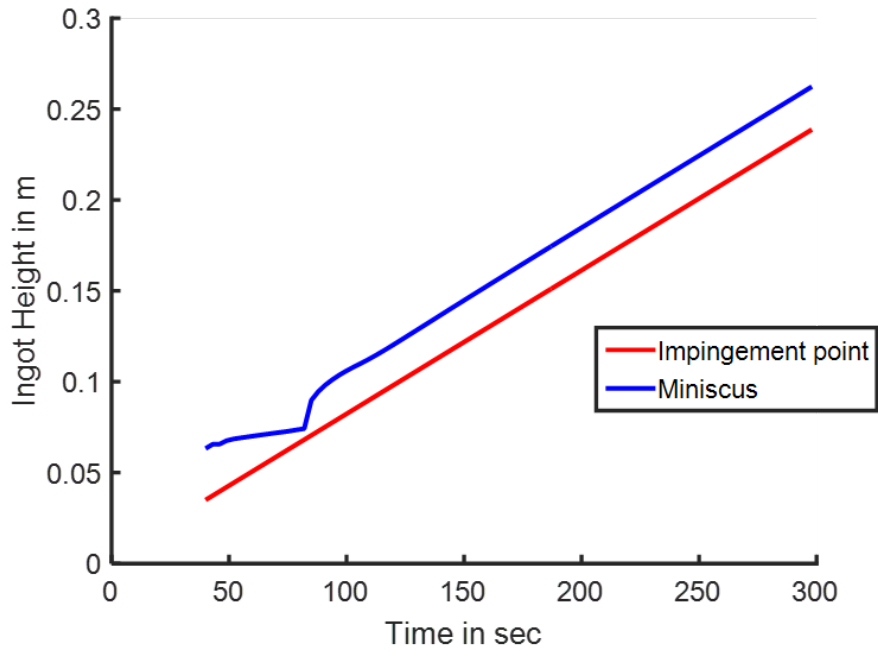


Figure 7.41: Distance between meniscus and impingement point for cold casting case

8. Conclusion

The DC casting process is mimicked in the laboratory to study the heat transfer occurring in the secondary cooling zone. The temperature on the back side of the metal sheet is measured with an infrared camera. The obtained thermal history data, with high local resolution, is analyzed further to obtain the boiling curve considering the difference in temperature between the quenching side and measuring side. The proposed method to determine the boiling curve is based on a Eulerian steady state solution. It is observed that this method is less sensitive to experimental and numerical error. This method also distinguishes between the region where cooling is because of advection in the axial direction and the region of water cooling. This is crucial to consider different boundary conditions in the regions.

Experimental investigations are conducted on an aluminium alloy AA6082, for parameters like initial temperature, casting speed, jet velocity and angle, water quality and temperature, different thickness and kind of metal sheet under moving sheet mechanism and stationary mechanism. The experimental results are analyzed further with the proposed model to quantify the influence of the parameter on the boiling curve.

It is observed that quenching parameters like water quality and temperature, jet velocity and angle does not have an influence on the boiling curve in the impingement zone. This is because of the high turbulence of the water film in the impingement zone. Turbulence will cause the formed bubbles on the surface to diffuse and fresh cooling water will come in contact near the metal surface. The boiling curve is observed to be dependent on the temperature at the point of impingement. For a thin sheet moving at higher speed gives identical boiling curve for thick sheet moving at lower speed, if the temperature at the point of impingement is same for the two cases. For impingement point temperature above 425°C , the maximum heat flux remained constant independent for quenching parameters. Further influence of various parameters is summarized in **Tab. 8.1**.

Table 8.1: Summary of influence of various parameters on heat transfer characteristics in the impingement zone

| Parameter (increase) | q_{max} | T_{DNB} | Width of pre-cooling region |
|------------------------------------|--------------|-------------------|-----------------------------|
| Water Quality | No influence | No influence | No influence |
| Water temperature | No influence | Increase | Slightly decrease |
| Thickness of metal | Increase | Decrease | Decrease |
| Jet velocity | No influence | Slightly decrease | Slightly increase |
| Jet angle | Increase | Decrease | Slightly increase |
| Casting speed | Increase | Decrease | Decrease |
| Initial Temperature of metal sheet | Increases | Increases | No influence |

In the free falling zone the turbulence in the water stream is less and water stream has no horizontal momentum. Because of this, the cooling characteristics will be

different compared to that in the impingement zone. In this analysis, the wetting front velocity cannot be controlled. Because of this, it is concluded that the heat transfer characteristics will be sensitive to various parameters. Water quality has an influence on the boiling curve. For water above $40^{\circ}C$ temperature, a drastic change in the boiling curve is observed. Similar to impingement zone, it is observed that above the initial temperature of $420^{\circ}C$, the boiling curves is not influenced further.

The DNB temperature in impingement zone and free falling zone does not vary with various parameters. The Maximum heat flux in the impingement zone is $\sim 7 MW/m^2$ whereas in case of the free falling zone the maximum heat flux is $\sim 3 MW/m^2$. Further influence of various parameters in the free falling zone is as described in **Tab. 8.2**.

Table 8.2: Summary of influence of various parameters on heat transfer characteristics in the free falling zone

| Parameter (increase) | q_{max} | T_{DNB} | Width of pre-cooling region |
|------------------------------------|-----------|-------------------------------------|-------------------------------------|
| Water Quality | Decreases | Decreases | Decreases |
| Water temperature | Decreases | No influence | Increase |
| Thickness of metal | Decreases | Slightly decrease | Increase |
| Jet velocity | Increase | No influence | Decrease |
| Jet angle | Decrease | Slightly increase and then decrease | Slightly decrease and then increase |
| Initial Temperature of metal sheet | Increases | Increases | Slightly increase |

In cases when a material point is not cooled sufficiently when it enters the free falling zone, it is observed that the water stream is ejected away from the surface. In the free falling zone, water stream has no momentum in the horizontal direction. So rapid formation of bubbles can throw the water film away from the metal surface, causing no cooling and hence no heat transfer with cooling water in this region. Because of this, the rate of cooling in the bottom region is less. Apart from this, followed by first wetting the downstream wetting front propagation velocity is observed to be very less. This is because when the water enters in the free falling zone, the water is heated owing to heat transfer in the impingement zone.

The thermal boundary conditions from the impingement zone and the free falling zone were incorporated in a 2D FE model to predict the susceptibility of ejection and to understand the physical effects causing water ejection. Experiments were conducted to validate the results from simulations and the influence of various parameters on water ejection is summarized in Tab. 8.3. The temperature of water and metal sheet as they enter in the free falling zone is observed to be most dominant factors causing water ejection. Apart from these, the quality of water and horizontal and vertical momentum also influences ejection.

To understand the heat transfer in the start-up phase of DC casting process, the understanding of water ejection phenomenon is incorporated in a 2D plane strain, in-house FE model simulating the DC casting process. With the understanding of distinguishing between impingement zone and the free falling zone and the heat transfer in these zones, the temperature profiles from simulation matches with the

Table 8.3: Influence of various factors on water ejection

| Parameter (increase) | Impingement Zone q_{max} | Free Falling Zone T_{RW} | Water Ejection |
|---------------------------------------|-------------------------------|-------------------------------|----------------|
| Water Quality | No influence | Increase | Decreases |
| Water temperature | No influence | Decreases | Increase |
| Thickness of metal | Increase | Decreases | Increase |
| Jet velocity | No influence | Increase | Decreases |
| Jet angle | Increase | Decreases | Increase |
| Casting speed | Increase | - | Increases |
| Initial Temperature of metal sheet | Increases | Increases | Increases |

temperature measurements from industry. Water ejection is also observed in the industrial casting process and the applied thermal boundary conditions are validated.

Finally, to understand the influence of evolution of stresses in DC casting process and effect of ejection on it, thermo-mechanical simulations were conducted for extreme cases. A case with very high water flow rate in which there is no water ejection named cold casting, another case with low water flow rate where wetting never occurs named hot casting are compared with the experimental case. Hot casting is an infeasible strategy as sufficient cooling of ingot does not occur. It can be concluded that without water ejection high stresses are observed in the bottom region during the first contact with water. This will increase the susceptibility of cracking as the temperature is above solidus temperature. In case of water ejection, compressive stresses occur in the bottom region of the ingot. Because of this, any crack formed can heal and will not propagate throughout the ingot.

Bibliography

- [1] N. B. Bryson. Casting of aluminium ingots. *Alcan, U.S. Patent*, 3411079, 1969.
- [2] H. Yu. A process to reduce d.c. ingot butt curl and swell. *Light Metals*, pages 613–628, 1980.
- [3] G. K. Singworth. Hot tearing of metals. *AFS Transactions*, 104:1053–1062, 1966.
- [4] D. G. Eskin, Suyitno, and L. Katgerman. Mechanical properties of aluminum alloys in the semi-solid state and hot tearing criteria. *Progress in Materials Science*, 49:629–711, 2004.
- [5] Suyitno. Hot tearing and deformation in direct-chill casting of aluminum alloys. *Ph.D. Thesis, Delft University, The Netherlands*, 2005.
- [6] W. van Haaften. Constitutive behavior and hot tearing during aluminium dc casting. *Ph.D. Thesis, Delft University, The Netherlands*, 2002.
- [7] M. Lalpoor, D. G. Eskin, and L. Katgerman. Cold-cracking assessment in aa7050 billets during direct-chill casting by thermomechanical simulation of residual thermal stresses and application of fracture mechanics. *Metallurgical and Materials Transactions A: Physical Metallurgy and Materials Science*, 40:3304–3313, 2009.
- [8] P. K. Penumakala. Thermomechanical simulation of continuous and semi-continuous casting of metals. *Ph.D. Thesis, OvG University, Magdeburg, Germany*, 2014.
- [9] P. Barral and P. Quintela. Numerical algorithm for prediction of thermomechanical deformation during the casting of aluminum alloy ingots. *Finite Elements in Analysis and Design*, 34:125–143, 2000.
- [10] Physical metallurgy of direct chill casting of aluminum alloys. *CRC Press*, 49.
- [11] M. Zaloznik and B. Sarler. Modeling of macrosegregation in direct-chill casting of aluminum alloys: Estimating the influence of casting parameters. *Materials Science and Engineering A*, 413:85–91, 2005.
- [12] M. Ishii. Study on emergency core cooling. *Nuclear Energy Socoty*, 14:237–242, 1975.
- [13] J. J. Carbajo. A study on the rewetting temperature. *Nuclear Engineering Design*, 84:21–52, 1984.
- [14] J. Filipovic, F. P. Incropera, and R. Viskanta. Rewetting temperatures and velocity in a quenching experiment. *Experimental Heat Transfer*, 8:257–270, 1995.

- [15] J. A. Bakken and T. Bergström. Heat transfer measurements during DC casting of aluminium part i : Measurement technique. *Journal of Light Metals*, pages 883–889, 1986.
- [16] E. F. Emley. Continous casting of aluminium. *International Metals Review*, pages 75–115, 1976.
- [17] J. Sengupta, S. L. Cockcroft, D. M. Maijer, M. A. Wells, and A. Larouche. The effect of water ejection and water incursion on the evolution of thermal field during start-up phase of the direct chill casting process. *Journal of Light Metals*, 2:137–148, 2002.
- [18] E. Caron. Secondary cooling in the direct-chill casting of light metals. *Ph.D. Thesis, The University of British Columbia*, 2008.
- [19] M. K. Agrawal and S. K. Sahu. Analysis of multi-region conduction-controlled rewetting of a hot surface with precursory cooling by variational integral method. *Applied Thermal Engineering*, 73:267–276, 2014.
- [20] J. F. Grandfield and P. T. McGlade. Dc casting of aluminium: Process behaviour and technology. *Materials Forum*, 20:29–51, 1996.
- [21] F. Kreith and M. Bohn. Principles of heat transfer. *West Publication Co.*, 1993.
- [22] J. Wiskel. Thermal analysis of the startup phase for dc casting of an aa5182 aluminium ingot. *Ph.D. Thesis, The University of British Columbia*, 1995.
- [23] I. J. Opstelten and J. M. Rabenberg. Determination of the thermal boundary conditions during aluminum dc casting from experimental data using inverse modeling. *Light Metals*, 1999.
- [24] D. C. Weckman and P. Niessen. A numerical simulation of the D. C. continuous casting process including nucleate boiling heat transfer. *Metallurgical Transactions B*, 13B:593–602, 1982.
- [25] B. Sarler and J. Mencinger. Solution of temperature field in dc cast aluminium alloy billet by the dual reciprocity boundary element method. *International Journal of Numerical Methods for Heat and Fluid Flow*, 9:269–295, 1999.
- [26] J. Zuidema. Modelling of glow phenomena during dc casting. *Ph.D. Thesis, Netherlands Institute for Metal Research*, 2005.
- [27] J. Grandfield and P. Baker. Variation of heat transfer rates in direct chill water spray of aluminium continuous casting. *International Conference on Solidification Processing*, 3:260–263, 1987.
- [28] S. Hibbins. Investigation of heat transfer in dc casting of magnesium alloys,. *International Symposium on Light Metals*, 27:265–280, 1988.
- [29] M. Zaloznik, I. Bajsoc, and B. Sarler. Nondestructive experimental determination of the heat flux during cooling of direct chill cast aluminum alloy billets,. *MATERIALI IN TEHNOLOGIJE*, 36:121–125, 2002.

- [30] B. Xue. Hot tearing and deformation in direct-chill casting of aluminum alloys. *Thesis, The University of Applied Science*, 2010.
- [31] D. Li. Boiling water heat transfer study during dc casting of aluminium alloys. *Thesis, The University of Applied Science*, 2000.
- [32] L. Maenner, B. Magnin, and Y. Caratini. A comprehensive approach to water cooling in dc casting. *Light Metals*, pages 701–708, 1997.
- [33] A. Larouche, Y. Caron, and D. Kooaeefe. Impact of water heat extraction and casting conditions on ingot thermal response during dc casting. *Light Metals*, pages 1059–1064, 1998.
- [34] L. Kiss, T. Meenken, A. Charette, Y. Lefebvre, and R. Levesque. Experimental study of the heat transfer along the surface of a water-film cooled ingot. *Light Metals*, pages 981–986, 2002.
- [35] E. Sorheim, D. Mortensen, S. Benum, and C. Stette. Inverse analysis of space and time variations in the boundary heat flux during water film cooling. *Light Metals*, pages 679–686, 2002.
- [36] J. V. Beck, B. Blackwell, and C. R. St-Clair. Inverse heat conduction - ill-posed problems. *Wiley, New York*, 1985.
- [37] M. Monde. Analytical methods in inverse heat transfer problem using laplace transform technique. *International Journal of Heat and Mass Transfer*, 43:3965–3975, 2000.
- [38] U. Z. Ijaz, A. K. Khambampati, M. C. Kim, S. Kim, and K. Y. Kim. Estimation of time-dependent heat flux and measurement bias in two-dimensional inverse heat conduction problems. *International Journal of Heat and Mass Transfer*, 50:4117–4130, 2007.
- [39] S. Deng and Y. Hwang. Applying neural networks to the solution of forward and inverse heat conduction problems. *International Journal of Heat and Mass Transfer*, 49:4732–4750, 2006.
- [40] C. H. Huang and H. H. Wu. An inverse hyperbolic heat conduction problem in estimating surface heat flux by conjugate gradient method. *Journal of Physics D-Applied Physics*, 39:4087–4096, 2006.
- [41] Q. W. Xue and H. T. Yang. Conjugate gradient method for the hyperbolic inverse heat conduction problem with multi-variables. *Chinese Journal of Computational Physics*, 22:417–424, 2005.
- [42] S. Groß, M. Soemers, A. Mhamdi, F. Al Sibai, A. Reusken, W. Marquardt, and U. Renz. Identification of boundary heat fluxes in a falling film experiment using high resolution temperature measurements. *International Journal of Heat and Mass Transfer*, 48:5549–5562, 2005.
- [43] M. Gradeck, J. A. Quattara, B. Rémy, and D. Maillet. Solution of an inverse problem in the hankel space infrared thermography applied to estimation of a transient cooling flux. *Experimental Thermal and Fluid Science*, 36:56–64, 2012.

- [44] E. Elias and G. Yadigarogul. A general one-dimensional model for conduction-controlled rewetting of a surface. *Nuclear Engineering and Design*, 42-2:185–194, 1977.
- [45] M. A. Wells, D. Li, and S. L. Cockcroft. Influence of surface morphology, water flow rate and sample thermal history on the boiling-water heat transfer during direct-chill casting of commercial aluminum alloys. *Metallurgical and Materials Transactions B*, 32B:929–939, 2001.
- [46] A. K. Nallathambi and E. Specht. Estimation of heat flux in array of jets quenching using experimental and inverse finite element method. *Journal of Materials Processing Technology*, 209:5325–5332, 2009.
- [47] A. K. Mozumder, M. Monde, and P. L. Woodfield. Delay of wetting propagation during jet impingement quenching for a high temperature surface. *International Journal of Heat and Mass Transfer*, 48:5395–5407, 2005.
- [48] M. Akmal, A. M. T. Omar, and M. S. Hamed. Experimental investigation of propagation of wetting front on curved surfaces exposed to an impinging water jet. *International Journal of Microstructure and Materials Properties*, 3:645–681, 2008.
- [49] E. Caron and M. A. Wells. Secondary cooling in the direct-chill casting of magnesium alloy az31. *METALLURGICAL AND MATERIALS TRANSACTIONS B*, 40B:585–595, 2009.
- [50] M. Hnizdil, M. Chabicovsky, and M. Raudensky. Influence of the impace angle and pressure on the spray cooling of vertically moving hot steel surfaces. *Materials and Technology*, 49:333–336, 2015.
- [51] D. A. Knool, D. B. Kothe, and B. Lally. New nonlinear solution method for phase-change problems. *Numerical Heat Transfer, Part B: Fundamentals*, 35, no. 4:439–459, 1999.
- [52] S. Koric and B. G. Thomas. Efficient thermo-mechanical model for solidification processes. *International Journal for Numerical Methods in Engineering*, 66, no. 12:1955–1989, 2006.
- [53] D. Celentano, E. Onate, and S. Oller. A temperature-based formulation for finite element analysis of generalized phase-change problems. *International Journal for Numerical Methods in Engineering*, 37, no. 20:3441–3465, 1994.
- [54] J. Sengupta. Mathematical modeling of the evolution of thermal field during start-up phase of the direct chill casting process for aa5182 sheet ingots. *Ph.D. Thesis, The University of British Columbia*, 2002.
- [55] P. Barral and P. Quintela. A numerical method for simulation of thermal stresses during casting of aluminium slabs. *Computer Methods in Applied Mechanics and Engineering*, 178:69–88, 1999.
- [56] Y. Kayamak. Modeling of metal quenching process and strategies to minimize distortion and stresses. *Otto von Guericke University, Magdeburg*, 2007.

- [57] A. K. Nallathambi. Thermomechanical simulation of direct chill casting. *Otto von Guericke University, Magdeburg*, 2010.
- [58] A. J. Williams, T. N. Croft, and M. Cross. Modeling of ingot development during the start-up phase of direct chill casting. *Metallurgical and Materials Transactions B: Process Metallurgy and Materials Processing Science*, pages 727–734, 2003.
- [59] B. Magnin, L. Maenner, L. Katgerman, and S. Engler. Ductility and rheology of an al-4.5to coherency temperature. *Materials Science Forum*, 217-222:1209–1214, 1996.
- [60] Suyitno, W. H. Kool, and L. Katgerman. Finite element method simulation of mushy zone behavior during direct-chill casting of an al-4.5 pct cu alloy. *Metallurgical and Materials Transactions A: Physical Metallurgy and Materials Science*, 35-A:2917–2926, 2004.
- [61] U. Alam, J. Krol, E. Specht, and J. Schmidt. Enhancement and local regulation of metal quenching using atomized spray. *Journal of ASTM International*, 5:1–10, 2008.
- [62] M. K. Agrawal and S. K. Sahu. Analysis of conduction-controlled rewetting of a hot surface by variational method. *Heat Mass Transfer*, 49:963–971, 2013.
- [63] Atsuo YAMANOUCI. Effect of core spray cooling in transient state after loss of coolant accident. *Journal of Nuclear Science and Technology*, 5(11):547–558, 1968.
- [64] H Kraushaar, R Jeschar, V Heidt, EK Jensen, and W Schneider. Correlation of surface temperatures and heat transfer by D. C. casting of aluminium ingots. *Light Metals (WARRENDALE PA)*, pages 1055–1059, 1995.
- [65] JF Grandfield, A Hoadley, and S Instone. Water cooling in direct chill casting: Part 1, boiling theory and control. *Light Metals (WARRENDALE PA)*, pages 691–700, 1997.
- [66] JB Wiskel and SL Cockcroft. Heat-flow-based analysis of surface crack formation during the start-up of the direct chill casting process: Part ii. experimental study of an aa5182 rolling ingot. *Metallurgical and Materials Transactions B*, 27(1):129–137, 1996.
- [67] Y Watanabe and N Hayashi. Light metals 1996, anaheim, ca, 1996, w. Hale, ed., TMS, Warrendale, PA, pages 979–984.
- [68] J. M. Drezet, M. Rappaz, G. U. Grün, and M. Gremaud. Determination of thermophysical properties and boundary conditions of direct chill-cast aluminium alloys using inverse methods. *Metallurgical and Materials Transactions A*, 31A:1627–1634, 2000.
- [69] E. Caron and M. A. Wells. Effect of advanced cooling front (acf) phenomena on film boiling and transition boiling regimes in the secondary cooling zone during the direct-chill casting of aluminum alloys. *Materials Science Forum*, 519-521:1687–1692, 2006.

- [70] Sabariman. Heat transfer analysis in metal quenching with sprays and jets. *Otto von Guericke University, Magdeburg*, 2015.
- [71] A. K. Mozumder, M. Monde, P. L. Woodfield, and Islam Md. A. Maximum heat flux in relation to quenching of a high temperature surface with liquid jet impingement. *International Journal of Heat and Mass Transfer*, 49:2877–2888, 2006.
- [72] El-Genk, S. Mohamed, and Z. Guo. Transition boiling from inclined and downward-facing surface in a saturated pool. *Journal of Refrigeration*, 16.6:412–422, 1993.
- [73] J. W. Westwater, J. J. Hwalek, and M. E. Irving. Suggested standard method for obtaining boiling curve by quenching. *Industrial and industrial chemistry fundamentals*, 21.4:685–692, 1986.
- [74] R. R. Sharp. The nature of liquid film evaporation during nucleate boiling. *National Aeronautics and Space Administration*, 1964.
- [75] U. Magrini and E. Nannei. On the influence of the thickness and thermal properties of heating wall on the heat transfer coefficient in nucleate pool boiling. *Journal of Heat Transfer*, 97.2:173–178, 1975.
- [76] J. M. Drezet and M. Rappaz. Modeling of ingot distortions during direct chill casting of aluminum alloys. *Metallurgical and Materials Transactions A: Physical Metallurgy and Materials Science*, 27:3214–3225, 1996.
- [77] E. K. Jensen, S. Johansen, T. Bergström, and J. A. Bakken. Heat transfer measurements during DC casting of aluminium. part ii: Results and verification for extrusion ingots. *Journal of Light Metals*, pages 891–896, 1986.
- [78] J. Sengupta, S. L. Cockcroft, D. M. Maijer, M. A. Wells, and A. Larouche. On the development of a three-dimensional transient thermal model to predict ingot cooling behavior during the start-up phase of the direct chill-casting process for an AA5182 aluminium alloy ingot. *Metallurgical and Materials Transactions B*, 35B:523–540, 2004.
- [79] Heat transfer characteristics during jet-impingement on a high temperature plate surface. *Applied Thermal Engineering*, 100.
- [80] Wagstaff. U.s. patent. 4693298, 1987.
- [81] P. J. Lamont and B. L. Hunt. The impingement of underexpanded, axisymmetric jets on perpendicular and inclined plates. *Journal of Fluid Mechanics*, 100.3:471–511, 1980.

Part I

Appendix

Appendix

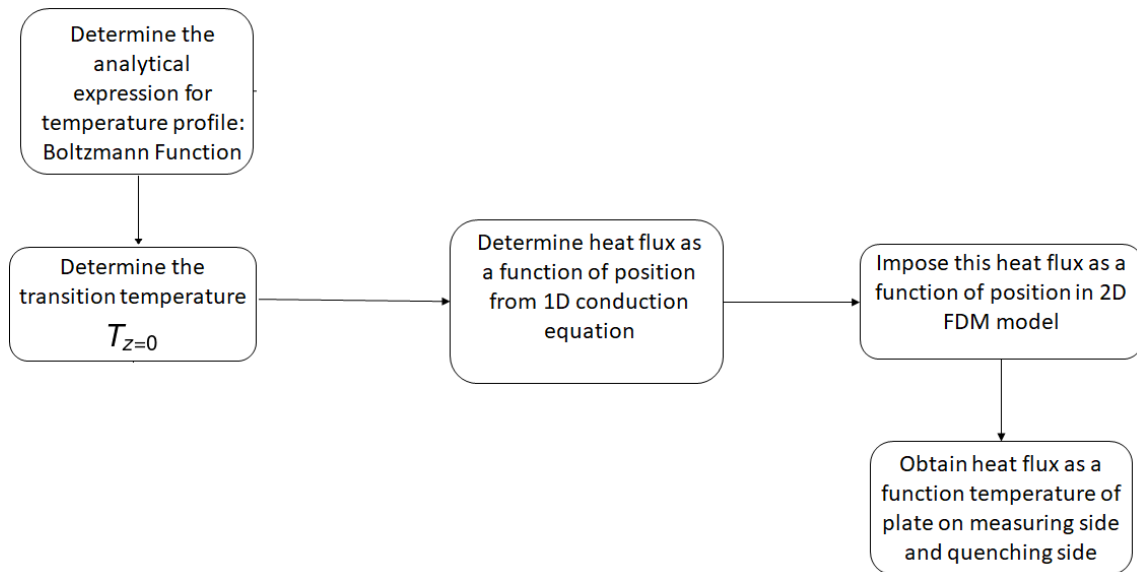


Figure 8.1: Algorithm for determining the boiling curve

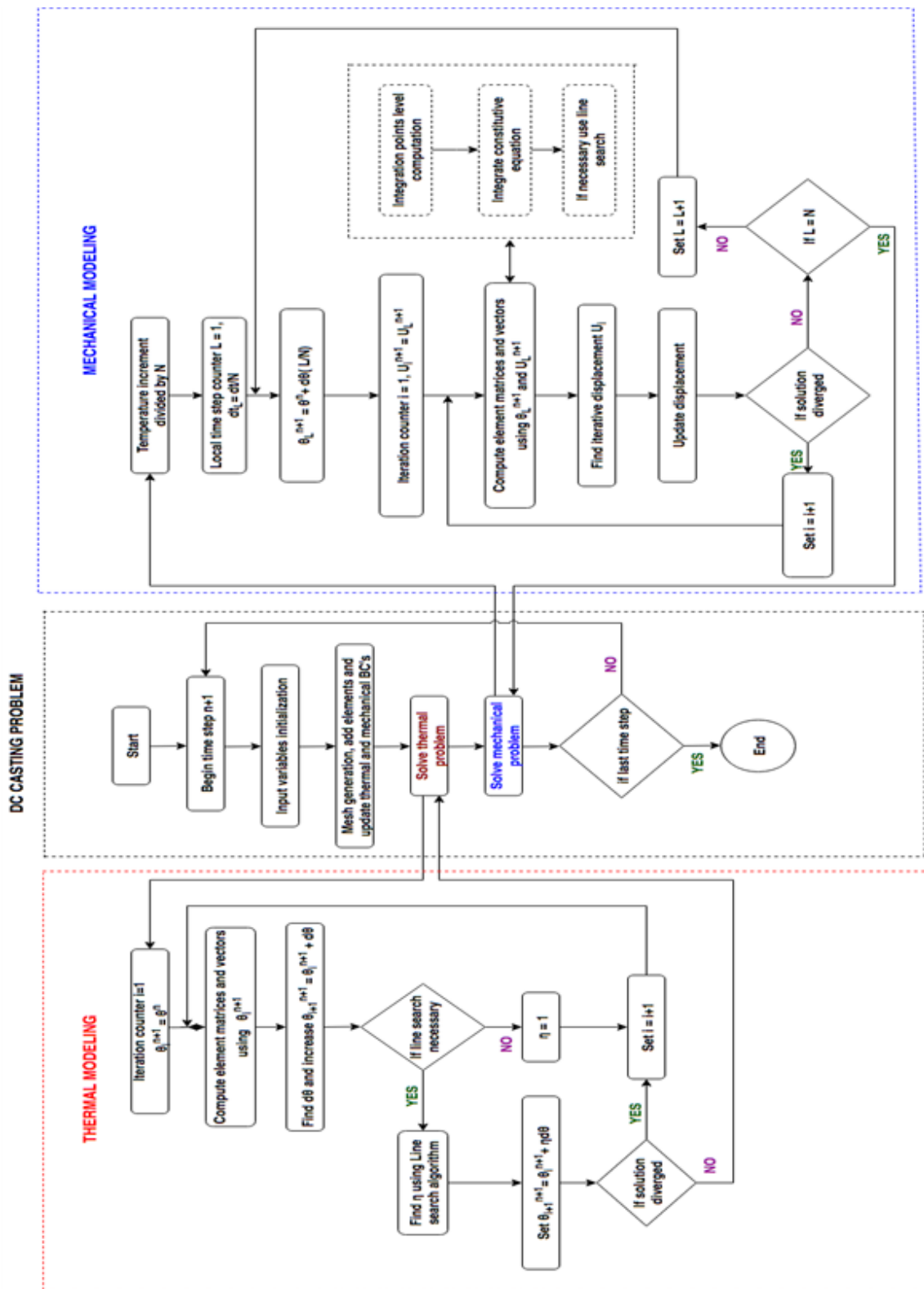


Figure 8.2: Flow chart for DC casting model in MATLAB

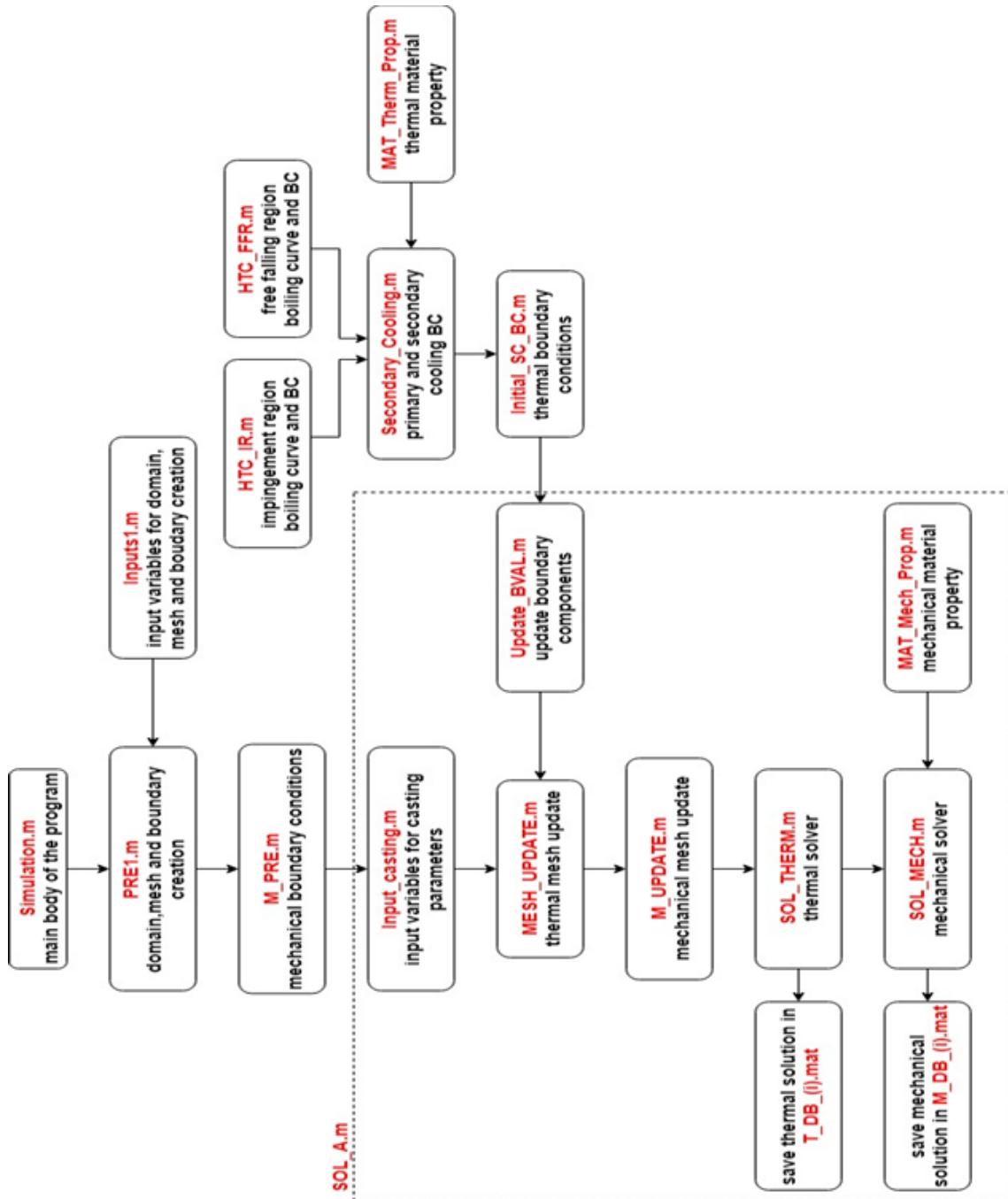


Figure 8.3: Flow chart for the algorithm of DC casting model

List of Publications

1. G. A. Kulkarni, A. K. Nallathambi, Y. Kaymak, and E. Specht, “Distortion Induced during Quenching of Seamless Tubed”, *Materials Science and Engineering*, DGM, Darmstadt, 2016.
2. G. A. Kulkarni, Sabariman, and E. Specht, “Jet Impingement Heat Transfer of Moving Metal Sheet”, *13th International Conference on Heat Transfer, Fluid Mechanics and Thermodynamics*, Portoroz, Slovenia, ISBN: 978-1-77592-140-0, pp. 393–400, 2017.
3. S. Ramasamy, G. A. Kulkarni, A. K. Nallathambi, and E. Specht, “Influence of Water Cooling on Stresses in DC Casting of Aluminum Alloys”, *Symposium and Workshop for Analytical Youth on Applied Mechanics*, 2018. ISBN: 978-9-38676-713-6.
4. S. B. Gopalkrishna, G. A. Kulkarni, A. K. Nallathambi, and E. Specht, “Thermal Stresses in Quenching of Moving plate by an Array of Jets”, *Symposium and Workshop for Analytical Youth on Applied Mechanics*, 2018. ISBN: 978-9-38676-713-6.
5. G. A. Kulkarni, E. Specht, “Quantifying the Parameters Influencing Heat Transfer during Quenching of Metal Plate”, *5TH International Conference on Heat Transfer and Fluid Flow*, Madrid, Spain, 2018.
6. S. B. Gopalkrishna, G. A. Kulkarni, A. K. Nallathambi, Y. Kaymak, and E. Specht, “Investigation of Distortion in Quenching of Seamless Tubes”, *Student technical Conference, Petroleum and Drilling Engineering related Geoscience Geothermics*, 2018.
7. G. A. Kulkarni, A. K. Nallathambi, and E. Specht, “ Eulerian Steady State Solution of Boiling Curve for Impinging Water Jet on Moving Hot Metal Plate”, *Heat and Mass Transfer*, 2018. (accepted)
8. G. A. Kulkarni, E. Specht, “Quantifying the Parameters Influencing Heat Transfer during Quenching of Metal Plate”, *Journal of Heat Transfer and Fluid Flow*, 2018. (accepted)

List of Thesis Supervised

1. Dumpala Sai Karunakar Reddy “Heat Transfer Analysis of Quenching with an Array of Jets on Aluminum sheet”, *Master Thesis, Otto-von-Guericke Universität Magdeburg*, 2017.
2. Lei Song “Influence of metal type and initial temperature on heat transfer of metal quenching with an array of jets”, *Master Thesis, Otto-von-Guericke Universität Magdeburg*, 2018.
3. Yaodong Xu “Heat Transfer Analysis of Metal Quenching with an Array of Jets in the Free Falling Region”, *Master Thesis, Otto-von-Guericke Universität Magdeburg*, 2018.
4. Subash Ramasamy “Influence of Water Ejection on Thermal Stresses in Direct Chill Casting”, *Master Thesis, Otto-von-Guericke Universität Magdeburg*, 2018.
5. Wenhao Hu “Influence of Spray Cooling on Stress Profiles on Continuous Casting of Steel”, *Master Thesis, Otto-von-Guericke Universität Magdeburg*, 2018.
6. Santosh Reddy Gurralla “Quantifying the parameters infusing water ejection during of Quenching with an Array of Jets on Aluminum Sheet”, *Master Thesis, Otto-von-Guericke Universität Magdeburg*, 2018.
7. Rahul Murkute “Forming of Stacked Metallic Plates using Shock Wave: An experimental and Numerical Study”, *Master Thesis, Rheinisch-Westfälische Technische Hochschule Aachen*, 2018.
8. Suresh Babu Gopalkrishna “Thermal Stresses in Quenching of Plate by Array of Jets and Sprays”, *Master Thesis, Otto-von-Guericke Universität Magdeburg*, 2018.
9. Vinay Kumar Bele “Thermo-Mechanical analysis of Quenching with an Array of Jets on Aluminum Sheet”, *Master Thesis, Otto-von-Guericke Universität Magdeburg*, 2018.

Curriculum Vitae

| | |
|----------------|---|
| First name | Gaurav Abhay |
| Family name | Kulkarni |
| Nationality | Indian |
| Date of birth | 05-10-1989 |
| Place of birth | Aurangabad, Maharashtra, India. |
| Parents | Abhay Kulkarni and Madhuri Kulkarni |
| Marital status | Married to Gauri Beedkar |
| 2007 – 2011 | Bachelor of Technology in Mechanical Engineering, Visvesvaraya National Institute of Technology, Nagpur, India. <i>Thesis:</i> Experimental and theoretical stress analysis using photoelasticity with special emphasis on stress concentration factor. |
| 2011 – 2012 | Engineer, Testing and Validation, Motorcycle Division, Bajaj Auto Ltd., India. |
| 2012 – 2015 | Master of Science in Computer Aided Conceptions and Production in Mechanical Engineering, Rheinisch-Westfälische Technische Hochschule Aachen, Germany. <i>Thesis:</i> Adaptive meshing based on contact boundary surface in 2D finite element computations |
| 2015 – 2018 | Doctorate of Engineering, Otto von Guericke University of Magdeburg, Germany <i>Thesis:</i> Local Heat Transfer and Stress Analysis of Direct Chill Casting Process |